The function of *cedA* of *Escherichia coli* and its relevance to urinary tract infections

by Tamika Ayisha Blair

Thesis submitted in fulfilment of the requirements for the degree of

Doctor of Philosophy

under the supervision of A. Prof. Iain Duggin, Dr. Bill Söderström and Prof. Elizabeth Harry

University of Technology Sydney
Faculty of Science

March 2021

[blank page]

CERTIFICATE OF ORIGINAL AUTHORSHIP

I, Tamika A. Blair, declare that this thesis, is submitted in fulfilment of the requirements for the award of Doctor of Philosophy, in the ithree institute at the University of Technology Sydney.

This thesis is wholly my own work unless otherwise referenced or acknowledged. In addition, I certify that all information sources and literature used are indicated in the thesis.

This document has not been submitted for qualifications at any other academic institution.

This research is supported by the Australian Government Research Training Program.

Signature: Production Note:
Signature removed prior to publication.

Date: 15/03/2021

Dada, I hope you are watching proudly

ACKNOWLEDGEMENTS

I would like to firstly thank Associate Professor Iain Duggin, for providing me with the opportunity to undertake a PhD under his guidance and supervision. Thank you for always being encouraging and a brilliant mentor. Your passion for science is inspiring. I would also like to thank the University of Technology Sydney for providing me with a UTS Doctoral Scholarship.

To Greg, you have honestly been a blessing during my time as a PhD candidate. You took me under your wings without hesitation and for that, I am extremely grateful. Thank you for helping me with everything related to the UTI infections and always being willing to discuss results over lunch together. Emma, thank you for your support through this journey and for reading this thesis. You are an extremely selfless person and I am so grateful to have met you. To Bill, thank you for taking the time to read a couple of chapters of this thesis and I am proud to pass the UPEC baton on to you. To past and present Duggin Lab members, Daniel, Roshali, Tayla, Solenne, Yan, Dora, Vinaya and Hannah, thank you for your support, friendship, and constant scientific discussions.

To my friends and family, this journey would not have been possible without your support. Tahlia and Tiana, thank you for always reminding me that there is life to enjoy outside of the lab. To Peter, thank you for putting up with me over these 4 years, we have been through so much and you have kept me level through it all. To my overseas family, Olivia and John, thank you for always checking in on my progress and sharing in my excitement when meeting milestones. Finally, to Mum and Dad, you have instilled in me the importance of education. Thank you for your sacrifices to ensure that I was given the best opportunity for education. Seeing you both strive for excellence through hard work has been inspirational and I hope this PhD makes you proud.

CONFERENCE PROCEEDINGS

2019 BMSV2019, Cape Town, South Africa. Oral Presentation titled, "***E. coli's*** **cell division activator, *cedA,* can prevent many pathways to bacterial filamentation: involvement in urinary tract infections**". **Blair, T.**

2018 ComBio, Sydney, Australia. Presented poster titled, "**Reversible cell filamentation of Uropathogenic Escherichia coli (UPEC) and the role of cedA gene in urinary tract infections". Blair, T**., Iosifidis, G., Mediati, D.G. & Duggin, I.G.

2017 BacPath, Adelaide, Australia. Presented poster titled, "**The Function of the *cedA* gene of Uropathogenic *Escherichia coli* and its Importance to Urinary Tract Infections". Blair, T**., Iosifidis, G., Mediati, D.G. & Duggin, I.G.

2015 New Horizons, Sydney, Australia. Presented poster titled, "**The Function of the *cedA* gene of Uropathogenic *Escherichia coli* and its Importance to Urinary Tract Infections". Blair, T**., Iosifidis, G., Mediati, D.G. & Duggin, I.G.

ABBREVIATIONS

A	Absorbance
Amp	Ampicillin
BLAST	Basic local alignment search tool
bp	basepair
Cm	Chloramphenicol
CO_2	Carbon dioxide
DMSO	Dimethyl sulfoxide
DNA	Deoxyribonucleic acid
DTI	Defined trypsin inhibitor
E.	*Escherichia*
EDTA	Ethylenediaminetetraacetic acid
et al.	and others
g	grams
GFP	Green fluorescent protein
h	Hours
HKGS	Human Keratinocyte Growth Supplement
IBC	Intracellular bacterial community
IL	Interleukin
IPTG	Isopropyl β-D-1-thiogalactopyranoside
Kan	Kanamycin
kb	Kilobase
L	Litres
LB	Luria Broth
LPS	Lipopolysaccharide
M	Molarity
m	meters
Min	The min protein system
min	minutes
mL	millilitres
MW	Molecular weight
n	nano (10^{-9})
NO	Nucleoid occlusion system
^{o}C	Degrees Celsius
OD	Optical density
PBS	Phosphate buffered saline
PCR	polymerase chain reaction
PFA	Paraformaldehyde
pH	Power of hydrogen
PS	Penicillin/Streptomycin
RNA	Ribonucleic acid
rpm	revolutions per minute
Spec	Spectinomycin
TAE	Tris/acetate/EDTA
TBE	Tris/borate/EDTA
TraDIS	Transposon-directed insertion-site sequencing

UP	Uroplakin
UPEC	Uropathogenic *Escherichia coli*
UTI	Urinary tract infections
V	Volts
v	Volume
w	Weight
WT	Wild-type
xg	Centrifugal force (x unit gravitational field)
Δ	Delta(change in)
μ	Micro (10^{-6})

Table of Contents

LIST OF FIGURES

LIST OF TABLES

ABSTRACT

Urinary Tract Infections (UTIs) are one of the most common bacterial infections worldwide. Eighty per cent of UTIs are caused by uropathogenic *Escherichia coli* (UPEC) which undergoes a multistage infection cycle. The regulatory mechanisms that control the stages of bacterial cell filamentation during dispersal from overwhelmed bladder cells, and filament reversal (re-division) to form rod cells and allow for reinfection are unresolved.

Previous work showed that overexpression of an *E. coli* gene, *cedA*, prevents filamentation in a mutant strain of *E. coli*, called *dnaA(cos)*. *cedA* was also shown to be under positive selection in UPEC strains and upregulated 8-fold during the dispersal (including filamentation) stage of the UPEC infection cycle in cultured human bladder cells.

We found that *dnaA(cos)*-mediated filamentation employs multiple pathways to lead to filamentation, suggesting that expression of *cedA* can prevent and/or reverse filamentation generally. We individually surveyed several other known pathways to filamentation and found that *cedA* can partially prevent filamentation caused by expression of *ftsZ-yfp*, *recAtif* (SOS response), and mild filamentation of *zwf*. *cedA* overexpression prevented the dispersal of filaments from infected bladder epithelial cells, via inhibition of bacterial growth and/or filamentation at this infection stage, and promoted division in wild-type (WT) cells grown under standard laboratory conditions.

Finally, we developed an infection growth competition assay aimed to test preliminary results from a previous genetic screen that suggested *cedA* might be required for the dispersal stage of UPECs infection cycle. Results revealed that *cedA* is dispensable for survival during the dispersal/filamentation and recovery (post-infection) stages of the infection cycle. However, division regulator, *slmA*, known to help prevent division from occurring over the DNA, appeared to play a role in the recovery stage. Understanding how it achieves this requires further work.

Overall, the work presented suggests *E. coli's cedA* has a general stimulatory effect on cell division. Possibly through metabolic regulators of division, and might control cell size under certain environmental conditions when its expression is induced, including the dispersal and recovery phases of UPECs infection cycle. Based on our results, we hypothesise that *cedA* prevents filamentation in the subset of intracellular bacterial communities that do not generate filaments during dispersal, possibly allowing for other types of differentiated bacteria that may benefit the species during the sudden change in conditions associated with dispersal. Therefore, this thesis initiates research into understanding the importance of *cedA* during infection and this may lead to possible future therapeutics for UTIs.

Chapter 1
Introduction

Urinary Tract Infections (UTIs) are one of the most common and significant bacterial infections worldwide. It has been reported that 40-50% of women will experience a UTI in their lifetime compared to 5% of men.[1] The discrepancy between the genders is due to women being more susceptible to UTIs because of their shorter urethra.[2] Approximately 4 million women will seek treatment annually and of these women at least 25% will experience a second UTI and 5% will experience a third UTI within 6 months from the initial infection.[3,4] The most commonly used method for treating UTIs is antibiotic treatments. However antimicrobial resistance has been increasing among pathogens that cause UTIs in community-acquired infections.[5] This elevates the importance of understanding how UTIs are capable of causing re-infection.

Economic expenditures for time lost at work and the cost of health care due to UTIs amounts to approximately $3.5 billion per annum in the United States.[6] Due to its detrimental effect on the population in terms of health and resources, UTIs are becoming a priority in research specifically focussed on finding new methods of treatment as well as prevention. Due to the rise in antibiotic-resistant bacteria, such as multi-drug resistant *E.coli* ST131, it is becoming increasingly difficult to treat UTIs.[7,8]

Uropathogenic *Escherichia coli* (UPEC) accounts for 80% of UTIs and is reported to have both intracellular and extracellular stages in its lifecycle.[9] Research has focused on the initial infection stages, these being attachment and invasion of bladder epithelial cells by UPEC, using the *in vivo* mouse model of infection. There is a considerable lack of understanding in the processes and mechanisms found in the later stages including the rupture of the bladder cells and the escape of the bacteria, which includes extensive filamentation of the bacteria, followed by reversal to reform its original size that can reinfect other epithelial cells.[10,11] Filamentation occurs when bacteria grow (elongate) without dividing.[10,12] Reversal is crucial to the continuation of the UPECs life cycle and the persistence of the UTI, for which the mechanism is still unknown.[10,12–14] It is hypothesised that a possible mechanism for filamentation reversal is through the expression of the *cedA* gene, which is found commonly but not limited to UPEC strains.[12] Very little is known about this gene, yet under some conditions, its expression can promote division of a filamentous *E. coli* strain *in vitro*.[15] Its mechanism and its potential role in the reversal of UPEC filamentation is unknown. Overall, the recurrence of UTIs

is high and with the rise in antibiotic resistance, there is a need to understand how the bacteria can reverse filamentation to cause re-infection. There are 3 key pieces of information that highlights *cedA* for its potential filament-reversal mechanism in UPEC. Firstly, it has been shown to be able to prevent filamentation in a non-pathogenic background.[15] Secondly, it is positively selected for in UPEC strains.[12] Thirdly, it has been shown it be upregulated 8-fold during that later stages of UPEC infection cycle.[16] The work in this thesis aims to address this question, by exploring the function of a relatively unknown gene *cedA* in the non-pathogenic standard lab K-12 *E. coli* strain and pathogenic UPEC strain, UTI89.[17]

1.1 Urinary Tract Infections

Urinary tract infections are caused by the presence of bacteria in the urinary tract.[1] UTIs are classified as either uncomplicated or complicated. An uncomplicated UTI affects healthy individuals who have no urinary tract abnormalities.[6,18] All remaining individuals who have a UTI are considered to have a complicated UTI where there are factors that compromise the urinary tract or host defence, for example, catheters, retention, immunosuppression and renal failure.[19] Complicated UTIs also have the potential of leading to kidney disease, lethal sepsis and increases in the risk of bladder and urinary tract cancers.[20] UTIs can be caused by both Gram-negative and Gram-positive bacteria however approximately 80% of UTI cases are caused by UPEC.[6] Other bacteria that can cause UTIs are *Klebsiella pneumonia, Staphylococcus saprophyticus, Enterococcus faecalis, Pseudomonas aeruginosa and Staphylococcus aureus.*[6]

UTIs are classified according to the site of infection and therefore when an infection is established in the bladder it is referred to as cystitis, in the kidney it is called pyelonephritis and in the urine, it is called bacteriuria.[21] The classic symptoms of UTIs once UPEC has colonised the urinary tract to cause cystitis are frequent and painful urination, as well as the urgency to urinate.[21] Treatment for UTIs is through the use of antibiotics such as ampicillin, trimethoprim, sulfamethoxazole and ciprofloxacin.[3] However, due to the increase of antibiotic resistance it is becoming difficult to treat UTIs through the current antibiotics on offer. For example, a relatively new strain of *E. coli*, ST131, is associated with UTIs and it carries fluoroquinolone, trimethoprim and sulfamethoxazole resistance through its plasmids.[7,22] This highlights the importance of understanding every aspect of the infection in order to develop new treatments.

Escherichia coli is found naturally occurring in the intestinal tract of humans and animals. A subset of *E. coli* is able to cause enteric disease while a different subset is able to cause extra-intestinal disease such as UTIs.[23] Due to a different combination of virulence factors, enteric disease-causing *E. coli* has 6 different pathotypes and these are enteropathogenic *E. coli* (EPEC), enteroinvasive *E. coli* (EIEC), enterohemorrhagic *E.coli* (EHEC), diffusely adherent *E. coli* (DAEC), enterotoxigenic *E. coli* (ETEC) and enteroaggregative *E. coli* (EAEC). Pathotypes for UTIs have not been distinguished as of

yet and therefore UPEC is commonly used for all *E. coli* strains causing UTIs. Virulence factors like adhesive organelles such as type I and P pili are necessary for UPEC to bind and invade the host cells and tissues within the urinary tract. Iron chelating factors or siderophores are important for UPEC to use the host iron stores.[24] Production and use of toxins such as hemolysin and cytotoxic necrotizing factor 1 allow UPEC to cause extensive tissue damage, therefore enabling bacterial dissemination through the host as well as releasing host nutrients and disabling host immune response.[24] These are just a few examples of the different types of virulence factors UPEC employs to cause infection.

A UTI comprises of interactions between the host, particularly urinary tract epithelial cells, and UPEC. Understanding these interactions is important to determine how UPEC can survive in a hostile environment and more importantly it might provide insight in other ways UTI can be treated. This section will describe the fundamentals of establishing an infection and the numerous morphological changes that UPEC undergoes to maintain and re-establish infection.

1.1.1 UPEC Infection Stages

UTIs are caused when UPEC from the gastrointestinal tract colonises the urethra.[6] From the urethra, UPEC moves into the bladder lumen where it undergoes an infection cycle which begins with the invasion of the bladder epithelium.[14] The infection cycle of UPEC is complex undergoing different morphologies to ensure its survival (Figure 1.1).[14] UPEC begins its lifecycle as a normal short rod-shaped bacteria. Its lifecycle consists of the attachment and invasion of bladder epithelial cells, proliferation, and formation of intracellular bacterial communities (IBCs) where some UPEC become filamentous during the late stage of intracellular infection and are released upon cell lysis.[14] After lysis, the filaments revert to short rod-shaped bacteria in order to effectively re-infect other surrounding bladder epithelial cells.[4,10,25,14] However, it is still unknown what mechanism allows for the reversal of filaments to enable the continuation of infection. Each stage of the infection cycle will be described in detail below.

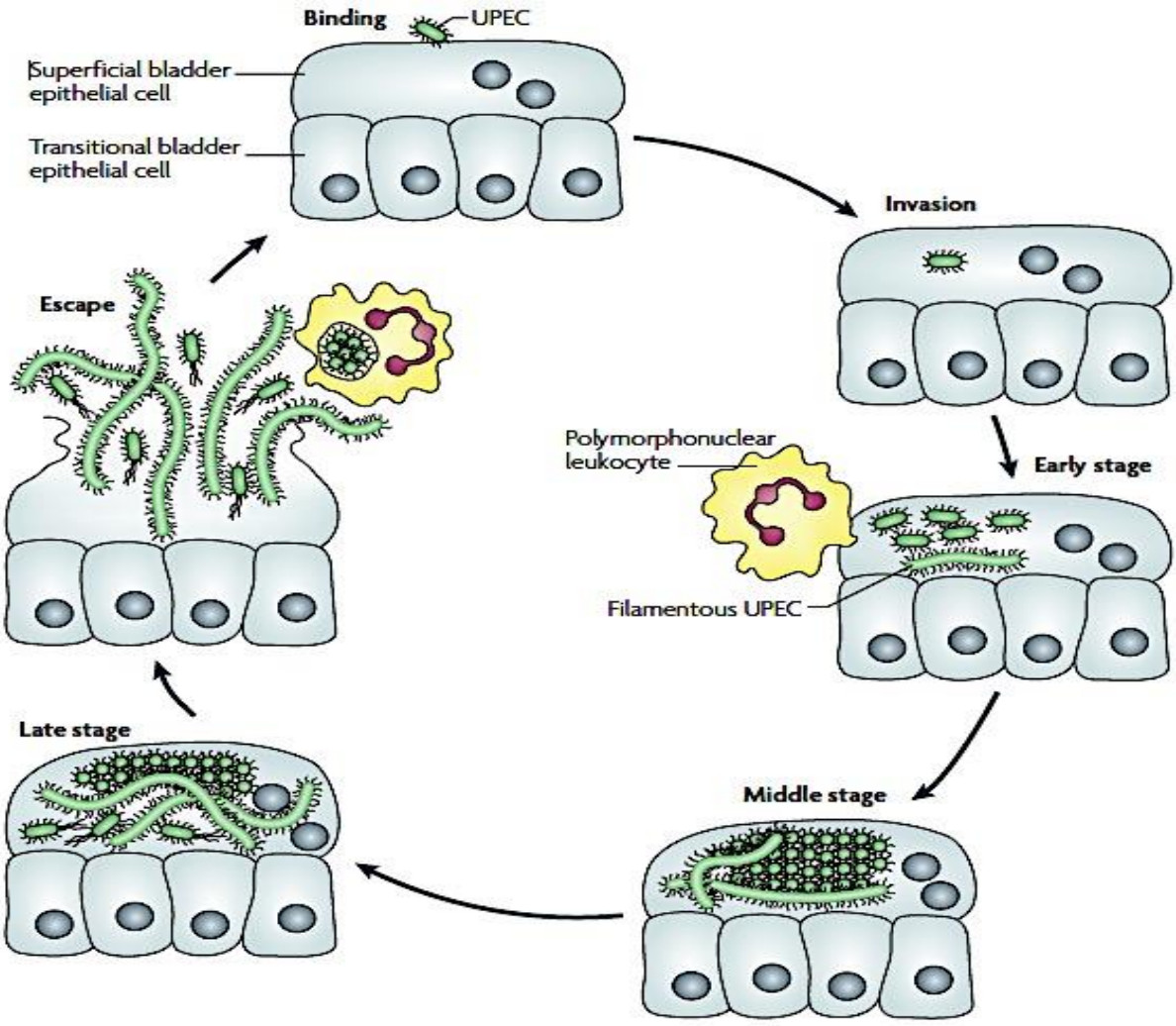

Figure 1.1 Lifecycle of Uropathogenic Escherichia coli (UPEC) causing urinary tract infections.
UPEC can bind to and invade the bladder epithelial cells (BECs) using type I pili. The early-stage denotes when the average length of UPEC is 3 µm and the formation of intracellular bacterial communities (IBCs). During the middle stage, the length of bacteria decreases to 1 µm and the IBC is more compact. In the late stage, the bacteria will grow back to their normal length of 3 µm. The escape stage sees filamentous bacteria detach from the IBC and attach to new BECs thereby facilitating the cycle to continue. Image taken from Justice et al.[14].

1.1.1.1 Bacterial Attachment and Invasion of Host cells

Critical to UPEC being capable to cause infection is its adherence to the host cells. This is mediated through filamentous adhesive organelles called type 1 pili which are the most common type amongst UPEC.[26] Type 1 pili can increase the virulence of *E. coli* by promoting bacterial persistence in the kidneys and bladder and induce an inflammatory

host response to infection.[27] The pili contain adhesin molecule, FimH, that binds to uroplakins (UPIa and UPIb), receptors that are found on the bladder luminal surface.[28] It has also been shown that FimH adhesin stimulates host cell signalling cascades to cause cytoskeletal rearrangements to internalise UPEC that has adhered to the cell surface through Type 1 pili mediation.[29] The invasion of bacteria into the epithelial cells is important to decrease the chances of the bacteria being cleared from the bladder by the increase in urine flow or addition of antibiotics such as gentamicin.[30]

Upon the attachment of UPEC to UPIa, the host recognises the bacterial lipopolysaccharide (LPS) via the Toll-like receptor 4 (TLR-4)-CD14 pathways and this leads to an influx of neutrophils into the bladder.[31] Another form of innate host defence is the exfoliation of infected or damaged bladder epithelial cells causing superficial epithelial cells to be shed into the urine and removed from the bladder. Mulvey, et al.[32] found that the clearing of bacteria through exfoliation implicated a caspase-mediated apoptosis-like mechanism shedding of epithelial cells in response to bladder infections. UPECs ability to overcome this exfoliation response is crucial to the persistence of infection.

1.1.1.2 Intracellular Bacterial Communities

Once contained within the host cell UPEC undergoes rapid replication and forms tightly associated bacterial clusters known as intracellular bacterial communities (IBCs) which occurs at 6 to 24 hours post-infection.[33] IBCs are usually globular in shape with tightly packed coccoid bacteria that eventually occupy most of the cytoplasm of the epithelial cell.[33] Justice, et al.[10] and Anderson, et al.[11] described three distinct phases of IBC formation: early, middle and late. Early IBCs occurs right after the binding and invasion of bladder cells (1 to 3 hours post-infection). The bacterial cells are normal rod-shaped and may be loosely associated at this point. Middle IBCs, between 6 - 8 h post-infection, the bacteria begin to form organised colonies with biofilm-like traits. During middle IBCs the bacterial cells reduce their length by half to become coccoid in shape.[34] Finally, late IBCs from 12 h post-infection saw the coccoid bacteria differentiate into normal rod-shaped bacteria and filamentous bacteria. It is hypothesised that bacterial cells may differentiate into filaments to help in the efflux of bacteria from the epithelial cells.[17]

Although these changes in morphology were observed it is still unknown what mechanisms cause these changes in shape or why UPEC undergoes these changes.

Andersen, et al.[31] performed freeze-fracture electron microscopy to have a more detailed look at UPEC within the bladder cells. It was found that the bacteria were organised in a polysaccharide-matrix which suggested that UPEC formed biofilms within the epithelial cells. This was an advantage for the bacteria as it made them more resistant to antibiotics, host defences and could lead to recurrent infections.[31] In addition to secreting a polysaccharide matrix IBCs are known to express surface proteins including type 1 pili, antigen 43.[10,31] Furthermore, there are a few genes that are essential for IBCs formation such as *surA* and *leuX*.[10,35] SurA is involved in folding extracytoplasmic proteins and has been shown to be essential for bacterial survival during stationary phase.[36,37] LeuX is a leucine tRNAs and tRNAs are required as adaptors to aide in synthesising proteins from mRNAs.[38] Justice, et al.[39] found that UTI89 *surA::kan* was deficient in binding and invasion of bladder cells and also was essential for bacteria to be able to progress into mature IBCs (Figure 1.2). Additionally, Hannan, et al.[40] found that a *leuX* mutation reduced UPECs ability to invade the bladder cell wall and its ability to form IBCs. It is thought that *leuX* is regulated by stress factor RpoH[41] and that it is necessary for the normal expression of iron scavenging effectors.[42] Therefore, LeuX may be necessary for bacterial stress responses in the urinary tract environment.

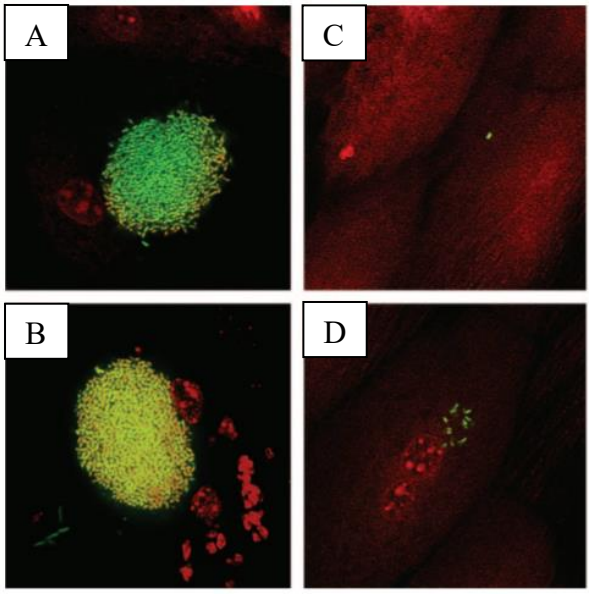

Figure 1.2 SurA is required for IBC maturation.
A) UTI89 at 6 h post-infection has formed an early IBC. B) UTI89 at 16 h post-infection has formed a mature IBC that consists of tightly packed coccoid bacteria. C) UTI89

surA:kan mutant is unable to form IBC at 6 h. D) At 16 h UTI89 surA:kan consists of 20 intracellular bacteria in 1 of 20 bladders infected. Taken from Justice, et al.[39].

1.1.1.3 Dispersal of UPEC and Filamentation

After IBC maturation at approximately 24 h post-infection it is thought that the bacterial load overwhelms the bladder cell (Figure 1.3A). As these infected epithelial cells erupt it may be possible that the compromised membrane integrity allows for the motile bacteria and filamentous bacteria to escape by protruding out of these epithelial cells (Figure 1.3B).[17] UPEC filaments after dispersal were observed to have partly assembled divisomes formed along the length of the cell (Figure 1.3C).[11] This suggested that cell division was blocked at an early stage of division before the constriction of the cell membrane. However, there are limited data to support this conclusion and more studies relating specifically to Z-ring formation in UPEC needs to be done. The processes of cell division and filamentation will be summarised below in *Sections 1.4* and *1.5*.

It was noted by Justice, et al.[10] that the eruption of IBCs during this late stage was not synchronous. It remains unknown what cues the bladder cells to erupt and release the bacteria. However, once UPEC had escaped from the infected bladder cells it spilled on to neighbouring cells to re-initiate another infection cycle (Figure 1.3D). The cycle of UPEC infection was demonstrated by the presence of small groups of UPEC in nearby infected bladder epithelial cells.[10]

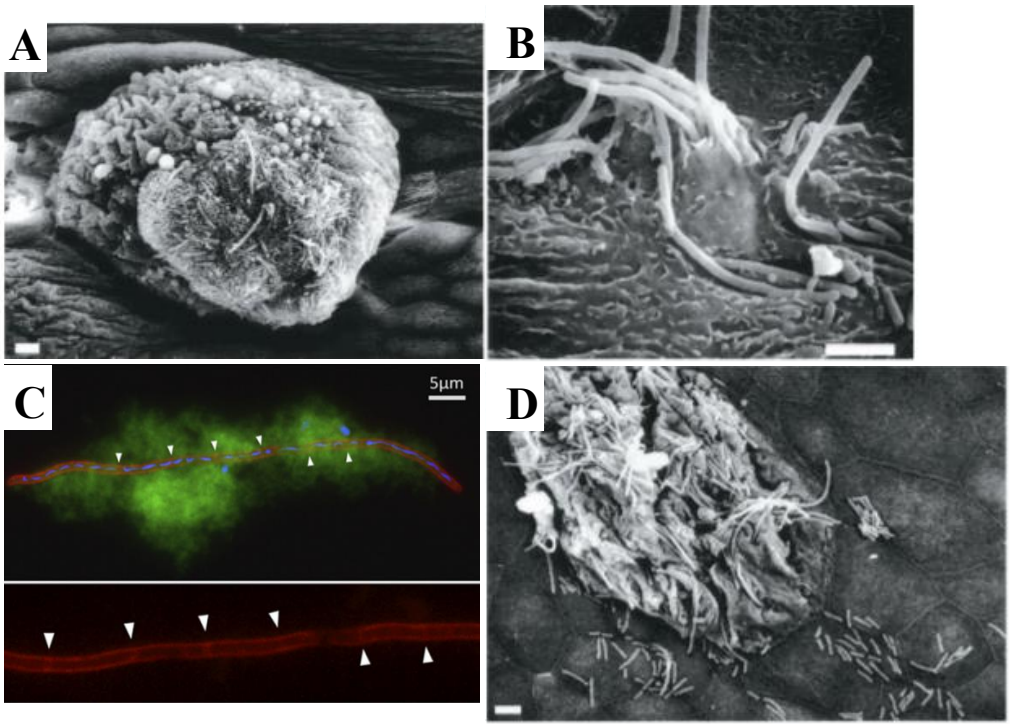

Figure 1.3 Scanning electron mircographs of UPEC escaping from bladder epithelial cells and fluorescence microscopy of UPEC filamentation.
A) Six hours after infection with UPEC the superficial bladder cell layer is undergoing exfoliation. B & D) The bacteria appear to be escaping the bladder cell and are spilling onto neighbouring bladder cells and they have differing morphologies from normal rod-shaped bacteria to filaments. C) A UPEC filament harvested from secondary in vitro infection. The membrane and DNA are stained with FM4-64 and DAPI respectively. The biofilm from infection can be visualised by the autofluorescence in the green channel. Partial cell division septa are indicated by arrowheads. Images taken from Berry, et al.[33] *and Andersen, et al.*[11].

For UPEC filaments to reinvade new epithelial cells, they must be able to revert to their normal rod-shape. Reversal of filamentation has been observed *in vivo* and *in vitro*.[10,11] Even filaments that were longer than 100 µm were capable of reversing into high numbers of single short rods.[11] This process usually occurred in two steps where 100 µm filaments became filaments of about 20 µm long after 1 hour. Then after another 3 hours, these filaments divided into normal rod-shaped bacteria (Figure 1.4).[11]

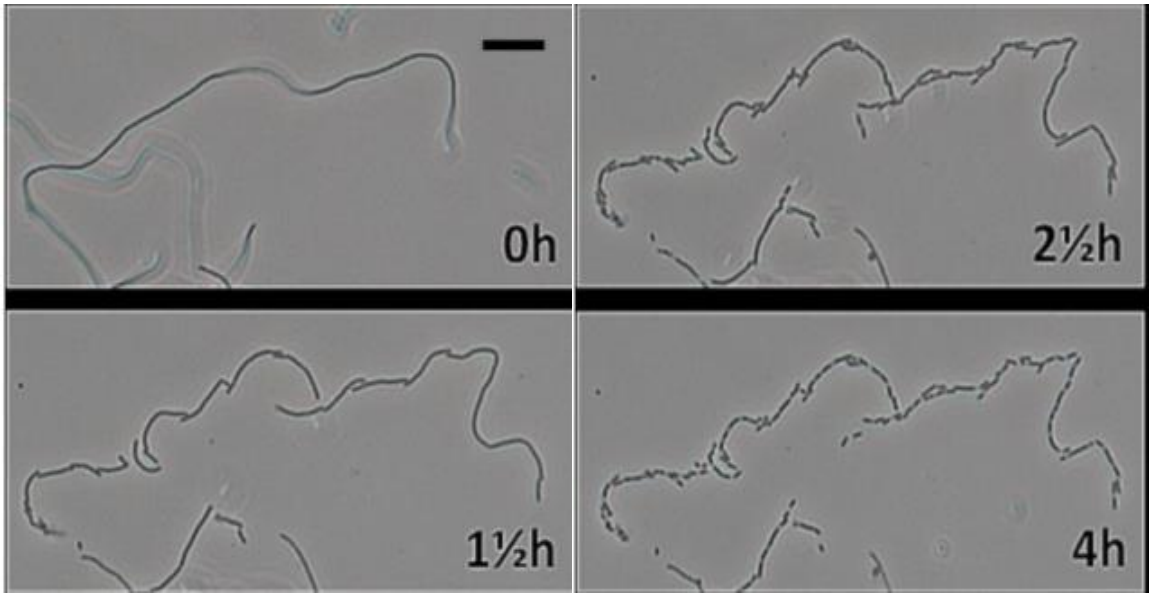

***Figure 1.4 Reversal of a UPEC filament over the course of 4 hours. Scale bar = 20* μm. *Taken from Andersen, et al.*[11].**

The exact mechanism that enables UPEC filament reversal is not understood. However, this thesis will examine how the *cedA* gene may have a role UPECs ability to undergo this process as it has already been shown to prevent filamentation of a DnaA mutant (*Section 1.6*). To understand what is known about CedA and the DnaA mutant and how this might help to unravel CedAs role in UTIs, the bacterial cell cycle will be discussed below. In particular chromosomal replication as DnaA initiates at the origin of replication on the chromosome (*Section 1.3*). Also, cell division and the mechanisms that regulate it will be discussed in detail (*Section 1.4*).

1.2 The Bacterial Cell Cycle

The bacterial cell cycle involves the replication of chromosomal DNA, growth of the cell and then the formation of the septum at mid-cell for the division into two identical daughter cells.[43] When the final stage, cell division, does not occur this results in filaments as seen in the UPEC lifecycle.

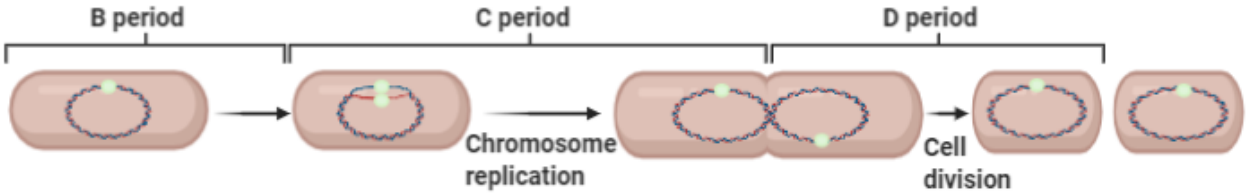

Figure 1.5 Overview of the bacterial cell cycle containing three phases: B, C and D. *Period B is the time from the birth of the cell to chromosomal replication. The C period is the time for replication to occur. The D period is the time for the completion of chromosomal replication to the end of cell division. The green circles mark the origin of replication. Image adapted from Wang and Levin.*[44]

The bacterial cell cycle consists of three different periods, termed the B, C and D (Figure 1.5).[44] The first period, B, is the time between cell division and chromosomal replication.[44] This is followed by the C period, the time it takes for chromosomal replication to occur.[44] In this period, *E. coli* replication of the single circular chromosome starts at a specific site called the origin of replication (*ori*C) and occurs bidirectionally.[45] Chromosomal replication itself goes through three stages: initiation, elongation, and termination.[46] Initiation starts with the binding of a protein DnaA to the *ori*C and the formation of a nucleoprotein complex.[47] During elongation, *E. coli* replication forks move along the chromosome at approximately 1kb/s.[48] Termination transpires in a region opposite to the *ori*C[49] when the forks reach one another in the circular chromosome and fuse, resulting in two complete chromosomes.[50]

After the termination of chromosomal replication, the final period of the bacterial cell cycle, is the D period. This is the time from when chromosomal replication ends to when the cell division is complete.[44] Filamentation, as seen in UPECs lifecycle is the result of ceased cell division during cell growth. It is, therefore, also important to understand how cell division occurs normally and its mechanisms for regulation. *cedA* was discovered as a multicopy suppressor of a mutation in the initiation of chromosome replication. In order

to understand how CedA does this, it is essential to understand the events that surround the initiation of chromosome replication, and this will be described further below.

1.3 Chromosomal Replication

CedA is thought to be able to reverse or prevent filamentation that is caused by a mutant protein that interferes with normal initiation of chromosomal replication. A previous study observed that the lethal effects of a mutant allele of the key regulator of chromosome replication DnaA, called *dnaA(cos),* was suppressed by an oversupply of *cedA.*[15] This suggests that CedA may also play a role in the filament-reversal mechanism in UPEC. Therefore, understanding the relevant aspects of the control of bacterial chromosomal replication is essential to understanding the function of CedA and its potential filament-reversal mechanism in UPEC.

Chromosomal replication involves the unwinding of DNA, starting at a site on the chromosome called the origin, *oriC*, to reveal two parental strands as templates for the synthesis of the two daughter strands using complementary base pairing. Chromosome replication in *E. coli* is initiated with the binding of key protein DnaA to the *ori*C in its ATP-bound active form.[51] The interaction between *ori*C and the DnaA protein leads to a local unwinding of the AT-rich region commanding the recruitment of the replisome proteins and formation of the replication fork (Figure 1.6).[52–54]

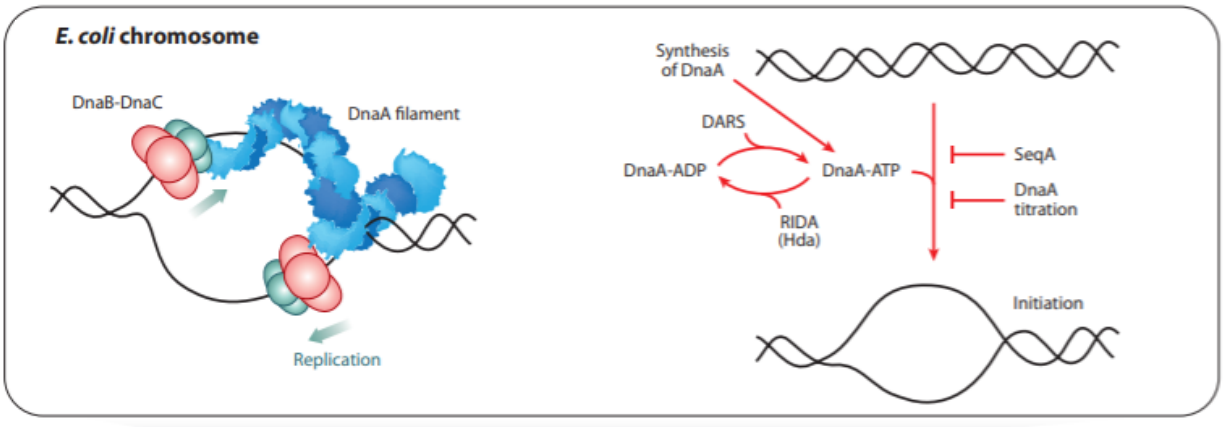

Figure 1.6 The initiation of chromosomal replication in E. coli.
A key step is the loading of the two helicases for bidirectional replication by DnaC at the origin of replication, which is unwound by ATP-bound DnaA. This is followed by the formation of the replisome. The image on the right shows the processes that control the levels of DnaA-ATP. Regulatory inactivation of DnaA (RIDA) can decrease the concentration of DnaA-ATP in the cell. While DnaA-reactivation sequences (DARS) increased the concentration of DnaA-ATP in the cell. Image taken from Reyes et al.[46].

Replication is closely regulated at the stage of initiation.[45] There are numerous mechanisms in place to ensure that chromosome replication only occurs once per cell cycle. This is important as cells with incomplete chromosome content or multiple copies of chromosomes can malfunction and die.

1.3.1 Mechanisms for the Regulation of Chromosomal Replication

The regulation of chromosomal replication is vital in controlling the amount of DNA being synthesised. This allows for the coordination of replication with the other stages of the cell cycle.[46] The most direct form of regulation is through the control of the levels of ATP bound to DnaA (DnaA-ATP), the initiator in the cell.[55] Only DnaA-ATP is able to initiate DNA replication and it is at low concentrations in the cell at all times except for during initiation.[51] After initiation, DnaA-ATP is converted to DnaA-ADP, an inactivated form of the complex, in a process known as the Regulatory Inactivation of DnaA (RIDA) (Figure 1.6).[53,56] The RIDA system involves elements of the replisome; the β-sliding clamp of DNA polymerase III and the Hda protein.[57] Kato and Katayama[56] showed that the Hda protein catalyses the conversion of ATP-DnaA to ADP-DnaA is a form of negative regulation. Furthermore, this form of the protein inhibits the over-initiation of replication, i.e. multiple initiation events at *oriC* per cell cycle.[56] On the other hand, before initiation, the binding of DnaA-ADP to DnaA-reactivation sequences (DARS) promotes the accumulation of DnaA-ATP which is needed for a new round of initiation of replication (Figure 1.6).[58]

Hda ("homolog of DnaA") is important to the RIDA system and like DnaA, is a protein from the AAA^+ type ATPase family and they have structural homology.[56] Kato and Katayama[56] demonstrated that Hda acts as a mediator between DnaA and the β-subunit of the sliding clamp. This is to promote the hydrolysis of ATP-DnaA which is vital for the RIDA system and the regulation of the initiation of chromosome replication. They were able to show that in the absence of Hda, DnaA was present in excessive amounts and over-initiation of replication was observed.[56]

Another form of DnaA regulation has been observed through the number of chromosomal *datA* sites present.[59] This site contains binding sites for DnaA and they contribute to the

inactivation of the protein's function at *oriC*.[59] Through a study that involved the oversupply of *datA* sites on a plasmid, Morigen, et al.[59] found that this led to a delay in initiation of replication and a block in cell division, thus making a connection between the two processes. It has also been shown that in the absence of *datA* over-initiation of replication occurs.[60] *datA* was first thought to ensure that excess DnaA is reduced therefore there is a restriction of the amount of DnaA that can bind to the *oriC*,[56] but recent research has suggested that this locus cooperates with the RIDA mechanism to help inactivate DnaA after initiation of replication.[61]

Another mechanism of regulation of replication initiation is through the protein SeqA and the functional sequestration of the *ori*C regions.[53,56] SeqA ensures that another round of replication does not occur immediately.[47] This was possible because when replication occurs it synthesises hemi-methylated GATC sites around *oriC* that bind SeqA.[62] It was observed that when SeqA was present the frequency of DnaA binding to the *oriC* decreased.[62]

Understanding the mechanisms that allow for the control of replication is important, as this study uses a mutant of DnaA, *dnaA(cos),* that is able to overcome this regulation and cause over-initiation of replication.

1.3.2 DnaA(cos)

Katayama and Kornberg[63] showed that a mutant allele of *dnaA*, called *dnaA(cos),* caused multiple initiations at *ori*C per cell cycle when the cells were grown at 30°C, a phenomenon termed "over-replication". It was also found that cell division was inhibited and bacterial filaments form under these conditions with the cells eventually dying. When grown at 42°C, however, the strain appeared normal with respect to the frequency of DNA replication and cell division. Thus, the strain was considered "cold-sensitive" owing to its defects in replication and survival at 30°C.[64] Felczak and Kaguni[65] suggested that at 30°C, the *dnaA(cos)* mutant is resistant to the normal regulatory mechanisms that limit initiation to once per cell cycle, although the precise details of the mechanisms underlying the *dnaA(cos)* mutant phenotype are not fully understood. At 42°C, the DnaA(cos) mutant

protein itself is less stable, so the mutations do not have an effect at this temperature and replication can occur as normal.[66,67]

To this day the mechanism that allows *dnaA(cos)* to cause filamentation is unknown and has only been casually linked to its role in hyper-initiation of chromosome replication. The cause of filamentation in *dnaA(cos)* is thought to be the result of fork collisions from the hyper-initiation of replication.[68] However, Katayama, et al.[15] first reported that *dnaA(cos)* causes filamentation in an SOS-independent manner. The SOS response is a process of DNA damage repair that requires RecA for the induction of downstream genes such as *sulA,* the process will be discussed further in detail in *Section 1.5*. Katayama, et al.[15] stated *dnaA(co*s) filamentation was SulA independent, as when a *sulA* mutation was introduced in the *dnaA(cos)* strain filaments still formed. They then went on to state that the same results were experienced with a *recA* mutant (to inactivate the whole SOS response) also with no data shown. Unfortunately, there are no other studies that attempt to show this result or attempt to determine whether filamentation caused by *dnaA(cos)* is SOS-dependent or independent.

Four point mutations in *dnaA(cos)* in comparison to *dnaA* have been identified; Q156L, A184V, H252Y, and Y271H. These mutations make the effects of the DnaA(cos) protein dominant over wild-type *dnaA*.[69] but only at the lower temperature (30°C). Though only 2 mutations are needed to cause the hyper-initiation phenotype seen in DnaA(cos): A184V and Y271H. The Q156L and H252Y mutations alone do not appear to cause any of the *dnaA(cos)* specific phenotypes. More specifically, it was found in genetic assays that the A184V mutation is dominant at 30°C and not at 42°C, causes hyper-initiation because it is defective in ATP binding,[70] hence making DnaA(cos) temperature-sensitive.[66] Whereas, the Y271H or Q156L mutation stabilises replication at 42°C and hence it is able to suppress the temperature-sensitive phenotype of A184V. When A184V mutation was combined with Y271H the hyper-initiation phenotype was observed at both temperatures.[66]

In addition to causing over-initiation, *dnaA(cos)* leads to filamentation and has previously been used as a model for studying this as described below in *Section 1.4*.

1.4 Bacterial Cell Division

Cell division in most bacteria occurs through binary fission.[71] Cell division begins with the selection of the division site, and the assembly of the FtsZ ring, which is anchored to the membrane and provides the foundation for the assembly of the divisome - the cell division apparatus.[72] The divisome constricts the cell, leading to septum formation, chromosome segregation, via the synthesis of cell wall material at the septum, and finally the splitting (hydrolysis) of the peptidoglycan cell wall to form two separate daughter cells (Figure 1.7).[72] When bacterial cell division does not occur due to a block in one of the stages, cells can continue to grow resulting in filamentation.[73] A critical stage where a block in cell division can occur to result in filamentation is at the assembly of a structure known as the "Z ring" made from FtsZ, as well as numerous other components.[74]

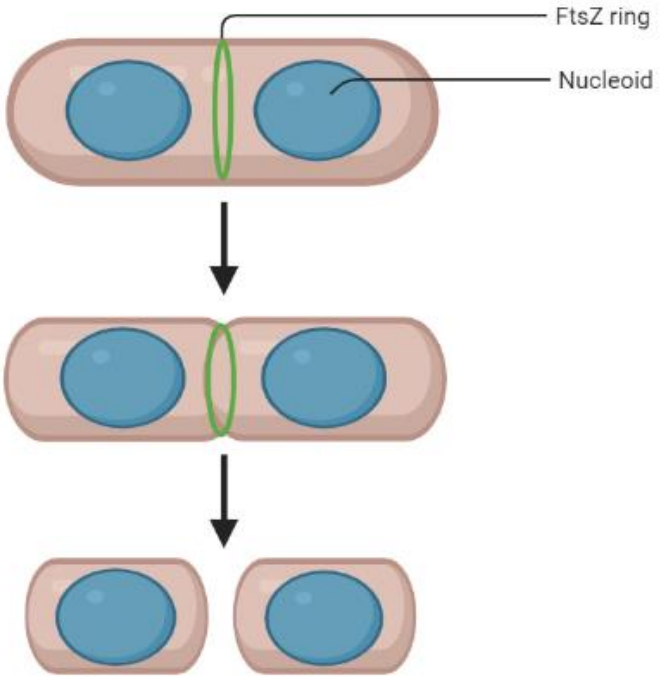

Figure* 1.7 *Cell division to form two daughter cells.
Once chromosomal replication is complete and the two nucleoids have separated the Z-ring is able to form at the mid-cell. The Z-ring begins to constrict to allow for cell division and the cell wall forms inwards following the ring constriction. Once complete cell division forms two identical daughter cells. Image adapted from Adams and Errington.[75]

1.4.1 Formation of the Z-ring

Bacterial cell division starts with the formation of the Z-ring at the mid-cell involving the assembly of its main component (FtsZ). FtsZ is a homologue of the eukaryotic protein tubulin, which forms the microtubule cytoskeleton.[76] The self-assembly of the Z-ring is the first step in cell division[74] and acts as a guide for the binding of the other important proteins involved in cell division, forming a complex known as the divisome at the mid-cell.[72,74,75] The assembly of the Z-ring is a key stage of successful cell division and it is therefore subject to tight regulation and control by several different mechanisms.

Z-ring formation relies on the polymerisation of the FtsZ protein.[77] This is dependent on the amount of FtsZ present in the cell. Also, the Z-ring must attach to the cell membrane at the division site, to provide the foundation for divisome assembly and later constriction of the cell membrane during division.[75] The Z-ring is attached to the membrane by two proteins ZipA and FtsA.[78,79] ZipA is imperative for the employment of other downstream proteins such as FtsK, which is furthermore needed for the recruitment of the other proteins in the divisome.[80] FtsA is related to the eukaryotic cytoskeleton protein actin.[81] FtsA anchors FtsZ to the inner surface of the cytoplasmic membrane via a membrane binding domain, and helps stabilise the Z-ring.[82]

FtsA and ZipA are important proteins to the stability of the Z-ring. Pichoff and Lutkenhaus[80] have demonstrated through the removal of either FtsA or ZipA that Z-rings remained stable. However, in the absence of both FtsA and ZipA, new Z-rings were unable to form and current Z-rings became unstable.[80] This suggests that both proteins contribute to stabilising the Z-ring structure. In the absence of both proteins elongated filaments formed with Z-rings in the correct position between the segregated nucleoids but were unable to divide.[75] Pichoff and Lutkenhaus[80] also showed that an FtsZ mutant, unable to interact with FtsA and ZipA, was unable to form Z rings, indicating that the interaction of FtsZ with either ZipA or FtsA is important to the formation of the Z-ring.

Other nonessential proteins involved in proper Z-ring formation are ZapA and ZapB.[79] ZapA interacts directly with FtsZ, and Gueiros-Filho and Losick[83] validated that in the absence of ZapA there were no obvious growth defects observed. However, in low

concentrations of FtsZ, cell division was dependent on ZapA.[83] This is because ZapA is able to stabilise FtsZ polymers and consequently aid in the formation of protofilaments for the Z-ring.[84] ZapB is a cell division factor that has only recently been characterised and is also important for the formation of Z-rings. In genetic studies, Ebersbach, et al.[85] found that the deletion of ZapB lead to cell elongation and imaging showed that the Z-rings that formed were not shaped like wild-type Z-rings. ZapB-GFP localised to the mid-cell and its dynamic localisation pattern depended on FtsZ, not FtsA or ZipA.[85] Nevertheless, ZapB still required functional FtsA or ZipA for the recruitment to the Z-ring.[85]

1.4.2 Regulators of Z-ring Assembly During Normal Cell Division

There are at least two known negative regulation systems and one known positive regulation system that helps to identify the mid-cell position for division, the Min protein system, nucleoid occlusion (NO) and the newer Ter-MatP system (Figure 1.8). Although these mechanisms of regulation are not directly involved in the mechanical function of the Z-ring constricting the cell during division, they are still crucial to the regulation of polymerisation of FtsZ, so that division occurs successfully.

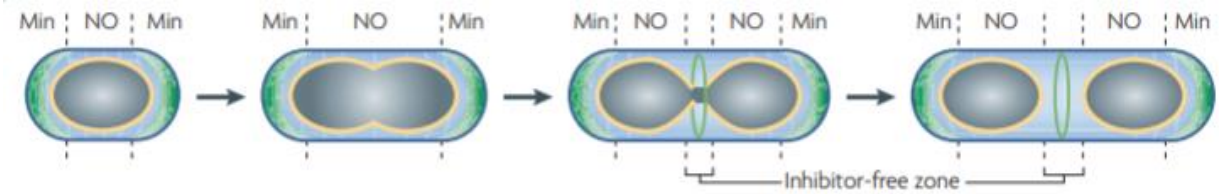

Figure 1.8 Spatial regulation of Z-ring assembly.
Nucleoid occlusion which is mediated by SlmA prevents the Z-ring from forming over or close to the nucleoids. The Min system inhibits the Z-ring from forming near the cell poles and it does this through oscillation. Image taken from Adams and Errington.[75]

The Min protein system oscillates from pole to pole, inhibiting the polymerisation of FtsZ near the cell poles,[86] and so indirectly promotes mid-cell assembly. It contains proteins MinC, MinD, and MinE. MinD is bound to the membrane, predominantly at the poles, and this process is ATP-dependent. MinD then recruits MinC, the inhibitor of FtsZ assembly.[87] MinE stimulates ATP hydrolysis by MinD[71,88] and is needed to concentrate the MinCD complex towards the pole. In a MinCDE mutant, polar division was seen (Figure 1.9), which gives rise to cell divisions that result in minicells.

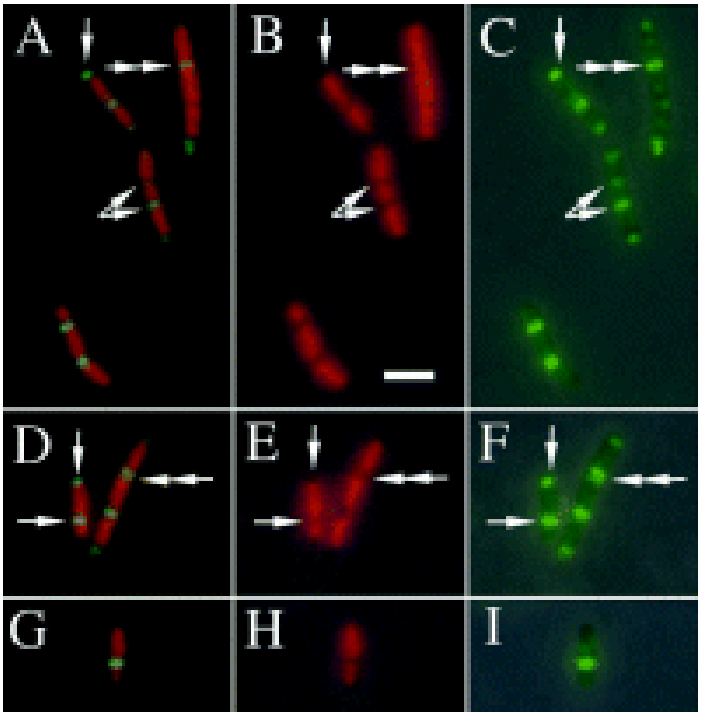

Figure 1.9 Fluorescence microscopy image of the localisation of FtsZ in the minCDE mutants.
A-C, D-F and G-I represent the different field of cells. G-I represent a cell with an off-centre Z-ring. The cells are stained with DAPI (red) and FtsZ staining (green). Arrows pointing down are FtsZ rings at the poles. Right pointing arrows are off-centre rings. Double right-pointing arrows are FtsZ rings that have unsegregated nucleoids, left-pointing arrows are FtsZ rings with different intensities. Image is taken from Yu, et al.[89].

Nucleoid occlusion is another negative regulatory system that ensures division occurs away from the nucleoid (DNA).[71] Mulder and Woldringh[90] proposed the NO mechanism when they used temperature-sensitive *E. coli* mutants and noticed that actively replicating nucleoids influenced the position of the division sites. Later studies revealed that the NO system involves a protein called SlmA, which associates with the DNA and directly interacts with FtsZ, preventing division over the chromosome.[91] Tonthat, et al.[92] later demonstrated that it is through SlmA binding to both DNA and FtsZ that it can prevent the formation of Z-ring over the nucleoid (Figure 1.10). Chromatin immunoprecipitation analyses showed that SlmA-binding sites (SBSs) are dispersed evenly along the chromosome except for the Ter region.[92] Therefore it is thought that with the help of the SBSs SlmA is able to bind FtsZ to prevent polymerisation and ultimately the formation the Z-ring.[93]

In the Ter-MatP system, the Ter macrodomain acts as a landmark for the Z-ring in the

presence of MatP ZapB, ZapA. Bailey, et al.[94] discovered that in the absence of MatP, ZapB or ZapA the positioning of the Z-ring was significantly affected. The four proteins work through the following process, ZapA interacts with FtsZ and links the Ter region to the Z-ring via ZapB.[94] ZapB then interacts with MatP to form a nucleoprotein complex with the Ter region.[95] Therefore, altogether these interactions help to stabilize and position the Z- ring.

It is possible that during a state of stress or damage, regulatory systems such as the Min System and nucleoid occlusion and Ter-MatP system (Figure 1.10) fail to continue normal cell division and this is when filamentation is most likely to occur. The different mechanisms that lead to filamentation will be discussed in the next section.

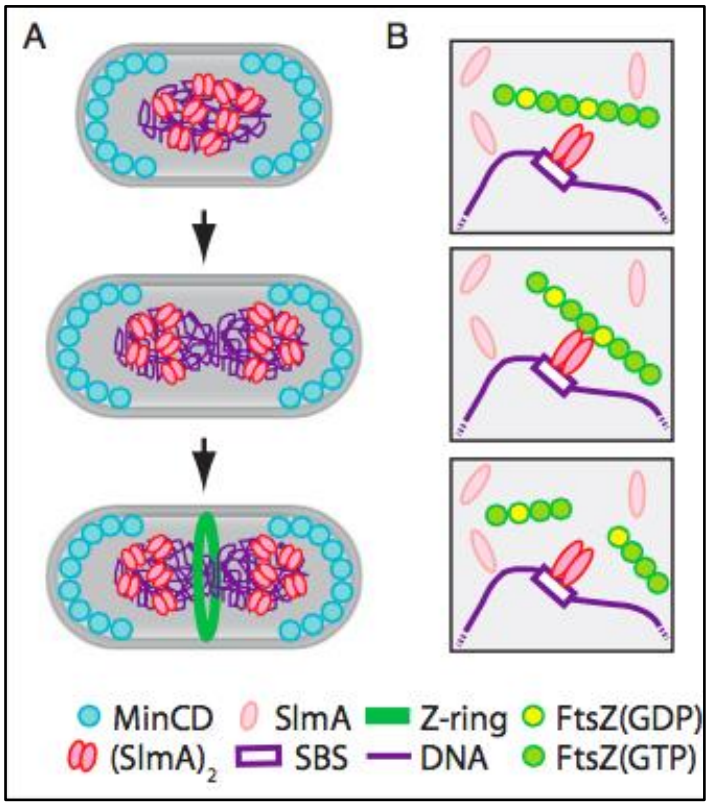

Figure* 1.10 *Proposed model of the interactions between SlmA, MinCD and FtsZ.
A) During cell development, the MinCD complex and SlmA ensure that the Z-ring does not form at the poles of the cells or over the nucleoid, respectively. SlmA binds to the SlmA-binding-sites (SBSs) in the regions that are near the origin. Overall, only the mid-cell is free from cell division inhibitors that allow the Z-ring to form. B) Monomers of SlmA in the cytoplasm are inactive. Once SlmA has bound to SBSs this stimulates the interaction between SlmA and FtsZ polymers. This leads to the breakdown of the polymers. Image is taken from Cho, et al.[93].

1.5 Mechanisms for Filamentation

There are numerous reasons for why transient filamentation could provide advantages for the cell.[14] It is thought to provide a selective advantage during stress, a response to restricted nutrient availability and inhibited metabolic pathways, and allows for the escape of the host's immune system.[14]

There is controversy surrounding the mechanism for filamentation during UTIs. The first filamentation response to be discovered was the result of the SOS response in the presence of the inhibitor SulA (Figure 1.11), whose expression is only induced during certain stress conditions in laboratory culture.[96] Evidence presented by Justice, et al.[14], suggested that SOS-mediated filamentation could be the mechanism that underlies the filamentation seen in UTIs. On the other hand Andersen, et al.[11] and Khandige, et al.[16] showed that filamentation occurs in the absence of SulA, suggesting that filamentation occurs via a non-SOS mechanism. Understanding the mechanism of filamentation is important in understanding the key stages of the infection cycle.

Bi and Lutkenhaus[97] studied the function of SulA by controlling its expression levels to determine the effect of its presence in the cell. They demonstrated that when SulA was expressed, cells would filament, and when its expression was suppressed, FtsZ was able to localise to the mid-cell and cell division occurred.[97,98] Naturally in the cell, SulA is suppressed by the Lon Protease which degrades SulA (Figure 1.11D) and allows cell division to proceed as normal.[99]

The SOS response is classically induced after DNA damage (Figure 1.11).[100,101] During this response, cell division is blocked, presumably to allow the cell time to repair damage and segregate the DNA before division. There are three distinct characteristics of the SOS response; (1) it is DNA damage inducible, (2) it requires *recA* and *lexA* genes (Figure 1.11) and (3) it requires *de novo* protein synthesis.[102] SulA, a key protein in the SOS response, is thought to inhibit the polymerisation of FtsZ, preventing the formation of the Z-rings, and blocking cell division.[75] In addition to SulA, RecA is also an important protein, which has been overlooked in many of the studies of SOS-induced filamentation. As well as being a part of the genetic regulation of the SOS response, RecA is directly

involved in DNA repair and stable DNA replication.[103] RecA is also the first protein expressed in response to DNA damage (Figure 1.11).[103]

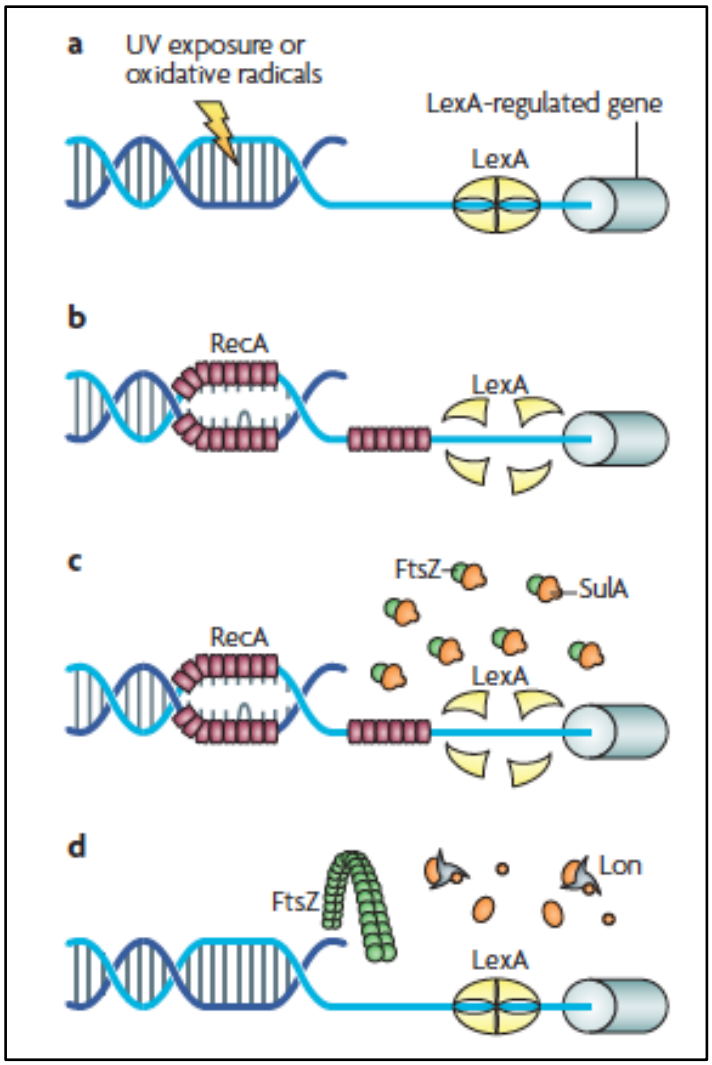

Figure 1.11 The SOS response.
A) showing the forms in which SOS response is induced i.e. through UV radiation or oxidative radicals which causes DNA damage. B) RecA, the inducer of the SOS response, is employed by the SOS response system to repair mismatched base pairs leading to single-stranded DNA. RecA is able to cause LexA, the repressor of the SOS response during non-stress conditions, to undergo an auto-cleavage reaction. C) SulA is able to prevent the transmission of mutant DNA to daughter cells by inhibiting the polymerization of FtsZ. D) once the amount of single stranded-DNA has decreased after DNA repair, RecA becomes inactive and new LexA represses the SOS response, the SOS response is inhibited and protease Lon degrades the remaining SulA so cell division can commence. Taken from Justice et al.[14].

One general proposal for why filamentation occurs in nature is due to the bacteria noticing a change in their environment causing them stress generally. Thus, UPEC might be forming filaments to provide itself with protection against stresses in the host's

environment, such as the immune responses.[14] UTIs have been studied in some detail using time-lapse video-microscopy[10] to help researchers understand UPEC interactions with the host's immune system, particularly with polymorphonuclear leukocytes (PMNs).[10] It became clear that when UPEC forms filaments it was able to evade killing by the PMNs (Figure 1.8). The PMNs are unable to phagocytise filamentous bacteria due to their size and it was this mechanism that allows the infection to persist (Figure 1.12E-H).[10]

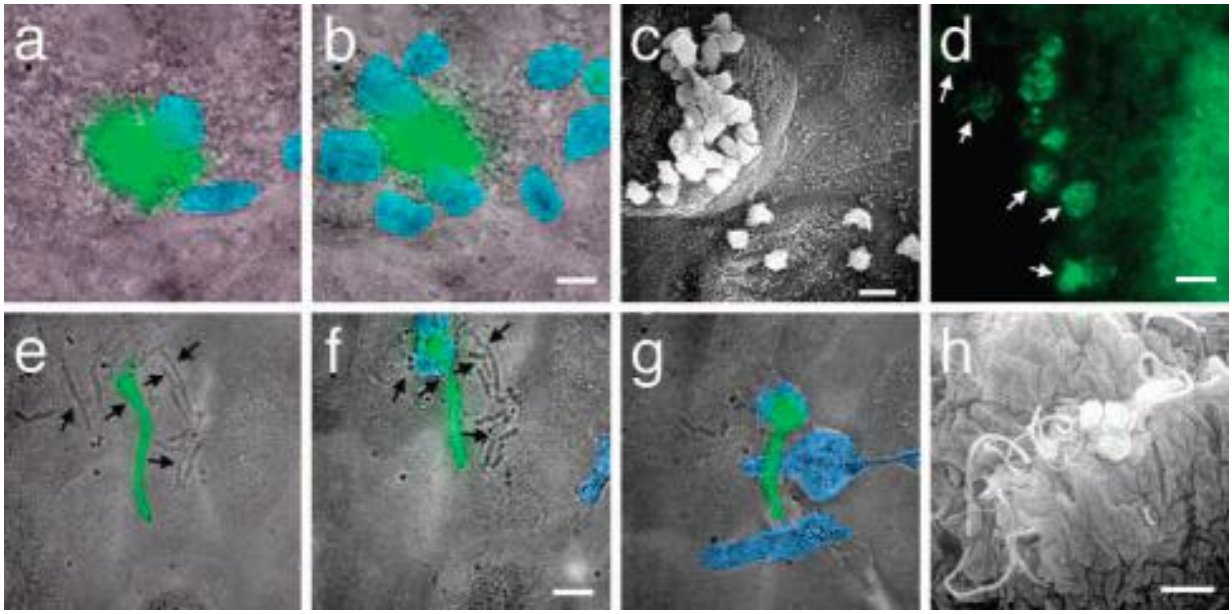

Figure 1.12 Fluorescence micrographs overlaid with transmitted light image showing UPEC being attacked by polymorphonuclear leukocytes (PMNs).
UPEC forms intracellular bacterial communities coloured green, which are protected against the PMNs (blue). A-B shows the PMNs trying to gain access to the IBC and finally consuming some of the community. E-H depicts the parts of the community that the PNMs are unable to consume i.e. the filaments. Image taken from Justice et al.[10].

In contrast to filamentation being caused by SulA, Andersen, et al.[11] constructed a SulA mutant in the UPEC strain, UTI89, to determine its degree of filamentation in their flow-chamber based culture system. Although the data was not shown it was reported that this mutant was able to filament to the same degree as the wild-type UTI89 suggesting that filamentation in this model was independent of the SOS response. Unfortunately, both studies by Justice, et al.[10] and Andersen, et al.[11] failed to test a *recA* mutant in UTI89. Since it is known that a cell division inhibitor, *sfiC*, which is independent of *sulA* is also induced during SOS, it is necessary to inactivate the SOS response completely by *recA* inactivation.[96] These experiments were also performed in our lab by a previous PhD

candidate, Greg Iosifidis[104] and it was found that the UTI89Δ*recA* strain was unable to grow inside the bladder cells compared to wild-type due to the sick nature of the cells and therefore the results from this experiment were inconclusive. Additionally, it was shown that UTI89Δ*sulA* was able to filament *in vitro*.

Andersen, et al.[11] also used their *in vitro* infection system to show that with urine of differing concentrations (from mildly dehydrated donors), the degree of filamentation also varied (Figure 1.13A-E). More recently, this system has been used to study the cause of UPEC filamentation further. Khandige, et al.[16] observed no filamentation in the UTI89Δ*damX* strain. DamX has been characterised as a gene that localises to the septal ring and has been shown to interact with other cell division proteins.[105] They also concluded that even though UTI89Δ*damX* could establish infection of bladders in the murine model, there were fewer IBC caused by this strain. Therefore, DamX is needed in order to cause a strong UTI and is essential to the filamentation response in UTI. This suggests that an SOS-independent mechanism of filamentation occurs in UTI.

Additionally, it was suggested by Anderson, et al.[11] that longer bacteria such as filaments would exhibit increased adhesion through increased contact points to the epithelial cells. This would be advantageous to UPEC as it would make it tougher to be cleared by phagocytes [25] and it would allow the bacteria to resist urine shear forces.[11] To support this Anderson, et al.[11] observed that filaments emerging from bladder epithelial cells were tightly associated (Figure 1.13F). They were also able to demonstrate the filaments from the infected cells were coated in type I pili (Figure 1.13G). Further work needs to be performed on the role of type I pili and FimH in later stages of infection such as dispersal filaments in order to understand the significance of this to the infection cycle.

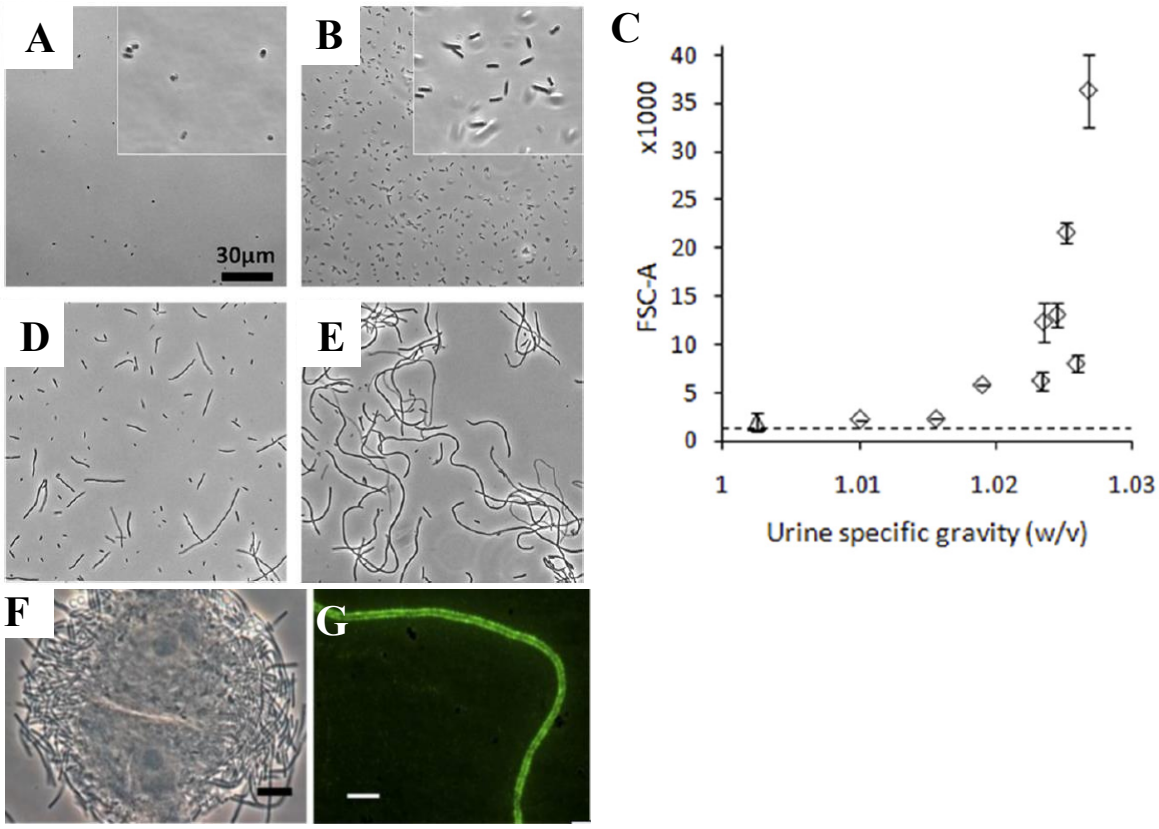

Figure 1.13 Induced secondary infection showcasing UPEC filamentation.
A) Phase-contrast microscopy of secondary infection in moderately concentrated urine. B) Filamentation in highly concentrated urine was 100%. C) Increase in urine concentrations (10 different concentrations) leads to increased filamentation of E. coli. On the y-axis is forward scatter (FSC-A) displayed as a function of the area otherwise considered as a relative measure of the size of the bacteria. On the x-axis is urine specific gravity which is a measure of the density of the urine to give a measurement for the urine concentration. D&E) Phase-contrast images of UTI89 grown in different concentrations of urine from 1.0025-1.0268g/L. F) Filament harvest from PDO7i showing tightly associated filaments. G) Fluorescence microscopy showing type I pili on a filament. Scale bars on H and I are 10 µM. Taken from Andersen, et al.[11].

Understanding the filament reversal mechanism is important to gain a holistic comprehension of how UPEC cause infection and is expected to be essential for ongoing infection. This aspect of UTIs has not been studied extensively, however, as mentioned in Section 1.1.1.3 Andersen, et al.[11] observed the reversal of filaments (longer than 100 µm) over time, as seen in Figure 1.14. Nothing is known about the mechanism regulating the re-initiation of division in filaments; this gap in knowledge is to be addressed in this thesis.

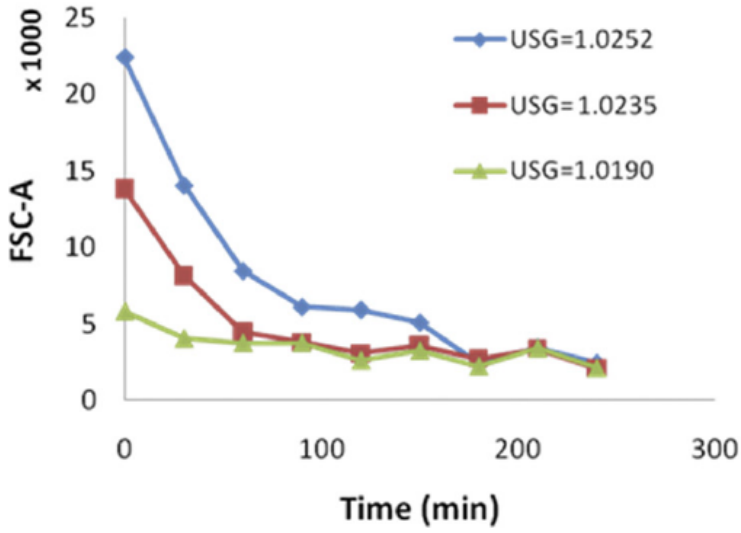

Figure 1.14 Graph of filament reversal in UTI89 to rod-shaped bacteria starting with three different degrees of filamentation.
The bacteria were grown in the presence of different urine concentrations and harvested after the secondary infection to measure the bacteria's efficiency in filament reversal. On the y-axis is forward scatter (FSC-A) displayed as a function of the area otherwise considered as a relative measure of the size of the bacteria. Image is taken from Andersen, et al.[11].

1.6 The *cedA* Gene

Katayama, et al.[15] discovered *cedA* ("cell division activator") as a multicopy suppressor of filamentation and lethality at 30 °C in the *dnaA(cos)* mutant (Figure 1.15). It was found that DNA replication still over-replicated during the suppression of *cedA*-mediated filamentation, suggesting that *cedA* does not simply reverse the effects of the *dnaA(cos)* on chromosome replication. Therefore, it was concluded that *cedA* has a regulatory role in cell division. Yet how *cedA* is able to restore cell division is unknown. Two possible mechanisms were raised by Katayama, et al.[15]. Firstly, when there was over-replication of the chromosome *cedA* could still be functional but overwhelmed by a factor associated with over-replication that causes filamentation somehow, such that extra CedA needs to be supplied for the cells to divide.[15] Secondly, an over-replication of the chromosome might allow for the overexpression of a cell division inhibitor that is normally repressed by CedA. CedA oversupply is therefore needed, to neutralise the inhibitor and reinstate cell division.[15] It is possible that the SOS response is activated in response to over-replication in the *dnaA(cos)* strain. Katayama, et al.[15] also suggested that the *cedA*-linked pathway was a necessary step for septum formation during over-replication, however, there was no evidence of this from the data presented.

Figure 1.15 The prevention of dnaA(cos) mutant strain filamentation with the overexpression of cedA.
A) Cell morphology of parental strain KH5402-1 (not containing dnaA(cos) mutant). B) of dnaA(cos) mutant strain KA441. C) dnaA(cos) mutant strain with pMK11 plasmid which contains cedA. Image taken from Katayama, et al.[15].

A genomic study from Chen, et al.[12] focused on identifying the positive selection of genes in UPEC strains. They identified 29 genes that showed evidence of positive natural selection in UPEC strains. These 29 genes were involved in an array of processes such as DNA metabolism, cell surface structure, urinary tract infection and the attainment of nutrients.[12] *CedA* was identified as one of these positively selected genes in UPEC strains although its presence is not limited to UPEC. Additionally, Khandige, et al.[16] used

microarrays on different stages of the UPEC infection cycle to identify genes with differing transcription levels. They found *cedA* to be upregulated during the filamentation phase by 8-fold.[16]

Lee, et al.[106] isolated RNA polymerase from *E. coli* strain O157:H7 Sakai, a strain that has a genome with 1,600 more genes compared to K-12 *E. coli*. They determined through affinity isolation and mass spectrometry that CedA was 1 of 29 proteins identified to associate with RNA polymerase.[106] All of these proteins identified were encoded in the core genome of *E. coli* and not specific to the O157:H7 Sakai strain.

1.6.1 The Structure of CedA

CedA has no sequence homology to any well-characterised protein, however, it can be found in other Gram-negative enterobacteria such as *Shigella sp.* and *Salmonella sp.* Chen, et al.[107] studied the structure of CedA to provide clues about its function through structural homology. This discovered that CedA consists of four anti-parallel β-strands and one α-helix.[107] The structure of the CedA protein has homology to certain DNA-binding proteins involved in transcriptional regulation (Figure 1.16).

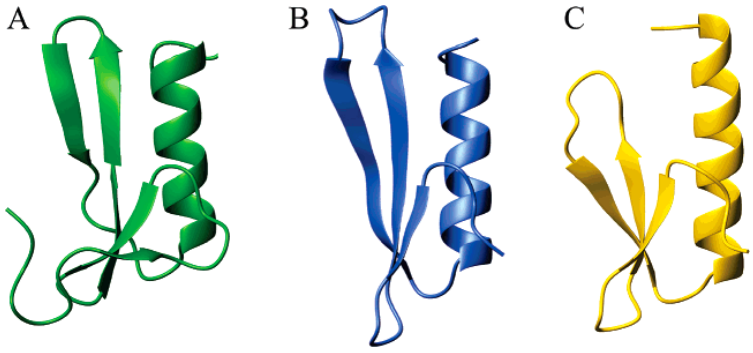

Figure 1.16 CedA has structural homology to DNA-binding proteins, for example, GBD and λ-INT-DBD.
A) 3D representation of CedA. B) 3D representation of GBD, which is a GCC box-binding domain of a transcription factor in Arabidopsis thalina. C) 3D representation of λ-INT-DBD. Image taken from Chen, et al.[107].

In order to test whether dsDNA is a ligand for CedA, Chen, et al.[107] undertook binding studies using gel-shift assays. The results suggested that CedA has a moderate, non-sequence specific affinity for dsDNA. Another characteristic proposed was the possibility

that CedA may be a transcription factor due to its structural homology to GCC box binding domain (GBD) in Figure 1.16.[107]

More recently, CedA was shown to interact with DNA through its N-terminus in non-specific and tight electrostatic binding.[108] CedA can also bind to DNA through sequence-specific weak hydrophobic interactions to its β-sheet.[84] Through *in vivo* experiments Abe, et al.[108] tested whether *cedA* mutants' repress filamentation in the *dnaA(cos)* strain. These mutants had amino-acid substitutions in its N-terminus, to inhibit the tight binding of CedA to DNA and RNA polymerase.[108] From growth assays of these mutants, all of the mutant strains experienced apparently normal reactivation of cell division. This suggested that is not CedA binding to DNA or RNA polymerase that causes reactivation of cell division. There were a few inconsistencies in the results presented by the pull-down assay and the *in vivo* experiment. In the *in vivo* experiment, the control strain with no amino-acid substitutions in the N-terminus did not have a complete population of filaments as it should have, and a low sampling number of cells made the results less convincing. These results should be considered preliminary until further analyses of the results are performed such as image analysis on more than just one field of view of the microscopy. Furthermore, there were additional protein bands in the RNA polymerase pull-down assay by Abe, et al.[108] that were unaccounted for. This might suggest that CedA is interacting with more proteins than just the RNA polymerase to reactivate cell division.

1.6.2 Possible CedA Binding Proteins

Sharma, et al.[109] demonstrated with pull-down assays and mass spectrophotometry that CedA interacts with proteins involved in transcription (RpoB, RplC, RplB and YbcJ), energy metabolism pathways (GlmS, Zwf and AceE) and cell cycle regulation (DnaK and LPP). It is known that pyruvate dehydrogenase complex E1 (AceE) converts pyruvate to acetyl-CoA and CO_2, and pyruvate is 1 of 12 precursor metabolites for the central carbon metabolism network.[110] Central carbon metabolism uses numerous enzymatic steps to convert sugars into metabolic precursors that are used to generate biomass of the cell, essentially governing the size of bacteria.[110] It is understood that increases in nutrient levels are followed by an increase in cell size and cell growth.[111] Zwf is an enzyme that catalyses the oxidation of glucose 6-phosphate to 6-phosphogluconolactone in the

pentose phosphate pathways which is a part of carbohydrate degradation. Sandoval, et al.[112] demonstrated that oxidative stress caused through tellurite increased transcriptional activation of *zwf* which lead to the increase in antioxidant molecules (NADPH and GSH). This decreased the amount of oxidized proteins and membrane lipids, therefore, protecting *E.coli* from oxidative stress.[112] CedA interacting with proteins involved in cell metabolism suggests that it may do so to control cell size during normal cell growth or even in stressful conditions.

CedA was also implicated in cell cycle regulation as it interacted with DnaK and Lpp. DnaK is a chaperone in protein folding, remodelling of protein complexes and protein disaggregation.[113] Unfortunately, it is known that DnaK interacts with approximately 700-1000 genes,[113] therefore, making it a very sticky protein for a pull-down assay and so this could be an unreliable interaction that needs to be tested further. Finally, CedA was found to interact with major outer membrane lipoprotein (Lpp). Lpp is required for maintaining the structural and functional integrity of the cell envelope. It is known that one-third of the protein is covalently linked to peptidoglycan and the remaining two-thirds is free form in the envelope.[114] Lpp could be required when CedA is necessary to prevent the filamentation that occurs when DnaA(cos) is overexpressed as mentioned previously. The interactions of all of these proteins with CedA still needs to be validated through *in vitro* and *in vivo* experiments.

Overall, CedAs interaction with these proteins may suggest that CedA could have a role in coupling cell division and chromosomal replication through energy metabolism by separately regulating each of these aspects of the cell. Whether CedA does this and how it is possible remains unknown and will be explored further in this thesis.

1.7 Aims and Objectives

UTIs are a widespread infectious disease that affects millions of women a year, leading to billions of dollars in expenses related to health care and employment.[3,4,6] As antibiotic resistance is set to rise in the coming years' attention is being turned to such infections where the means for treatment is becoming significantly challenging.[8] The most common causative agent for UTIs is UPEC, and as mentioned previously UPEC has many virulence factors that play a specific role in aiding its pathogenicity. As UPEC undergoes a multi-stage infection cycle a lot of research has been focused on how UPEC is able to establish an infection. Unfortunately, limited research has been conducted on the later stages of infection such as filamentation, dispersal and reversal. These stages would provide insight on how UPEC is able to maintain a persistent infection by re-invading nearby bladder epithelial cells. As mentioned previously it is thought that in order to re-invade healthy epithelial cells UPEC must be in its original normal rod shape. This would mean that the filaments that disperse from the infected bladder cells must undergo reversal.

Little is known about the mechanisms involved in the reversal of filamentation however *cedA* has been implicated to preventing filamentation in *dnaA(cos)* and is upregulated during the filament phase of UPECs infection cycle. The present PhD study raises the possibility that *cedA* is important and under strong selection in UPEC strains due to its potential requirement during the dispersal and/or reversal of filamentation response seen in UTI. Therefore, the work in this thesis aimed to understand the function of *cedA* in K-12 *E. coli* strain, BW25113 and UPEC cystitis isolate, UTI89.[17]

Therefore to address this aim the objectives of the thesis were:

1. To understand how *dnaA(cos)* can cause filamentation.

As *cedA* was originally identified as a multi-copy suppressor of *dnaA(cos)* **Chapter 3** aims to understand how *dnaA(cos)* can cause filamentation and therefore which pathway *cedA* is able to regulate. Five mutant strains of BW25113 were used, these were: BW25113Δ*recA,* BW25113Δ*slmA,* BW25113Δ*minC,* BW25113Δ*ymfM*Δ*sulA* and TB43

(BW25113Δ*minCDE)*. This chapter uses the overexpression of *dnaA(cos)* in these strains to determine which if any of these pathways (SOS response, Min System or Nucleoid occlusion) are needed to cause *dnaA(cos)* filamentation.

2. **To determine if *cedA* can prevent and/or reverse filamentation caused through other pathways in the cell.**

Chapter 4 aims to determine whether in addition to preventing *dnaA(cos)* filamentation, can *cedA* overexpression prevent filamentation caused through another pathway in the cell. The pathways that lead to filamentation under examination were metabolism (*zwf)*, inhibition of cell division (*ftsZ-yfp)*, SOS response (*recAtif)*, nucleoid occlusion (*slmA* and *slmA*-SBS) and UPEC filamentation. In addition to questioning whether cedA can prevent filamentation from occurring it was also examined whether *cedA* can reverse filaments that are pre-formed. Finally, this chapter explored the effect of *cedA* overexpression in wild type *E. coli*.

3. **To verify if *cedA* and *slmA* are required for the dispersal and reversal of UPEC during *in vitro* bladder epithelial cell infections, respectively.**

There is limited knowledge of the genes required for the dispersal and reversal of filaments during the UPEC infection cycle. Recently, in a TraDIS genetic screen performed by previous PhD candidate Daniel Mediati, *cedA* and *slmA* were identified to be required for dispersal and reversal respectively. Therefore, **Chapter 5** aims to verify these results using UTI89Δ*cedA* and UTI89Δ*slmA* during infection through competition assays with UTI89 in 6-well dished and single *in vitro* flow chamber infections. Both of these methods use human bladder cell culture line PDO7i and required concentrated human urine. Before the role of the *cedA* mutant was explored in infection it was characterised in standard laboratory conditions to provide insight on its phenotype and function through cell growth, cell volume, initiation of replication and FtsZ ring positioning and timing.

Chapter 2
General Materials and Methods

2.1 Bacterial Strains and Plasmids

Table 2.1 and 2.2 contain the list of *E. coli* strains and plasmids that were provided and used throughout this thesis. All other bacterial strains and plasmids that were created will be described where appropriate. *E. coli* strains were grown to stationary phase in an overnight culture and stored at -80°C in 16% (v/v) glycerol. Mammalian bladder cell line PDO7i was used for infection model.[11]

Table 2.1 General E. coli strains used during this thesis

***E. coli* Strain**	**Genotype**	**Source**
HC328 pHC534	*ΔslmA P sbs ::lacZ/pUC-2xSBS*	Cho and Bernhardt[115]
JM12	*F-, thr-1, araC14, leuB6(Am), Δ(gpt-proA)62, lacY1, tsx-33, qsr'-0, glnX44(AS)?, galK2(Oc), λ-, Rac-0, hisG4(Oc), rfbC1, recA441(ts), rpsL31(strR), kdgK51, xylA5, mtl-1, argE3(Oc), thiE1*	*E. coli* Genetic Stock Center (Yale University, USA).
JW1165-1	*ΔminC765::kan*	*E. coli* Genetic Stock Center (Yale University, USA).
JW1720-1	*ΔcedA730::kan*	*E. coli* Genetic Stock Center (Yale University, USA).
JW2669-1	*ΔrecA774::kan*	*E. coli* Genetic Stock Center (Yale University, USA).
JW5641-1	*ΔslmA747::kan*	*E. coli* Genetic Stock Center (Yale University, USA).
K-12 BW25113	Wild-type	Baba et al.[116]
K-12 BW25113Δ*ymfM*Δ*sulA*	*ΔsulAΔymfM::kan*	Ansari, et al.[117]
K-12 DH5α	*fhuA2 Δ(argF-lacZ)U169 phoA glnV44Δ(lacZ)M15 gyrA96 recA1 relA1 endA1 thi-1 hsdR17 F-ompT hsdSB(rB-, mB-) gal dcm araB::T7RNAP-tetA*	New England Biolabs (NEB).
TB28	*ΔLacIZYA <>frt*	Bernhardt and De Boer[91,118]
TB28 pTB67	P_{tac}*::slmA*	Bernhardt and De Boer[91]

TB43	TB28 *ΔminCDE <>frt*	Bernhardt and De Boer[91,118]
UTI89	Wild-type	Moller-Jensen, J.[17]
UTI89Δ*cedA*	Δ*cedA:kan*	D. Mediati (UTS)
UTI89Δ*slmA*	Δ*slmA:kan*	This work

Table 2.2 General plasmids used during this thesis

Plasmid	Purpose	Size (bp)	Selection	Source/Reference
pBAD24	Arabinose inducible expression	4500	AmpR	Moller-Jenson, J./ Guzman, et al[119]
pBAD24/*dnaA(cos)*	Arabinose inducible expression of *dnaA(cos)*	5904	AmpR	This work
pBAD24/*damX*	Arabinose inducible expression of *damX*	5778	AmpR	This work
pGI5	Constitutive expression of GFP	4547	SpecR	Iosifidis and Duggin[120]
pGI6	Constitutive expression of mCherry	4542	SpecR	This work
pLAU80	Arabinose inducible expression of *ftsZ-yfp*	6395	AmpR	J. Moller Jensen/ Lau et al.[121]
pTAB1	IPTG inducible expression	4503	CmR	This work
pTAB1/*zapB-gfp*	IPTG inducible expression of *zapB-gfp* to visualise Z-rings	5501	CmR	This work
pTAB2	Anhydrotetracycline inducible expression	3345	CmR	This work
pTAB2/*cedA*	Anhydrotetracycline inducible expression of *cedA*	3633	CmR	This work
pTAB2/Δ*18cedA*	Anhydrotetracycline inducible expression of a truncated *cedA* (first 18 amino acids of the protein removed)	3579	CmR	This work
pTAB2/*cedA-gfp*	Anhydrotetracycline inducible expression of *cedA* tagged with GFP on the C-terminus	4353	CmR	This work

2.2 Bacterial and Mammalian Growth Media

Bacterial growth media used in this thesis are listed in Table 2.3. All media underwent sterilisation in the autoclave.

Table 2.3 Bacterial and mammalian growth media

Growth Media	Composition[a,b]
Epilife Medium	Epilife, 10% (v/v) HKGS, 1% (v/v) PS. (Epilife composition is as stated in Epilife medium formulations sheet, Life Technologies, USA)
Luria-Bertani	1% tryptone, 0.5% yeast extract, 1% NaCl
M63	0.2% $(NH_4)_2SO_4$, 0.14% KH_2PO_4, 0.5 mg $FeSO_4.7H_2O$, 1 mM $MgSO_4.7H_2O$, 10 mL of 20% Maltose, 2 mL of 0.05% Vitamin B1 (thiamin).
Minimal-media M9	Composition as in Burke, et al.[122]. Carbon source was 0.4% glucose and 0.4% casamino acids.
SOB	2% peptone, 0.5% yeast extract, 10 mM NaCl, 2.5 mM KCl, 10 mM $MgCl_2$, 10 mM MgSO4 in MQW.
SOC	2% tryptone, 0.5% yeast extract, 10mM NaCl, 2.5mM KCl, 10mM $MgCl_2$, 20mM glucose.

[a] All percentages are given as (w/v) unless stated otherwise.

[b] Solid LB contains 1% (w/v) agar unless stated otherwise.

2.3 Chemicals, Solutions and Reagents

The list of manufacturers for chemicals and reagents is in Table 2.4. Commonly used buffers and solutions are listed in Table 2.5.

Table 2.4 General chemicals, reagents and solutions used in this thesis

Chemical	Source
Agarose	Bioline, Australia

Ampicillin	Sigma-Aldrich, USA
Anhydrotetracycline	Sigma-Aldrich, USA
Bacteriological Agar	Oxiod, Australia
Chloramphenicol	Sigma-Aldrich, USA
Chloroform	Bio-Strategy, Australia
Defined Trypsin Inhibitor (DTI)	Gibco, Life Technologies, USA
Difco LB Broth Base (Luria-Bertani)	Becton Dickinson, USA
DMSO	New England BioLabs, USA
Ethanol	Sigma-Aldrich, USA
Ethidium Bromide	Sigma-Aldrich, USA
Gel-Red	Biotium
Gentamicin sulfate	Sigma-Aldrich, USA
Glucose	Sigma-Aldrich, USA
Glycerol	Sigma-Aldrich, USA
Human Keratin Growth Supplement (HKGS)	Gibco, Life Technologies, USA
Kanamycin	Sigma-Aldrich, USA
Paraformaldehyde (PFA)	Sigma-Aldrich, USA
PBS tablets	Astral Scientific, Australia
Penicillin/Streptomycin (PS)	Life Technologies, USA
Phenol	Thermo Fisher, USA
Spectinomycin	Sigma-Aldrich, USA
Triton X-100	Sigma-Aldrich, USA
Trypsin-EDTA	Gibco, Life Technologies, USA
Tween 20	Sigma-Aldrich, USA

Table 2.5 List of aqueous buffers and solutions used during this thesis

Solution	**Composition[a]**
1x PBS	150 mM Potassium Phosphate, 50 mM Tris-Cl, pH 7.4
TBE	89 mM Tris, 89 mM Boric acid, 2.5 mM EDTA, pH 8.3

TAE	40 mM Tris, 20 mM Acetate,1 mM EDTA, pH 8.6
Lysis solution	0.5% trypsin-EDTA, 0.1% triton X-100.
Hoechst Staining Solution	20 mM Tris-Cl, 10 µg/mL RNAase A, 1 µg/mL Hoechst 33342
10% Paraformaldehyde	1 x PBS, 40g PFA powder, 1 M NaOH, pH adjust with HCl to 6.9
Solution 1 for RNA purification	10 mM NaCitrate, 10 mM NaAcetate pH 4.5, 2 mM EDTA
Solution 2 for RNA purification	10 mM NaAcetate pH 4.5, 2% SDS
Acidic phenol	100 mL Phenol, 3.33 mL 3 M NaAcetate, pH 4.5

[a] All percentages are given as (w/v) unless stated otherwise

2.4 General Growth Conditions for *E. coli*

To culture *E. coli,* scrapings from the -80°C glycerol stock was used to inoculate solid LB containing the appropriate antibiotics (Table 2.3) and was left to incubate for at least 16 h at 37°C. An individual colony was selected from the solid agar and used to inoculate liquid LB, M9, M63 or SOC growth media (Table 2.3) where appropriate and was incubated for at least 16 h at 37°C with 180 rpm.

2.4.1 Electrocompetent Preparation and Transformation of *E. coli*

After the growth of *E.coli* in liquid LB as stated above, the culture was diluted into 100 mL of fresh LB media and left to grow until mid-log phase (A_{600} = 0.4-0.6). The culture was left on ice for 20 mins and then centrifuged at 4000 rpm for 15 mins. The pellet was then resuspended in 25 mL of ice-cold milliQ water and centrifuged as before. This was repeated 4 more times with decreasing volumes of ice-cold water. After the final centrifugation, the pellet was resuspended in 500 µL ice-cold 10% glycerol (Table 2.4). Aliquots of 50 µL were then stored at -80°C.

For the electrocompetent transformation of *E. coli,* a single aliquot was thawed out on ice and then mixed with 20-50 ng of DNA. The mixture was added to an ice-cold 0.2mm electroporation cuvette (BioRad, USA) and electroporated using PowerPac Basic Eletroporator (BioRad, USA) as 25 μF (capacitance), 2.5 kV (voltage) and 200 ohm (resistance). Immediately after electroporation, 1 mL of SOC media (Table 2.3) was added to the cuvette and the transformation was transferred to a 1.5 mL Eppendorf tube and left to recover at 37°C for 1 h at 300 rpm. The cells were plated onto selective solid LB and incubated for at least 16 h at 37°C. Negative control was also performed and this contained competent *E. coli* cells without DNA and it was treated identically.

2.4.2 Chemically Competent Transformation of *E. coli*

For chemically competent transformations, an aliquot of ligation was mixed with an aliquot of chemically competent DH5α and was left on ice for 30 minutes. The cells were then heat shock[123] at 42°C for 1 minute and returned to ice for 2 mins. Then SOC (Table 2.1) was added and the cells were incubated at 37°C for 1 hour. The cells were then plated on LB plus antibiotics for selection and incubated overnight at 37°C. Negative controls were also run alongside where the DH5α cells did not contain DNA and they were treated the same.

2.5 General Mammalian Growth Conditions

Human bladder cell line PDO7i was regularly cultured at 37°C with 5% CO_2 to confluency in EpiLife medium with 60 mM calcium, supplemented with 1% Human Keratinocyte Growth Supplement (HKGS) and 1% Penicillin/Streptomycin (PS) (Table 2.4) as previously described.[33] The cells were cultured in T75 culture flasks and the media was changed every 2 days.

2.5.1 Splitting Mammalian Cells for Bladder Infection Model

To detach the bladder cells from the tissue culture flask the media was removed from the flask and 5 mL Trypsin-EDTA (0.5%) (Table 2.4) was added. The flask was left to

incubate at 37°C with 5% CO_2 for 10 mins and then it was gently tapped to release the bladder cells from the surface. A 1x Defined Trypsin Inhibitor (DTI) (Table 2.4) was added to the flask and the cell suspension was transferred to a 50 mL falcon tube for centrifugation at 1000 xg for 4 mins. The supernatant was removed and the cells were resuspended in 12 mL of PBS.

Then 100 uL of the cells were taken obtain a cell per millilitre count on the Coulter Counter (Beckman). The cells were centrifuged as stated and resuspended in EpiLife medium with no antibiotics to either a minimum of $1x10^5$ cells/mL for large scale infections and $3x10^6$ cells/mL for flow chamber infections.

2.6 General Methods and Protocols

A number of methods were used during this thesis and these are outlined below. Any changes that were made from the manufacturer's protocol are noted. More detailed methods can be found in the results chapters below.

2.6.1 Extraction of DNA from Bacteria

Plasmid and genomic DNA was purified from *E. coli* using Bioline Isolate II plasmid DNA kit and Bioline Isolate II genomic kit (Bioline, Australia). For the elution step the elution buffer was preheated to 70°C and 25 µL of the buffer was loaded onto the silica pad. The column was centrifuged following the protocol and this was repeated once more for a final volume of 50 µL. Concentrations of DNA was tested on the NanoDrop One spectrophotometer.

2.6.2 Polymerase Chain Reaction (PCR)

To amplify DNA, PCR was used regularly with between 10-50 ng of template DNA (prepared as in Section 2.6.1) in a final volume of 50 µL. Oligonucleotide primers manufactured by Macrogen Inc (South Korea) or Integrated DNA Technologies (IDT) were dissolved in TE buffer to a concentration of 100 µM and stored at -20°C. The list of

the oligonucleotide primers can be found in the relevant result chapter below. A PCR reaction was prepared as per the Phusion® PCR protocol standards with the addition of 50 mM $MgCl_2$ and DMSO where noted. In summary, each reaction contained template DNA, 1 mM of forward and reverse primers, 10 mM dNTPS, Phusion GC buffer, MQW and Phusion DNA polymerase enzyme. All PCR reactions underwent a general temperature cycle suing thermocycler (Mastercycler, Eppendorf); 2 min at 98°C (for the initial denaturation of the template), followed by 30 cycles of 95°C for 15 secs (template denaturation), X°C for 30 secs (primer annealing to the template) and 72°C for 60 secs (extension), followed by 1 min at 72°C or a final extension and then the PCR was held at 4°C until downstream application (where X= predicted annealing temperature for oligonucleotide primer pair). The PCR products were routinely cleaned up using Bioline Isolate II PCR clean-up kit following the manufacturer's protocol (Bioline, Australia). All PCR products were visualised using agarose gel electrophoresis (Section 2.6.3).

2.6.3 Agarose Gel Electrophoresis

For most gels, a 1% TBE agarose gel was used (Bioline, Australia) and it was prepared with 1 µL of Gel-Red or 0.1 ug/mL of ethidium bromide (Table 2.4). In some cases, a 0.7% agarose gel was used instead and this will be noted where appropriate. DNA loading buffer (New England BioLabs) to a final concentration of 1x was added to 50-100 ng of each DNA sample and then this was loaded into the gel wells. DNA electrophoresis was run at 110 V for 60 mins and visualised with exposure to UV light (254 nm) using a transilluminator (Ingenius3, Syngene) and recorded using charge-coupled device (CCD) camera (Synoptics CAM-FLXCM, Syngene) linked to GeneSys molecular imaging software, version 1.5.0.0 (Syngene).

Alternatively, when performed a gel purification of DNA fragments a 0.7% TAE agarose gel (Bioline, Australia) with 1 µL of Gel-red was used. The gel was run at 60 V for 120 mins and visualised in the same manner as mentioned above. Once the correct bands of DNA were excised from the gel they were purified and cleaned up using the Bioline Isolate II PCR clean-up kit as per the manufacturer's protocol. The final concentration of DNA was determined using the NanoDrop One spectrophotometer.

2.6.4 DNA Sanger Sequencing

Throughout this work plasmids that were created had their PCR regions confirmed by Sanger Sequencing. Between 600-1000 ng of the purified plasmid DNA as outlined in Section 2.6.1, along with the appropriate primers at a concentration of 10 pmol/µL was sent to Australian Genome Research Facility (AGRF) were the sequencing reactions were performed. Then the sequencing data was analysed using SnapGene Viewer 4.1.9.

2.6.5 RNA Extraction from *E. coli*

For the extraction of RNA from *E. coli* a home-made Hot Phenol Total RNA Purification method was used and the RNA was used downstream for transcriptomics. Initially, 10 mL of *E. coli* culture was spun down at 4000 rpm for 10 mins and then the pellet was resuspended in Solution 1 (Table 2.5) with the addition of 400 µL of phenol (Table 2.4) and 150 µL of Solution 2 (Table 2.5) prewarmed to 65^{o}C. The contents were then vortexed and incubated at 65^{o}C for 3-4 mins at 1300 rpm. After vortexing, the samples were frozen in liquid nitrogen for 30 secs and then centrifuged at room temperature for 10 mins at 11000 rpm. The aqueous layer was transferred to a new tube and 400 µL of phenol was added and the tube was frozen and centrifuged as mentioned previously. This was repeated once more and then the aqueous layer was transferred to a new tube and 200 µL of phenol and 200 µL of chloroform was added. The tubes were vortexed and centrifuged at 11000 rpm for 5 mins at 4^{o}C. The aqueous layer was transferred to a new tube and 400 µL of chloroform was added. The tube was vortexed and centrifuged as before and then the aqueous layer was transferred to a new tube with 2.5x of the sample volume of 100 % (v/v) ethanol, 1/10 of the sample volume of 3 M NaAcetate and 1 µL glycogen (1 µg/ µL). The samples were then stored at -20^{o}C overnight. The next day the samples were spun at 20000g for 1 hour at 4^{o}C and the supernatant was discarded. The pellet was washed in 1 mL of 70% ethanol and spun for 5 mins at 11000 rpm. The supernatant was removed and the pellet was dried and dissolved in RNAase free H_20. The RNA was run on a bleach gel (see Section 2.6.6) and then samples were added to RNAstable tube (Sigma-Aldrich, USA) and spin-dried ready for shipping to McGill University Genome (Quebec, Canada).

2.6.6 Bleach Gel for RNA Visualisation

To determine if the RNA had been degraded during the extraction and purification the RNA was run in a bleach gel.[124] A 1 % TAE agarose gel was used (Bioline, Australia) and 1 % (v/v) of Chlorite bleach was added and the solution was incubated at room temperature for 5 mins with occasional swirling. Then the solution was heated to melt the agarose and once it cooled 1 µL of ethidium bromide was added (Table 2.4). DNA loading buffer (New England BioLabs) to a final concentration of 1x was added to 1 µL of RNA sample. The gel was run at 100 V for 35 mins in 1x TAE buffer and visualised with exposure to UV light (254 nm) using a transilluminator (Ingenius3, Syngene) and recorded using charge-coupled device (CCD) camera (Synoptics CAM-FLXCM, Syngene) linked to GeneSys molecular imaging software, version 1.5.0.0 (Syngene).

2.6.7 Transcriptomics

RNA was extracted (Section 2.6.5) from BW25113 *pBAD24 pTAB2,* BW25113 *dnaA(cos) pTAB2,* BW25113 *dnaA(cos) cedA,* and BW25113 *pBAD24 cedA.* The RNA was visualised on a bleach gel (Section 2.6.6) to observe any degradation and good samples were sent to McGill University Genome (Quebec, Canada) for RNA sequencing (RNA-seq). The sequencing performed was Illumina 150-bp paired-end. The FASTQ files from the RNA-seq were uploaded and analysed through Galaxy.[125] The files underwent quality control analysis using FASTQC software took (Andrew, S. 2010) version 0.72, http://bioinformatics.babraham.ac.uk/projects/fastqc/. The last 5 bp from the forward and reverse reads were trimmed using Trim sequences software tool (Assaf Gordan, 2010) version 1.0.1, http://hannonlab.cshl.edu/fastx_toolkit/. The sequence read mapping to *E. coli* BW25113 genome (Genbank NZ_CP009273.1) was performed by Bowtie2[126] using the default settings. The frequency of the mapped reads was determined by HTseq defaults[127] and visualised using Artemis (Artemis, version 17.0.1). For the differential gene expression analysis DESeq2[128] was used. DESeq2 requires replicates to be entered during the analysis and cannot perform the analysis on one replicate alone. This is because without replicates DESeq2 is unable to provide proper statistical inference on the differences between groups and therefore it cannot estimate the biological variability of each gene.

2.6.8 Chromosomal Runouts

To study the synchrony of initiation of chromosome replication, chromosomal runouts were used.[129] Firstly the strains of interest were diluted down to OD_{600} = 0.01 from an overnight culture and then grown for 2 hours at 37°C. The culture was then diluted down to OD_{600} = 0.01 in fresh media and grown until an OD_{600} = 0.1 where initiation of replication was inhibited by rifampicin (300 μg/mL) and cephalexin (15 μg/mL). Another culture was also made in fresh media containing only rifampicin (200 μg/mL). The cultures were left to grow for 3 hours in the presence of the antibiotics and then 300 μL of cells were fixed in 700 μL of 100% ethanol and the samples were stored at 4°C.

2.7 General Cloning

All enzymes used in the cloning process were obtained from New England BioLabs.

2.7.1 Sub-cloning of *dnaA(cos)*

The *dnaA(cos)* gene was amplified by PCR using Phusion polymerase, using primers listed in Table 2.6, in reactions containing 1 M betaine. The PCR product was cleaned up using the Isolate II PCR and gel-extraction kit (Bioline) and the product digested NcoI-HF and HindII-HF. This product was ligated with pBAD24, which had been digested with NcoI-HF and HindII-HF, and treated with Antarctic phosphatase. Ligations were done with T4 DNA Ligase overnight, and hen transformed into DH5α using the heat shock method, and the cells plated on LB-ampicillin (100 μg/mL). Six cloned were picked for restriction digest screening to confirm their structure, and one clone was sequenced (Sanger sequencing, AGRF).

Table 2.6 Oligonucleotides and their respective restriction enzymes used for cloning dnaA(cos) into pBAD24

Name	Sequence (forward 5' → 3')	Source
DnaA_BAD_Nco_F	GGG CCA TGG GCT CAC TTT CGC TTT GGC	Macrogen
DnaA_BAD_Hin_R	GGG AAG CTT ACG ATG ACA ATG TTC TG	Macrogen

2.7.2 Construction of Plasmid for Expression of *zapB-gfp*

In order to visualise Z-rings during work in this thesis, a plasmid was created to allow for the expression of *zapB-gfp* in conjunction with the expression of genes in pBAD24 vector. A novel low copy number plasmid, pTAB1, was constructed from the backbone of pACYC184 which contained the p15A origin of replication and chloramphenicol resistance, and the laqIq repressor and multi-cloning site of pNDM220 (Figure 2.1).

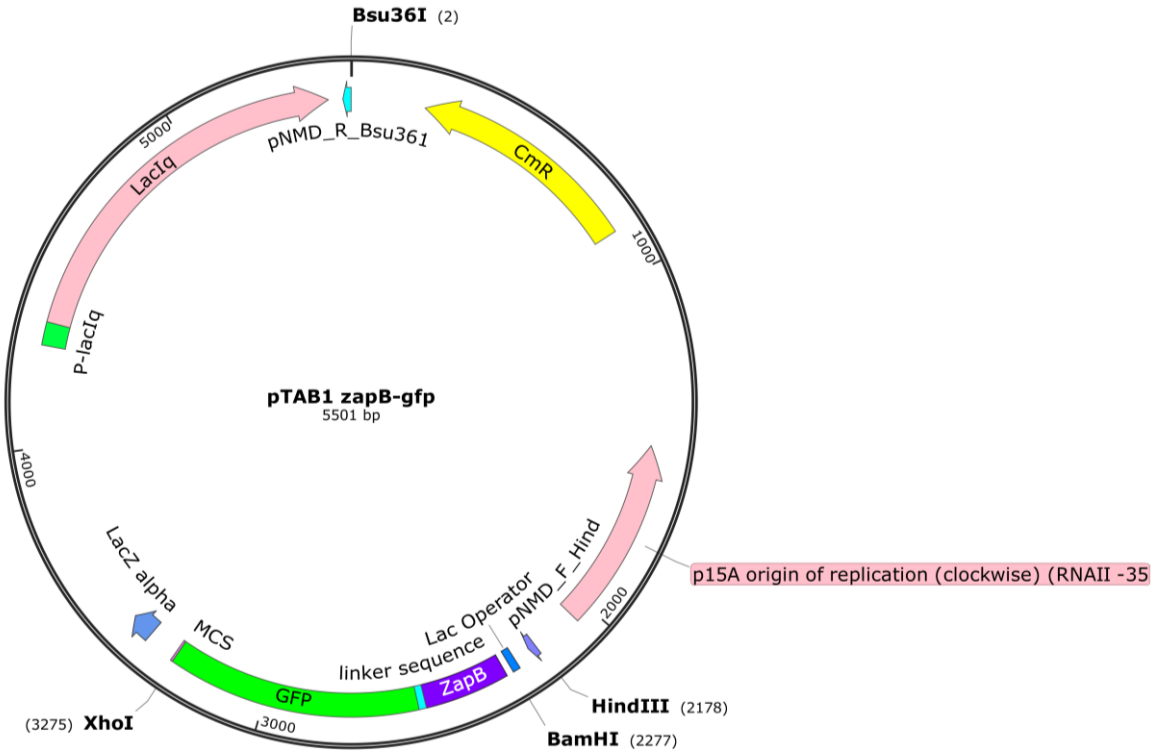

Figure 2.1 Plasmid of pTAB1 containing zapB-gfp in multiple cloning site.

Firstly, a specific region of pNDM220 was amplified using primers pNDM_F_Hind and pNDM_R_Bsu361 (Table 2.7).

Table 2.7 Oligonucletiodes and their respective restriction enzymes used for cloning zapB-GFP into pTAB2

Name	Sequence (forward 5' → 3')	Source
pNDM_F_Hind	GGG CCC AAG CTT CGC TCT AGG ATC AAG ATC TCC C	Macrogen
pNDM_R_Bsu361	GGC CCT GAG GGG AAG CAT AAA GTG TAA AGC CTG G	Macrogen

msf_gfp_F_OE	GAG CTC TTA ATT AAG GAC GTC AGT AAA GGT GAA GAA CTG TTC ACC	Macrogen
msf_gfp_R_xho	GCC CCG CTC GAG TTA TTT GTA GAG TTC ATC CAT G	Macrogen
zapB_N_F	GTC GGA TCC AGG AGG TCT AGA TAA TGA CAA TGT CAT TAG AAG TGT TTG AG	IDT
zapB_N_R	GGTACCCGCGGCCGCGCTAGCGACCTCTTG CATGCGACCC	IDT

To create this plasmid pACYC184 and amplified pNDM220 region were digested with restriction enzyme Bsu361 following the manufacturer's instructions to remove any remaining template DNA from the PCR reaction. Then pACYC184 was further digested with HindIII-HF and SalI and pNDM220 were only digested with HindIII-HF. Bsu361 digestion was performed separately from HindIII-HF and SalI because they were not compatible enzymes and Bsu361 only works when it digests DNA alone. The digestions were checked on a 0.7 % (w/v) agarose gel in 1 x TBE buffer for 60 minutes at 110V.

Once the digestions were confirmed the digested pACYC184 was gel purified by running the sample on a 0.5% (w/v) agarose gel in 1x TAE buffer for 90 minutes at 60V. A digital image of the gel was taken on the EDAS 290 gel documentation system (KODAK) and then the fragment of the correct size was extracted. To purify the DNA the Bioline Isolate II PCR clean-up kit was used following the manufacturer's protocol (Bioline, Australia). Once pACYC184 was purified it was ligated to the digested pNDM220 fragment using T4 DNA Ligase following manufacturers protocol for an overnight reaction. The resulting plasmid was transformed into DH5α as stated in section 2.4.2 and cells were selected for on chloramphenicol (35 µg/ml). Clones that looked correct via restriction enzymes digest check were then sent off for sequencing with Australian Genome Research Facility (AGRF).

Once the sequence of pTAB1 was confirmed *zapB* and *gfp* were PCR amplified using primers zapB_N_F, zapB_N_R, msf_gfp_F_OE and msf_gfp_R_xho (Table 2.4). *zapB* was amplified from MG1655 genome and monomeric superfolding *gfp* was amplified from pGI5.The PCR reactions were set up as per the Phusion® PCR protocol standards. The fragment sizes of the PCR were confirmed by agarose gel electrophoresis. The genes were then fused using PCR amplification with overlap extension. After confirmation of a successful overlap extension through agarose gel electrophoresis, *zapB-gfp* and pTAB1

were digested with BamHI-HF and XhoI using manufacturers' protocol. They were then ligated with T4 DNA Ligase following manufactures protocol and the ligation mixture was transformed into DH5α. Resulting clones underwent a restriction enzyme digest check and one clone that looked correct was sent for sequencing at AGRF.

2.8 *In vitro* Flow Cell Infection Model

After the 100 µL of PDO7i cells were resuspended to a concentration of $3x10^6$ cells/mL following the splitting of mammalian cells (Section 2.5.1) the cells were added to an IBIDI flow chamber and incubated overnight at 37°C with 5% CO_2. The flow cell system was set up as shown in Figure 2.2. In this system, the media bottle is attached to the bubble trap, after which the media flows through the flow chamber where the PDO7i cells are seeded. The media is pulled through the peristaltic pump and into the waste beaker. The entire set up is placed into an incubator at 37°C with 5% CO_2. The flow rate for the system was 50 µL/min and Epilife media without antibiotics was pumped through the system overnight. After the set up of the flow chamber, static bacterial cultures were made of the strains of interest and they were left to incubate overnight at 37°C.

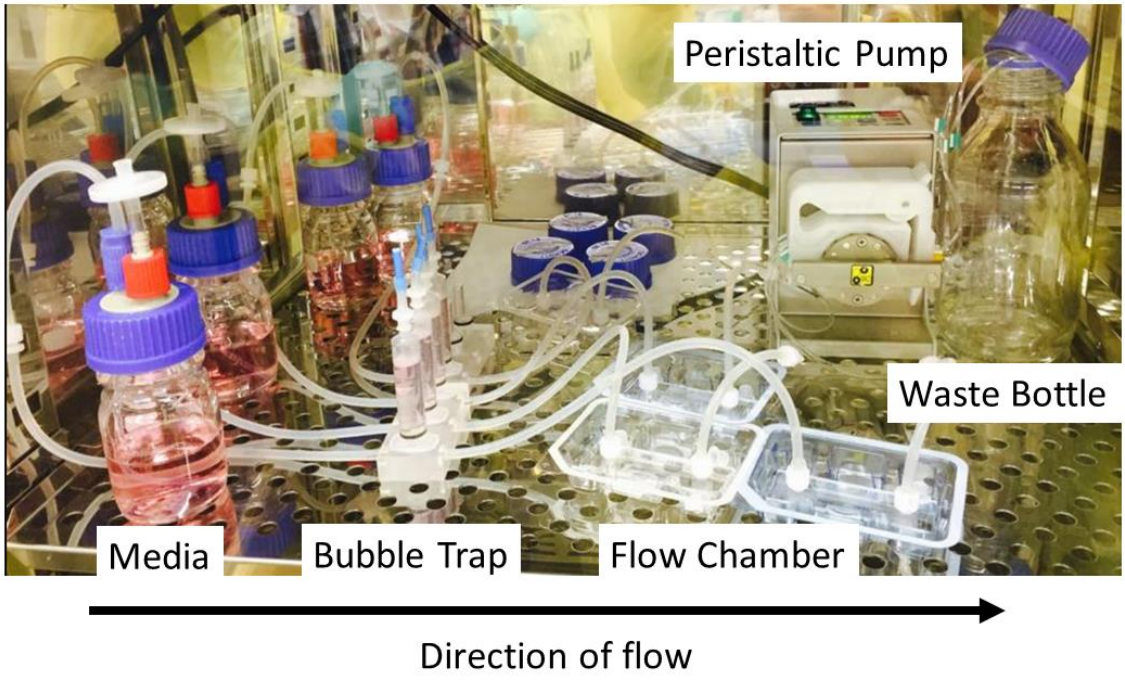

Figure 2.2 Flow chamber set up of infection model.

2.8.1 Preparation of Urine Samples

Concentrated urine was required for filamentation in all work related to the UTI infection models. This was achieved by a donor collecting urine while dehydrated, this was done first thing in the morning as the donor would have gone some time without water during the night. The urine samples were then stored at -4^{o}C for 2-3 days. The samples were centrifuged at 4000 xg for 10 minutes to remove any precipitate and debris to allow the urine to be passed through a 0.2 μm filter. To measure the concentration of urine a density meter (Densito, Mettler Toledo) was used. To ensure that filamentation would be achieved by urine during the infections, its concentration was measured every batch and only a concentration of 1.025 g/ml or over would be used. In addition to the concentration of urine, pH was also tested using Eutech pH 700 meter and only urine with a pH of 5-6 was used. If the urine passed both selection criteria then it would be filter sterilized and stored at -20^{o}C until used. To reduce variability this study only had 2 donors.

2.8.2 From Infection to Dispersal and Filamentation

For the infection of the *in vitro* model, the bacterial culture was centrifuged for 10 minutes at 4000 xg and resuspended to an OD_{600} = 0.2. The system was stopped and the tubing before the flow chambers were disconnected. Using a syringe a small piece of tubing was filled with the bacterial suspension and one end of the tubing was connected to the flow chamber ensuring that there were no bubbles present. The other end of the tubing was placed in the falcon tube containing the bacterial suspension and flow was resumed for 20 minutes. After 20 minutes the pump was stopped, the extra tubing was removed and the initial tubing was reconnected with the flow resuming for 9 hours.

After 9 hours the pump was stopped and all of the media was drained from the media bottles and the bubble traps. They were then filled with Epilife media containing 100 μg/mL gentamicin. This media flowed through the system for 20 hours. After 20 hours the pump was stopped, and the media bottles and bubble traps were drained again. This time sterile water was used to flush the system of any remaining gentamicin before adding concentrated urine (Section 2.7.1). The urine was left to flow through the flow chambers for 20 hours. To harvest the bacteria the flow chamber was disconnected, and the

supernatant was removed using a pipette into a 1.5 mL centrifuge tube. Then 200 µL of PBS was added to the chamber and pipetted back and forth to remove an excess sample and it was pooled with the initial supernatant. The sample was centrifuged at 5000 xg for 5 minutes and the pellet was resuspended in 2% paraformaldehyde and stored at 4°C.

2.9 Analysis of Bacterial Cells

To collect data on the cell size, cell volume and cell morphology different instruments and methods were used, and these are outlined below. First, the bacterial cells were cultured to mid-log phase (A_{600} = 0.3-0.6) unless mentioned otherwise and then 200 – 500 µL of the culture was fixed in 0.4% PFA (Table 2.5).

2.9.1 Coulter Counter

A Coulter counter measures the size of particles, like bacterial cells, which are suspended in an electrolyte buffer. The size of the bacteria is reported as a volume (μm^3)[130] and this is proportional to the cell length in rod-shaped bacteria such as *E. coli*. To prepare the sample for reading on the Coulter Counter (Multisizer 4, Beckman Coulter Inc) 100 µL of the fixed bacterial culture was added to 9.9 mL of filtered Isoflow electrolyte and the 30 µm aperture tube was used to read 200 µm of the sample from 0.3 µm to 30 µm on a logarithmic scale unless stated otherwise. The software programme Multisizer™ 4 Particle Analyzer was used to export the data so that Graphpad Prism 8 could be used to make graphs of the data and perform analysis. For visualisation, the x-axis of the graph was transformed to $\log_{10}$ and the data was offset for better visualisation of replicates and samples.

As the Coulter counter can count hundreds of thousands of cells per sample, every difference includes those that are very small are statistically significant. This is also true for two samples from the same strain and therefore do not always indicate biological significance. Therefore, statistical analysis was not used to determine significant differences between strains. Instead, a combination of visual differences from the Coulter distribution graphs along with correlation analysis from Graphpad Prism 8 was used. For

analysis of the cell volume distributions, a Pearson correlation was used to calculate the correlation between two samples that were performed on the same day. This value would then be able to be used to compare the results of the same experiment performed on another day. The correlation coefficient allows for the interpretation of the correlation where 1 is a very high positive correlation and the two samples cell volume distributions are highly similar. Zero is for two samples that do not vary together and therefore have a negligible correlation and finally -1 is for a very negative correlation.

2.9.2 Microscopy

The fixed cells were spun down by centrifugation at 5000 rpm for 5 mins to remove the paraformaldehyde. The supernatant was removed, and cells re-suspended in 1 mL of 20 mM Tris-Cl (pH 7.4). This was then spun again at 5000 rpm for 5 mins and the supernatant discarded. Finally, the cells were re-suspended in 0.5 mL of Hoechst staining solution (Table 2.5) and left to stain for at least 15 mins before microscopy.

For microscopy, the Zeiss Axioplan 2 fluorescence microscope was used, and 1% (w/v) agarose pads were prepared on glass slides. Oil immersion on the 100x objective was used to view the cells, unless stated otherwise. Phase contrast and Hoescht fluorescence were used for the nucleoid staining for all strains. Images were taken using a Zeiss AxioCam MRm camera and image analysis was performed using ImageJ 1.51s.

2.9.3 Flow Cytometry

The BD LSR II Flow Cytometer was used to measure cell length by running at least 200 µL of the fixed bacterial culture in a FACS tube. If the sample was too concentrated then at least 300 µL of PBS was also added to the tube to dilute the sample. For each reading, 100 000 events were recorded and the parameters used were forward scatter (FSC), side scatter (SSC) and a fluorescence channel depending on the strain which will be mentioned in the results chapter. The side scatter parameter was used to threshold the readings. Once all of the samples had been run a tube of 1% bleach was run for 5 mins followed by FACS rinse and then sterile water, each tube was run for 5 mins. For analysis and visualisation of the data, FlowJo V.10.1 was used.

Chapter 3
Cell filamentation induced by a dominant mutant of the replication initiator protein, *dnaA(cos)*, is a multifaceted process

3.1 Introduction

DNA replication in *Escherichia coli* is heavily regulated, with an emphasis on the regulation of its initiation (Section 1.3). Normally, during initiation of DNA replication, DnaA begins replication from the chromosomal origin known as *oriC.*[131] It is thought that DnaA plays a positive role in regulating the frequency of initiation.[132] To do this, DnaA must be in its active form, with ATP bound, in order to be able to bind to the *oriC*. The cellular concentration of ATP-DnaA is known to fluctuate and peak at the time of initiation of replication.[133] In addition, the binding of DNA-bending protein IHF (integration host factor) to *oriC* is required to form the initiation complex.[134] This complex promotes the unwinding of an AT-rich region of *oriC* and the loading of DnaB helicases onto the single-stranded DNA.[134] Thereby, forming sister replisomes and leading to bidirectional chromosomal replication.[45]

There are artificial instances where the oversupply or conformational change of DnaA can increase and/or control the frequency of initiation, respectively.[63]

A DnaA mutant that leads to unregulated initiation, *dnaA(cos)*, was first used by Katayama and Kornberg[63] to understand the functional regulation of DnaA in initiation. It was found that *dnaA(cos)* was able to cause excessive initiation at a restrictive temperature of 30^{o}C without an increase in DnaA protein levels.[63] There are many features of the *dnaA(cos)* mutation: 1) it is dominant over the wild-type allele;[69] 2) it is cold-sensitive (30^{o}C);[135] 3) its hyper-initiation comes about from two base-substitutions;[66] 4) hyper-initiation of chromosomal replication occurs at the restrictive temperature with or without *de novo* protein synthesis;[135] 5) hyper-initiation occurs at or near the *oriC,*[63] 6) *dnaA(cos)* induces bacterial filamentation at the restrictive temperature.[15]

To begin to understand how *dnaA(cos)* was capable of causing inhibition of cell division (the underlying cause of filamentation), Katayama, et al.[15] isolated 7 groups of multicopy suppressors of the cold-sensitive phenotype, and one gene which was common to 5 groups, was a gene they named *cedA*. It was found that oversupply of *cedA* enabled cells

to continue cell division at the restrictive temperature in the *dnaA(cos)* mutant. However, since DNA over-replication still occurred in this strain, the promotion of cell division was considered independent of overcoming the hyper-initiation of chromosomal replication itself.[15] Katayama, et al.[15] also reported that *dnaA(cos)* formed filaments in the absence of the SOS genes *sulA* and *recA.* SulA and RecA are proteins in the SOS response, a regulatory pathway responsible for DNA repair in response to DNA damage. However, very limited data was published to support this claim, and the pathway or mechanism of cell division activation by *cedA* remains unknown.

Despite it being shown that CedA can prevent DnaA(cos) filamentation, it is important to understand through which pathway *dnaA(cos)* inhibits cell division, as this would indicate the pathway that is acted on by *cedA* and might thereby shed light on how *cedA* can prevent filamentation. There are several direct inhibitors of the cell division complex, or 'Z-ring', in *E. coli,* and they mostly function by affecting the activity and self-association of the key cell division protein FtsZ.[136] [137,138] Inhibitors of FtsZ include the proteins MinC, SulA, and SlmA. MinC together with MinDE, known as the Min System, prevents the formation of Z-rings near the cell poles by inhibiting FtsZ polymerisation there (Section 1.4.2). Whereas, SlmA, involved in a process known as nucleoid occlusion, prevents the Z-ring forming over the nucleoid by directly binding FtsZ (Section 1.4.2). SulA binds to FtsZ monomers through a process known as sequestration and inhibits FtsZ polymerization, thus allowing the cell time to repair DNA damage before attempting to divide.[139] Of note, the SOS response is induced by the damage sensor RecA which causes LexA, the repressor of the SOS response during non-stress conditions, to undergo an auto-cleavage reaction.[140]

This chapter sets out to test the requirement for the known division inhibitory pathways in *dnaA(cos)* filamentation, as this may help understand how *cedA* maintains normal cell division under these conditions, which could help identify *cedA*'s role during the filamentation stage of cellular infection in UTIs.

3.2 Results

To understand through which pathway *dnaA(cos)* causes filamentation, *E. coli* BW25113 mutants (Δ*minC,* Δ*slmA,* Δ*recA and* Δ*ymfMsulA)* and TB43 (Δ*minCDE)* were examined for their ability to produce filaments when *dnaA(cos)* was overexpressed at the restrictive temperature. We selected Δ*recA* as RecA is the first protein to be expressed during the SOS response and it enables the transcription of downstream SOS genes by causing the repressor LexA to undergo auto-cleavage.[140] Additionally, we selected Δ*ymfMsulA* as it has been shown that both of these downstream SOS genes need to be deleted in order to block filamentation induced by the SOS response.[141] Strain TB43 was used as this has the entire *min* operon deleted.[91] In this background, there is a mixed population of minicells and mildly filamentous cells, as a result of polar cell division.[97] The parent to this strain is TB28. All strains were examined for their ability to cause hyper-initiation of chromosomal replication using flow cytometry. To determine whether there was hyper-initiation of chromosomal replication, DNA ratio (*see Section 3.2.4 for explanation)* was determined using nucleoid staining.

All cell size data were obtained using a Coulter Counter, which measures the cell volumes of hundreds of thousands of cells per sample, which provides a histogram distribution of cell size in the population (*Section 2.9.1)*. To analyse the cell volume distributions, a Pearson correlation statistical analysis was performed to determine how similar the distributions were for samples performed on the same day (*Section 2.9.1*). Additionally, to test the other phenotype of *dnaA(cos)* filamentation which is over-replication we measured DNA staining per cell using flow cytometry. The DNA ratio content per cell was worked out by dividing the mean DNA fluorescence by the mean cell size to provide an arbitrary number for the DNA ratio (*Section 3.4.2)*. Overall from these studies, if *dnaA(cos)* was able to cause filamentation and hyper-initiation of replication in the absence of *minC, minCDE, slmA, recA* or *ymfMsulA* then this would indicate that that pathway is not required for *dnaA(cos)* filamentation.

3.2.1 Δ*recA* has a reduced growth rate compared to other strains

Firstly, the doubling times of all strains used in this study were measured. All strains, with and without pBAD24-*dnaA(cos),* were cultured at 30°C and sampled every 30 minutes. It was found that all strains without *dnaA(cos)* (carrying pBAD24 only), except the *recA* mutant (Δ*recA*), displayed biomass doubling times no different to the WT control (Figure 3.1 and Table 3.1). When *dnaA(cos)* was overexpressed in any of the backgrounds the doubling time increased. For example, the doubling time for BW25113 pBAD24 (WT) at 30°C was 33.03 ± 4.32 mins and when *dnaA(cos)* was overexpressed in BW25113 the doubling time increased to 52.58 ± 8.45 min. However, the Δ*recA dnaA(cos)* growth defect was more severe, with a doubling time of 87.94 ± 34.16 mins compared to Δ*recA* vector-only with a doubling time of 53.37 ± 3.15 mins. Additionally, it can be noted that Δ*recA* with *dnaA(cos)* overexpression was unable to reach a high OD_{600} (Figure 3.1C), so samples were harvested at OD_{600} = 0.1 for Δ*recA*. Additionally, an OD_{600} = 0.3 was used as a later time point to investigate whether the *dnaA(cos)* strains acquired any suppressor mutations that inhibit filamentation via *dnaA(cos)*. We expected to see suppressors because suppressors of *dnaA* are common when there is elevated levels of *dnaA* and its mutants in the cell.[142]

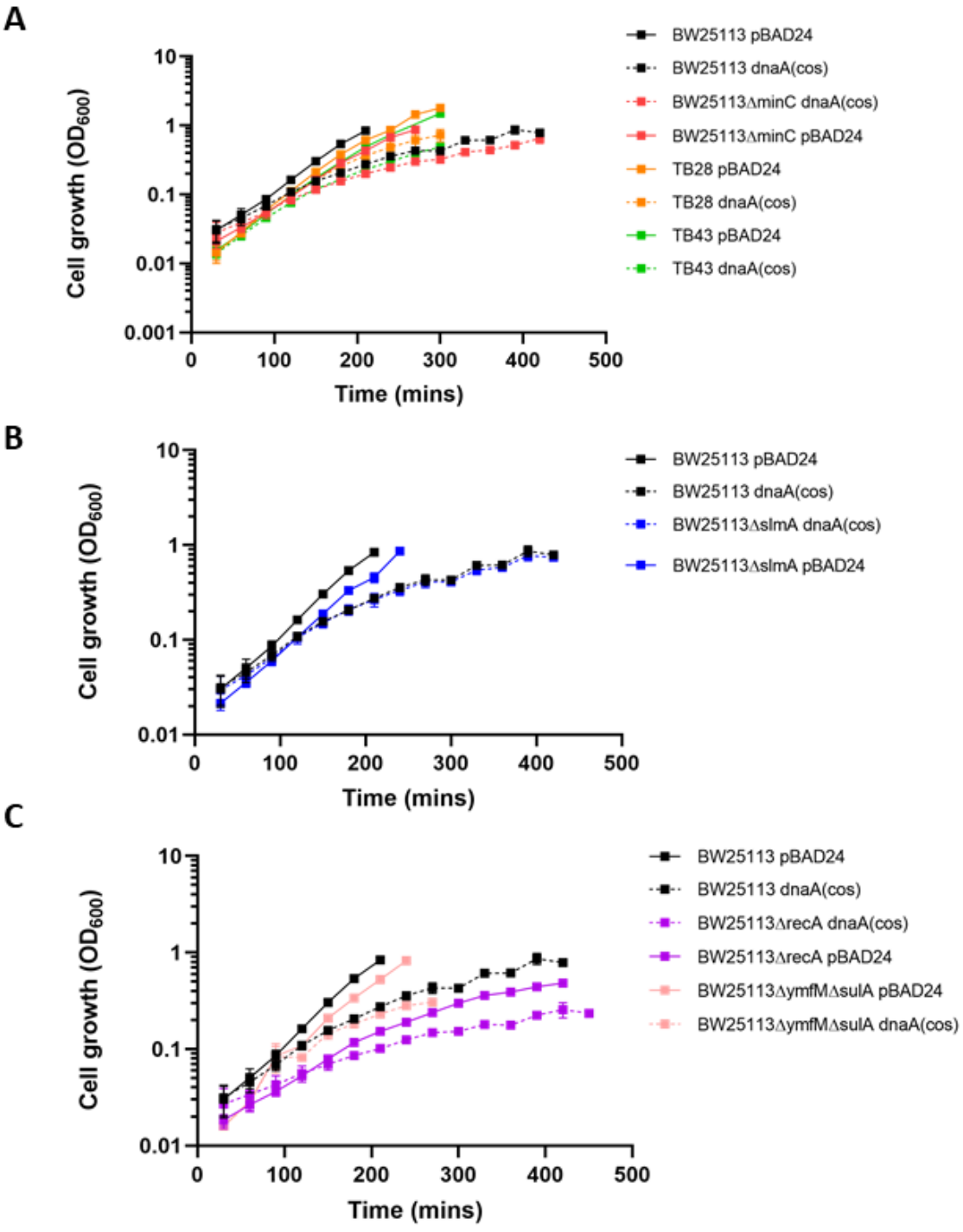

Figure 3.1 Growth Curve of BW25113, TB28 and their mutants.
BW25113 and its mutants ΔrecA, ΔslmA ΔminC, and double mutant ΔymfMΔsulA along with TB43 (ΔminCDE) and its parental strain TB28 were first cultured for 2 hours at 42 from an overnight liquid culture in LB containing ampicillin (100 µg/mL), then samples were diluted into LB containing 0.2% (w/v) L-arabinose and grown until a late OD_{600}. The optical density (OD) was plotted on a log scale against time in minutes. Triplicate data has been averaged to find mean and SEM which has been plotted. Each graph contains the same BW25115 pBAD24 and BW25113 dnaA(cos) plots for comparison purposes as all of the strains were grown at the same time. A) Growth curves for Min

System B) Growth Curves for nucleoid occlusion C) growth curves for SOS response genes.

Table 3.1 Doubling times of BW25113, TB28 and their indicated mutants.

Strain	Doubling time[a] (minutes) ± SD
BW25113 pBAD24	33.03 ± 4.32
BW25113 *dnaA(cos)*	52.58 ± 8.45
TB28 pBAD24	32.35 ± 0.80
TB28 *dnaA(cos)*	39.26 ± 6.17
TB43 pBAD24	34.88 ± 0.03
TB43 *dnaA(cos)*	44.21 ± 1.42
BW25113Δ*minC* pBAD24	37.77 ± 1.55
BW25113Δ*minC dnaA(cos)*	59.01 ± 18.77
BW25113Δ*slmA* pBAD24	36.37 ±1.88
BW25113Δ*slmA dnaA(cos)*	51.74 ± 11.82
BW25113Δ*recA* pBAD24	53.37 ± 3.15
BW25113Δ*recA dnaA(cos)*	87.94 ± 34.16
BW25113Δ*ymfMΔsulA* pBAD24	48.16 ± 20.74
BW25113Δ*ymfMΔsulA dnaA(cos)*	75.01 ± 29.62

[a] mean doubling time from triplicate data

3.2.2 Min System is not required for *dnaA(cos)* filamentation

Initially, to test the requirement for the Min System in the *dnaA(cos)* filamentation pathway, a *minC* mutant (Δ*minC*) was used; if the MinC division inhibitor were required for *dnaA(cos)* filamentation, then this strain should not form filaments. To determine if filamentation has occurred in the strains the Coulter counter was used to measure the cell size distribution of the population. As expected, the cell size distribution of BW25113 *dnaA(cos)* was negligibly correlated to BW25113 pBAD24, with an average Pearson correlation coefficient of 0.142 ± 0.240 (Table 3.2) because *dnaA(cos)* has caused filamentation. The relatively high standard deviation reflects filamentation from *dnaA(cos)* overexpression that varied from experiment to experiment even though the culturing methods were applied consistently. This variation may have been a response to the suppressors that appeared to commonly arise in this background. Flow cytometry

showed a higher DNA content per cell, consistent with the expected over-replication (Figure 3.2C).

It was found that Δ*minC* alone leads to long filaments (Figure 3.2A, green line and Figure 3.2B). Therefore, when *dnaA(cos)* was overexpressed in the Δ*minC* background it was difficult to distinguish if there was any additional filamentation occurring. The average correlation between Δ*minC* vector-only compared to Δ*minC* with *dnaA(cos)* overexpression was 0.576 ± 0.175, suggesting that they had a moderate positive correlation (Table 3.2). Finally, it was demonstrated through flow cytometry that *dnaA(cos)* overexpression in Δ*minC* causes hyper-initiation of chromosomal replication, seen by the increase in DNA ratio (arbitrary number) from 7.1 for Δ*minC* vector-only to 8.6 for Δ*minC* with *dnaA(cos)* (Figure 3.2C). This was much like the increase of DNA ratio seen when comparing WT to BW25113 *dnaA(cos)* from 5.6 to 8.6 respectively. Due to the unexpected extensive filamentation that Δ*minC* causes, the *minCDE* mutant was also used to test whether *dnaA(cos)*-filamentation requires the Min system.

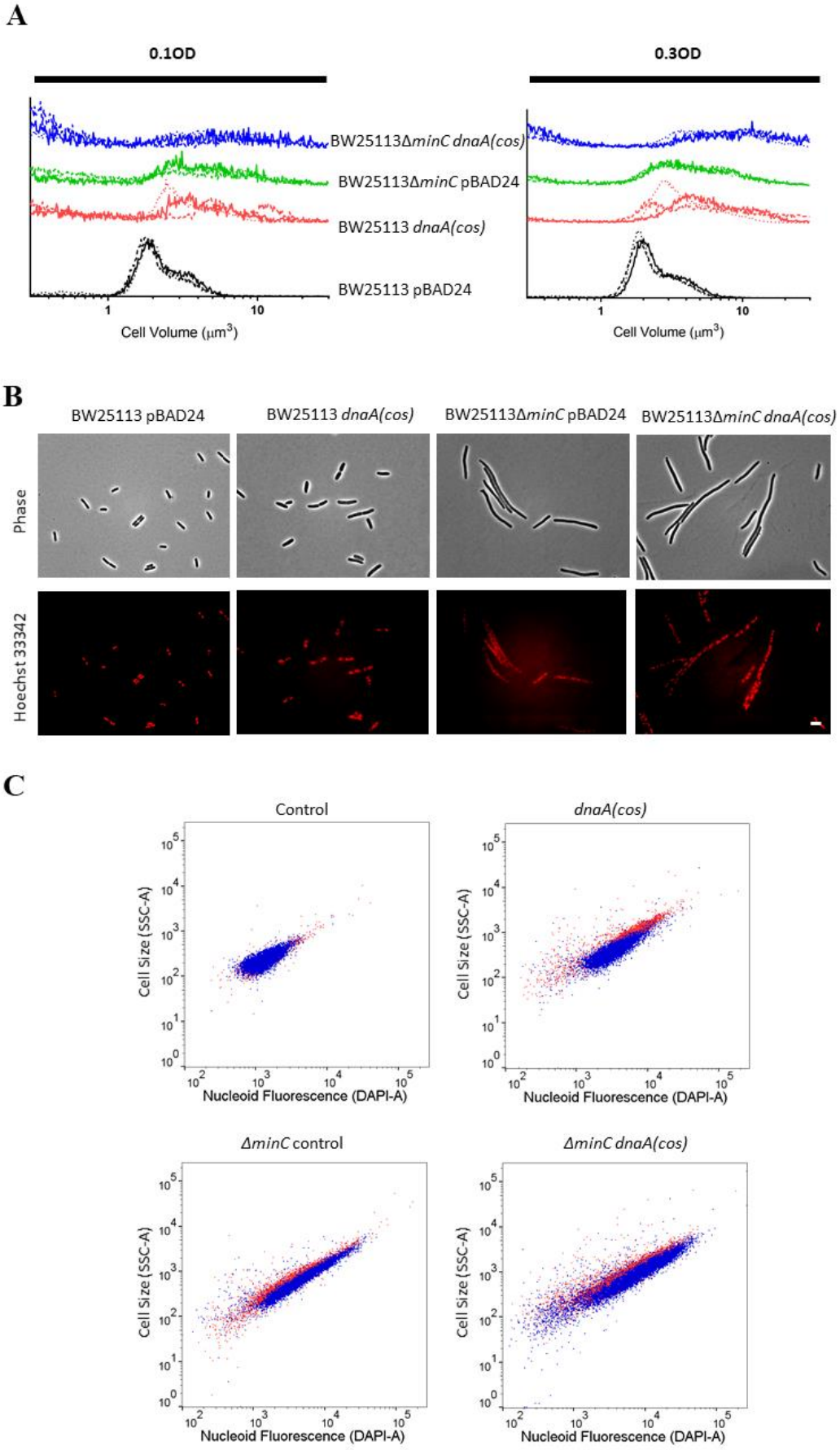
A
0.1OD
0.3OD
BW25113ΔminC dnaA(cos)
BW25113ΔminC pBAD24
BW25113 dnaA(cos)
BW25113 pBAD24
Cell Volume (μm3)
B
BW25113 pBAD24
BW25113 dnaA(cos)
BW25113ΔminC pBAD24
BW25113ΔminC dnaA(cos)
Phase
Hoechst 33342
C
Control
dnaA(cos)
ΔminC control
ΔminC dnaA(cos)
Cell Size (SSC-A)
Nucleoid Fluorescence (DAPI-A)

Figure 3.2 minC is not required for dnaA(cos)-mediated filamentation
The open reading frame of dnaA(cos) was cloned into expression plasmid, pBAD24. With fresh transformants, the strains BW25113 pBAD24, BW25113 dnaA(cos), BW25113ΔminC pBAD24 and BW25113ΔminC dnaA(cos) were grown at 42°C for 2 hours and then diluted into LB containing 0.2% (w/v) L-arabinose and grown at 30°C. The cultures were sampled at OD_{600} = 0.1 and 0.3. A) Coulter counter analysis of cell size distributions. The X-axis represents cell volume (μm³) and the Y-axis represents the percentage of cells at any given volume. Data are shown in triplicates, the same dash-type refers to same-day experiments. B) Phase-contrast and fluorescent microscopy depicting cell morphology and DNA staining (Hoechst 33342) at OD_{600} = 0.1. The images were acquired on the Zeiss Axioplan microscopy using 100x magnification, Scale bar = 5 μM. C) Flow cytometry performed at OD_{600} = 0.1 with BW25113 pBAD24 (control, which was mostly short cells), BW25113 dnaA(cos) (mostly filaments), BW25113ΔminC pBAD24 and BW25113ΔminC dnaA(cos). In these graphs, the dots represent single events plotted with side scatter area on the x-axis (for cell length) and DAPI area on the Y-axis (for nucleoid intensity). Replicate data shown one in red and the other in blue.

Table 3.2 Correlation matrix of cell size distributions from Coulter counter data when dnaA(cos) was overexpressed in a minC mutant (mean ± SEM)[a]

	BW25113 *dnaA(cos)*	**BW25113Δ*minC* pBAD24**	**BW25113Δ*minC* *dnaA(cos)***
BW25113 pBAD24	0.142 ± 0.240	0.219 ± 0.074	-0.151 ± 0.064
BW25113 *dnaA(cos)*		0.608 ± 0.094	0.413 ± 0.076
BW25113Δ*minC* pBAD24			0.576 ± 0.175

[a] mean and standard deviation from triplicate data

In addition to MinC, the Min system is comprised of MinD and MinE, which work together to prevent cell division near the cell poles, thus restricting division to midcell. TB43 containing the entire *minCDE* operon deleted does not undergo filamentation like the *minC* only deletion. As may be seen in Figure 3.3, *dnaA(cos)* filamentation in the WT background of TB28 did not lead to the same extent of filamentation as in BW25113 background. The combination of TB28 and pBAD24 have been used in a previous study for the overexpression of helicase *dnaB*.[143] This suggests that the overexpression of *dnaA(cos)* is working in this background but the effects of filamentation are subdued. The average correlation value between TB28 vector-only and TB28 *dnaA(cos)* was 0.717 ± 0.107 (Table 3.3). Also, it was found that *dnaA(cos)* expression led to an increase in the proportion of debris (<1 μm³) in Δ*minCDE* (Figure 3.3A, blue line) compared to Δ*minCDE* vector-only (Figure 3.3A, green line). The average correlation value between

these two strains was 0.323 ± 0.254, suggesting that these two strains had a low positive correlation. *dnaA(cos)* overexpression also led to hyper-initiation of chromosomal replication in the Δ*minCDE* background (Figure 3.3C). The DNA ratio of TB43 (*minCDE* mutant*)* was 5.7 compared to 6.4, that of TB43 *dnaA(cos)*. Overall, it appears that in the absence of the Min system *dnaA(cos)* is able to cause filamentation.

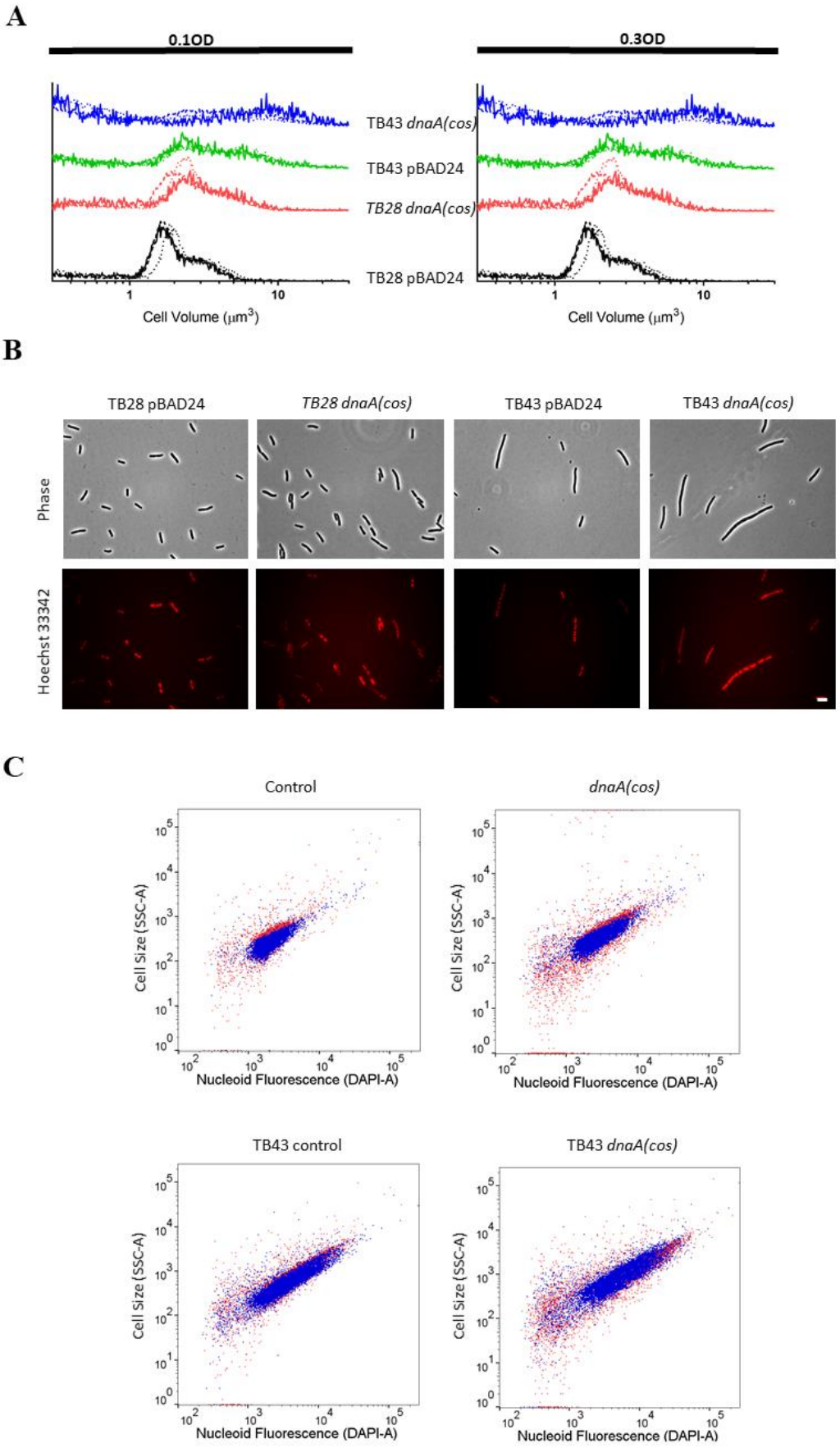
A
0.1OD
0.3OD
TB43 dnaA(cos)
TB43 pBAD24
TB28 dnaA(cos)
TB28 pBAD24
Cell Volume (μm3)
Cell Volume (μm3)
B
TB28 pBAD24
TB28 dnaA(cos)
TB43 pBAD24
TB43 dnaA(cos)
Phase
Hoechst 33342
C
Control
dnaA(cos)
TB43 control
TB43 dnaA(cos)
Cell Size (SSC-A)
Nucleoid Fluorescence (DAPI-A)

Figure 3.3 minCDE is not required for dnaA(cos)-mediated filamentation.
The open reading frame of dnaA(cos) was cloned into expression plasmid, pBAD24. With fresh transformants, the strains TB28 pBAD24, TB28 dnaA(cos), TB43 (ΔminCDE) pBAD24 and TB43 dnaA(cos) were grown at 42°C for 2 hours and then diluted into LB containing 0.2% (w/v) L-arabinose and grown at 30°C. The cultures were sampled at both OD_{600} = 0.1 and 0.3. A) Coulter counter analysis of cell size distributions. The X-axis represents cell volume (μm^3) and the Y-axis represents the percentage of cells at any given volume. Data is shown in triplicates, the same dash-type refers to same-day experiments. B) Phase-contrast and fluorescent microscopy depicting cell morphology and DNA staining (Hoechst 33342) at OD_{600} = 0.1. The images were acquired on the Zeiss Axioplan microscopy using 100x magnification, Scale bar = 5 μM. C) Flow cytometry performed at OD_{600} = 0.1 with TB28 pBAD24 (control, which was mostly short cells), TB28 dnaA(cos) (mostly filaments), TB43 pBAD24 and TB43 dnaA(cos). In these graphs, the dots represent single events plotted with side scatter area on the x-axis (for cell length) and DAPI area on the Y-axis (for nucleoid intensity). Replicate data shown one in red and the other in blue.

Table 3.3 Correlation matrix of cell size distributions from Coulter counter data when dnaA(cos) is overexpressed in minCDE mutant (mean ± SEM)[a]

	TB28 *dnaA(cos)*	**TB43 (Δ*minCDE)* pBAD24**	**TB43 *dnaA(cos)***
TB28 pBAD24	0.717 ± 0.107	0.544 ± 0.046	0.008 ± 0.176
TB28 *dnaA(cos)*		0.822 ± 0.023	0.150 ± 0.232
TB43 pBAD24			0.323 ± 0.254

[a] mean and standard deviation from triplicate data

3.2.3 Nucleoid occlusion is not required for *dnaA(cos)* filamentation

To prevent Z-rings from forming over the nucleoid, nucleoid occlusion provides spatial and temporal regulation of the Z-ring during the cell cycle. In this study, *dnaA(cos)* overexpression in the *slmA* mutant (Δ*slmA)* background led to increased filamentation over time (Figure 3.4). As seen previously, *dnaA(cos)* overexpression in WT background caused a swelling of the cells, and the nucleoids in all strains appeared to be evenly separated throughout the cell length (Figure 3.4B). For comparison as the experiments were run on the same day in parallel, we have added the controls, BW25113 pBAD24 and BW25113 *dnaA(cos)* as shown in Figure 3.2 to the following figures. The average correlation value between Δ*slmA* vector-only (Figure 3.4A, green line on the left graph) and Δ*slmA dnaA(cos)* (Figure 3.4A) at OD_{600} = 0.1 was 0.578 ± 0.068 (Table 3.4), suggesting that these distributions have a moderate positive correlation and that

dnaA(cos) is slightly causing filamentation in the Δ*slmA* background. Additionally, the average correlation value between Δ*slmA dnaA(cos)* and BW25113 *dnaA(cos)* was 0.583 ± 0.219 compared to an average correlation value between WT and Δ*slmA dnaA(cos)* of 0.090 ± 0.161. This suggests that *dnaA(cos)* overexpression leads to cells displaying a filamentous phenotype rather than a short cell phenotype. As time progressed (at OD_{600} = 0.3) *dnaA(cos)* was able to create longer filaments in Δ*slmA* as expected (Figure 3.4A). Nucleoid analysis demonstrated that *dnaA(cos)* overexpression leads to hyper-initiation in Δ*slmA*, the DNA ratio of Δ*slmA* vector-only was 8.6 compared to 9.5 for Δ*slmA dnaA(cos)* (Figure 3.4C). Additionally, a phenotype of Δ*slmA* is an increase of short cells that contain large amounts of DNA content. Interestingly, in this study when *dnaA(cos)* was overexpressed this sub-population of cells decreased (Figure 3.4C).

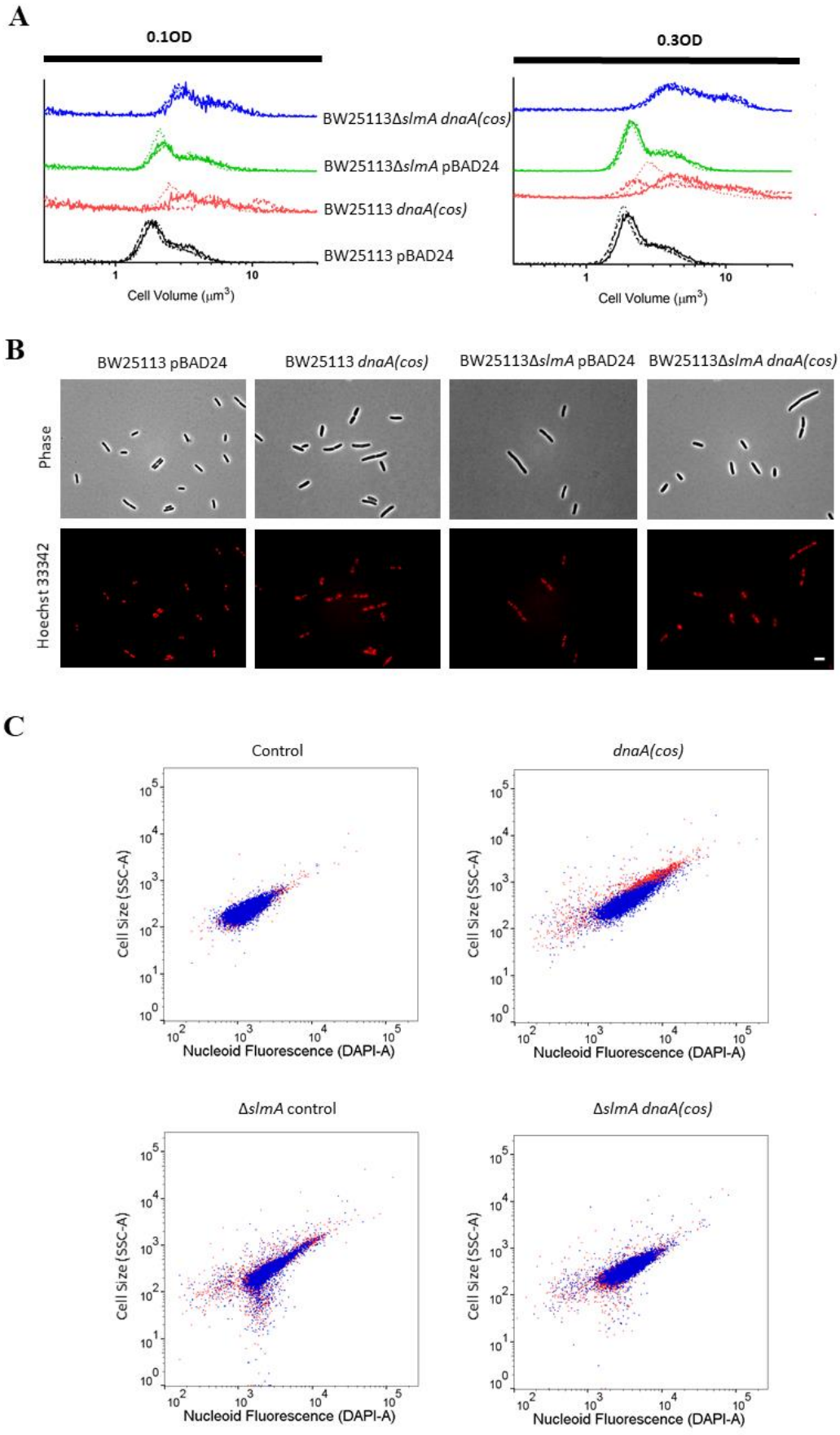
A
0.1OD
0.3OD
BW25113ΔslmA dnaA(cos)
BW25113ΔslmA pBAD24
BW25113 dnaA(cos)
BW25113 pBAD24
Cell Volume (μm3)
B
BW25113 pBAD24
BW25113 dnaA(cos)
BW25113ΔslmA pBAD24
BW25113ΔslmA dnaA(cos)
Phase
Hoechst 33342
C
Control
dnaA(cos)
ΔslmA control
ΔslmA dnaA(cos)
Cell Size (SSC-A)
Nucleoid Fluorescence (DAPI-A)

Figure 3.4 slmA is not required for dnaA(cos)-mediated filamentation.
The open reading frame of dnaA(cos) was cloned into expression plasmid, pBAD24. With fresh transformants, the strains BW25113 pBAD24, BW25113 dnaA(cos), BW25113ΔslmA pBAD24 and BW25113ΔslmA dnaA(cos) were grown at 42°C for 2 hours and then diluted into LB containing 0.2% (w/v) L-arabinose and grown at 30°C. The cultures were sampled at both OD_{600} = 0.1 and 0.3. A) Coulter counter analysis of cell size distributions. The X-axis represents cell volume (μm^3) and the Y-axis represents the percentage of cells at any given volume. Data is shown in triplicates, the same dash-type refers to same-day experiments. B) Phase-contrast and fluorescent microscopy depicting cell morphology and DNA staining (Hoechst 33342) at OD_{600} = 0.1. The images were acquired on the Zeiss Axioplan microscopy using 100x magnification, Scale bar = 5 μM. C) Flow cytometry performed at OD_{600} = 0.1 with BW25113 pBAD24 (control, which was mostly short cells), BW25113 dnaA(cos) (mostly filaments), BW25113ΔslmA pBAD24 and BW25113ΔslmA dnaA(cos). In these graphs, the dots represent single events plotted with side scatter area on the x-axis (for cell length) and DAPI area on the Y-axis (for nucleoid intensity). Replicate data shown one in red and the other in blue.

Table 3.4 Correlation matrix of cell size distributions from Coulter counter data when dnaA(cos) is overexpressed in slmA mutant (mean ± SEM)[a]

	BW25113 *dnaA(cos)*	**BW25113Δ*slmA* pBAD24**	**BW25113Δ*slmA* *dnaA(cos)***
BW25113 pBAD24	0.142 ± 0.240	0.759 ± 0.085	0.090 ± 0.161
BW25113 *dnaA(cos)*		0.418 ± 0.197	0.583 ± 0.219
BW25113Δ*slmA* pBAD24			0.578 ± 0.068

[a] mean and standard deviation from triplicate data

3.2.4 *dnaA(cos)* filamentation does not require the SOS response

The SOS response is controlled by two key genes, *lexA* and *recA*. RecA senses DNA damage and is required for the cleavage of the SOS response repressor LexA to enable the transcription of a set of downstream genes in the SOS response. Therefore, to initially address whether the SOS response could be required for *dnaA(cos)* filamentation, the *recA* mutant (Δ*recA)* was used. It was found that *dnaA(cos)* overexpression in Δ*recA* did not lead to extensive filamentation, although cell size was more heterogeneous compared to WT and larger than the Δ*recA* only strain (OD_{600} = 0.3, Figure 3.5A). The average correlation between Δ*recA* pBAD24 (Figure 3.5A, green line) and Δ*recA dnaA(cos)* (Figure 3.5A, blue line) at OD_{600} = 0.1 was 0.732 ± 0.079, suggesting that these strains have a high positive correlation. Whereas the average correlation between Δ*recA dnaA(cos)* and BW25113 *dnaA(cos)* (Figure 3.5A, red line) was 0.350 ± 0.231 (a low

positive correlation), suggesting that Δ*recA dnaA(cos)* was not filamentous like BW25113 *dnaA(cos*). Overall, these results were inconclusive, most likely due to these cells being unwell and not fit for performing an experiment of this nature where a lethal gene is being expressed. From the microscopy, it can be seen that in Δ*recA dnaA(cos)* the DNA staining in these cells appears sporadic and not binucleated like WT (Figure 3.5B).

Also, during these studies, it was found that Δ*recA* may not have been viable after long periods of growth with exposure to *dnaA(cos)*. This is demonstrated from the growth curves (Figure 3.1) and from the Coulter counter data (Figure 3.5A, the graph on the right), which shows that at OD_{600} = 0.3, Δ*recA* pBAD24 cells are shorter than WT demonstrating possible premature division. Δ*recA* also appears to decrease the DNA content of the cells (Figure 3.5C). This can also be noted from the DNA ratio values of 7.8 for Δ*recA* pBAD24 and 4.0 for Δ*recA dnaA(cos)*. The degradation of DNA in the Δ*recA dnaA(cos)* background could be due to RecA's role in DNA recombination repair and therefore these results were difficult to interpret. So, instead, the double mutant of *ymfM* and *sulA* was used as these genes are upregulated during the SOS response and required for the direct inhibition of cell division.[139,141]

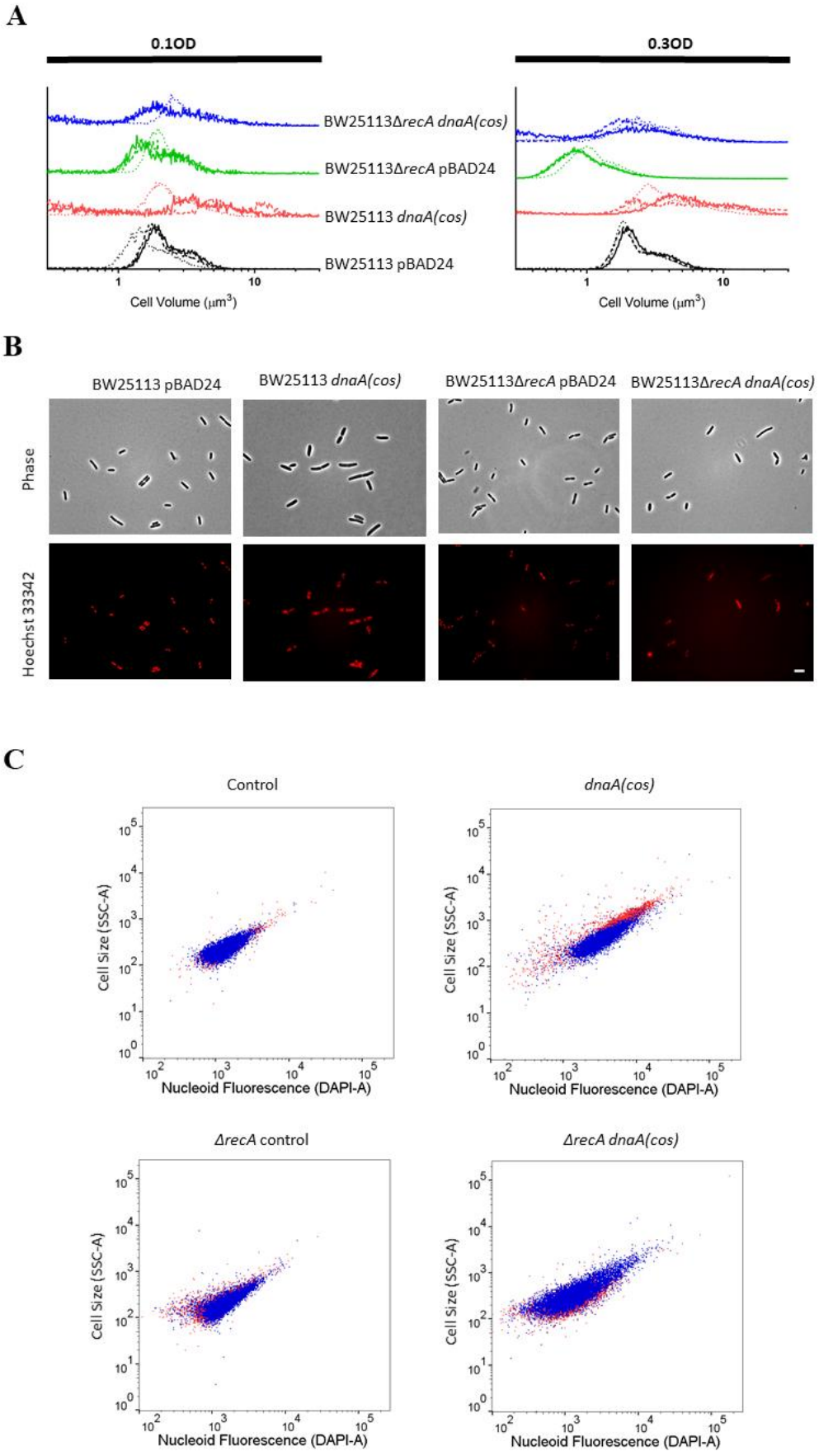
A
0.1OD
0.3OD
BW25113ΔrecA dnaA(cos)
BW25113ΔrecA pBAD24
BW25113 dnaA(cos)
BW25113 pBAD24
Cell Volume (μm3)
B
BW25113 pBAD24
BW25113 dnaA(cos)
BW25113ΔrecA pBAD24
BW25113ΔrecA dnaA(cos)
Phase
Hoechst 33342
C
Control
dnaA(cos)
ΔrecA control
ΔrecA dnaA(cos)
Cell Size (SSC-A)
Nucleoid Fluorescence (DAPI-A)

Figure 3.5 recA is not required for dnaA(cos)-mediated filamentation

The open reading frame of dnaA(cos) was cloned into expression plasmid, pBAD24. With fresh transformants, the strains BW25113 pBAD24, BW25113 dnaA(cos), BW25113ΔrecA pBAD24 and BW25113ΔrecA dnaA(cos) were grown at 42°C for 2 hours and then diluted into LB containing 0.2% (w/v) L-arabinose and grown at 30°C. The cultures were sampled at both OD_{600} = 0.1 and 0.3. A) Coulter counter analysis of cell size distributions. The X-axis represents cell volume (μm^3) and the Y-axis represents the percentage of cells at any given volume. Data is shown in triplicates, the same dash-type refers to same-day experiments. B) Phase-contrast and fluorescent microscopy depicting cell morphology and DNA staining (Hoechst 33342) at OD_{600} =0.1. The images were acquired on the Zeiss Axioplan microscopy using 100x magnification, Scale bar = 5 μM. C) Flow cytometry performed at OD_{600} = 0.1 with BW25113 pBAD24 (control, which was mostly short cells), BW25113 dnaA(cos) (mostly filaments), BW25113ΔrecA pBAD24 and BW25113ΔrecA dnaA(cos). In these graphs, the dots represent single events plotted with side scatter area on the x-axis (for cell length) and DAPI area on the Y-axis (for nucleoid intensity). Replicate data shown one in red and the other in blue.

Table 3.5 Correlation matrix of cell size distributions from Coulter counter data when dnaA(cos) is overexpressed in recA mutant (mean ± SEM)[a]

	BW25113 *dnaA(cos)*	**BW25113Δ*recA* pBAD24**	**BW25113Δ*recA* *dnaA(cos)***
BW25113 pBAD24	0.142 ± 0.240	0.735 ± 0.095	0.893 ± 0.034
BW25113 *dnaA(cos)*		-0.333 ± 0.173	0.350 ± 0.231
BW25113Δ*recA* pBAD24			0.732 ± 0.079

[a] mean and standard deviation from triplicate data

To determine whether the SOS response is required for *dnaA(cos)* filamentation, a double mutant of *ymfM* and *sulA* (Δ*ymfM*Δ*sulA)* was used. It was found that with *dnaA(cos)* overexpression in this strain, slight filamentation was observed, and it increased over time (Figure 3.6A). The average correlation between Δ*ymfM*Δ*sulA* pBAD24 (Figure 3.6A, green line) and Δ*ymfM*Δ*sulA dnaA(cos)* (Figure 3.6A, blue line) at OD_{600} = 0.1 was 0.697 ± 0.145 demonstrating that these two strains have a moderate positive correlation. The average correlation between *dnaA(cos)* and Δ*ymfM*Δ*sulA dnaA(cos)* was 0.853 ± 0.118 which may suggest that filamentation is also occurring in the double mutant strain with *dnaA(cos)* overexpression. There were no obvious DNA defects from the DNA staining (Figure 3.6B).

In the Δ*ymfM*Δ*sulA* background, it was difficult to reproduce adequate filamentation. This may suggest that there is another condition that is required in addition to these genes absence to lead to filamentation. DNA ratios of these stains also varied highly through replicates and it was found that Δ*ymfM*Δ*sulA* pBAD24 had DNA ratios of 4.0 and 6.5 on day 1 and 2, respectively (Figure 3.6C). Whereas Δ*ymfM*Δ*sulA dnaA(cos)* has DNA ratio values of 4.1 and 8.3 on day 1 and 2, respectively (Figure 3.6C). Day 1 results suggest that *dnaA(cos)* overexpression does not lead to hyper-initiation whereas Day 2 results suggest that it does. Overall, due to the variability of the results, the data is inconclusive. Therefore, the next approach we used to determine which pathway *dnaA(cos)* requires to cause filamentation was transcriptomics.

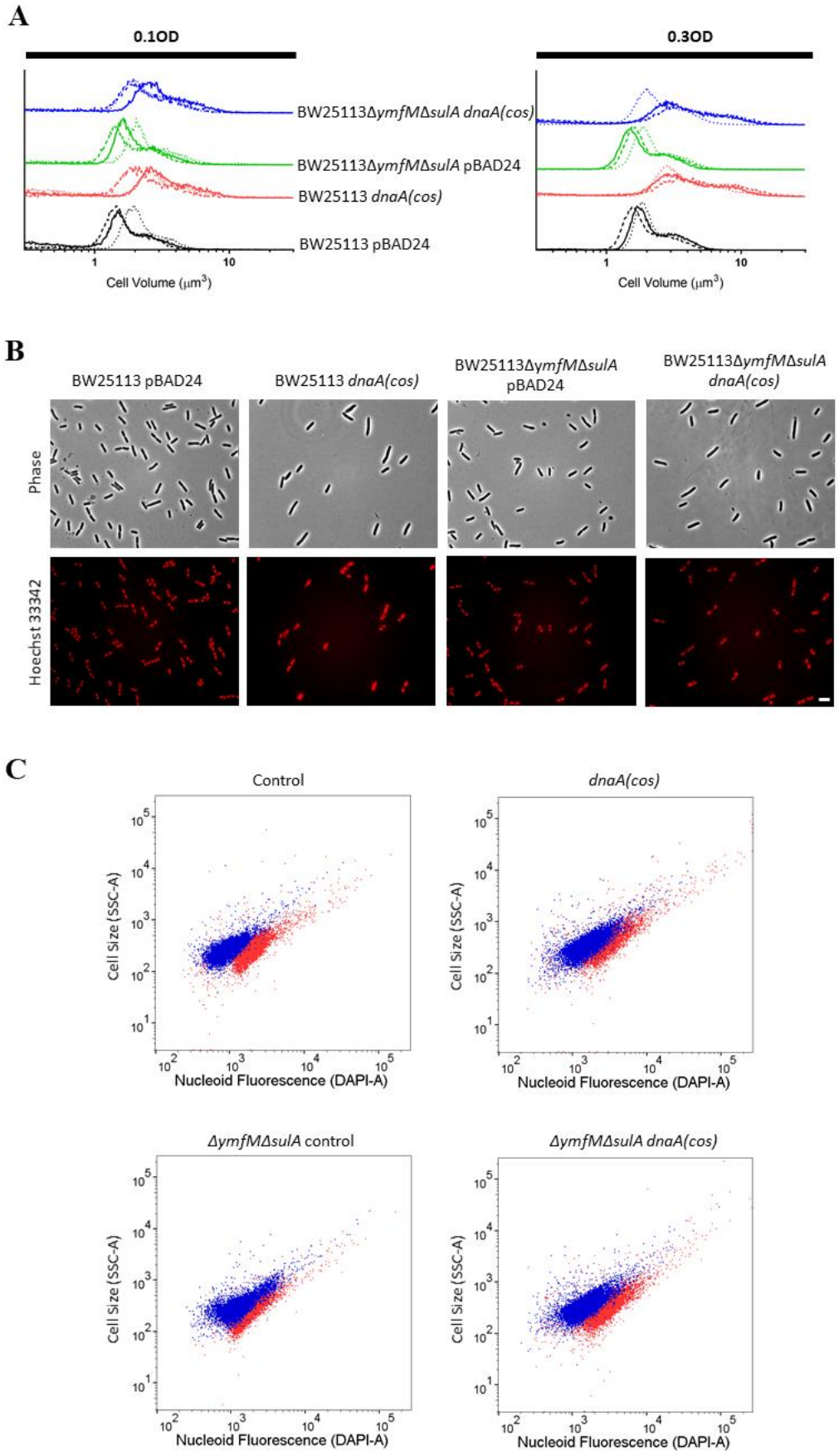
A
0.1OD
0.3OD
BW25113ΔymfMΔsulA dnaA(cos)
BW25113ΔymfMΔsulA pBAD24
BW25113 dnaA(cos)
BW25113 pBAD24
Cell Volume (μm3)
B
BW25113 pBAD24
BW25113 dnaA(cos)
BW25113ΔymfMΔsulA pBAD24
BW25113ΔymfMΔsulA dnaA(cos)
Phase
Hoechst 33342
C
Control
dnaA(cos)
ΔymfMΔsulA control
ΔymfMΔsulA dnaA(cos)
Cell Size (SSC-A)
Nucleoid Fluorescence (DAPI-A)

Figure 3.6 ymfM and sulA are not required for dnaA(cos)-mediated filamentation
The open reading frame of dnaA(cos) was cloned into expression plasmid, pBAD24. With fresh transformants, the strains BW25113 pBAD24, BW25113 dnaA(cos), BW25113ΔymfMΔsulA pBAD24 and BW25113ΔymfMΔsulA dnaA(cos) were grown at 42°C for 2 hours and then diluted into LB containing 0.2% (w/v) L-arabinose and grown at 30°C. The cultures were sampled at both OD_{600} = 0.1 and 0.3. A) Coulter counter analysis of cell size distributions. The X-axis represents cell volume (μm^3) and the Y-axis represents the percentage of cells at any given volume. Data is shown in triplicates, the same dash-type refers to same-day experiments. B) Phase-contrast and fluorescent microscopy depicting cell morphology and DNA staining (Hoechst 33342) at OD_{600} =0.1. The images were acquired on the Zeiss Axioplan microscopy using 100x magnification, Scale bar = 5 μM. C) Flow cytometry performed at OD_{600} =0.1 with BW25113 pBAD24 (control, which was mostly short cells), BW25113 dnaA(cos) (mostly filaments), BW25113ΔymfMΔsulA pBAD24 and BW25113ΔymfMΔsulA dnaA(cos). In these graphs, the dots represent single events plotted with side scatter area on the x-axis (for cell length) and DAPI area on the Y-axis (for nucleoid intensity). Replicate data shown one in red and the other in blue.

Table 3.6 Correlation matrix of cell size distributions from Coulter counter data when dnaA(cos) is overexpressed in ymfM sulA double mutant (mean ± SEM)[a]

	BW25113 *dnaA(cos)*	**BW25113Δ*ymfM*Δ*sulA* pBAD24**	**BW25113 Δ*ymfM*Δ*sulA* *dnaA(cos)***
BW25113 pBAD24	0.437 ± 0.116	0.942 ± 0.022	0.628 ± 0.195
BW25113 *dnaA(cos)*		0.555 ± 0.109	0.853 ± 0.118
BW25113 Δ*ymfM*Δ*sulA* pBAD24			0.697 ± 0.145

[a] mean and standard deviation from triplicate data

3.2.5 Identification of genes regulated during *dnaA(cos)* filamentation

As we were unable to link the Min system, nucleoid occlusion or the SOS response to *dnaA(cos)* filamentation we used a transcriptomics approach to search for genes that responded to overexpression of *dnaA(cos)*. Strains BW25113 (carrying pBAD24 and pTAB2 vectors) and BW25113 *dnaA(cos)* (carrying pBAD24-*dnaA(cos)* and pTAB2) were induced and grown until OD_{600} = 0.3 and then RNA from duplicate cultures were extracted and then rRNA-depleted RNA was prepared and high-throughput sequenced on an Illumina system (Section 2.6.5). The RNA-seq analysis was performed on the Galaxy interface using DeSeq2 for downstream differential gene expression analysis (Section 2.6.7). The full table of data from this analysis can be found in Supplementary Table S1.

The genome was plotted on a scatterplot of log_2FC versus p-adjusted (i.e. the false discovery rate), and 179 genes were identified to meet the criteria of a p-adjusted value of ≤ 0.05 and $log_2FC \geq \pm 2$ (Figure 3.7, green). Amongst the top two upregulated genes was *ibpB* and *ibp*A, small heat-shock proteins. Two of the most downregulated genes were *btsT*, a pyruvate transporter and BW25113_RS18405, a putative MFS transporter which are located in separate places on the genome.

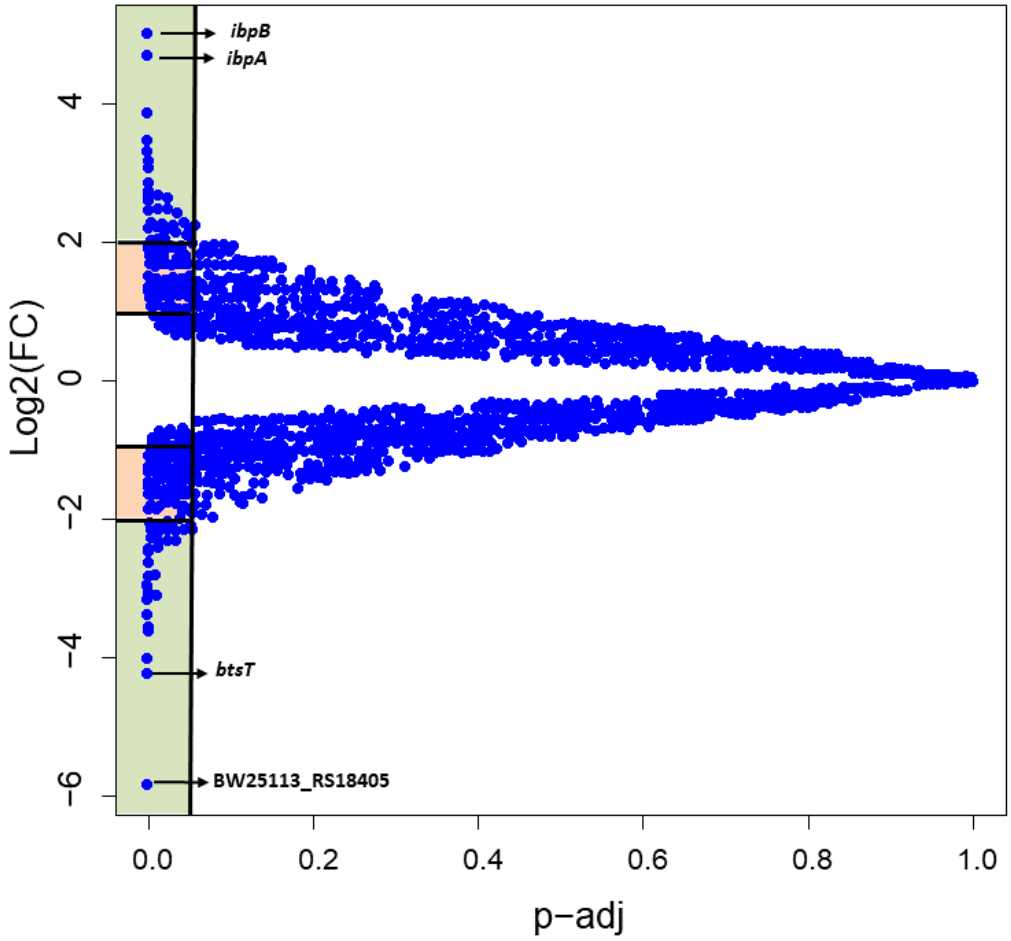

Figure 3.7 Scatterplot summary of genome-wide expression changes in condition BW25113 dnaA(cos) pTAB2 versus BW25113 pBAD24 pTAB2.
There was a total of 640 genes identified to have met the selection criteria of p-adjusted value ≤ 0.05 and $log_2FC \geq \pm 1$ from duplicate experiments (orange shaded boxes plus green shaded boxes). Of these 640, 179 genes were identified to have met the criteria of p-adjusted value ≤ 0.05 and $log_2FC \geq \pm 2$ (green shaded boxes).

The 179 genes found to be significant in the RNA-seq data were characterised by their Clusters of Orthologous Groups (COG) function category, to identify any specific groups that were more regulated than others (Figure 3.8). Interestingly, the results identified

carbohydrate transport and metabolism as the most regulated COG category. Most of the genes downregulated in the carbohydrate transport and metabolism category are involved in galactitol (*gatABZY)*, maltose (*malEFGKMX* and *lamB*), fructose (*fruAK)* metabolism. The downregulation in the maltose system is of interest as it has been reported previously that *E. coli* grown in Luria-Bertani (LB) use maltose and maltodextrins as the first substrates to support growth.[144]

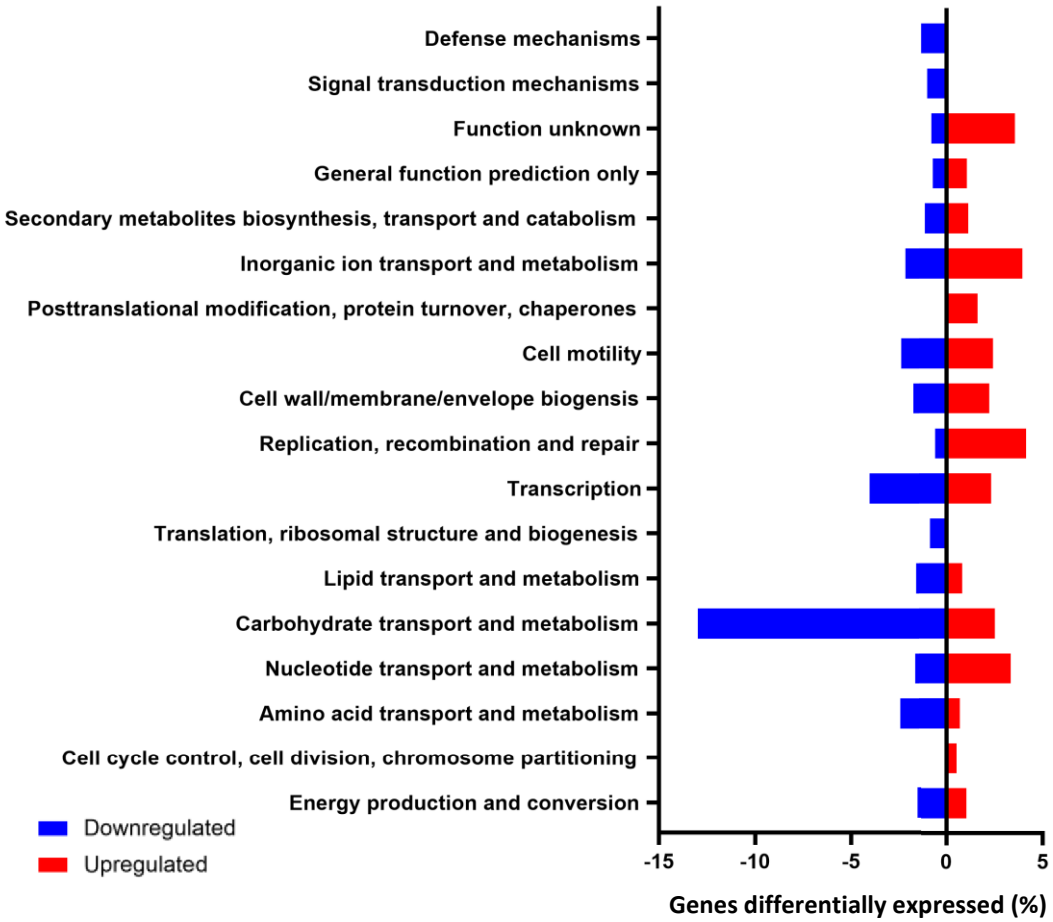

Figure 3.8 Percentage of genes differentially expressed per COG category for condition BW25113 dnaA(cos) pTAB2 versus BW25113 pBAD24 pTAB2
The genes were identified by DeSeq2 and have a p-adjusted value of ≤ 0.05 and 2 ≤ log_2FC ≤ -2 from duplicate experiments.

Out of interest, the transcriptomics data was mined for SOS-specific genes, nucleoid occlusion and Min system genes. Intriguingly, it was found that many of the SOS response genes were found to be upregulated (Figure 3.9). It was noted that *lexA* is also amongst the genes that were upregulated, and this was also seen by Courcelle, et al.[145] when studying the SOS response in mutant *lexA E. coli* to identify the expression profiles of *lexA* dependent and independent genes. Additionally, it was found that the *minC* gene

was significantly downregulated, the *minDE* genes were not regulated and *slmA* was significantly upregulated during *dnaA(cos)* filamentation (Supplementary Table S1).

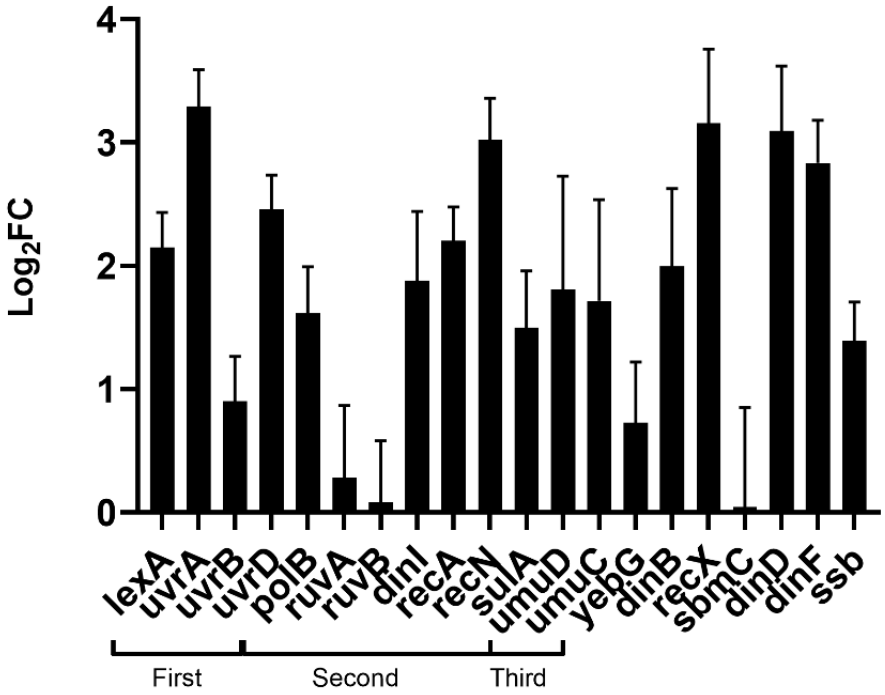

Figure 3.9 Upregulation of expression levels for genes involved in the SOS response. *First, second and third refer to the different stages of SOS induction when the genes are known to be expressed. The log_2FC for each gene from replicate data was determined by DeSeq2 along with the SD.*

Overall, the transcriptomics data combined with the targeted genetics study may suggest that *dnaA(cos)* has numerous effects on the cells. Through transcriptomics, we were able to demonstrate that the SOS response is induced however using the *ymfmsulA* double mutant we were unable to block filamentation during *dnaA(cos)* overexpression. Therefore this may suggest that *dnaA(cos)* causes filamentation through multiple pathways as we were unable to link one specific pathway that was required to cause filamentation.

3.3 Discussion

The purpose of this chapter was to initiate an investigation into which known inhibitory pathway that leads to filamentation is required for the *dnaA(cos)* filamentous phenotype. This would, in turn, provide a better understanding of which pathway of cell division inhibition *cedA* can overcome. This chapter studied several well-known pathways that lead to filamentation such as the Min system, nucleoid occlusion, and the SOS response.

To investigate whether *dnaA(cos)* filamentation required *minCDE, slmA, recA* or *ymfMsulA, dnaA(cos)* was overexpressed from pBAD24 in the mutant backgrounds. In the absence of *minCDE, slmA, recA* and *ymfMsulA* filamentation was observed when *dnaA(cos)* was expressed, demonstrating that DnaA(cos) filamentation does not require the Min System, nucleoid occlusion, or the SOS response. Also, DNA ratio data showed that in the Δ*slmA* Δ*ymfM*Δ*sulA* and Δ*minCDE* backgrounds *dnaA(cos)* was able to cause hyper-replication, further supporting the view that these pathways are not required for the *dnaA(cos)* phenotype. Additionally, the DNA ratio of Δ*recA dnaA(cos)* overexpression was decreased compared to the Δ*recA* empty vector, suggesting that perhaps in Δ*recA dnaA(cos)*-overexpression, hyper-initiation of DNA replication is causing a large number of DNA lesions that are leading to an increase of linear DNA that is being degraded (possibly by RecBCD). In DNA recombinational repair, RecBCD forms an exonuclease complex that works along with RecA and repairs DNA damage detected during DNA replication.[146] After RecBCD unwinds and degrades the double-stranded DNA, it interacts with RecA to promote strand exchange with a homologous DNA region.[146] It was found by Kuzminov and Stahl[147] that in the absence of RecA, χ sites (a regulatory element that acts to control the degradative function of RecBCD)[148] do not work and therefore RecA is needed to turn off degradation caused by the RecBCD enzyme.[147] Therefore, it was speculated that due to hyper-initiation causing breaks in the DNA strands, in the absence of RecA this damage is not repaired and leads to DNA degradation.

Genetic studies did not reveal one pathway that was responsible for *dnaA(cos)* filamentation therefore we employed transcriptomics studies to help identify any specific gene expression that could be responsible. In addition to the upregulation of the SOS

genes, this study showed that the two most upregulated genes during *dnaA(cos)* filamentation were heat shock proteins *ibpA* and *ibpB*. It is known that some heat shock proteins are induced to make bacterial cells tolerate the heat and other stresses such as oxidative stress.[149] More specifically it was found that the overexpression of *ibpA* and *ibpB* increased *E. coli* cells resistance to heat, ethanol and superoxide stress.[150] Interestingly, *ibpA* and *ibpB* were found to be induced during the study by Courcelle, et al.[145] in a LexA-dependent manner during the SOS response. Even though the SOS response is induced during *dnaA(cos)* filamentation, filamentation was still observed in Δ*ymfMΔsulA dnaA(cos)*. It has been demonstrated that by deleting both *ymfM* and *sulA* filamentation will be blocked during the SOS response.[141] This suggests that *dnaA(cos)* triggers multiple filamentation mechanisms including the SOS response. Katayama, et al.[15] also concluded that filamentation caused by *dnaA(cos)* in the KA441 strain was independent of *sulA*. They stated that in the absence of *sulA* the cells still appeared to have a filamentous shape, although the data for this was not presented.

This study found the downregulation of many pathways involved in carbohydrate metabolism such as the *gat, mal,* and *fru* operons in response to *dnaA(cos)* expression. These pathways were also found to be downregulated during UV irradiation by Courcelle, et al.,[145] but the reason for why these pathways are specifically downregulated remains unknown. However, it stands to reason that this further supports the hypothesis that *dnaA(cos)* could cause filamentation, at least in part, by activating the SOS response.

For the first time, the work presented in this chapter shows that *dnaA(cos)* may cause filamentation at its permissive temperature of 30°C through both SOS-dependent and SOS-independent pathways. Further work is required to identify the molecular mechanisms that lead to filamentation in the *dnaA(cos)* mutant. Overall, these results suggest that *cedA* may be able to overcome multiple pathways of inhibition of cell division through a direct or indirect manner, and this will be explored further in Chapter 4.

3.4 Methods

3.4.1 Bacterial Strains and Growth Conditions

E. coli BW25113 and the mutations in genes: *recA, slmA, minC* were obtained from the *E. coli* Genetic Stock Center (Yale University, USA). TB28 (WT) and TB43 (*minCDE* mutant) were kindly provided by Bernhardt and De Boer [91,118]. The BW25113 double mutant of *ymfM* and *sulA* was kindly provided by S. Ansari (UTS). The strains were all transformed with pBAD24 and pBAD24-*dnaAcos.* The strains were routinely transformed through electroporation (Section 2.4.1) for each experiment and each colony selected was cultured at 42°C overnight in liquid Luria Broth (LB) containing ampicillin (100 μg/mL). On the day of the experiment, the cultures were diluted down to OD_{600} = 0.1 from an overnight culture and incubated for 2 hours at 42°C. After 2 hours the cultures were diluted into LB containing 0.2% (w/v) L-arabinose and incubated at 30°C until 0.1 and OD_{600} = 0.3 (3.5 and 5.5 generations, respectively) where samples were collected and fixed in 0.4% PFA. This was to determine whether *dnaA(cos)* was able to cause filamentation without toxicity or cell death as seen by the cell length continuing to increase over the generations.

3.4.2 Measuring DNA Ratio

Flow cytometry was used to measure DNA content through Hoechst 33342 staining (Section 2.9.3). The median of the nucleoid fluorescence area (DAPI-A) was divided by the median of side scatter area (SSC-A) to provide an arbitrary value of the ratio of DNA content per cell.

Chapter 4
CedA can prevent many modes of filamentation

4.1 Introduction

Uropathogenic *E. coli* (UPEC) is commonly found in the human intestinal tract where it is rarely the cause of disease. However, UPECs virulence factors allow it to disseminate and colonise the urinary tract and undergo a multi-stage intracellular infection cycle within bladder cells.[10] During the infection cycle, UPEC undergoes numerous morphological changes from short rod-shaped bacteria, to a coccoidal shape during the formation of biofilm-like IBCs, to filamentous bacterial cells accompanying rupture of the bladder cells during bacterial dispersal, and finally, they undergo reversal back to their original short rod shape which has the capacity to re-infect neighbouring bladder cells.[10] The mechanisms that are required for filamentation and reversal remain unknown.

Bacterial filamentation is thought to be a survival mechanism used under stressful conditions, for example when UPEC infects the urinary tract. It is thought that the cells undergo filamentation to 1) evade the host immune system and, 2) provide a stronger attachment to surfaces to overcome shear forces from urine flow.[14] Despite filamentation known to be a critical process that the cell undergoes, the molecular mechanisms are unknown. Recently, Khandige et al.[16] found that UPECs reversible filamentation requires *damX*. DamX is known to participate in cytokinesis in bacteria as its mutation in combination with *dedD* or other cell division genes lead to division defects.[105,151] However, the complete mechanism that allows for UPEC filamentation remains to be solved. In addition to filamentation, there is little known about how the filaments can then divide into rod-shaped cells, to allow re-infection of neighbouring bladder cells.[10,11] One gene that has been implicated in the prevention of bacterial filamentation is *cedA*.[15,108]

Although *cedA* was first discovered in 1997 there have been limited studies to understand its function in *E. coli*. There are data to suggest that *cedA* is upregulated during the later (dispersal) stages of UPECs lifecycle[16] and that *cedA* overexpression is capable of preventing filamentation and cell death in a mutant strain of *E. coli* K-12, *dnaA(cos)*, which at a reduced growth temperature over-initiates chromosome replication and filaments extensively before cell death.[15] However, there is little data to explore whether its ability to prevent filamentation is restricted to replication initiation, as seen in the

dnaA(cos) background, or whether it is a more general response to many or all forms of filamentation, including that seen in UTIs. As we demonstrated in Chapter 3, *dnaA(Cos)* filamentation may be caused through multiple pathways. Therefore as *cedA* can prevent *dnaA(cos)* filamentation this suggests that *cedA* may be able to prevent filamentation caused by many cell division blocks. Additionally, it is not known whether *cedA* can promote the reversal of filaments into short-rod shaped bacteria, in particular, when they are already formed.

In this chapter, we used a combination of phylogenetics, transcriptomics, genetic studies, and an *in vitro* flow chamber UTI model to explore the function of CedA through its overexpression. A major aim of this chapter was to determine whether *cedA's* ability to prevent filamentation of *dnaA(cos)* as shown by Katayama, et al.[15] was specific to *dnaA(cos)* or a general function of *cedA.* To approach this question, several different genes and mutants that are known to cause filamentation (referred to as filamentors) were tested. These include genes and mutants involved in different aspects of cell biology such as metabolism (*zwf),* cell division (*ftsZ-yfp),* the SOS (DNA damage) response (*recAtif)*, nucleoid occlusion (*slmA and slmA*-DNA complexes), and DNA replication (*dnaA(cos))* were chosen. To perform this study, a novel plasmid vector, pTAB2, was constructed for the co-expression of *cedA* with a filamentor expressed from pBAD24. This plasmid was constructed to allow for low-copy number gene expression and compatibility of inducers (as it was found that inducers arabinose and IPTG are not compatible due to sugar crosstalk).[152] Additionally as the inducer for pTAB2 is anhydrotetracycline it may be used in future to express genes within mammalian cells.[153] We also aimed to determine whether induction of *cedA* could reverse pre-formed filaments.

The next aim of this chapter was to identify the pathways that are regulated during *cedA* overexpression in WT cells and when *cedA* is preventing filamentation of *dnaA(cos),* using transcriptomics.

The final aim was to explore whether *cedA* overexpression in an *in vitro* flow chamber UTI model could also lead to the prevention of UPEC filamentation. A combination of these approaches was expected to allow for a better understanding of why *cedA* is

upregulated during the later stages of UPEC lifecycle and whether it can prevent and/or reverse filamentation in a general manner.

4.2 Results

4.2.1 CedA phylogenetics

CedA is known to have structural homology to known transcription factors but does not have any sequence homology to any other known proteins.[107] It is known that CedA is conserved amongst UPEC strains,[12] however, there is little phylogenetic information on the evolution and conservation of CedA. Using a bioinformatics approach, we set out to understand in which branches of life CedA can be found. Using a combination of JACKHMMER and Blastp database searches, protein sequences of CedA were gathered that had the highest query coverage, an E-value score of 3.5e-29 or less and had undergone a reciprocal Blastp search in order to verify them as homologs. From a MUSCLE multiple sequence alignment, a bootstrapped maximum-likelihood (ML) consensus tree was generated (Figure 4.1).

Interestingly, CedA was only found in the Bacteria domain of life, and more specifically, it was only found in 20 genera of bacteria as seen in Figure 4.1. All of the genera identified fall into the Enterobacteriaceae family. Nine out of the 20 genera are also bacteria that are commonly found to inhabit and/or cause infection in the gastrointestinal tract, and in some cases, also the urinary tract; for example, *Salmonella sp.*, *Citrobacter sp.*, *Kluyvera sp., Klebsiella sp., Pseudoescherichia sp.* and *Enterobacter sp.* Five of the 20 genera, namely *Franconibacter sp., Superifiebacter sp., Phyotobacter sp., Izhakiella sp.,* and *Cedecea sp.,* are not well known and their possible role in disease has not been explored. Additionally, CedA was also found in non-pathogenic genera such as *Shimwellia sp.* and *Mangrovibacter sp.*

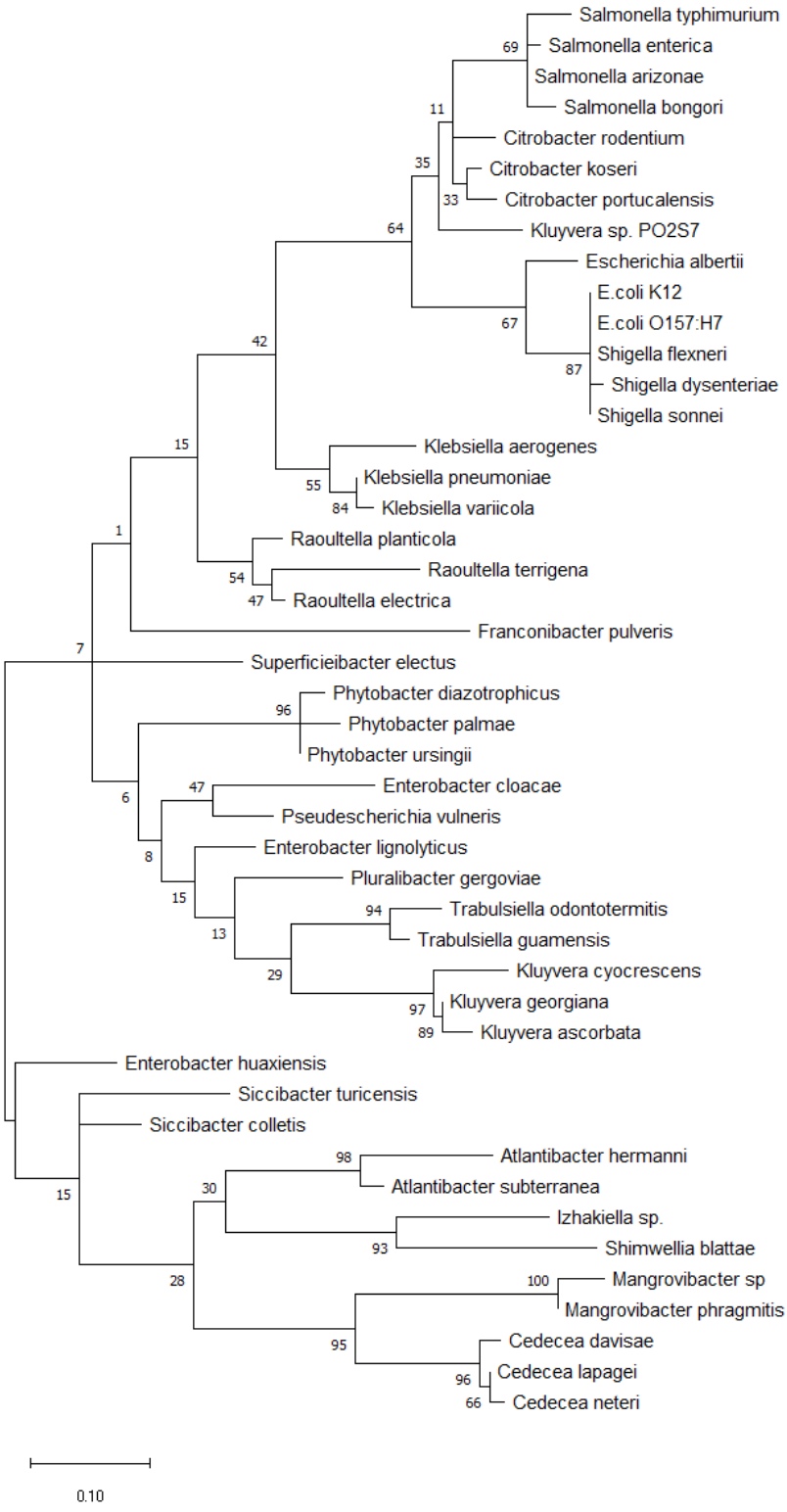

Figure 4.1 Phylogenetic analysis of CedA demonstrates it is only found in the Enterobacteriaceae family.

A bootstrapped maximum likelihood tree was generated in MEGA-X from a multiple sequence alignment built from CedA homologs identified by a survey of the three domains of life using JACKHMMER and Blastp searches. Bootstrapping provides a measure of confidence in each branchpoint in the phylogenetic tree. The branch lengths are measures of the average number of substitutions per amino acid site.

4.2.2 CedA overexpression in WT cells can promote cell division

Katayama, et al.[15] reported with one replicate of flow cytometry data that when *cedA* was overexpressed in WT background *cedA* overexpression led to a change in the timing of cell division. There is no other published data on what phenotype *cedA* overexpression has in WT *E. coli*. This project set out to determine what effect *cedA* overexpression had on the cell in terms of cell growth, cell size, and initiation of DNA replication. To test this, *E. coli* strains BW25113 and UTI89 were used, due to them being pertinent to the work in this thesis. *cedA* was expressed from pTAB2 using 0.2 µg/mL anhydrotetracycline for induction through multiple culture passages, maintaining mid-log growth to ensure that growth was steady and that the effect of the overexpression would be seen in effectively all cells. All cell size data were obtained using a Coulter Counter, which measures the cell volumes of hundreds of thousands of cells per sample, which provides a histogram distribution of cell size in the population (*Section 2.9.1)*. To determine how similar any two cell volume distributions were, a Pearson correlation statistical analysis was performed. A value of 1 indicates that the two distributions being compared are a perfect correlation. A value of 0 means that the samples are not correlated and a value of -1 means that the samples are perfectly anti-correlated.

As summarised in Table 4.1, it was found that *cedA* overexpression did not significantly affect the growth rate when compared to vector-only in either BW25113 or UTI89 (Figure 4.2A). Interestingly, Coulter cytometry showed that during *cedA* overexpression the bacterial cells became shorter than WT in both backgrounds (Figure 4.2B). The average correlation between BW25113 and BW25113 *cedA* was 0.730, while the average correlation between UTI89 and UTI89 *cedA* was 0.145. It is evident that *cedA* overexpression leads to a greater difference in the UTI89 background compared to the BW25113 background. There were a lot more instances of shorter cells in the UTI89 *cedA* strains when compared to UTI89 as can be seen by microscopy (Figure 4.2C). Additionally, DNA staining showed that there was no obvious difference between WT and *cedA* overexpression in either background, as each cell appeared typically binucleated (Figure 4.2C). Overall, from the cell size distributions, it is evident that the overexpression of *cedA* leads to the promotion of cell division without changing the growth rates.

Finally, we determined whether *cedA* overexpression could affect the frequency and synchronicity of initiation of DNA replication, as *cedA* has been implicated in regulating cell division in strains with altered replication initiation (*dnaA(cos)*). To do this, we used the chromosomal runout method, which combines the antibiotics rifampicin, to inhibit transcription and therefore new rounds of chromosome replication, and cephalexin to inhibit cell division (*Section 2.6.8*). After chromosomal runouts, the cells will only contain complete chromosomes and then flow cytometry is used to count the number of chromosomes per cell. This will provide information on the status of chromosomal replication when the antibiotics were added. However, for unknown reasons we found that the chromosomal runout method did not work in the UTI89 strain, as there were no peaks for the different numbers of chromosomes (data not shown). The method did work in BW25113, a K-12 strain for which the method has previously been validated, and the results showed that *cedA* overexpression does not affect the synchrony of initiation of chromosome replication in the cells compared to the WT (Figure 4.2D). We observed from the flow cytometry data that there are two distinct peaks in both BW25113 and BW25113 *cedA* and they both have approximately the same intensity for nucleoid staining, suggesting that both strains contain the same number of nucleoids, and therefore have equivalent frequency and synchronicity of initiation of chromosome replication.

Table 4.1 Doubling times of cedA overexpression in E. coli backgrounds BW25113 and UTI89

	BW25113 pTAB2	**BW25113 *cedA***	**UTI89 pTAB2**	**UTI89 cedA**
Doubling Time[a]	28.90 ± 3.48	29.10 ± 2.45	29.32 ± 6.64	29.58 ± 4.83
p-value[b]	0.5086		0.5473	

[a] Averaged doubling times from replicate data

[b] The p-value is from an unpaired t-test comparing vector-only to *cedA* for each strain.

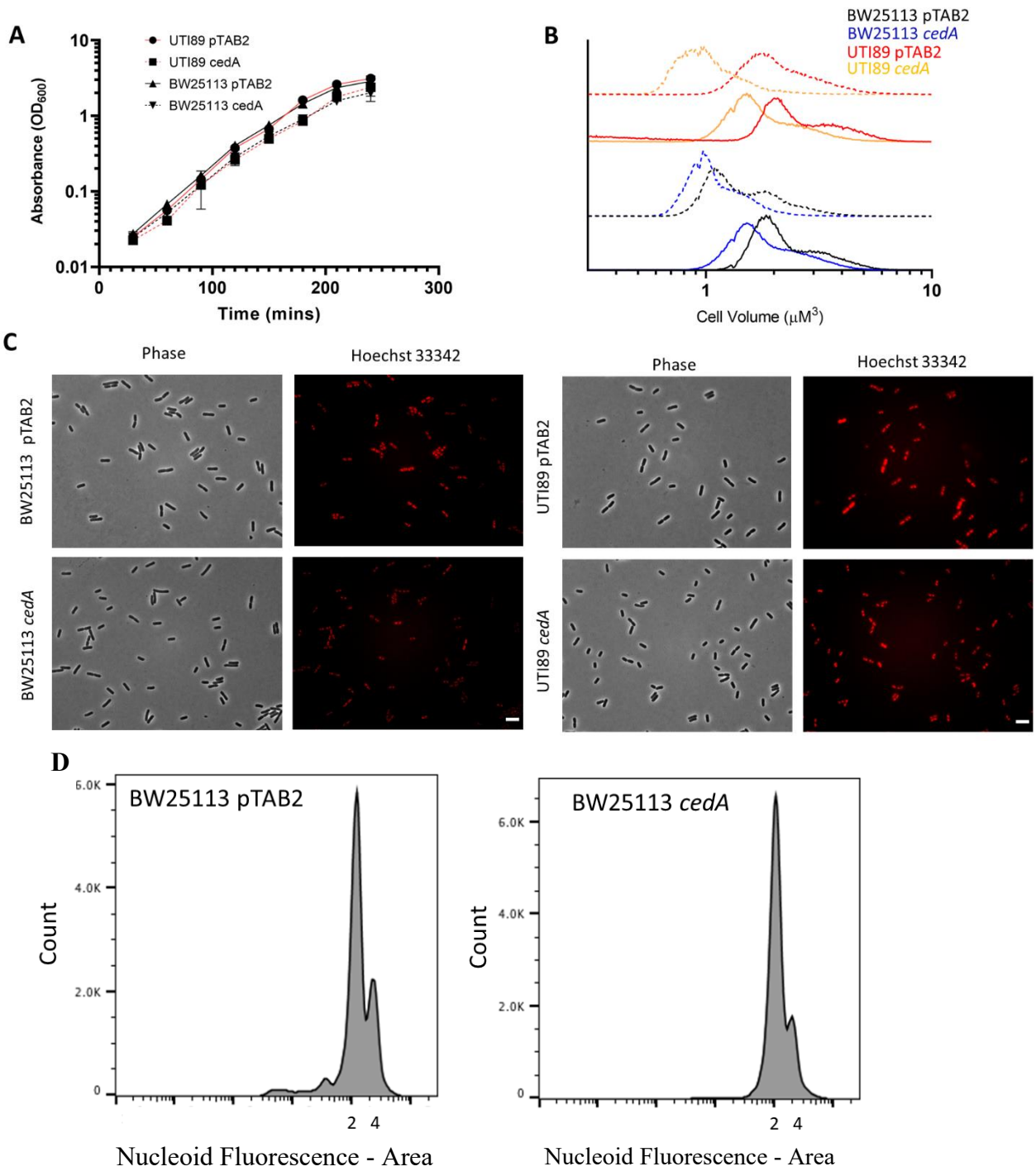

Figure 4.2 cedA overexpression in BW25113 and UTI89 promotes cell division.
The cedA open reading frame was cloned into pTAB2 and induced with 0.2 μg/ml of anhydrotetracycline through two passages whereby the cultures were diluted down to OD_{600} = 0.01 and grown to mid-log a total of 3 times. A) A comparison of cell growth between WT and cedA overexpression was performed by measuring optical density and it was plotted against time in minutes. Duplicate data was averaged and plotted on this graph. In both backgrounds, cedA overexpression showed no significant difference in growth compared to the vector only. B) The cell volume of each strain was also measured using the Coulter counter as this is generally proportional to cell length. Cell volume

distributions from Coulter counter data in replicates (replicate 1 (solid lines) and replicate 2 (semi-solid lines)) at OD_{600} = 0.5. Cell length distributions demonstrated that cedA overexpression in either background led to shorter cells. C) Phase-contrast and fluorescence microscopy of all four strains. The DNA of the bacterial cells was stained with Hoechst 33342 to observe any nucleoid morphology. Scale bar = 5 μM. (Section 2.9.2). D) To determine if cedA overexpression led to any changes in DNA replication initiation chromosomal runouts were performed. To count the number of chromosomes per cell the cells were stained with DAPI and the flow cytometer was used to detect the relative number of nucleoids in the bacterial cells. For the chromosome runouts the antibiotics rifampicin (300 μg/mL) and cephalexin (15 μg/mL) were added each culture at OD_{600} = 0.1 and left to incubate for 3 hours. The graphs are from one replicate and the trend was similar in the second replicate.

4.2.3 Identification of genes that are regulated during *cedA* overexpression

To enhance our understanding of how *cedA* can promote cell division in WT cells, we used transcriptomics to identify which genes and/or pathways that are regulated during *cedA* overexpression in BW25113 compared to vector-only. We performed the experiment, as mentioned in the previous section, with strains BW25113 pBAD24 pTAB2 (WT, vector-only) and BW25113 pBAD24 pTAB2-*cedA* (*cedA* overexpression) in rich medium. The bacterial cells were harvested at an OD_{600} = 0.5 and the RNA was extracted (*Section 2.6.5).*

RNA-seq data analysis was performed on the Galaxy platform using DeSeq2 for the differential gene expression analysis (*Section 2.6.7*). The full table of data from this analysis can be found in Supplementary Table S2. The genome was plotted on a scatterplot of log_2FC versus p-adjusted (false discovery rate) and the genes that met the criteria are found in the shaded orange box on the scatterplot (Figure 4.3). In total 191 genes were identified to have a p-adjusted of ≤ 0.05 and $log_2FC \geq \pm 1$. As expected, the overexpression of *cedA* was found to be high; 8-fold (log_2) upregulated.

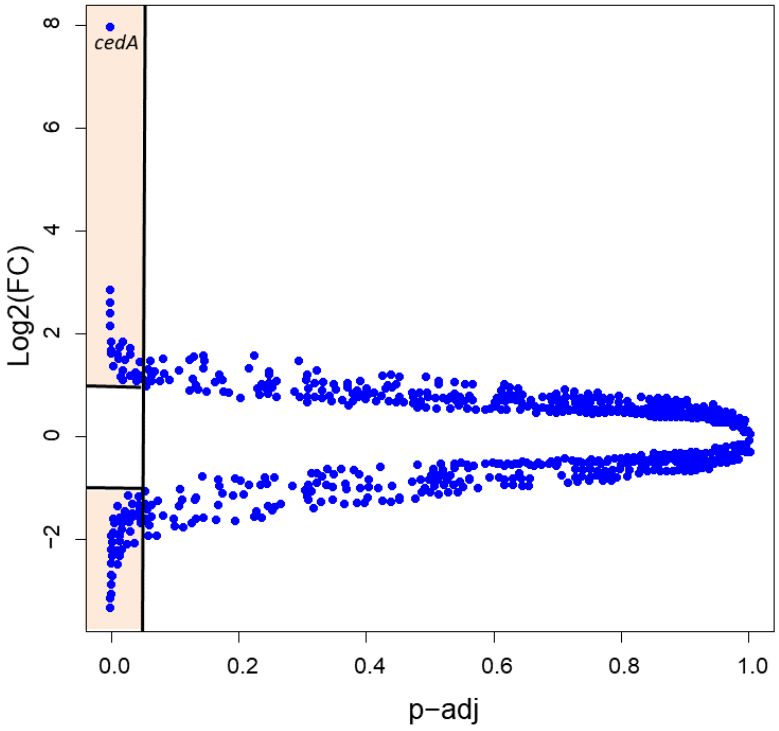

Figure 4.3 Scatterplot summary of genome-wide expression changes in condition BW25113 pBAD24 pTAB2-cedA versus BW25113 pBAD24 pTAB2.
The orange boxes indicate the selection criteria of p-adjusted value ≤ 0.05 and $log_2FC \geq \pm 1$ from duplicate experiments.

There were 191 genes found to have met the selection criteria. There were no obvious genes related to our current knowledge of cell division that would help explain how CedA is able to promote cell division. Therefore, the genes were then characterised by their Clusters of Orthologous Groups (COG) functional category to help identify any specific groups that were regulated more than others (Figure 4.4). This indicated that carbohydrate transport and metabolism, as well as amino acid transport and metabolism, were two of the COG categories with the most regulation. Most genes in these two categories were downregulated during *cedA* overexpression, suggesting that it reduces the use of cell metabolism pathways that would use different carbon sources from glucose.

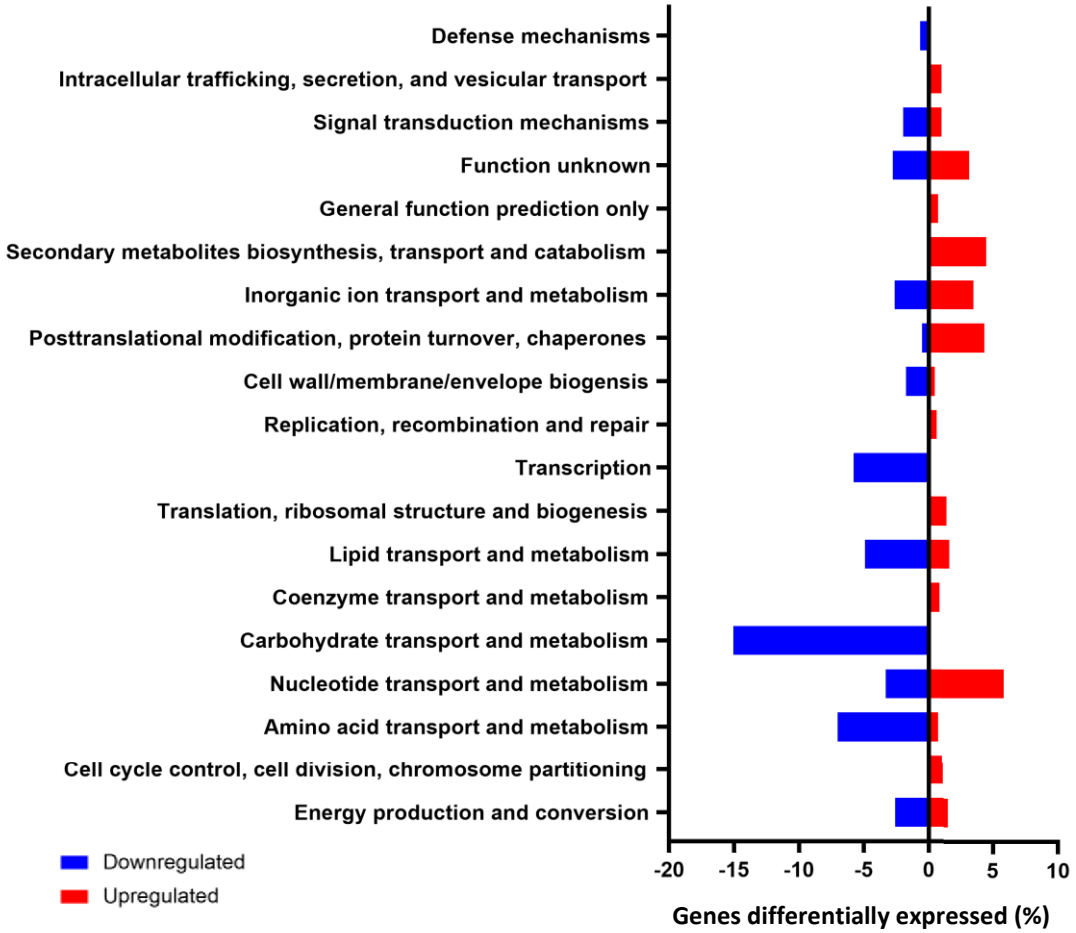

Figure 4.4 Percentage of genes differentially expressed per COG category for condition BW25113 pBAD24 pTAB2 versus BW25113 pBAD24 cedA.
Only the 191 genes that were identified by DeSeq2 and have a p-adjusted value of ≤ 0.05 and 1 ≤ log_2FC ≤ -1 from duplicate experiments were used for the COG analysis.

For example, one pathway that is downregulated between -1.8 to -3.2 log_2FC during *cedA* overexpression is the fructose operon (*fruA, fruK* and *fruB*) which metabolises fructose to fructose 1,6-bisphosphate. Fructose 1,6-bisphosphate is required for the gluconeogenesis pathway. *E. coli* uses gluconeogenesis to synthesise glucose 6-phosphate (a precursor of glycogen and other sugars used in the biosynthesis of cell surface structures). Therefore, it may be possible that *cedA* is able to indirectly reduce to the level of glycogen leading to smaller cell size. Additionally, the entire *rbs* operon (*rbsDACBKR)* was found to be downregulated. This operon encodes for the ribose transport complex and the pathway involves an ATP-binding cassette (ABC) to hydrolyse ATP to transport ribose in the cell in order to use it as a carbon source.[154] Another large proportion of genes downregulated in the carbohydrate transport and metabolism

category is the maltose system. Almost all of the genes involved in this system (*malP, malT, malGFE, malKM, lamB and malX*) are significantly downregulated with log_2FC changes between -1.36 to -2.78. The maltose system has been extensively studied as it is positively regulated by MalT which is only induced in the presence of maltose or maltodextrin in the medium.[155] Overall, the downregulation of these operons demonstrates *cedAs* ability to directly or indirectly control cell metabolism.

On the other hand, most of the *ent* operon (*entCEBAHF)* was upregulated from 1.4 to 1.8 log_2FC. Along with these genes, it was found that *fes* and *fepA* were upregulated too. These genes are involved in iron acquisition, with the *ent* operon involved in siderophore synthesis and *fes* and *fepA* a part of a collection of genes involved in enterobactin uptake and export.[156] Interestingly, genes in the *ent* operon were previously found to be in the top 50 genes upregulated *in vivo* during an *E. coli* UTI.[157] Another example of an upregulated operon during *cedA* overexpression is the *codBA* operon for cytosine deaminase, with an increase of 1.8 and 2.4 log_2FC. These genes are known to be upregulated during culture in a nitrogen-limiting medium. Cytosine deaminase cleaves cytosine to ammonia (the source of nitrogen) and uracil.[158] Nitrogen limitation is also a problem that UPEC must face in the urinary tract as it can lack the urease enzyme to catalyse the hydrolyses of urea to ammonia and CO_2.[157] The majority of the genes downregulated in the amino acid transport and metabolism pathway are involved in isoleucine and valine biosynthesis (*ilv)*. They include *ilvA, ilvBN, ilvC, ilvD, ilvE, ilvL,* with log_2FC values between -1.58 to -3.33. This might suggest that *cedA* is able to control cell metabolism as these cultures were grown in rich media containing high amounts of amino acids.

Overall, this transcriptome study did not clearly implicate any known cell division genes which could explain how CedA is able to promote cell division. For example, *ftsZ* had a log_2FC of 0.538 with a p-adjusted value of 0.548. However, it did suggest that the division effects seen by the overexpression of *cedA* may be a consequence of indirect changes in metabolism regulation. So, the next set of studies was to understand more about the specificity of CedA by looking at how to acts with other modes of division block.

Chapter 4 | cedA can prevent many modes of filamentation

4.2.4 Confirmation that *cedA* can prevent filamentation caused by *dnaA(cos)* in a co-expression system

To determine whether *cedA* has a specific role in preventing *dnaA(cos)* filamentation or a more general role in preventing all filamentation pathways, we created a system that would allow for the simultaneous co-expression of the gene that causes filamentation and *cedA*. We used the plasmids pTAB2 and pBAD24 for simultaneous expression of *cedA* and a filamentor, respectively. To ensure that this system was functional we tested it with *dnaA(cos)* to compare the results found in the previous study, which involved the chromosomal expression of DnaA(cos).[15] In addition to full-length *cedA*, we also tested a truncated *cedA* which had the first 18 amino acids (Δ18*cedA*) deleted as described in Abe, et al.[108] to determine whether the N-terminus of *cedA* would be required for preventing filamentation of different pathways, as it was found that the N-terminus is required for DNA and RNA polymerase binding.[108] We also tested a GFP tagged version of *cedA* (*cedA-gfp*) to determine if this fusion was functional and therefore could be trusted for determining the subcellular localisation of *cedA* in cells during the prevention experiments.

Our co-expression system successfully replicated the prevention of *dnaA(cos*)-caused filamentation by *cedA* (Figure 4.5). To analyse the Coulter cell volume distributions, a correlation statistical analysis was performed to determine how similar the distributions were. Data for the Pearson correlation is from triplicate data, each row shows correlations from same day experiments and should not be compared to values from different rows (Table 4.5B). It is important to note that the cell size distributions in most of the backgrounds exhibited obvious variation day to day despite how smooth the distribution curves are. This is because hundreds of thousands of cells are being measured to create a smooth curve but small changes such as different batches of media can create these day to day differences.

When *dnaA(cos)* was overexpressed in BW25113 (*dnaA(cos)* overexpression), the cells became longer than WT demonstrating filamentation (blue and red lines respectively, Figure 4.5A) and the average correlation between the two strains was 0.263 ± 0.127

demonstrating that these strains have a negligible correlation (Table 4.5B). Once *cedA* was simultaneously expressed with *dnaA(cos)* in BW25113 (*dnaA(cos)* prevention) there was an obvious shift to the cell size distribution (green line, Figure 4.5A) indicating that these cells are shorter. The average correlation between *dnaA(cos) cedA*-prevention and *dnaA(cos)* overexpression was 0.390 ± 0.130 (Figure 4.5B). Whereas the correlation between *dnaA(cos) cedA*-prevention and WT was 0.750 ± 0.381, indicating that *cedA* overexpression can prevent *dnaA(cos)* filamentation in our co-expression system (Table 4.5B). Additionally, Δ18*cedA* and *cedA-gfp* (purple line and orange line respectively, Figure 4.5A) were able to partially prevent filamentation caused by *dnaA(cos)* with average correlation values of 0.717 ± 0.150 and 0.687 ± 0.251 compared to *dnaA(cos)* overexpression. We observed no subcellular localisation of *cedA-gfp* during the prevention of *dnaA(cos)* filamentation, although green fluorescence was seen uniformly throughout the cytoplasm (data not shown).

From the microscopy, we observed that when *dnaA(cos)* is overexpressed, cells become rounder and slightly wider (Figure 4.5C). DNA staining of the *dnaA(cos)* overexpression demonstrates that the cells are no longer binucleated like WT but rather the nucleoids appear larger and smeared along the cell length, consistent with chromosome over-replication (Figure 4.5C). In the *dnaA(cos)* prevention it appears that the overexpression of *cedA* recovers approximately normal nucleoid organisation. Once it was established that this system could prevent *dnaA(cos)* filamentation with *cedA,* as previously seen by Katayama, et al.[15] other pathways that lead to filamentation were tested to determine if *cedA* could also prevent filamentation in the following sections.

A

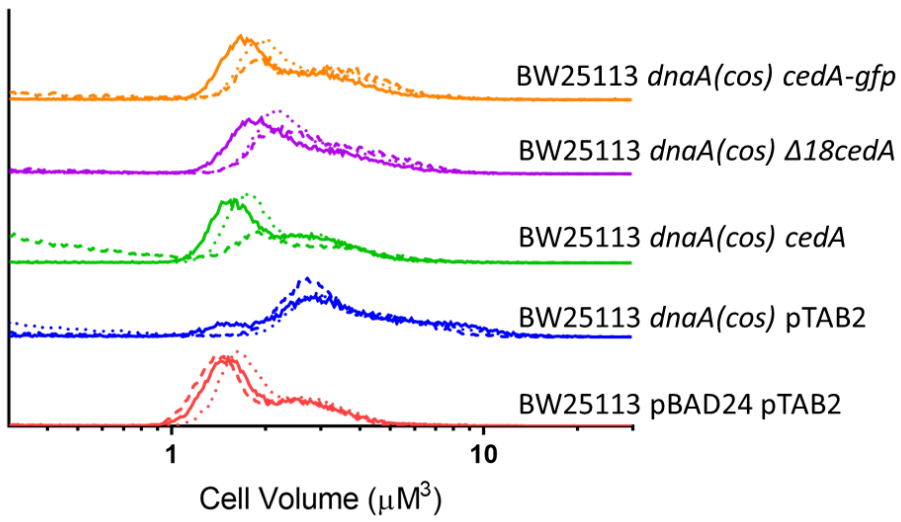

B

	dnaA(cos) **pTAB2**	*dnaA(cos)* *cedA*	*dnaA(cos)* **Δ18***cedA*	*dnaA(cos)* *cedA-gfp*
pBAD24 pTAB2	0.41	0.97	0.75	0.87
	0.19	0.31	0.31	0.40
	0.19	0.97	0.61	0.79
***dnaA(cos)* pTAB2**		0.52	0.64	0.58
		0.39	0.89	0.74
		0.26	0.62	0.48

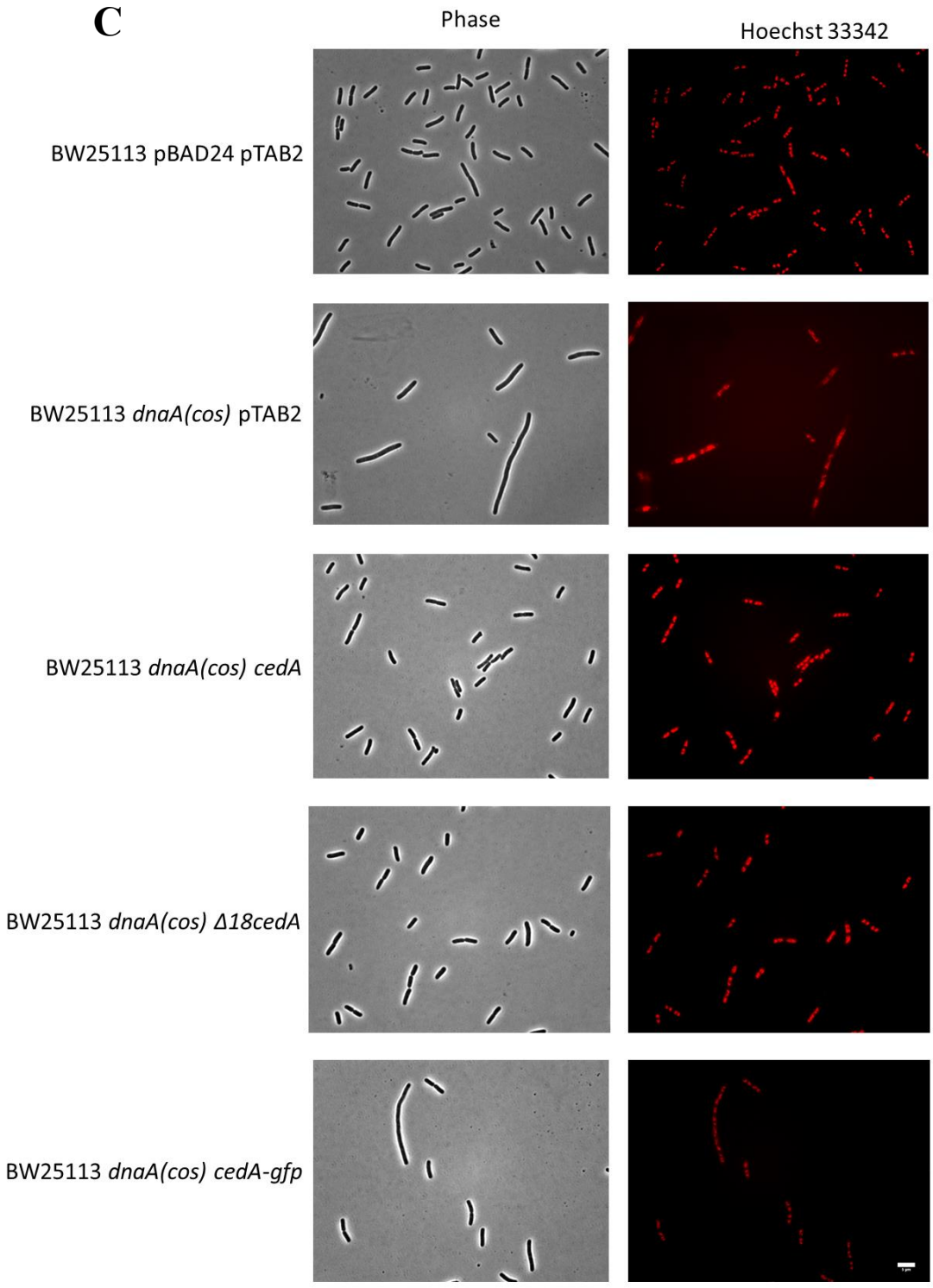

Figure 4.5 CedA can prevent filamentation that is induced by dnaA(cos) overexpression.

dnaA(cos) was cloned into pBAD24 and expressed with 0.2% L-arabinose in LB media. Full-length cedA, truncated cedA (Δ18cedA) and cedA-gfp were all cloned into pTAB2 and expressed with 0.2 μg/mL of anhydrotetracycline. The genes were expressed simultaneously, and the cells were fixed at $0D_{600}$= 0.3. They were then analysed by

Coulter counter to obtain cell volume distributions where over 50,000 cells were counted, overlaid, and offset vertically for visualisation (data shown in triplicate independent cultures of the strain by the different line patterns) (A). Matrix of Pearson correlation coefficients of triplicate data for dnaA(cos) prevention by cedA (B) and microscopy to observe cell morphology and DNA staining using Hoechst 33342. Scale bar = 5 μm (Section 2.9.2)(C).

4.2.5 Identification of genes required for the prevention of *dnaA(cos)* filamentation by *cedA*

Bacterial filamentation that is caused by the DNA replication initiator mutant, *dnaA(cos)*, is a known pathway that can be prevented by the overrepresentation of *cedA*.[15] Though, how *cedA* promotes cell division in these cells is unknown. Through the use of transcriptomics, we aimed to identify which genes and/or pathways are regulated that may allow cell division in a cell that would normally filament. For this, we compared BW25113 *dnaA(cos) cedA* to BW25113 *dnaA(cos)*. We performed the filamentation-prevention experiment, where *cedA* was expressed from pTAB2 and *dnaA(cos)* was expressed from pBAD24. For this style of experiment, the strains were initially grown in liquid LB with no inducers to mid-log at 42°C and then diluted to OD_{600} = 0.01 in LB containing 0.2 μg/mL of anhydrotetracycline and 0.2% (w/v) L-arabinose. Once the cultures reached OD_{600} = 0.3 the RNA was extracted for RNA-seq, as described in *Section 2.6.5*. The RNA-seq analysis was performed using DeSeq2 for the differential gene expression analysis (*Section 2.6.7*). The full list of the significantly differentially expressed genes can be found in Supplementary Table S3. All the genes were plotted on a scatterplot of log_2FC versus p-adjusted (FDR) and the genes that met the inclusion criteria requirements are displayed in the shaded orange box on the scatterplot (Figure 4.6). In total, 378 genes were identified to have a p-adjusted of ≤ 0.05 and $log_2FC \geq \pm 1$. As expected, *cedA* was found to be strongly (8-fold log_2FC) upregulated.

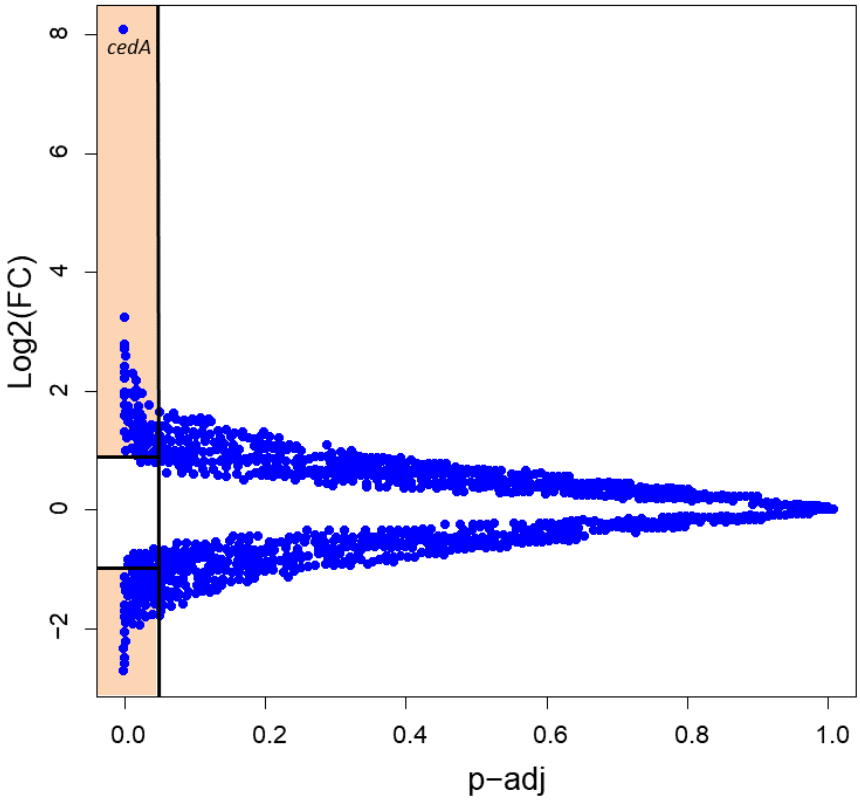

Figure 4.6 Scatterplot summary of genome-wide expression changes in condition BW25113 dnaA(cos) cedA versus BW25113 dnaA(cos) pTAB2.
The orange boxes indicate the selection criteria of p-adjusted value ≤ 0.05 and $\log_2$FC ≥ ±1 from duplicate experiments.

The 378 genes were then characterised by their Clusters of COG functional category to determine if any specific functional groups were prominent (Figure 4.7). From this analysis, a broad range of functional categories were changed, including amino acid transport and metabolism, carbohydrate transport and metabolism, and cell wall, membrane and envelope biogenesis were all major functional classes identified. Of note, when we compared the *dnaA(cos) cedA* prevention strain to WT during the transcriptomics study to determine the differential gene expression. We found that the COGs with the most regulation was nucleotide transport and metabolism and carbohydrate transport and metabolism (Supplementary Table S4). In the nucleotide transport and metabolism functional group, all of the genes were upregulated, suggesting that *cedA* is able to cause the prevention of filamentation by possibly upregulating cell metabolism.

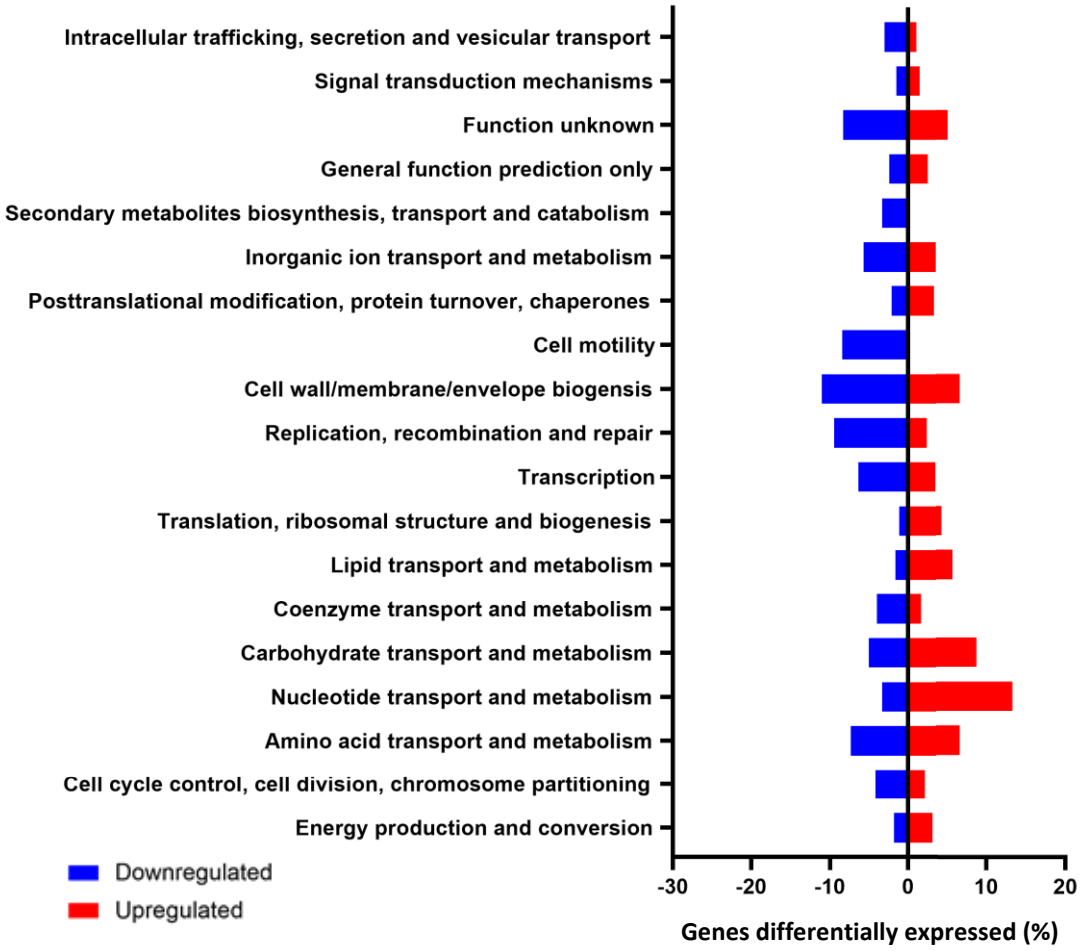

Figure 4.7 Percentage of genes differentially expressed per COG category for condition BW25113 dnaA(cos) cedA versus BW25113 dnaA(cos) pTAB2.
Three-hundred and seventy eight genes were identified by DeSeq2 and have a p-adjusted value of ≤ 0.05 and 1 ≤ Log_2(FC) ≤ -1 from duplicate experiments were used for the COG analysis.

An interesting group of genes found to be upregulated during *cedA*-overexpression in *dnaA(cos)* when compared to *dnaA(cos)* overexpression, are in the lipid transport and metabolism category and are involved in fatty acid synthesis (FAS). Fatty acid biosynthesis is the first stage in membrane lipid biogenesis, and recently FAS has been linked to controlling cell size by setting the cell envelope capacity.[159] The genes found to be upregulated when *cedA* prevents *dnaA(cos)* filamentation in the fatty acid biosynthesis pathway were *fabAGFI* (logFC 1.15 to 1.75), additionally, *fabR* which is a transcriptional repressor, was downregulated -1.26 log_2FC.

A number of membrane and envelope biogenesis genes were found to be downregulated. An example of this was the *wec* gene cluster, which are genes responsible for the synthesis of the Enterobacterial common antigen (ECA). The ECA is a glycolipid on the outer membrane and is found in all Gram-negative members of the Enterobacteriaceae family.[160,161] It was found that the entire *wec* cluster (*wecABCDEFG* and *rffG*) was downregulated with $\log_2$FC between -1.14 to -1.65. On the other hand, *omp* genes (*ompACFX*) were found to be upregulated with $\log_2$FC between 1.12 to 1.90. These genes encode for outer membrane porins which are necessary the minimise the access of toxic compounds and maximise the access of nutrients.[162] OmpC and OmpF are known to control the permeability of the outer membrane to glucose and nitrogen uptake during nutrient deprivation.[163]

As mentioned in Chapter 3, BW25113 pTAB2-*dnaA(cos)* overexpression leads to the upregulation of genes involved in the SOS response which may be the reason for the filamentation that is observed. Therefore, we wanted to explore if, in the *dnaA(cos)* prevention, the overexpression of *cedA* could lead to the downregulation of the SOS genes, which might thereby prevent an SOS response and filamentation. As may be seen in Figure 4.8, the genes involved in the SOS response were induced strongly in the *dnaA(cos)* cells, but this was prevented when *cedA* was also overexpressed in the *dnaA(cos)* + *cedA* strain. Specifically, it was found that the SOS response was not significantly regulated during *cedA* overexpression (BW25113 *cedA* vs WT) or *cedA* prevention control (BW25113 *dnaA(cos) cedA* vs WT) (Figure 4.8). During *dnaA(cos)* overexpression (BW25113 *dnaA(cos)* vs WT) the SOS was significantly upregulated, and the opposite was observed during *dnaA(cos)* prevention (BW25113 *dnaA(cos) cedA* vs BW25113 *dnaA(cos)*) where the SOS response was significantly downregulated. This indicates that *cedA* overexpression prevents SOS induction, either by directly blocking SOS induction or by preventing the conditions or signals that trigger SOS induction in DnaA(cos) strain. Thus, it is possible that SOS and/or other pathways that lead to filamentation are causing the observed filamentation in DnaA(cos) strains, that *cedA* can prevent. The effects of *cedA* on SOS and other known pathways to filamentation will be examined below.

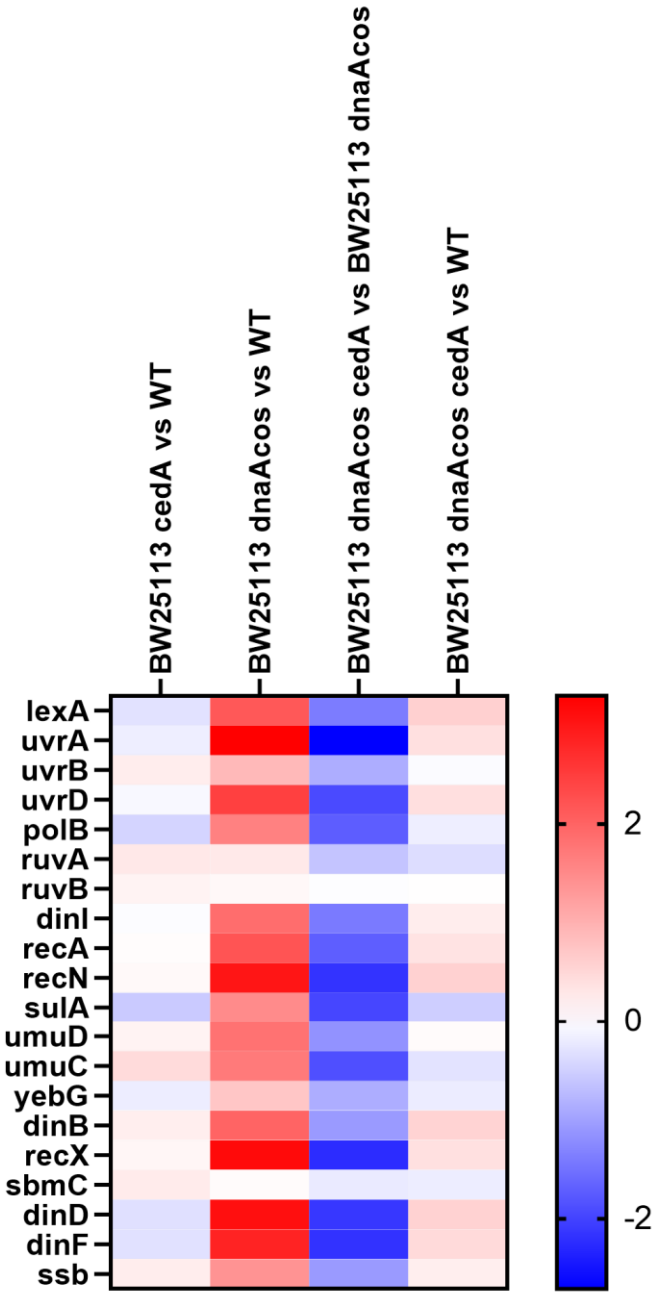

Figure 4.8 Heatmap data for SOS response genes shows log$_2$FC for all conditions. *First column is cedA overexpression (BW25113 cedA vs WT), second column is dnaA(cos) overexpression (BW25113 dnaA(cos) vs WT), third column is dnaA(cos) prevention (BW25113 dnaA(cos) cedA vs BW25113 dnaA(cos)) and the fourth column is cedA prevention control (BW25113 dnaA(cos) cedA vs WT). Only the well-known SOS genes were selected for this analysis.*

4.2.6 CedA can partially prevent filamentation caused by *ftsZ-yfp, recAtif, zwf* and *damX*

To further elucidate the function of *cedA* in *E. coli*, the testing of different pathways that are known to lead to filamentation was necessary to determine if *cedA* has a specific role in preventing the DnaA(cos) over-replication pathway or instead a general role in cell division control. *ftsZ-yfp* was used as it is known to cause filamentation by directly blocking Z-ring formation. In theory, due to this form of filamentation being so severe, *cedA* should not be able to overcome this. The *ftsZ* gene with a *yfp* tag was cloned into pBAD24 and is named pLAU80.[121]

To induce *ftsZ-yfp*, 0.2% (w/v) L-arabinose was included during continuous mid-log growth in batch culture, and then cell size was assessed at an $OD_{600} = 0.5$. When *ftsZ-yfp* was overexpressed (blue line, Figure 4.9A) filamentation was observed, as expected, demonstrated by the cell volume distribution shifting to the right compared to WT (red line, Figure 4.9A) with an average correlation value of 0.373 ± 0.150 (Table 4.9B). When *cedA* was simultaneously expressed with *ftsZ-yfp* (*ftsZ-yfp* prevention) (green line, Figure 4.9A) a degree of prevention was observed when compared to *ftsZ-yfp* overexpression with an average correlation value of 0.730 ± 0.171 (Table 4.9B). It is also evident from the microscopy that while the cells in the *ftsZ-yfp* prevention are shorter than *ftsZ-yfp* overexpression they are still not as short as WT (Figure 4.9C). Although full-length *cedA* was able to partly prevent *ftsZ-yfp* filamentation, we observed that the same was not true for Δ18*cedA* and *cedA-gfp.* We observed that the average correlation between *ftsZ-yfp* overexpression with Δ18*cedA* and *cedA-gfp* compared to *ftsZ-yfp* overexpression was 0.920 ± 0.070 and 0.890 ± 0.085, respectively. This suggested that the distributions have very high positive and high positive correlations, respectively, and therefore they are filamentous.

A

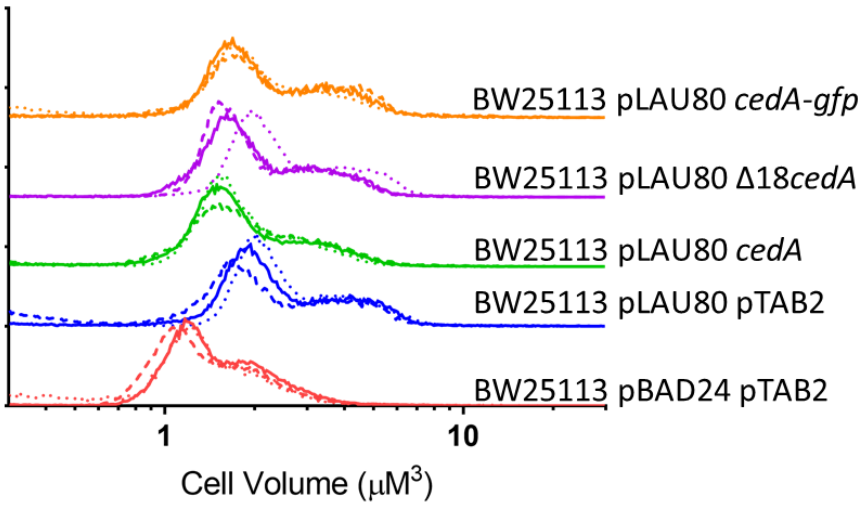

B

	pLAU80 pTAB2	pLAU80 *cedA*	pLAU80 Δ18*cedA*	pLAU80 *cedA-gfp*
pBAD24 pTAB2	0.45 0.47 0.20	0.77 0.68 0.68	0.67 0.50 0.26	0.58 0.46 0.52
pLAU80 pTAB2		0.71 0.91 0.57	0.85 0.92 0.99	0.90 0.97 0.80

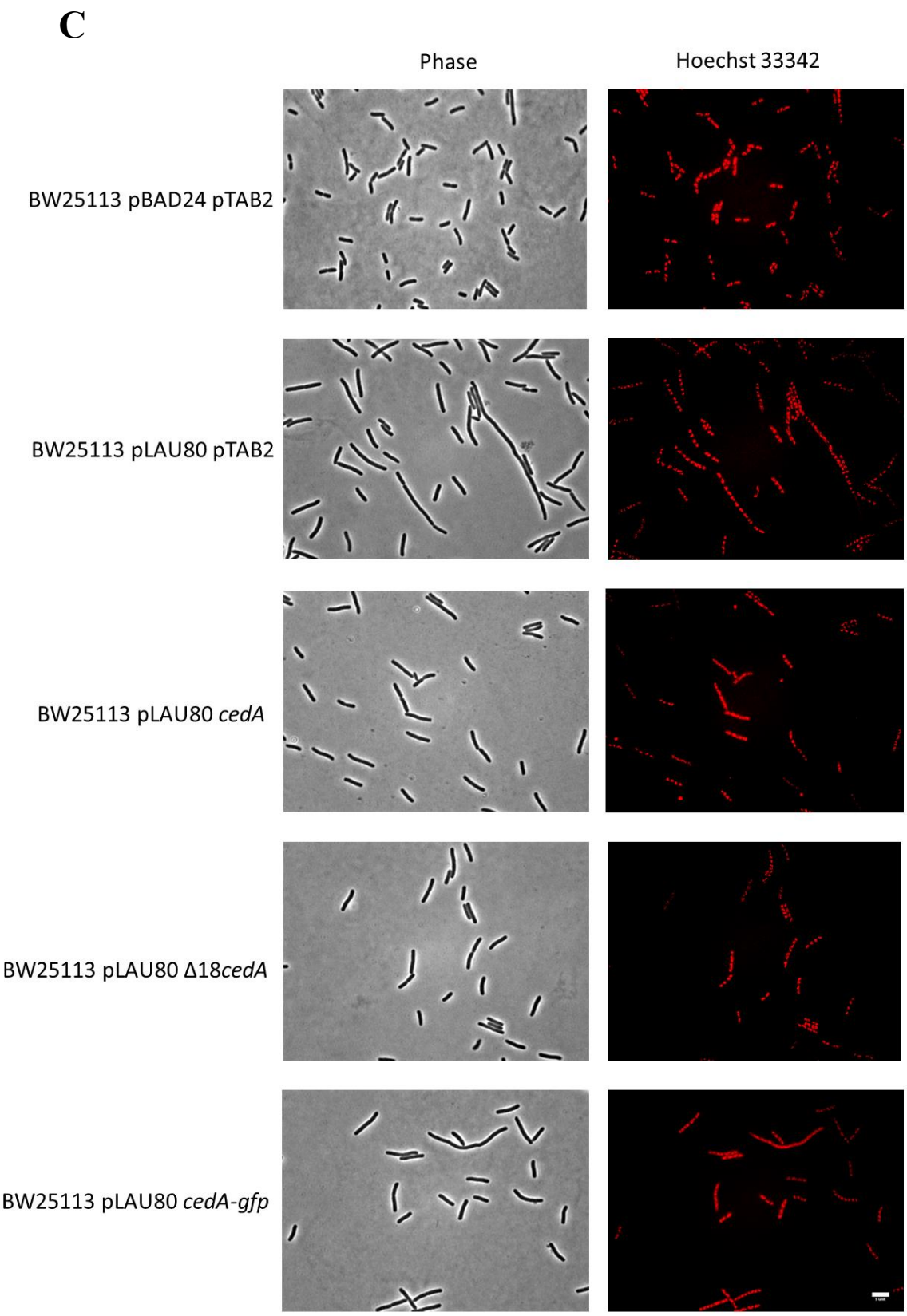

Figure 4.9 CedA can partially prevent filamentation caused by ftsZ-yfp overexpression. *pLAU80 which was provided to this experiment was expressed with 0.2% L-arabinose in LB media. cedA, Δ18cedA and cedA-gfp in pTAB2 were expressed with 0.2 μg/mL of*

anhydrotetracycline. The genes were expressed simultaneously and the cells were fixed at 0.5OD$_{A600}$. They were then analysed by coulter counter to obtain cell volume distributions where over 50,000 cells were counted, overlaid, and offset for visualisation (data shown in triplicate independent cultures of the strain by the different line patterns) (A). Matrix of Pearson correlation coefficients of triplicate data for ftsZ-yfp prevention by cedA (B). Microscopy to observe cell morphology and DNA staining using Hoechst 33342. Scale bar = 5 μm (Section 2.9.2) (C).

Additionally, as expected the Z-rings in *ftsZ-yfp* expression were chaotic and organized randomly along the cell length (Figure 4.10). Although it appears that *cedA* can partially prevent *ftsZ-yfp* induced filamentation this is independent of the formation of the Z-rings along the midcell as these cells still had randomly localising Z-rings along the cell length (Figure 4.10).

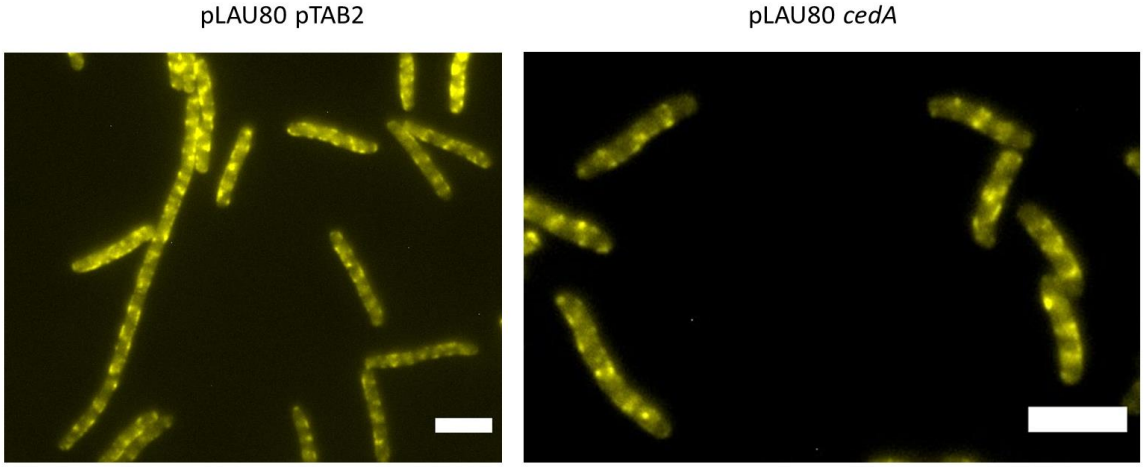

Figure 4.10 CedA can partially prevent ftsZ-yfp induced filamentation independent of repairing the misplacement of the Z-rings*. BW25113 pLAU80 pTAB2 and BW25113 pLAU80 cedA were grown to an OD$_{600}$ of =0.5. The cells were then used for fluroescence microscopy of the Z-rings using ftsZ tagged to fluorescent protein YFP. Scale bar = 5 μm (Section 2.9.2).*

Next, the SOS response was considered as a filamentation pathway that *cedA* could prevent. For these experiments, strain JM12 was used as it carries the *recAtif* mutation. This strain was used as opposed to the plasmid (pBAD24-*recAtif*) as it appeared to have consistent filamentation when induced under correct conditions, i.e. minimal media (M63), adenine and 42°C.[96] This mutant contains two amino acid substitutions, E38K and I298V.[164] It is known that the E28K mutation leads to the constitutive expression of the SOS response, and the I298V mutation is responsible for its temperature-sensitivity. To activate the *recAtif* mutant for the SOS response the strain must be at its non-permissive

temperature of 42°C and adenine must be added to the cells to enhance the activity of the mutant.[165] For experiments with JM12, cultures were harvested at 3 hours post-induction of *recAtif* at 42°C and analysed.

Filamentation caused by the *recAtif* mutant in the JM12 strain was not as severe as the filamentation that is caused by *dnaA(cos) (*Figure 4.8A), The average correlation of the cell size distributions between WT (red line, Figure 4.11A) and JM12 vector-only (*recAtif* overexpression) (blue line, Figure 4.10A) was 0.735 ± 0.177 (Table 4.11B) suggesting that they have a high positive correlation. When *cedA* (green line, Figure 4.11A) was simultaneously expressed with *recAtif* (*recAtif* prevention) there was an average correlation value of 0.785 ± 0.148 when compared to *recAtif* expression alone. The average correlation between *recAtif* prevention and WT was 0.975 ± 0.021 and therefore these strains have a very high positive correlation. Additionally, it was found that Δ18*cedA* (purple line, Figure 4.11A) and *cedA-gfp* (orange line, Figure 4.11A) were unable to prevent filamentation of *recAtif* as there was a high positive to very high positive correlation between those strain and JM12 vector-only of 0.895 ± 0.035 and 0.965 ± 0.007, respectively (Table 4.11B). There were no obvious morphological or nucleoid organizational differences between the strains (Figure 4.11C).

A

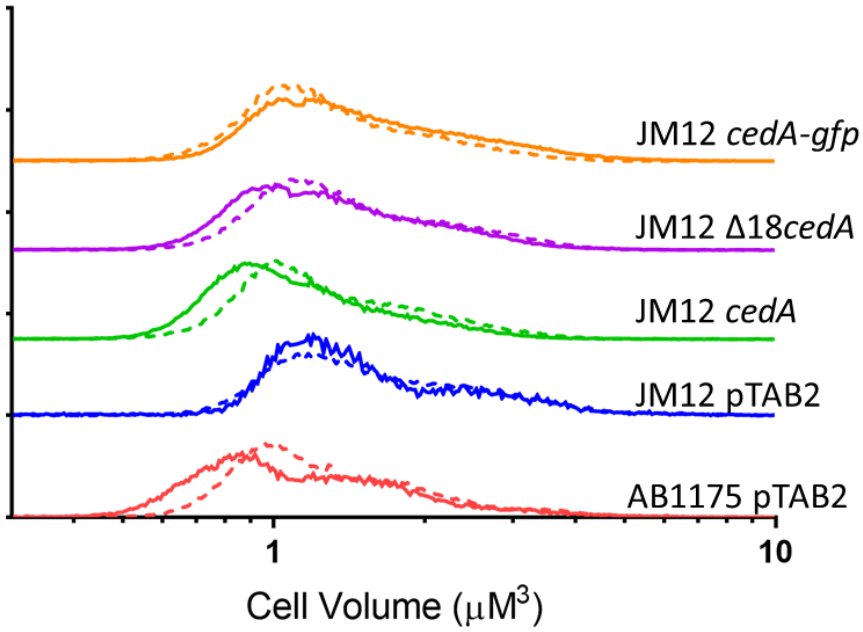

B

	JM12 pTAB2	JM12 *cedA*	JM12 Δ18*cedA*	JM12 *cedA-gfp*
AB1157 pTAB2	0.61 0.86	0.96 0.99	0.89 0.94	0.75 0.97
JM12 pTAB2		0.68 0.89	0.87 0.92	0.96 0.97

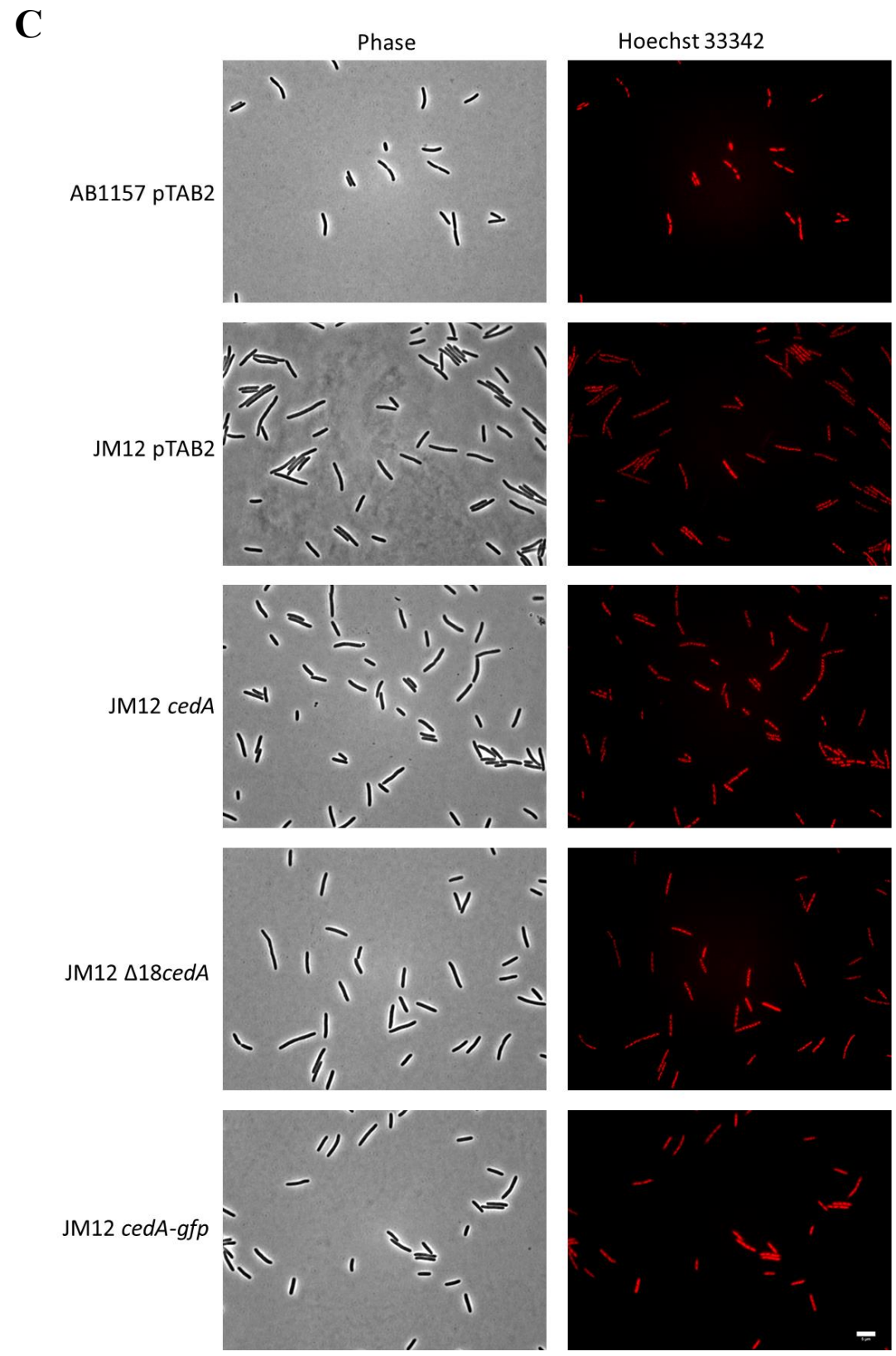

Figure 4.11 CedA can partially prevent filamentation caused by recAtif.
JM12 carrying the recAtif mutation was transformed with the three cedA plasmids and

the cells were grown in M63 media containing 0.4% casamino acids and 0.4% glycerol. To induce the recAtif mutation, adenine (100 µg/ml) was added to the culture and the temperature was shifted to 42°C and 0.2 µg/mL of anhydrotetracycline was also added at this time. The genes were expressed simultaneously and the cells were fixed 3 hours after induction. They were then analysed by Coulter counter to obtain cell volume distributions where over 50,000 cells were counted, overlaid, and offset vertically for visualisation (data shown in triplicate independent cultures of the strain by the different line patterns) (A). Matrix of Pearson correlation coefficients of replicate data for recAtif filamentation prevention by cedA (B). Microscopy was used to observe cell morphology and DNA staining using Hoechst 33342. Scale bar = 5 µm (Section 2.9.2) (C).

The next pathway that was examined was related to central carbon metabolism. For this pathway, *zwf*, which encodes for Glucose-6-phosphate 1-dehydrogenase in the first step of the pentose phosphate pathway, was selected as this was identified in a screen by Mediati, et al.[166] to cause filamentation. However, this has not been verified to determine if it did, in fact, cause filamentation. *Zwf* was also identified as a protein that interacts with CedA, as mentioned in Section 1.6.2.

The open reading frame of *zwf* was cloned into pBAD24 and induced with 0.2% (w/v) L-arabinose. Filamentation caused by *zwf* overexpression in BW25113 (blue line, Figure 4.12A) was found to be very mild, with only a small shift in cell volume when compared to WT. The average correlation between these two distributions was 0.683 ± 0.140 (Table 4.12B) suggesting that have a moderate positive correlation. Therefore, *zwf* overexpression causes the cells to be only slightly longer than short WT cells. When *cedA* was also induced with *zwf* ("*zwf* prevention") (green line, Figure 4.12A) there was a slight shift back towards the smaller cell sizes, suggesting prevention of cell elongation; the average correlation between *zwf* prevention strain and WT was 0.970 ± 0.017. While the average correlation between *zwf* prevention and *zwf* overexpression was 0.793 ± 0.055. These results suggest that *zwf* prevention is similar to WT. It was found that Δ18*cedA* was unable to prevent filamentation, with an average correlation value of 0.960 ± 0.036 when compared to *zwf* overexpression demonstrating that these cells have a very high positive correlation and are highly similar. Additionally, *cedA-gfp* was found to be similar to both WT and BW25113 *zwf* pTAB2 with average correlation values of 0.910 ± 0.066 and 0.900 ± 0.017, respectively. This suggests the cell distributions of BW25113 *zwf cedA-gfp* remains half-way between WT and BW25113 *zwf* pTAB2 as can be seen in the Coulter histograms (Figure 4.12A). DNA staining revealed that the nucleoids in some of the

filaments caused by *zwf* appeared to have lost its organisation and was instead spread along the cell length similar to that seen in *dnaA(cos)* filamentation (Figure 4.12C, green arrows).

A

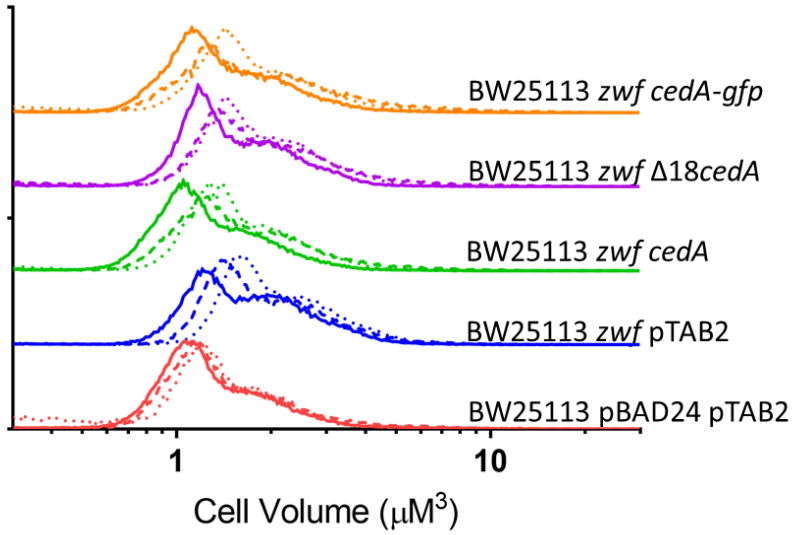

B

	zwf pTAB2	*zwf cedA*	*zwf* Δ18*cedA*	*zwf cedA-gfp*
pBAD24 pTAB2	0.82	0.99	0.90	0.98
	0.69	0.96	0.76	0.90
	0.54	0.95	0.78	0.85
***zwf* pTAB2**		0.79	0.97	0.91
		0.85	0.99	0.91
		0.74	0.92	0.88

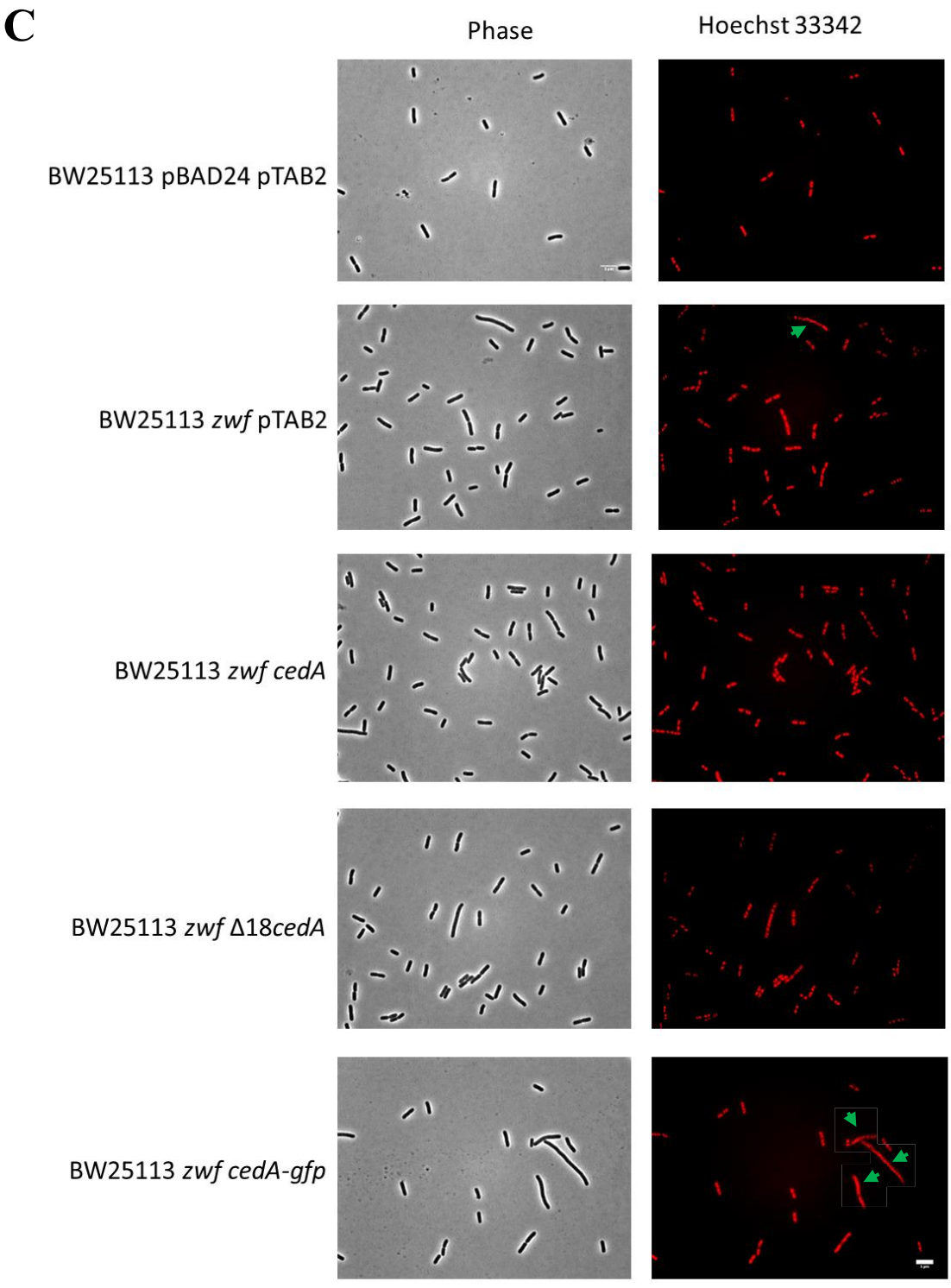

Figure 4.12 CedA can partially prevent filamentation that is induced by zwf overexpression
zwf was cloned into pBAD24 and expressed with 0.2% L-arabinose in LB media. Full-length cedA, Δ18cedA and cedA-gfp in pTAB2 were expressed with 0.2 μg/mL of anhydrotetracycline. The genes were expressed simultaneously and the cells were fixed

at OD_{600} = 0.5. They were then analysed by Coulter counter to obtain cell volume distributions where over 50,000 cells were counted, overlaid, and offset for visualisation (data shown in triplicate independent cultures of the strain by the different line patterns) (A). Matrix of Pearson correlation coefficients of triplicate data for zwf prevention by cedA (B). Microscopy was used to observe cell morphology and DNA staining using Hoechst 33342. Scale bar = 5 μm (Section 2.9.2) (C).

Next, we wanted to investigate *damX* as this was identified as causing the reversible filamentation that UPEC undergoes during infection.[16] The open reading frame of *damX* was cloned into pBAD24 and induced with 0.2% L-arabinose. Filamentation caused by *damX* was found to be time-dependent meaning that as time went on the longer exposure of the cells to *damX* lead to more filamentation (Figure 4.13). This meant that *damX* could not be sampled at mid-log phase like the other strains as we did not observe filamentation or an increase of cell volume compared to WT at OD_{600} = 0.5. The average cell volume for OD_{600} = 0.3, 0.5, and 0.7 was 2 μm, 2.5 μm, and 3 μm, respectively. A Kruskal-Wallis test was performed on the median of the cell volume for the different ODs and it found that the difference was statistically significant ($p < 0.0001$). At any OD_{600} before 0.7 the cells were the same size as wild-type and filamentation was not observable. This was different from all of the other strains used in this study as filamentation would normally be observable from OD_{600} = 0.1. This time-dependent effect for *damX* suggests that there might need to be a certain level of the protein in cells that has to build up before it leads to filamentation, which has been observed previously.[167] For this reason, for the *damX* experiments, the cultures were sampled at an OD_{600} = 0.7 when the cells displayed the highest level of filamentation.

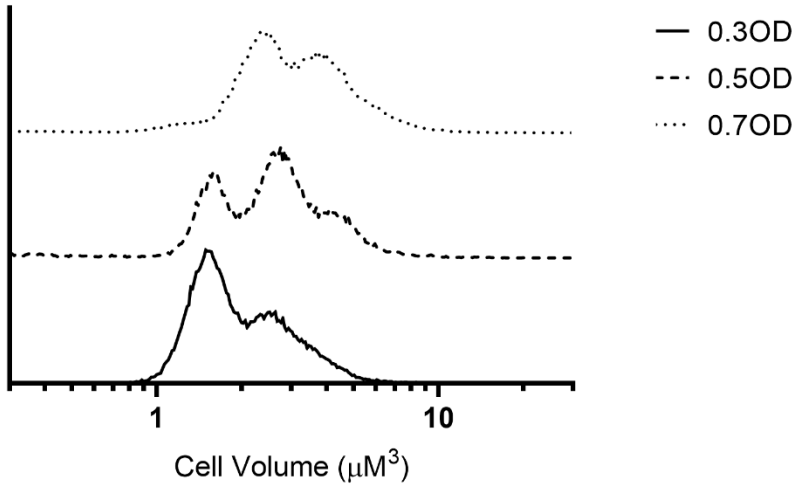

Figure 4.13 Coulter counter data shows that damX cell length increases as absorbance (OD_{600}) increases.
BW25113 damX pTAB2 was cultured at 37C in LB containing 0.2% (w/v) L-arabinose. Cells were harvested at OD_{600} = 0.3, 0.5 and 0.7. The x-axis represents the cell volume (μm^3).

At an OD_{600} = 0.7 the cell volume distributions of BW25113 *damX* pTAB2 (*damX* overexpression) (blue line, Figure 4.14A) shifted to the right compared to WT (red line, Figure 4.14A) suggesting filamentation. The average correlation value between these two strains was 0.093 ± 0.155 suggesting that the cell volume distributions were negligibly correlated (Table 4.14B). When *cedA* was simultaneously overexpressed with *damX* (*damX* prevention) (green line, Figure 4.14A) there was an average correlation of 0.680 ± 0.191 when compared to *damX* overexpression suggesting that the distributions have a moderate correlation suggesting that *cedA* is able to partially prevent *damX* overexpression filamentation. However, there is no prevention seen with Δ18*cedA* (purple line, Figure 4.14A) and *cedA-gfp* (orange line, Figure 4.14A), when compared to *damX* overexpression these had correlation values of 0.923 ± 0.070 and 0.877 ± 0.040, respectively. This suggested that these distributions have a high positive to very high positive correlation and therefore, these versions of *cedA* also cannot prevent filamentation. It should be mentioned that in 2 out of the 3 triplicates, the correlation values between *damX* and WT were found to not be statistically significant. Thus, suggesting that *damX* filamentation is variable or the strain is potentially subject to suppressors. Finally, there were no obvious differences in the nucleoid organisation or morphology between the strains (Figure 4.14C).

A

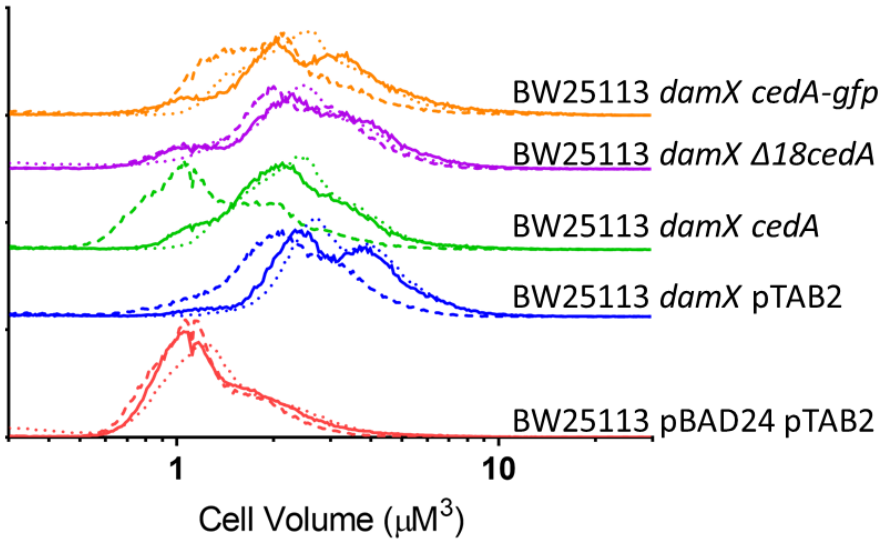

B

	damX pTAB2	*damX cedA*	*damX* Δ18*cedA*	*damX cedA-gfp*
pBAD24 pTAB2	0.03	0.40	0.32	0.28
	0.27	0.96	0.30	0.51
	-0.02	0.34	0.34	0.31
***damX* pTAB2**		0.80	0.93	0.90
		0.46	0.99	0.90
		0.78	0.85	0.83

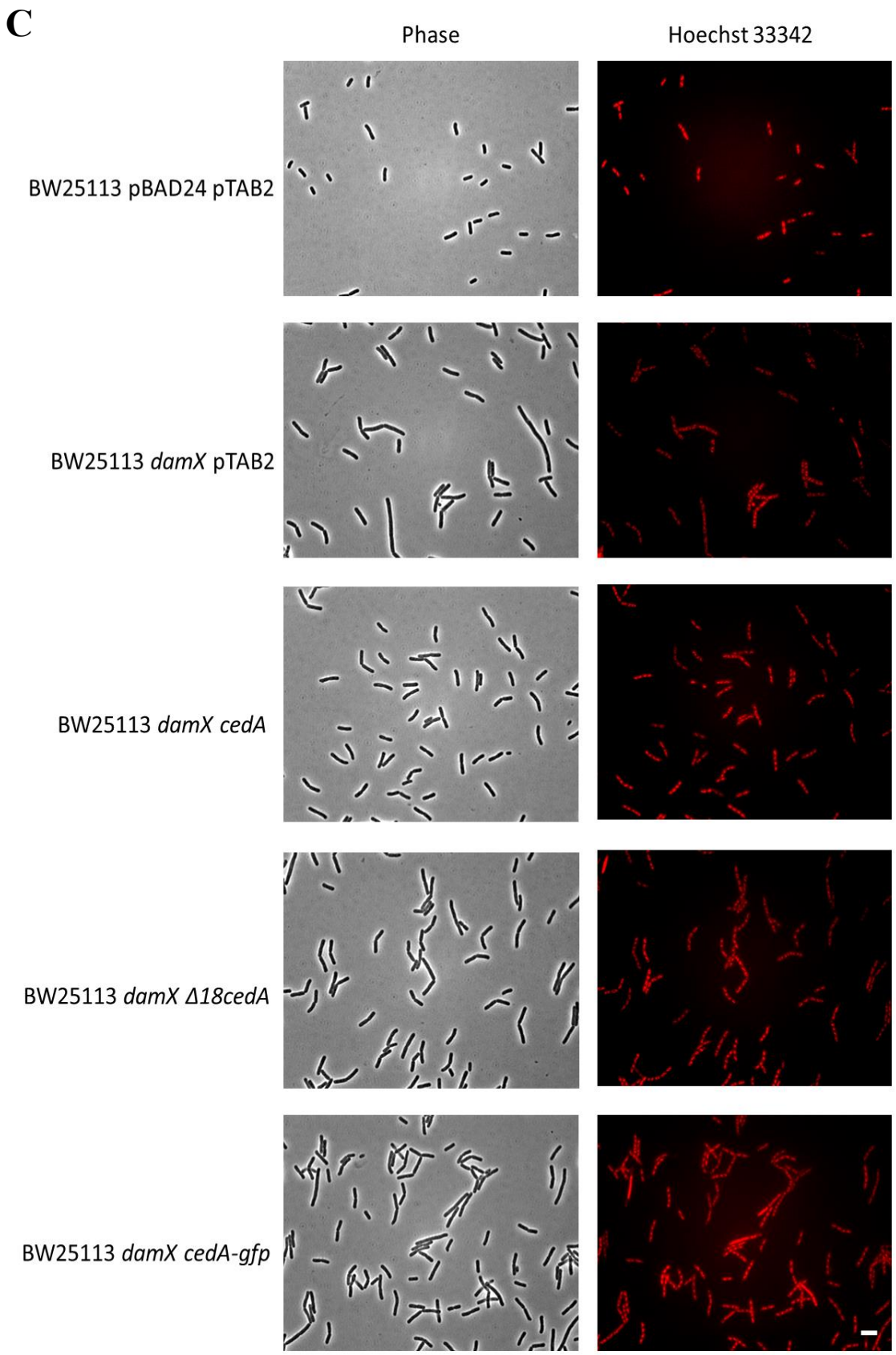

Figure 4.14 CedA can partially prevent filamentation that is induced by damX overexpression.

damX was cloned into pBAD24 and expressed with 0.2% L-arabinose in LB media. Full-length cedA, Δ18cedA and cedA-gfp were all cloned into pTAB2 and expressed with 0.2 µg/mL of anhydrotetracycline. The genes were expressed simultaneously and the cells were fixed at 0.7 OD_{A600}. They were then analysed by Coulter counter to obtain cell volume distributions where over 50,000 cells were counted, overlaid, and offset for visualisation (data shown in triplicate independent cultures of the strain by the different line patterns) (A). Matrix of Pearson correlation coefficients of triplicate data for damX prevention by cedA (B). Microscopy was used to observe cell morphology and DNA staining using Hoechst 33342. Scale bar = 5 µm (Section 2.9.2) (C).

4.2.7 No strong evidence to suggest that CedA can prevent filamentation caused by *slmA* and *slmA*-SBS overexpression

The final pathway explored was nucleoid occlusion through *slmA*. This system ensures that Z-rings do not form over nucleoids, and there are two ways of inducing filaments using *slmA*, 1) the overexpression of *slmA* alone, or 2) overexpression of *slmA* and its SlmA binding sites (SBS), which are placed all over the chromosome to allow *slmA* to bind (*described in Section 1.4.2*).

First, *slmA* was expressed from the plasmid pTB67 with 50 µM IPTG and all cultures were harvested at an OD_{600} = 0.1, due to the toxicity of large amounts of *slmA*. When *slmA* was overexpressed it led to very long filaments (Figure 4.15C) (blue line, Figure 4.15A). The average correlation with WT (red line, Figure 4.15A) was -0.310 ± 0.070 showing that had a low negative correlation. When *cedA* (green line, Figure 4.15A), Δ18*cedA* (purple line, Figure 4.15A) and *cedA-gfp* (orange line, Figure 4.15A) were co-expressed with *slmA* their average correlation values were 0.760 ± 0.098, 0.220 ± 0.413, and 0.493 ± 0.091, respectively compared to *slmA* overexpression, suggesting that *cedA* is unable to prevent filamentation caused by *slmA*.

A

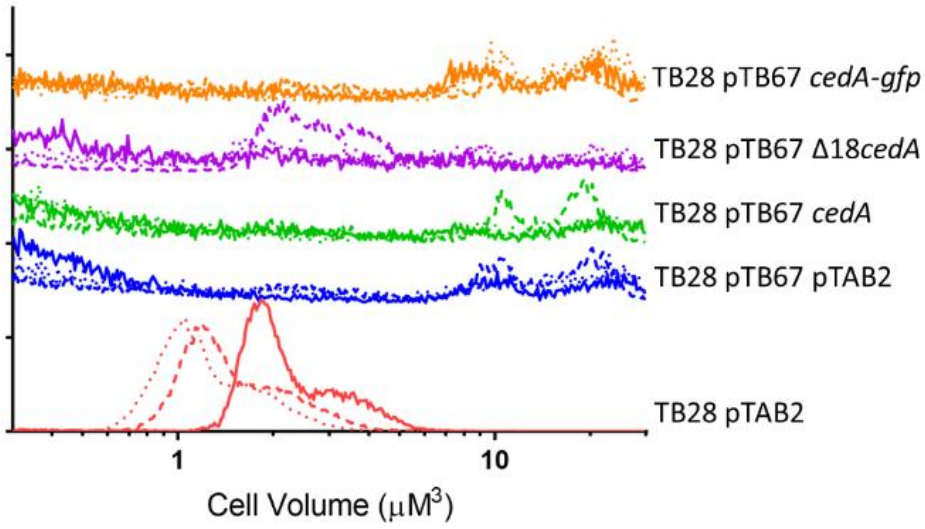

B

	pTB67 pTAB2	pTB67 *cedA*	pTB67 Δ18*cedA*	pTB67 *cedA-gfp*
pBAD24 pTAB2	-0.36	-0.22	0.03	-0.38
	-0.34	-0.21	0.13	0.00
	-0.23	-0.08	-0.04	-0.32
pTB67 pTAB2		0.84	0.68	0.39
		0.79	-0.12	0.56
		0.65	0.10	0.53

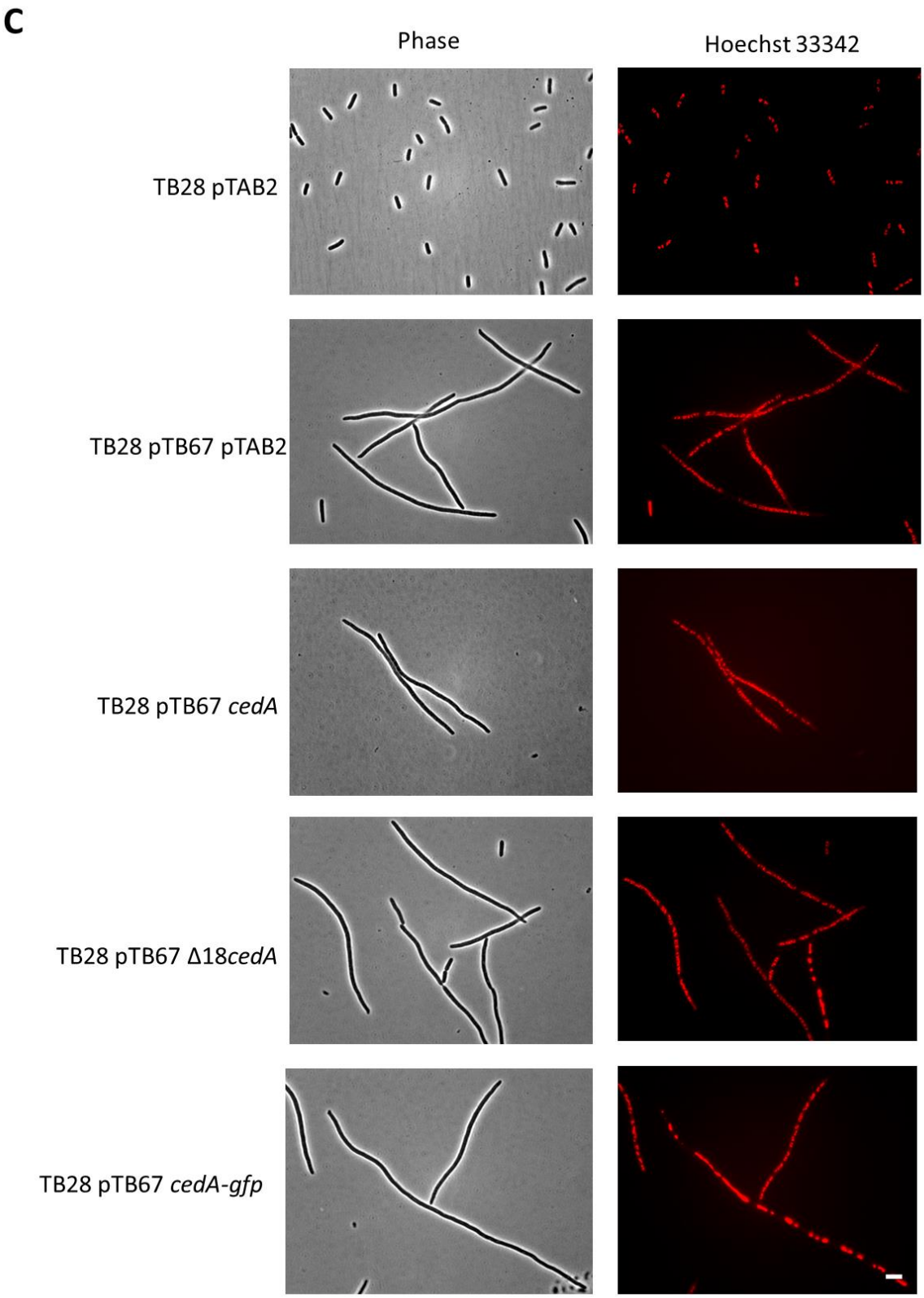

Figure 4.15 Filamentation caused by slmA overexpression cannot be prevented by CedA

slmA was overexpressed from plasmid pTB67 in strain TB28 using 50 µM IPTG and cedA, Δ18cedA and cedA-gfp were simultaneously expressed with 0.2µg/mL

anhydrotetracycline. The cultures were grown to an OD_{600} = 0.1 and fixed. They were then analysed by Coulter counter to obtain cell volume distributions where over 50,000 cells were counted, overlaid, and offset for visualisation (data shown in triplicate independent cultures of the strain by the different line patterns) (A). Matrix of Pearson correlation coefficients of triplicate data for slmA prevention by cedA (B). Microscopy was used to observe cell morphology and DNA staining using Hoechst 33342. Scale bar = 5 μm (Section 2.9.2) (C).

To confirm that *cedA* cannot prevent filamentation caused by *slmA*, *slmA-SBS* was also tested. In strain HC328, a plasmid pHC534 contained *slmA*-SBS and it was induced using 1 mM IPTG. The strains were again induced until an OD_{600} = 0.1 because of the toxicity that comes from *slmA* overexpression. When *slmA*-SBS was overexpressed, the cells became very filamentous (Figure 4.16C) as seen with *slmA* overexpression, and the correlation between *slmA*-SBS overexpression and WT was -0.245 ± 0.035. When *cedA* (green line, Figure 4.16A), Δ18*cedA* (purple line, Figure 4.16A) and *cedA-gfp* (orange line, Figure 4.16A) were co-expressed with *slmA*-SBS they had similar average correlation coefficients when compared to *slmA*-SBS overexpression (0.630 ± 0.085, 0.550 ± 0.255, and 0.550 ± 0.057, respectively). These results reaffirm that *cedA* is unable to prevent filamentation caused through the nucleoid occlusion pathway.

A

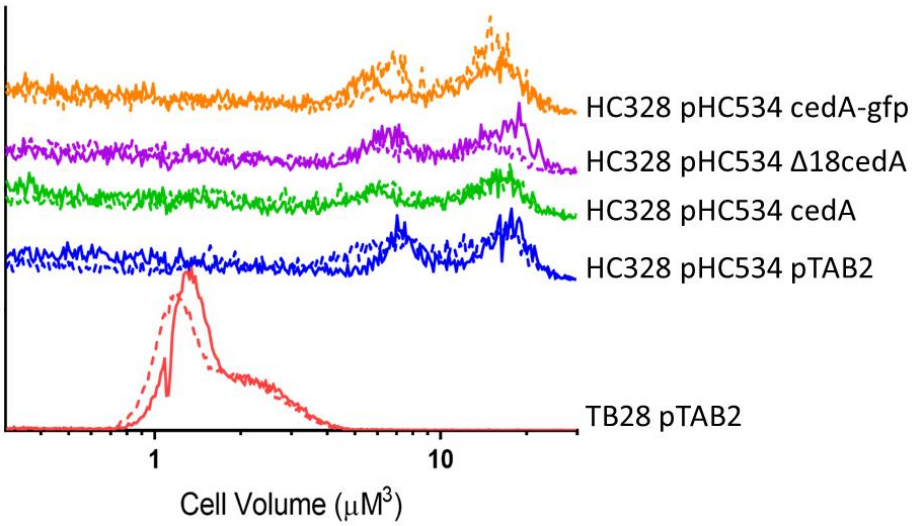

B

	HC328 pHC534 pTAB2	**HC328 pHC534 *cedA***	**HC328 pHC534 Δ18*cedA***	**HC328 pHC534 *cedA-gfp***
pBAD24	-0.22	-0.18	-0.29	-0.26
pTAB2	-0.27	0.00	0.00	-0.32
HC328 pHC534 pTAB2		0.57 0.69	0.73 0.37	0.51 0.59

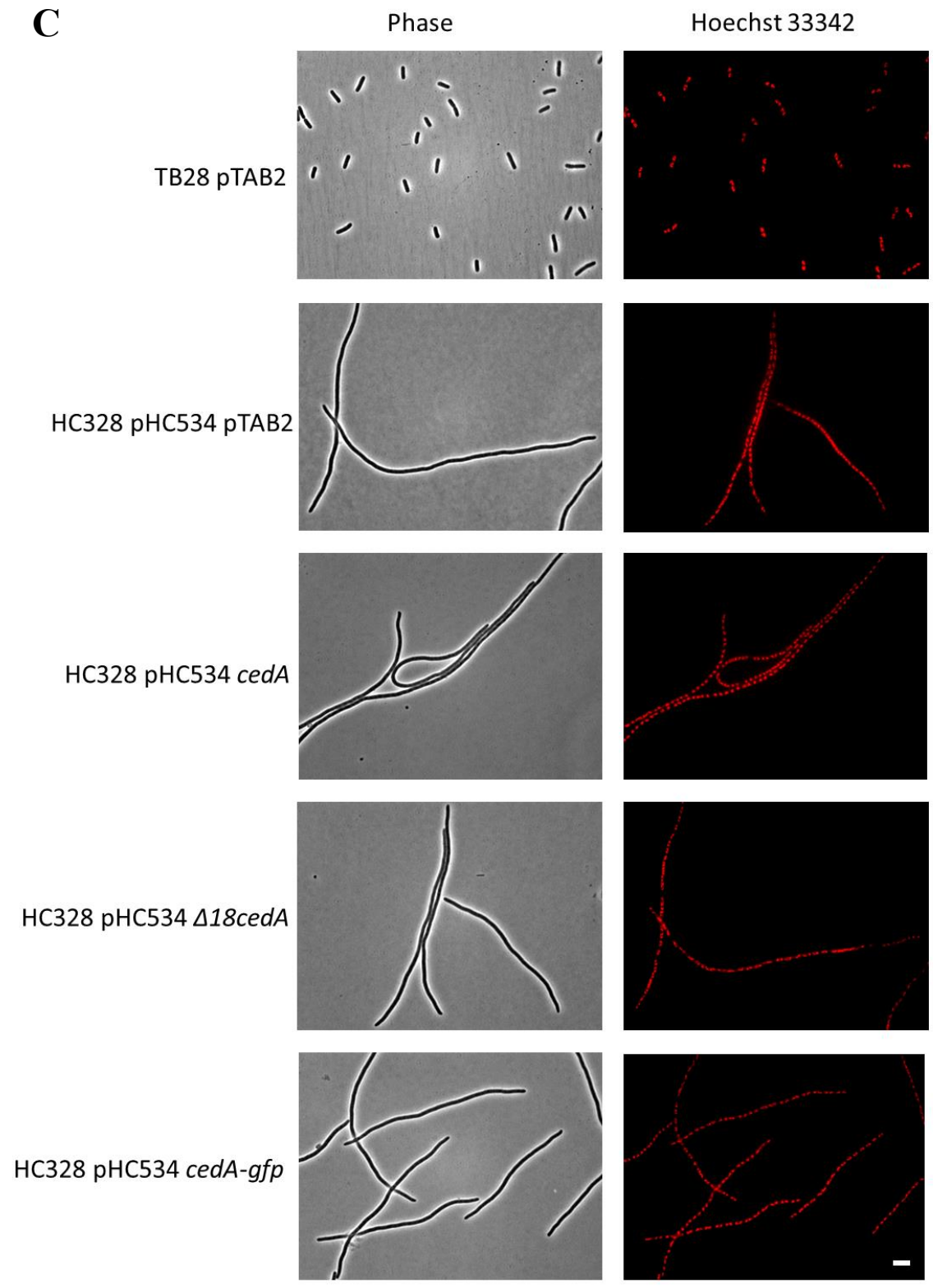

Figure 4.16 CedA cannot prevent filamentation caused by the overexpression of slmA-SBS.

slmA-SBS was overexpressed from HC328 containing pHC534 using 1 mM IPTG. Full-length cedA, Δ18cedA and cedA-gfp were expressed simultaneously with slmA-SBS using 0.2µg/mL anhydrotetracycline. The cultures were grown to an OD_{600} = 0.1 and fixed.

They were then analysed by Coulter counter to obtain cell volume distributions where over 50,000 cells were counted, overlaid, and offset for (data shown in triplicate independent cultures of the strain by the different line patterns) (A). Matrix of Pearson correlation coefficients of replicate data for slmA-SBS prevention by cedA (B). Microscopy was used to observe cell morphology and DNA staining using Hoechst 33342. Scale bar = 5 μm (Section 2.9.2) (C).

In summary, it was found that, through *cedA's* simultaneous overexpression with a filamentor, in addition to *dnaA(cos), cedA* can prevent filamentation of *ftsZ-yfp, recAtif, zwf* and *damX.* While it was found that *cedA* cannot prevent filamentation of*, slmA* and *slmA*-SBS overexpression. Therefore, this could suggest that *cedA* may have a dose-dependent effect on blocking filamentation. This was further supported by *cedA*s inability to prevent the severe filamentation of *slmA* and *slmA*-SBS.

4.2.8 *cedA* overexpression during UTIs

The final filamentation pathway tested was that caused by UPEC during UTIs. This study was performed using an *in vitro* flow chamber infection model[11] as described in *Section 2.7*. Filamentation during the infection model is induced with concentrated urine; anhydrotetracycline was added to the urine to induce *cedA*, Δ18*cedA* and *cedA-gfp* at the same time. One replicate experiment is shown below, and the second replicate can be found in Supplementary Figure S1. WT UTI89 pTAB2 (vector only) caused filamentation as expected with 10.4% of the population of cells being categorized as filamentous compared to the control at 0.68%, which was the same strain grown overnight at 37°C in LB (Figure 4.17A). Intriguingly, when *cedA* and *cedA-gfp* were overexpressed during the infection, while it appeared to prevent filamentation, with filamentous populations of 0.69% and 0.31%, respectively. It was possible that not all of the cells were viable and some appeared to have lysed (Figure 4.17B) which was also evident from the clear supernatant collected from the flow chamber compared to the very cloudy supernatant collected from WT. Also after being collected from the flow chamber the cells were added to LB media to recover growth and UTI89 pTAB2/*cedA* and UTI89 pTAB2/*cedA-gfp* did not grow while WT recovered growth as expected. This could suggest that when *cedA* is overexpressed during an *in vitro* infection of *BECs* these cells are unable to continue through the normal infection cycle. Using time-lapse microscopy on this study would allow for the visualization of these cells to determine if they are able to invade epithelial

cells, form IBCs and release as short-rods due to the overexpression of *cedA*. Or do the UPEC cells form IBCs and then due to the overexpression of *cedA* they die. Additionally, there was no localisation of *cedA-gfp* observed in the dispersed bacteria.

Furthermore, it appears that Δ18*cedA* was unable to cause full prevention of filamentation with a filamentous population of 5.50%. This is a level that is lower than WT and therefore, it may be partial prevention. From the microscopy, it can be seen that the filaments from the infection do not have separated nucleoids and in some cases, they appear to be compacted (Figure 4.17B). This may suggest that UPEC filamentation may be caused by its inability to overcome nucleoid occlusion.

A

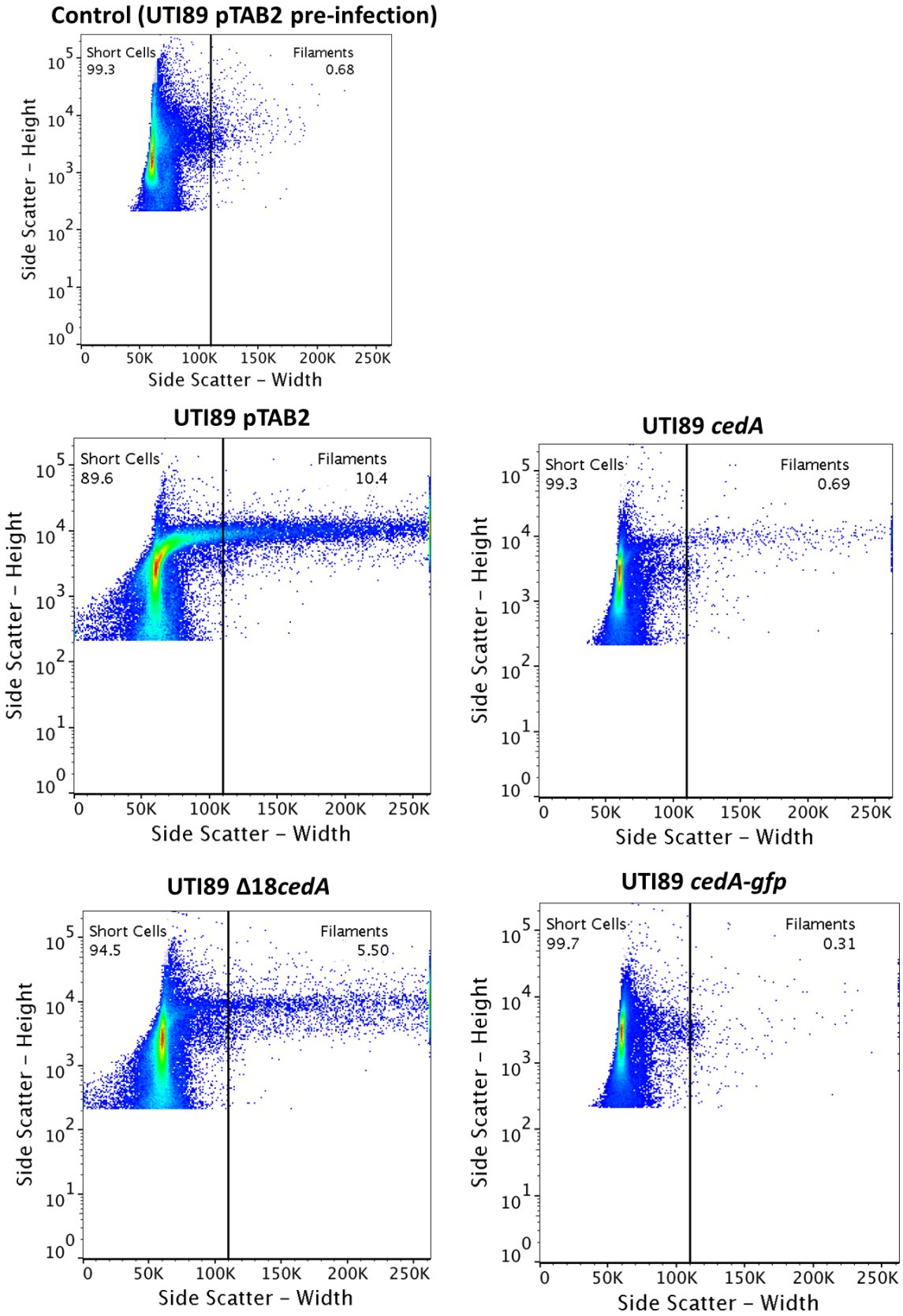
Control (UTI89 pTAB2 pre-infection)
Short Cells
99.3
Filaments
0.68
UTI89 pTAB2
Short Cells
89.6
Filaments
10.4
UTI89 cedA
Short Cells
99.3
Filaments
0.69
UTI89 Δ18cedA
Short Cells
94.5
Filaments
5.50
UTI89 cedA-gfp
Short Cells
99.7
Filaments
0.31
Side Scatter – Height
Side Scatter – Width
0
50K
100K
150K
200K
250K

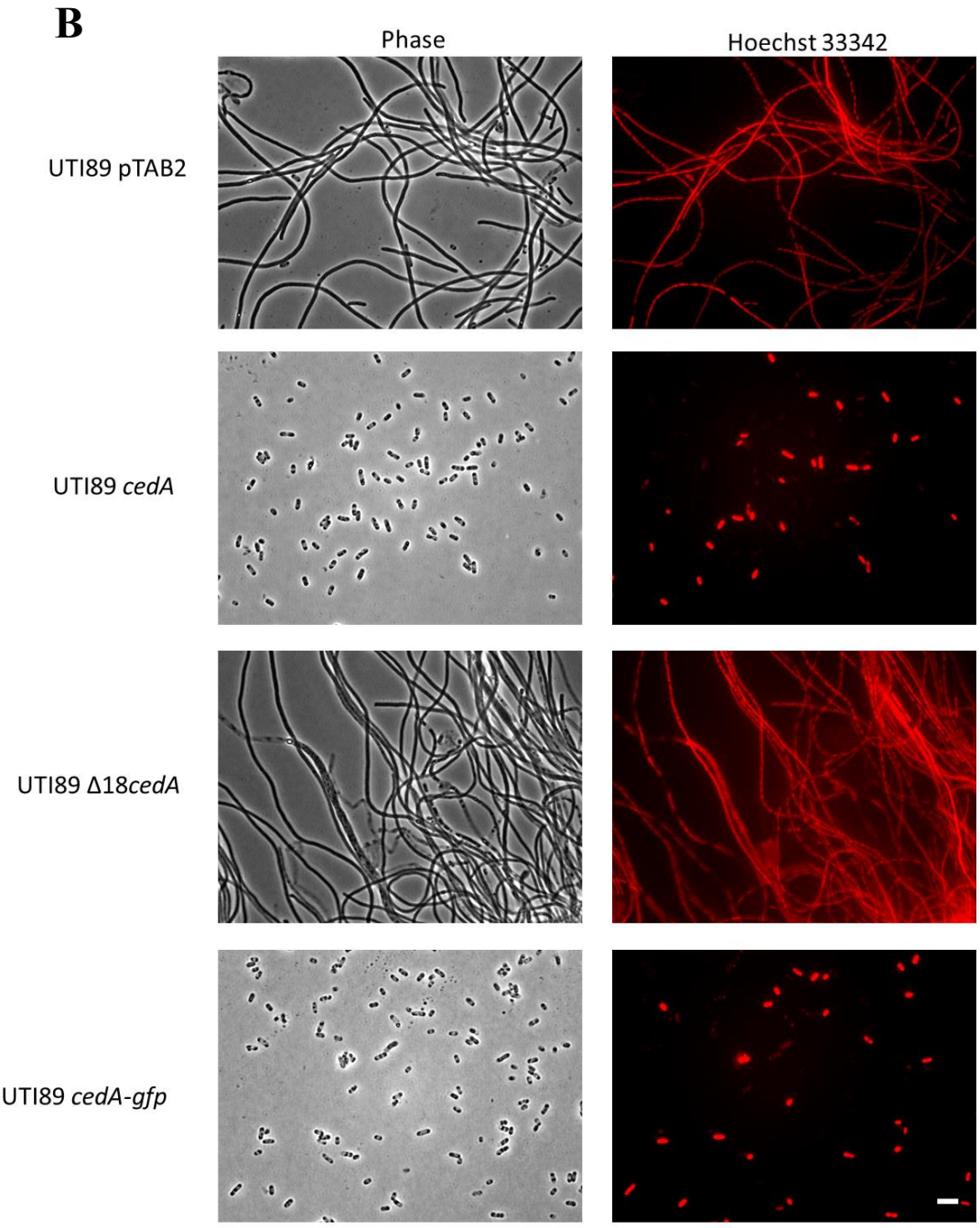

Figure 4.17 CedA overexpression may lead to the death of UPEC and therefore prevent filamentation that is caused during in vitro BEC infection.
Control (UTI89 pTAB2 grown in LB overnight), UTI89 pTAB2, UTI89 cedA, UTI89 Δ18cedA, and UTI89 cedA-gfp underwent infection of bladder cells (PDO7i) in an in vitro flow chamber infection model. A) The fraction of filamentous bacteria were obtained from flow cytometry. A scatterplot of the cells was gated based on the control (UTI89 pTAB2 grown overnight in LB) and was named short cells and all other cells were names filaments with side scatter width and height on the x and y axes respectively. B) Microscopy was used to observe cell morphology and DNA staining using Hoechst 33342. Scale bar = 5 μm (Section 2.9.2). This is data shown from one replicate.

4.2.9 *cedA* cannot reverse pre-formed filaments

It is known that *cedA* can prevent filamentation of *dnaA(cos)* and now we have found that it can also prevent or partially prevent filamentation of *ftsZ-yfp*, *recA(tif), zwf and during UPEC* cellular infection. This suggests that *cedA* may have a role in a general pathway that regulates cell division. Next was to determine if *cedA*_could reverse filaments that were already formed and by doing so reactivate cell division where it has already ceased. To do this *dnaA(cos)* and *ftsZ-yfp* were selected as these genes are from different biological pathways in the cell and would examine *cedA*s versatility in function.

To perform these experiments the gene to cause filamentation was induced for 2 hours with 0.2% (w/v) L-arabinose in the absence of *cedA* induction to allow for filamentation. After filamentation was observed *cedA* was induced with 0.2 µg/mL anhydrotetracycline and the cultures were left to grow for 2 hours. Results suggest that *cedA, Δ18cedA* and *cedA-gfp* were unable to reverse filaments of *dnaA(cos)* or *ftsZ-yfp* back into short rod-shaped cells after 2 hours (Figure 4.18). Over time with the induction of the filamentor gene, it allows the cells to continue to get longer in the presence of *cedA.* As can be seen in Figure 4.18 at time point 0 filamentation has occurred in the strains containing filamentors *dnaA(cos)* and *ftsZ-yfp* compared to WT. After 0 mins the inducer for *cedA* was added to the culture and it can be seen that the addition of *cedA* and its variants are unable to reverse the filaments that have already been formed. Additionally, the strains containing the filamentors and the different *cedA* variants appear to become more filamentous over time. Overall, this data suggests that *cedA* is unable to reverse or overcome blocks to cell division that are already in place.

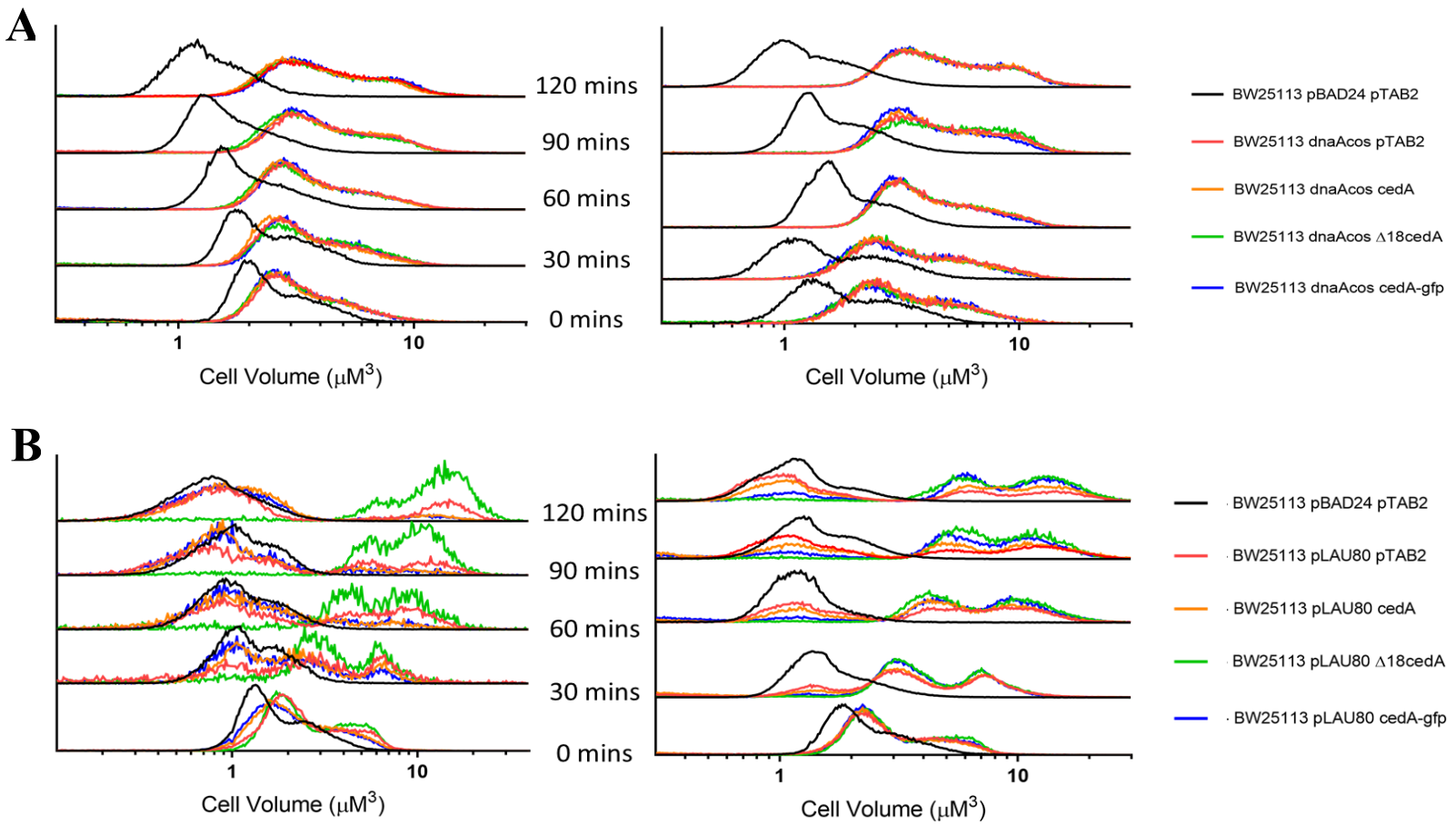

Figure 4.18 CedA cannot reverse preformed filaments.
Cell volume distributions as determined by the Coulter counter of dnaA(cos) (A) and ftsZ-yfp (B). Replicates are show on separate graphs.

4.3 Discussion

Very little is known about the role of CedA in *E. coli*, however, it appears to be a small protein that has a role in regulating cell division. The work in this chapter set out to preliminarily understand the function of CedA in *E. coli* through its overexpression. It has already been shown that *cedA* overexpression can prevent *dnaA(cos)* filamentation,[15] therefore, this chapter also surveyed *cedA's* ability to prevent other pathways that lead to filamentation. We also questioned whether CedA was able to reverse pre-formed filaments. The combination of transcriptomics and genetics from this study provides a preliminary insight into how CedA functions.

4.3.1 CedA is conserved in strains that inhabit and cause infection of the gastrointestinal tract and/or urinary tract

Bioinformatics demonstrated that CedA is widely conserved within the Enterobacteriaceae family of the Bacteria domain of life. It also found that CedA is specifically found in strains that inhabit or cause infection of the gastrointestinal tract and urinary tract, suggesting that CedA has a biological function in the pathogenesis of bacteria. There were only 2 out of 46 species that CedA was found in that are not known to cause infection. Currently, based on its 3D structure, CedA has similarity to transcription factors,[107] however, there is little *in vivo* data to support this potential function. It can also be seen to bind to DNA.[107,108] There does not appear to be any strong conservation amongst the terminal ends of the amino acid sequence of the protein and the protein does not appear to have any domains found in other proteins. This suggests a possible importance of *cedA*'s unknown function to gastrointestinal infections.

4.3.2 CedA can promote cell division in WT cells

Limited data on the effects of the overexpression of *cedA* in WT *E. coli* has demonstrated that it can lead to the alteration in the timing of cell division during the cell cycle.[15] To further our understanding of *cedA* we overexpressed it in BW25113 and UTI89. It was found that in the absence of a significant change in the growth rate *cedA* overexpression

led to significantly smaller cell size, therefore, suggesting that CedA can promote cell division. Interestingly, the effect of *cedA* overexpression leading to smaller cells was more prominent in UTI89 than BW25113. The hypothesised reason for the difference between backgrounds may be due to the faster maturation of the FtsZ-ring in UTI89 as it is known that does not affect the growth rate.[168] A known example of gene concentration affecting cell size is *ugpT* whereby during nutrient-poor conditions it allows unhindered cell division and therefore smaller cells are produced.[169]

To understand how *cedA* was able to promote cell division in WT cells transcriptomics was employed. Using RNA-seq, we found that 191 genes were significantly changed in BW25113 *cedA* overexpression. More specifically, carbohydrate and amino acid transport and metabolism were found to have the highest level of change. Notably, the fructose operon and the *rbs* operon were downregulated. This result may be considered expected as the cultures were grown in Luria Broth, a rich-medium. In line with previous findings, these genes are not deemed essential during growth in nutrient-rich conditions.[170] On the other hand, it was found that the *ent* operon and *codBA* were upregulated and they are required for iron acquisition and cytosine deaminase, respectively. It is known that both of these pathways are also upregulated during UTIs as there is limited iron and nitrogen within the urinary tract.[157] Therefore, the upregulation of these pathways might explain why CedA is conserved amongst bacterial strains that inhabit and infection of the GI tract and urinary tract.

4.3.3 CedA can partially prevent filamentation caused by *ftsZ-yfp*, *recAtif*, *zwf* and *damX*

For this study to successfully control the expression of a gene that causes filamentation and *cedA,* a co-expression system was successfully created. As expected *cedA* overexpression was able to prevent *dnaA(cos)* filamentation in our novel co-expression system. To further understand what pathways are regulated when *cedA* prevents *dnaA(cos)* filamentation transcriptomics was used. This analysis demonstrated that *cedA* was also able to downregulate the SOS response, which would normally be upregulated when *dnaA(cos)* causes filamentation (*Section 3.2.4*). Katayama, et al.[15] suggested that in

dnaA(cos) cedA overexpression cells although *cedA* was able to prevent filamentation these cells still had a higher copy number of chromosomes compared to WT. This demonstrated that while *cedA* could overcome the block to cell division it was unable to overcome over-replication of the chromosome. In addition to our findings, we hypothesise that the SOS response may be induced after the main cause of over-replication has occurred and therefore DnaA(cos) filamentation is caused by the SOS response and *cedA* can prevent it.

In addition to the SOS response, transcriptomics of the *dnaA(cos)* filamentation prevention by *cedA* identified some of the genes involved in the fatty acid synthesis (FAS) pathway were upregulated. This is of interest because FAS is thought to control bacterial cell size, by setting the cell envelope capacity.[159] Therefore, it is possible that in response to imminent filamentation, the upregulation of *cedA* also leads to an increase in genes involved in FAS to increase phospholipid content and therefore, maintain normal cell shape. It was also found that the *omp* gene cluster was upregulated in our study, which may allow a greater influx of nutrients to maintain proper cell division. During *dnaA(cos)* filamentation it was found that Δ18*cedA* was able to prevent filamentation although it was not to the same extent as *cedA*. Similarly, *cedA-gfp* was also able to prevent filamentation to a slightly lesser extent than *cedA,* demonstrating that the fusion is functional and can be used in future studies, suggesting that the C-terminus and N-terminus are not required for the reactivation of cell division. Abe, et al.[108] have already demonstrated that Δ18*cedA* can reactivate cell division.

To build on the knowledge that *cedA* can prevent filamentation in *dnaA(cos)* this study tested an array of genes known to cause filamentation through a variety of pathways. This study found that *cedA*, Δ18*cedA* and *cedA-gfp* can partially prevent filamentation caused by *ftsZ-yfp*, *recAtif,* and *zwf*. While only *cedA* and not its variants can partially prevent filamentation caused by *damX,* therefore, suggesting that *cedA* can prevent filamentation that is caused by a direct block to cell division, the SOS response, metabolism and UPEC reversible filamentation, respectively. This work was the first to verify whether *zwf* overexpression could cause filamentation as it was a hit in an overexpression screen to identify genes in UTI89 that cause filamentation.[166] It was found that *zwf* overexpression

does not lead to the formation of very long filaments but rather a slight elongation of the cell length. However, it does not matter the extent of filamentation, as *cedA* may have the ability to sense an upcoming arrest in proper cell division and can prevent this from occurring. As Katayama, et al.[15] concluded, *cedA*s ability to prevent filamentation was independent of changes to the nucleoid structure in the *dnaA(cos)* background. This study also found that in the *zwf* background the nucleoid organisation was unaffected by *cedA* overexpression.

This study found pathways of filamentation that *cedA* was unable to prevent such as *slmA,* and *slmA-SBS* overexpression. It is clear from the results that *slmA* and *slmA-SBS* overexpression led to severe filamentation and therefore these strains were regularly subjected to suppressor mutations. which very often led to their inability to filament. Therefore, it is possible that due to their toxicity and possible high abundance of SlmA in the cell CedA was unable to overcome its high presence so that it could prevent filamentation. Another possibility is that through CedA ability to bind DNA it competes with SlmA or SlmA counteracts CedA function in the prevention of filamentation. Additionally, we found that CedA is unable to reverse filamentation. There are no results in the literature that have considered the difference between prevention and reversal of filamentation by *cedA*. These are biologically significant because prevention suggests that CedAs protein levels may need to match that of the protein causing filamentation in order to continue normal cell division processes. Whereas in a reversal, filamentation has already happened and CedA must work to reactivate cell division and this may be independent of the protein levels. This study found that CedA is unable to reverse filamentation that is caused by a defect in replication initiation (*dnaA(cos)*) and a direct block to cell division (*ftsZ-yfp*).

4.3.4 CedA can prevent UPEC filamentation

Finally, we tested the effect of *cedA* overexpression in UTIs using an *in vitro* flow chamber infection model. It was found that *cedA* overexpression in UTI89 leads to a prevention of filamentation that is caused during infection. However, it appears that the dispersed bacteria during the prevention are ghostly in appearance and may not be viable. Due to time restraints, we were unable to develop an assay that would allow us to ensure

that the infection was equal for both WT and *cedA* overexpression before dispersal and then quantify the difference in viability between these strains after dispersal. Additionally, it was found that Δ18*cedA* was not able to prevent filamentation like *cedA* and *cedA-gfp*, suggesting that the N-terminus of *cedA* is required during UPEC infection for the reactivation of cell division. This would suggest that the mechanism of prevention during infection is different from the other pathways that were tested in this chapter. Therefore, these results suggest that during infection the increase of *cedA* expression during the later stages may create the diversity seen in the morphology of the bacterial cells. It is known that when the bladder cells erupt both filaments and short cells are released. It is possible that the short cells have remained short due to the upregulation of *cedA* in these cells. Also, recently Iosifidis, et al.[120] found that not all bladder cells will release filamentous bacteria and that some IBCs do not progress to filaments and remain as short rod-shaped cells. It is possible that the IBCs that remain as rods have *cedA* upregulated in them to ensure that when the bladder cells erupt, the short cells can immediately infect neighbouring bladder cells as this is imperative for the continuation of the infection.[10,11]

Overall, this chapter has demonstrated that CedA can prevent the arrest of cell division by multiple pathways, such as a direct block to cell division (*ftsZ-yfp)*, the SOS response (*recAtif)*, metabolism (*zwf*), and UPEC infection. This suggests that CedA does not specifically work to prevent filamentation due to an excessive chromosomal number as suggested by Katayama, et al.,[15] but rather may overcome general cell division inhibition by promoting the expression of genes involved in FAS or carbohydrate metabolism. We found that CedA is unable to reverse filamentation and prevent filamentation caused by *slmA* and *slmA-SBS* overexpression. This may be due to a dose-dependent effect of CedA, whereby CedA must be able to neutralise the protein causing the inhibition of cell division.

The work in this chapter can be further expanded by follow-up experiments relating to the transcriptomics results. For example, to understand whether CedA upregulates FAS during prevention to control cell size would provide insight into the mechanisms of CedA. FadR is a transcriptional regulator that controls fatty acid metabolism and its overexpression in WT leads to an increase in cell size.[159] Therefore, a future study could

use the overexpression of *fadR* during *dnaA(cos), ftsZ-yfp, recAtif, zwf* and *damX* filamentation to determine if FAS can prevent filamentation. This would then suggest that CedA regulated metabolism to control cell size. Also, by using the *in vitro* flow chamber model and cell sorting it would be possible to determine whether *cedA* is expressed in the filaments or short cells after the dispersal stage of infection. It is hypothesised from this work that the short cells would have an upregulation or higher expression level of *cedA* compared to the filaments. As there is very little known about the later stages of UPECs infection cycle this information would be crucial for future therapies.

4.4 Methods

4.4.1 Bacterial Strains and Plasmids

E. coli BW25113 and JM12 were obtained from the *E. coli* Genetic Stock Center (Yale University, USA). *E. coli strains* TB28 pTB67 and HC328 pHC534 were kindly provided by T. Bernhardt. *E. coli* plasmids pBAD24 and pLAU80 were kindly provided by J. Moller-Jensen. BW25113 and TB28 pTB67 were routinely cultured at 37ºC on solid or liquid Luria broth (LB). HC328 pHC534 was routinely cultured at 30ºC on solid or liquid LB. JM12 was routinely cultured in M63 supplemented with adenine (100 μg/mL).

For the prevention and reversal style experiments a plasmid that was compatible with pBAD24 was created named pTAB2. This plasmid contained a Tet repressor that allowed for the expression of *cedA* and its variants (*Δ18cedA* and *cedA-gfp*) using anhydrotetracycline. pTAB2 contained the backbone of pASKIBA5C which consisted of the multiple cloning site, chloramphenicol and the Tet repressor; also the p15A origin of replication from pACYC184 (Figure 4.19).

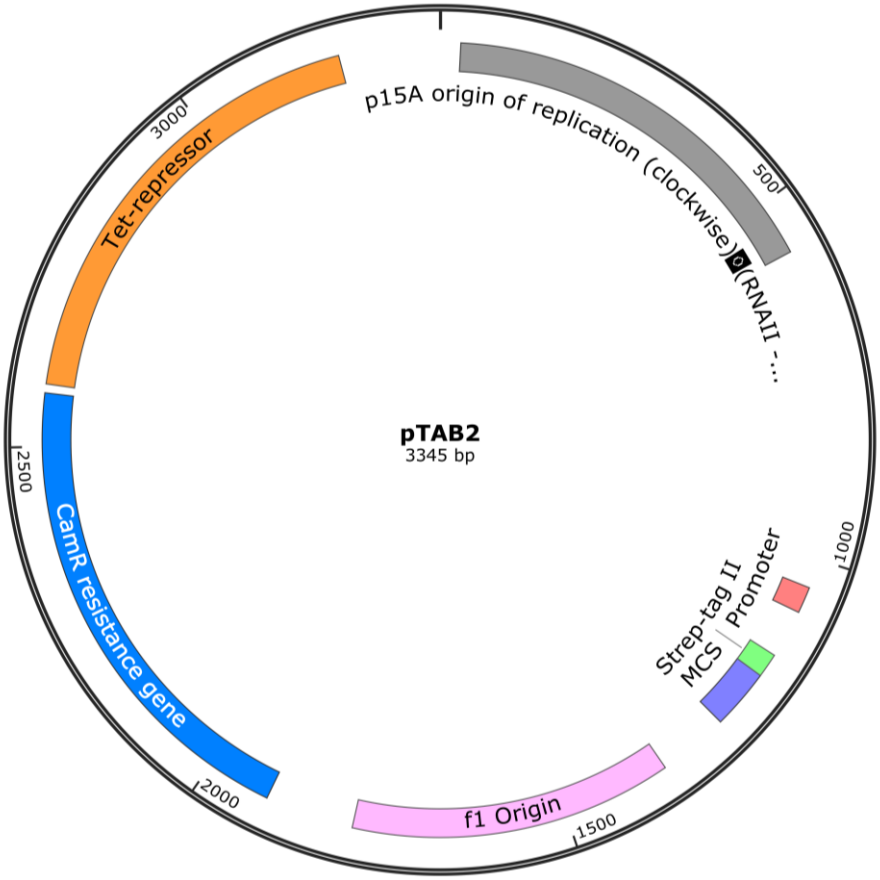

Figure 4.19 Plasmid map of pTAB2

In order to, clone these two parts of the novel plasmid together, PCR with Phusion DNA polymerase (NEB) was employed to amplify the regions of interest using primers pASK_F_NotI and pASK_R_ApaI to amplify the region of interest from pASKIBA5C and p15A_F_NotI and p15A_R_ApaI to amplify the region of interest from pACYC184 (Table 4.2). After the completion of the PCR, a DpnI (NEB) treatment was performed on the reaction to remove any template DNA that it would interfere with downstream cloning. The products were purified using Isolate II PCR and gel-extraction kit (Bioline) before a sequential digest with restriction enzymes ApaI and NotI. The ligation mixtures were then transformed into chemically competent DH5α and then clones selected on solid LB agar supplemented with chloramphenicol (35 µg/mL) were chosen for a restriction digest check. To confirm the sequence of the clone it was sent for sequencing with the Australian Genome Research Facility (AGRF).

A similar approach was used to sub-clone genes *cedA*, Δ*18cedA* (first 18 amino acids of *cedA* removed from the N-terminus)[108] and *cedA-gfp* (monomeric super folding GFP fused to the C-terminus of *cedA*) into pTAB2 and *zwf* and *damX* into pBAD24. The DNA oligonucleotide and the integrated restriction sites are listed in Table 4.2. After PCR the products were cleaned up using Isolate II PCR and gel-extraction kit (Bioline) and double digests were performed. The genes for pTAB2 were selected for on chloramphenicol (35 μg/mL) and genes for pBAD24 were selected for on ampicillin (100 μg/mL). All clones selected were confirmed by DNA Sanger sequencing at AGRF.

Table 4.2 Oligonucleotides and their respective restriction enzymes used for the construction of pTAB2. Sub-cloning cedA, 18ΔcedA, cedA-gfp into pTAB2 and zwf and damX into pBAD24.

Name	Sequence (forward 5' → 3')	Source
pASK_F_NotI	GGC AGG GCG GCC GCC TTT TGC TGG CCT TTT GCT C	Macrogen
pASK_R_ApaI	GCC CCG GGG CCC TTT TCT ACG GGG TCT GAC GC	Macrogen
p15A_ F_NotI	GGC AGG GCG GCC GCA CTG ATT TAG TGT ATG ATG G	Macrogen
p15A_R_ApaI	GCC CCG GGG GCC CTC TGA TTA ATA AGA TGA TCT T	Macrogen
cedA_F_XbaI	GCC CCG TCT AGA AGG AGG AAT TCC ATA TGC GTT TAG TGA AGC CAG TAA TG	IDT
cedA_K12_R_XhoI	GCC CCG CTC GAG TTA CTC AGT CAC TTC CCC	IDT
msf_gfp_R_xho	GCC CCG CTC GAG TTA TTT GTA GAG TTC ATC CAT G	IDT
KO18cedA_F_XbaI_NdeI	GCC CCG TCT AGA AGG AGG AAT TCC ATA TGA TTA GCT ATG TCC CAC GC	IDT
zwf_F_NcoI	GGG GCC ATG GCC GCG GTA ACG CAA ACA GC	IDT
zwf_R_HindIII	GCG CCG AAG CTT TTA CTC AAA CTC ATT CCA GGA A	IDT
DamX_F NcoI	CG CCA TGG ATG AAT TCA AAC CAG AAG A	IDT
DamX_R Hind	GCT AAG CTT ACT TCA GAT CGG CCT GTA	IDT

4.4.2 Phylogenetic Analysis

The CedA sequence (VWQ02694.1) was obtained from NCBI and used as a query in JACKHMMER version 2.41.1[171] in all predefined representative, one at a time. This

search displayed 38 query matches with the highest E-value of $1.2x10^{-11}$. From here blastp was used restricting each search to a specific organism genus as provided by JACKHMMER. The top 3 matches with the highest coverage of the protein and lowest E-value were selected for the alignment. In some cases, there were only 1 or 2 species per genus.

A MUSCLE[172] multiple sequence alignment was built from the sequences collected and then a maximum likelihood phylogenetic analysis was performed in MEGA-X.[173] The maximum likelihood was bootstrapped with 500 replicates.

4.4.3 Prevention and Reversal of Genes that cause Filamentation

Several different genes that cause filamentation (filamentors) were selected to survey different biological pathways in the cell. The first style of experiments performed were prevention experiments. In these experiments *dnaA(cos) zwf, damX* and *ftsZ*-yfp were expressed from pBAD24 with 0.2% (w/v) L-arabinose. *recA(tif)* was expressed from JM12, *slmA* from TB28 pTB67 and *slmA*-SBS from HC328 pH534 with adenine (100 µg/mL) and IPTG (1mM and 0.5mM), respectively. Simultaneous to the expression of these filamentors, *cedA*, Δ*18cedA* and *cedA-gfp* in pTAB2 were induced with 0.2 µg/mL of anhydrotetracycline. Firstly, the strains were cultured overnight in liquid LB with chloramphenicol (35 µg/mL) and ampicillin (100 µg/mL) at 37°C or 30°C for HC328 pHC534. Then the next morning the cultures were diluted down to OD_{600} = 0.01 and left to grow at the same temperature as overnight for 2 hours. After 2 hours the cultures were diluted down to OD_{600} = 0.01 in LB containing the appropriate antibiotics and the inducers. JM12 was handled differently from the other strains, from a colony on a plate on the day of the experiment the strain was cultured in M63 media with chloramphenicol (35 µg/mL) at 30°C for 2 hours. After 2 hours the culture flasks were switched to 42°C and adenine (100 µg/mL) and anhydrotetracycline (0.2 µg/mL) was added. The samples were harvested when the cells reached the appropriate OD_{600} that allowed for observable filamentation which was between OD_{600} = 0.1 for *slmA* and *slmA*-SBS, OD_{600} = 0.3 for *dnaA(cos)*, OD_{600} = 0.5 for *zwf* and OD_{600} = 0.7 for *damX.* for the different strains. JM12 was harvested 3 hours after the switch of temperature to 42°C.

Once the cells were harvested, they were fixed on 2 % (w/v) paraformaldehyde and stored at 4°C for downstream analysis. The samples were run on the Beckman Coulter Counter (*Section 2.7.1*) and cell volume distributions were used for correlation analysis in Graphpad Prism 8. For microscopy (*Section 2.7.2*), the cells were stained with Hoechst (1 µg/mL) and were mounted on a 1% (w/v) agarose gel pad (in phosphate-buffered saline). The cells were then imaged in phase contrast and epifluorescence with a Zeiss Axioplan 2 microscope using the 100x oil objective.

For reversal experiments, instead of inducing the filamentor and *cedA* at the same time, the filamentors were induced for approximately 2 hours before the induction of *cedA* to allow for filamentation. After 2 hours *cedA* was induced (with 0.2 µg/mL anhydrotetracycline) and the cells were harvested every 30 minutes for 2 hours. The samples were fixed and analysed as mentioned previously.

For *damX* filamentation, to analyse the significance of the increasing cell volume as the OD_{600} increases a Krustal-Wallis test was used on the median cell volume at each OD. This is a nonparametric test where the null hypothesis assumes that the samples are from identical populations.

Chapter 5
CedA is not required for the dispersal of filaments during UPECs infection cycle

5.1 Introduction

UPEC is a part of the human intestinal microbiome where it rarely causes disease. However, it has the ability to disseminate and colonise the urinary tract, which is possible through the use of various virulence factors (*Section 1.1*). Furthermore, these virulence factors have specific roles for the various stages of the intracellular infection within bladder cells.[10] During this multi-stage infection, UPEC undergo numerous morphological changes that allow for the formation of biofilm-like intracellular bacterial communities (IBCs), followed by dispersal of bacterial filaments, and then the reversal of these filaments back into their short rod-shaped cells.[10,11]

To initiate infection, UPEC adheres to the luminal surface of the bladder epithelium, using adhesive fibres such as Type-1 pili, which recognise mannosylated glycoproteins receptors present on the bladder epithelium.[29] After the attachment of UPEC to the bladder surface, it becomes internalised via endocytosis.[32] Once inside the bladder cell, UPEC begins to replicate rapidly, forming IBCs, where the rod-shaped bacteria divide into coccoid daughter cells that are tightly packed together.[31] Then, as the IBC reaches its last stage of development, subpopulations of filamentous UPEC develop.[10] As the IBC begins to overwhelm the bladder cell due to the high density of bacterial cells, it is thought to lead to the rupture of the bladder cell and dispersal of bacteria.[10] UPEC filaments are thought to be advantageous as they provide a stronger attachment to the bladder cell wall, allowing UPEC to survive the shear force of urine.[11] Additionally, filamentation allows the bacteria to avoid consumption by phagocytosis through the host immune response.[14] Filaments are then able to revert into short rod-shaped bacteria that can continue to divide as normal and thus, initiate a new infection cycle.[11] Despite the different stages that occur within UPEC infection cycle being well defined, the specific genes that are required are lesser-known.

Recently, genes that are required for each stage of UPEC infection have been identified in a high-throughput Transposon Directed Insertion Site Sequencing (TraDIS) analysis of the genetic requirements of UPEC during an *in vitro* infection.[174] Mediati, et al.[174] identified genes in the IBC phase, dispersal phase, and recovery phase of UPEC infection.

Of interest to the present study, *cedA* was identified as a gene putatively required for the dispersal phase. Additionally, *cedA* has previously been linked to the filamentous stage of infection, as it was shown to be upregulated 8-fold from systematic transcriptional profiling of UTI89 during infection using a microarray.[16] This suggests that *cedA* may have a role in the formation of filaments during UPEC infection. However, Khandige, et al.[16] observed using an *in vitro* flow chamber UTI model that UTI89Δ*cedA* was able to form IBCs and filaments to approximately the same extent as WT UTI89. Therefore, the role that *cedA* has during the later stages of filamentation and dispersal of UPEC remains unclear. This thesis aims to quantify uTI89Δ*cedA* during dispersal in comparison to WT during a competition style experiment to investigate whether Δ*cedA* is required for normal IBC and filament formation. Interestingly, another gene that has been studied in this thesis, *slmA,* was identified in the TraDIS screen. *slmA* was putatively essential during the recovery of UPEC filaments into normal rod-shaped cells.[174] SlmA is a nucleoid occlusion factor that inhibits FtsZ polymerisation over the nucleoid.[91] The nucleoid structure in UPEC filaments has not been studied in detail and it was of interest to elucidate how SlmA is involved in filament reversal.

In this chapter, we initially set out to phenotypically characterise the deletion of *cedA* (Δ*cedA)* in *E. coli* backgrounds BW25113 and UTI89, as these are the parental strains of the majority of the strains used in this thesis. Next, we used an *in vitro* human bladder cell culture to perform competition assays between UTI89, UTI89Δ*cedA,* and UTI89Δ*slmA*. This study set out to determine whether *cedA* was required for the dispersal stage of infection and whether *slmA* was required for the reversal of filaments during recovery. The mechanisms during these two stages of UPEC infection cycle remain largely unknown and thus, characterising the role of these two genes during infection may shed light on new strategies used by UPEC to cause re-infection and subsequently, help to uncover new treatments and therapies for UTIs in the future.

5.2 Results

5.2.1 *cedA* deletion does not have any obvious phenotypes

In Chapter 4, the overexpression of *cedA* demonstrated that, in addition to having a role in normal cell growth, CedA may have a role in promoting cell division in various situations that lead to filamentation. This suggests that it may function broadly to promote cell division. To further investigate this hypothesis, Δ*cedA E. coli* strains were used to determine its effects on cell morphology, cell growth, and Z-ring formation. Since it is established that c*edA* is not essential, this mutant can be further characterised (according to profiling of *E. coli* chromosome).[175] BW25113 and UTI89 *E. coli* backgrounds were used for the deletion experiments. It was hypothesised that *cedA* may have an effect on cell division and therefore, to visualize the Z-rings, a GFP-tagged Z-ring structural protein, *zapB* was utilized. A ZapB fusion has been previously determined to be functional[85]. In this study, *zapB-gfp* was cloned into pTAB1 (*Section 2.7.2*) and it was determined that a concentration of 0.05 mM IPTG was appropriate for inducing *zapB-gfp* to visualize the Z-rings (Figure 5.1). The bacterial cells were grown in liquid LB media and passaged twice until mid-log phase, at which point they were fixed and analysed. Notably, any concentration higher than 0.05 mM IPTG would lead to the formation of ZapB-GFP inclusion bodies at the poles and filamentation, also previously reported (Figure 5.1).[85]

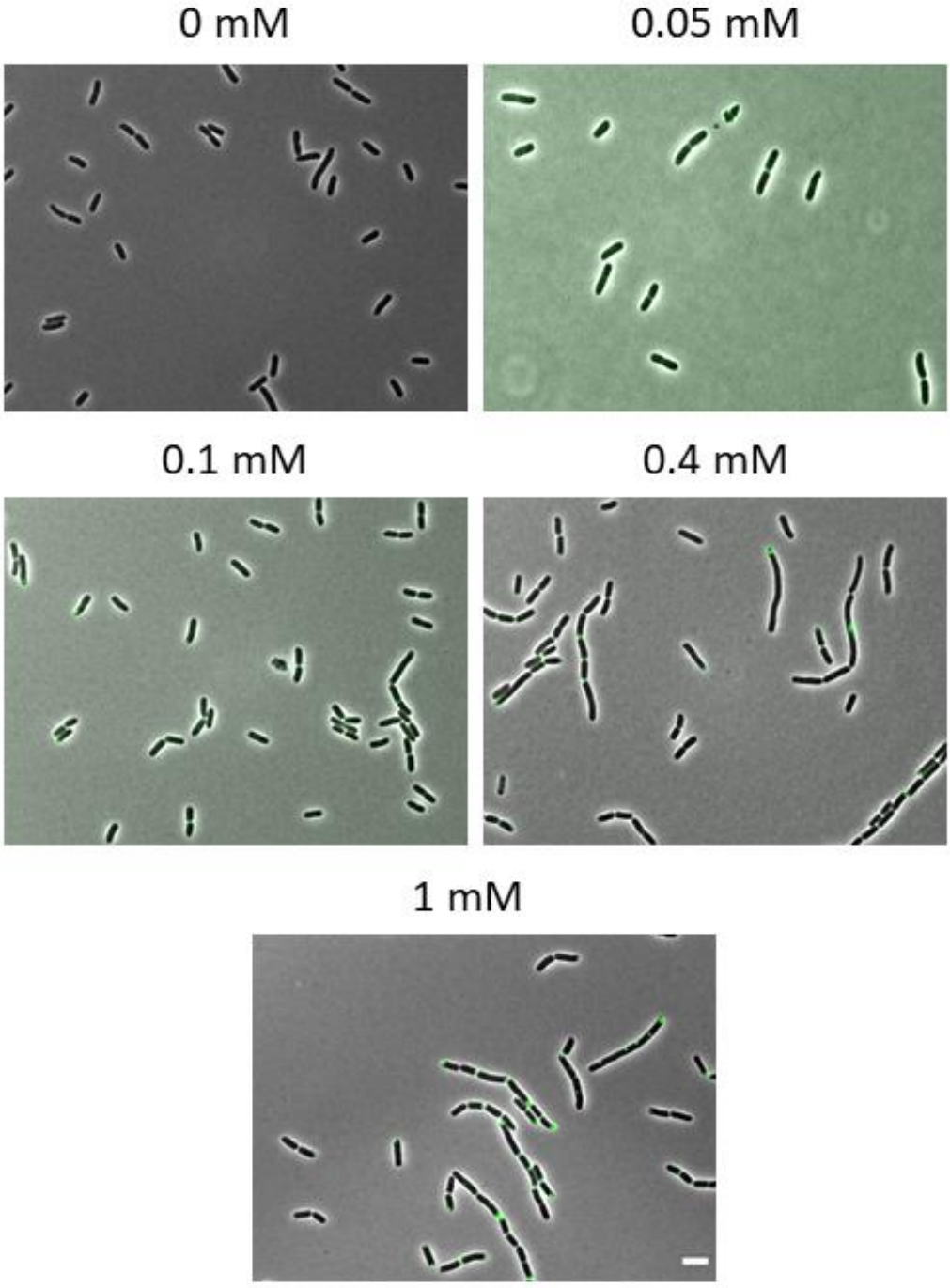

Figure 5.1 ZapB-GFP expression in UTI89 to visualise Z-rings.

UTI89 3 was transformed with pTAB1 zapB-gfp and cultured in LB containing 35 µg/mL chloramphenicol. To induce zapB-gfp various concentrations of IPTG was added to the diluted culture at OD_{600} = 0.01, the culture was left to incubate until OD_{600} = 0.5 when the cells were fixed. Scale bar is 5µm (Section 2.9.2).

From the initial characterisation studies, it was found that Δ*cedA* did not have an effect on cell size in LB media, as WT and Δ*cedA* in both of *E. coli* backgrounds had the same

cell size distributions (Figure 5.2A). Additionally, Δ*cedA* did not have an effect on Z-ring positioning (Figure 5.2B, C) or the timing of Z-ring formation (Figure 5.2D), as it was found to always form at the mid cell in the Δ*cedA* in both backgrounds. However, it was noted that the Z-ring formation began at a shorter cell length in BW25113 when compared to UTI89. This demonstrates that although these backgrounds are considered WT they act slightly different from one another. Finally, the synchrony of the initiation of DNA replication was assessed using chromosomal runouts on the BW25113 only.[129] Of note, as mentioned in Chapter 4 chromosomal runouts do not work within the UTI89 background. For unknown reasons, we found that the chromosomal runout method did not work in the UTI89 strain, as there were no peaks for the different numbers of chromosomes (Figure 5.2F). It was found that there was no difference between WT and Δ*cedA* in BW25113, with the standard number of chromosomes for bacterial cells growing fast in a rich-medium (Figure 5.2E).[176] Overall, it appears that Δ*cedA* does not have any obvious phenotypic traits in a single deletion strain under standard laboratory growth conditions. To further support this finding, transcriptomics data (*Section 2.6.7*) found that in WT BW25113 there were very low reads for *cedA*, suggesting that under normal growth conditions *cedA* is not expressed or required.

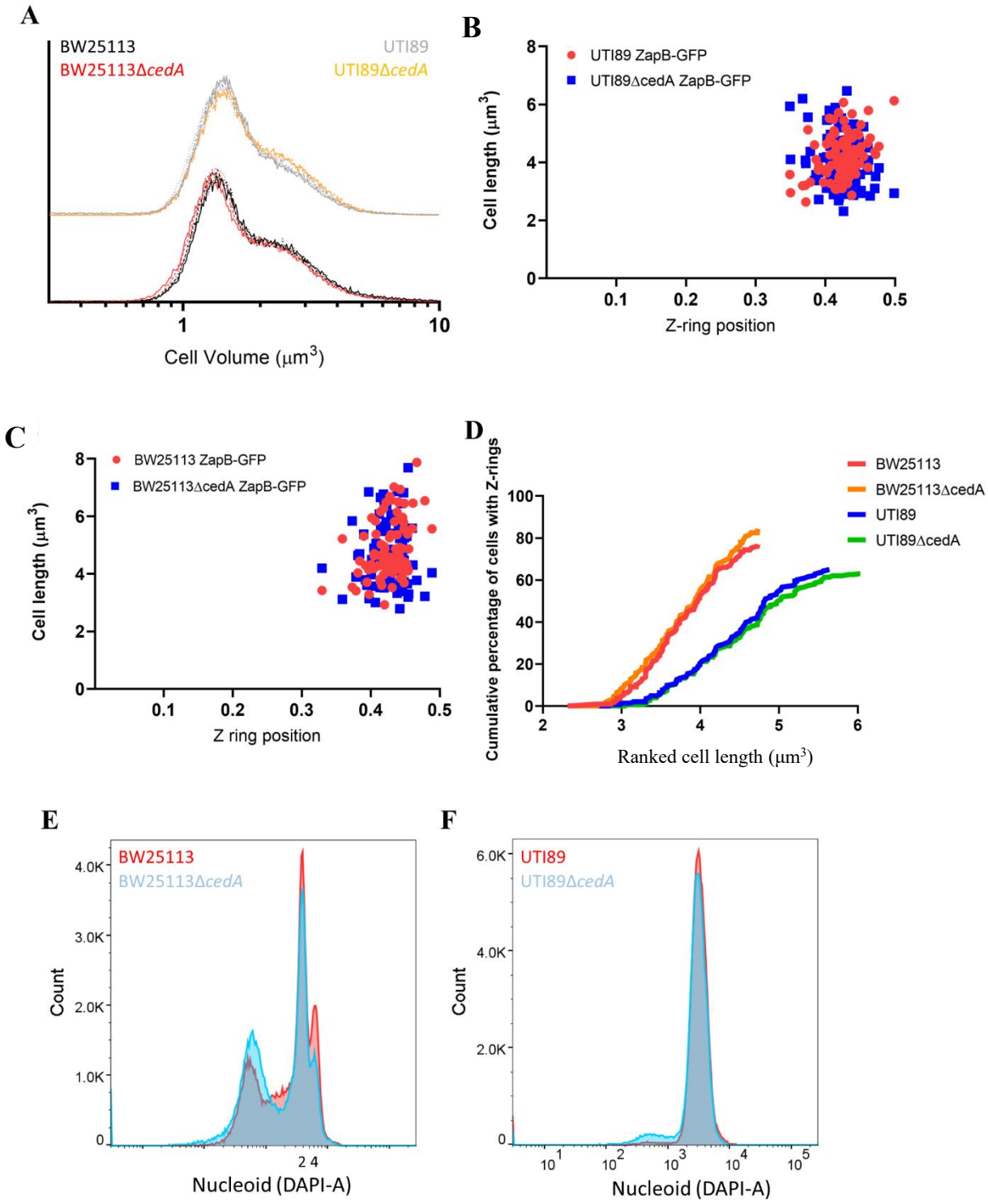

Figure 5.2 ΔcedA does not affect E. coli growth, morphology or the timing of mid-cell Z-ring formation.

The open reading frame of cedA was deleted from UTI89 and Keio collection BW25113ΔcedA were transformed with pTAB1 zapB-gfp grown in LB medium with and without chloramphenicol (35 μg/mL) at 37°C. A) Cells were fixed at mid-log and they were measured on the Coulter counter to obtain cell volume distributions. Triplicate data shown as different line patterns. B&C) Z-ring positioning in UTI89 and BW25113

backgrounds were determined using ZapB-GFP, induced with 0.05 mM IPTG. The x-axis is the position of the Z-ring along the cell length and the y-axis is the cell length. Over 100 cells were measured and are represented by an individual dot. D) The timing of Z-ring position in both backgrounds, the x-axis is the cell length ranked in increasing order and the y-axis is the cumulative percentage of the cells that contain a Z-ring (Section 5.4.2). E&F) Chromosomal runouts to determine the number of chromosomes per cell in the UTI89 and BW25113 backgrounds. When the cultures reached OD_{600} = 0.1, 5mL of the culture was added to a flask containing cephalexin (15 μg/mL) and rifampicin (300 μg/mL). After 3 hours of incubation, the cells were fixed. The cells were then stained with DAPI and analysed on the flow cytometer. On the x-axis is the nucleoid intensity from the DAPI stain and the y-axis is the count. The most left peak is in the BW25113 background is noise. Data is representative of replicate data.

5.2.2 *cedA* is not required for the dispersal of UPEC from BECs *in vitro*

In a TraDIS screen to identify the essential gene profile set of UPEC during an infection model, *cedA* was shown to be essential during the dispersal phase of infection.[174] This was defined as a 10-hour window, 34 hours post-infection, where the bacterial cells undergo morphological changes and subsequent dispersal from the bladder cell.[10,11] The TraDIS screen also identified *slmA* as a gene required during the bacterial reversal phase. This phase was defined as after the dispersal the cells from the infection, they were then grown in LB for 18 hours for recovery.

We began our studies with Δ*cedA* during infection. It has previously been demonstrated that UTI89Δ*cedA* is able to form IBCs and filaments during a flow chamber UTI infection model.[16] This study set out to determine whether UTI89Δ*cedA* could undergo dispersal to the same extent as WT. To determine the more fit strain, we devised a competition-style UTI infection model in 6-well dishes (*Section 5.4.1*). The competition-style assays were perfectly controlled for due to both WT and UTI89Δ*cedA* being treated in identical ways. Briefly, each well contained PD07i bladder cells infected with both UTI89 and UTI89Δ*cedA*. In order to distinguish WT from UTI89Δ*cedA*, the strains were transformed with pGI5 (constitutive GFP expression[120]) or pGI6 (constitutive mCherry expression) and also the reverse order of plasmids in the strains. Three different samples were collected from the Δ*cedA* infection; 1) pre-infection sample, which contained an equal mixture of the strains, 2) sample 1, which was 20 hours post-infection during the IBC phase assess each strain's relative capacity to infect the bladder cells, and 3) sample 2,

which was 35 hours post-infection during the dispersal phase where the bacterial cells would have undergone morphological changes and the bladder cells would have erupted and released the bacteria. This study set out to determine whether *cedA* is required for the dispersal of UPEC from the bladder cells, and it was hypothesised that UTI89Δ*cedA* would have a fewer number of cells compared to WT in sample 2. Each sample was analysed using flow cytometry and microscopy. To control the flow cytometry analysis, individually labelled cells that contained either pGI5 (green) or pGI6 (red) were used to set the gates for all of the samples. This determined that the red cells (pGI6) were found in upper left quadrant (H1-UL) and lower left quadrant (H1-LL) as these contain the cells with only the red signal. The green cells were found in the lower right quadrant (H1-LR) as this contains the cells with only the green signal. There appear to be cells that are fluorescing both colours and these are a small proportion that was found in the upper right quadrant (H1-UR). This appears to be an artefact of the mCherry signal overlapping the GFP channel. Additionally, microscopy image analysis was performed to count the number of cells fluorescing each colour (Table 5.1). Due to filaments becoming tangled and overlapping in the images quantification of filament numbers was not considered accurate (sample 2 for *cedA* experiments and sample 1 for *slmA* experiments). For these samples flow cytometry was relied on.

As expected, from the flow cytometry, the pre-infection samples showed almost an equal mixture of WT (41%) and UTI89Δ*cedA* (59%) (Figure 5.3, panel A). IBC phase sample 1 also almost had an equal mixture of WT (54%) and UTI89Δ*cedA* (46%), suggesting that Δ*cedA* does not affect the ability of UTI89 to invade and progress to IBCs in bladder cells, previously concluded by Khandige, et al.[16]. Microscopy analysis also demonstrated that there were equal amounts of WT (42%) compared to UTI89Δ*cedA* (57%) (Table 5.1). After 15 hours of exposure of urine leading to the filamentation and dispersal of bacteria, there are slight more UTI89Δ*cedA* cells (58%) compared to WT (42%) on average from triplicate flow cytometry data (Figure 5.3; panel C; sample 2). This suggests that *cedA* is not required for the dispersal stage as previously suggested from the TraDIS screen.

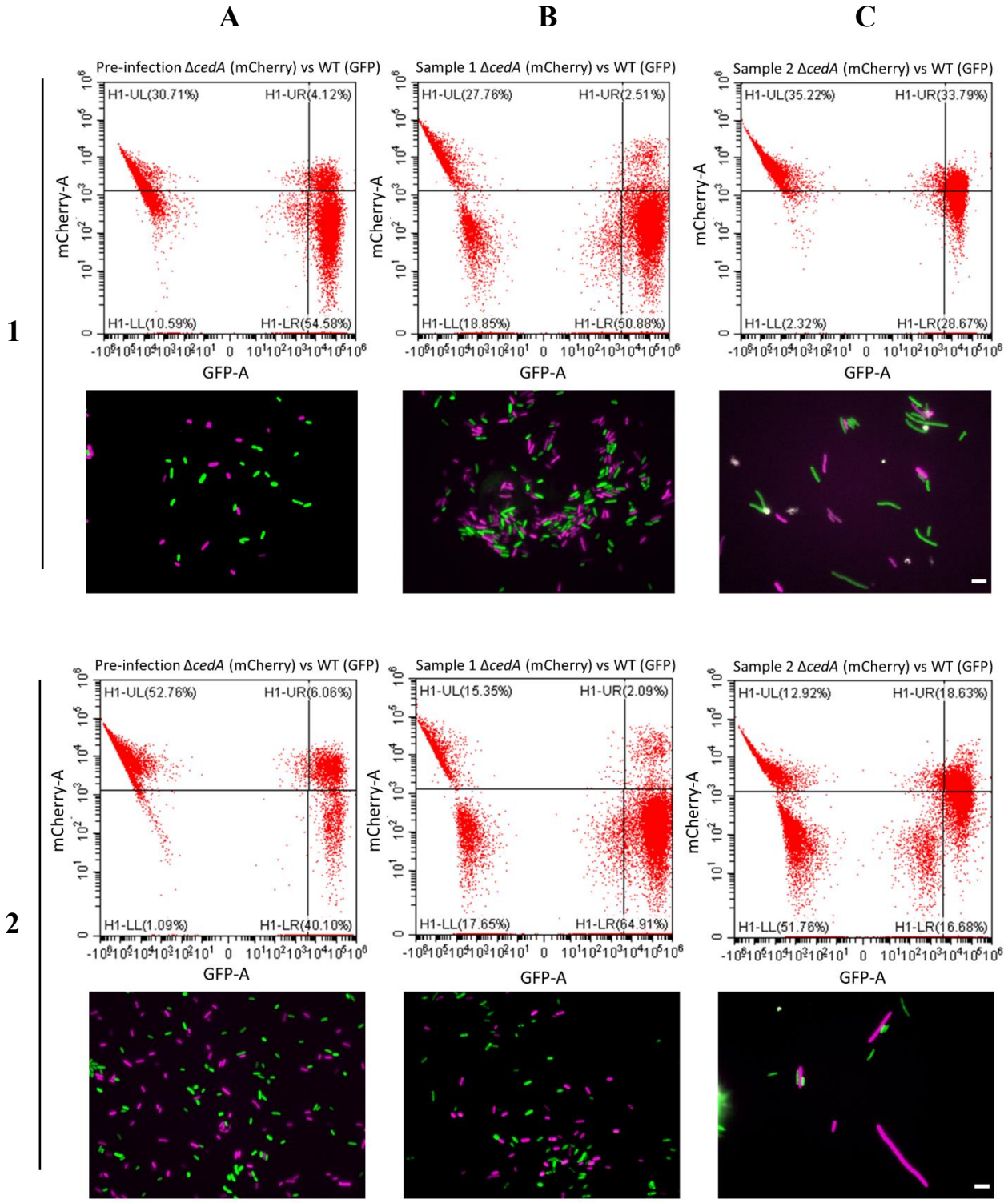

Figure 5.3 cedA is not required for the dispersal of filaments from IBCs.
Competition assays were performed using an up-scaled bladder cell infection model. Two sets of representative data are shown (1&2) (performed 4 times). PD07i bladder cells were infected with an equal mixture of UTI89 and UTI89ΔcedA (both containing a constitutive fluorescent plasmid pGI5 (GFP) or pGI6 (mCherry)) (panel A, pre-infection sample). Twenty hours post-infection IBCs were lysed, and the samples were fixed and analysed (panel B, sample 1). Concentrated urine was added to induce filamentation and

after 15 hours some of the cells were fixed and analysed (panel C, sample 2). All samples were analysed using flow cytometry and compensation was performed to reduce bleed-through signal. The x-axis shows the GFP labelled cells while the y-axis shows the mCherry labelled cells. The samples were gated using a GFP only control and a mCherry only control. Cells that are only green will appear in the H1-LR quadrant and cells that are red will appear in the H1-LL and H1-UL quadrants. There are some cells that appear to fluoresce both red and green and these make up a small proportion of cells which appear in the H1-UR quadrant. Scale bar = 5 μm (Section 2.9.2).

Table 5.1 Percentages from flow cytometry and microscopy analysis of ΔcedA competition-style infection assays.

	Pre-infection						**Sample 1**						**Sample 2**					
Triplicate	1		2		3		1		2		3		1		2		3	
Strain	WT	Δ*cedA*	WT	Δ*cedA*	WT	Δ*cedA*	WT	Δ*cedA*	WT	Δ*cedA*	WT	Δ*cedA*	WT	Δ*cedA*	WT	Δ*cedA*	WT	Δ*cedA*
Flow cytometry	23	77	56	44	43	57	61	39	36	64	66	34	8	92	96	4	21	79
Microscopy	45	55	60	40	46	54	47	53	21	78	59	40	-	-	-	-	-	-

5.2.3 *slmA* improves growth for the recovery of dispersed UPEC from BECs *in vitro*

The *slmA* gene was also identified in the TraDIS screen for genes required for UPECs infection cycle.[174] After the dispersal, the filamentous UPEC have the ability to revert to rod-shaped bacteria through an unknown mechanism.[10] This process is critical for UPECs survival and invasion of other bladder cells to the initiation of a new infection cycle.[11] *slmA* was identified as a candidate gene required during the bacterial reversal phase (in LB) after the dispersal stage of infection during the screen. It is known that SlmA is an inhibitor of FtsZ polymerisation and prevents the formation of the Z-ring over the nucleoid.[71] We hypothesised that *slmA* is required during bacterial reversal of UPEC to ensure that the reversal of the filaments does not lead to division over DNA in the daughter cells. As performed previously for the *cedA* confirmation, competition assays were also performed between WT and UTI89Δ*slmA, however,* the time for the sample collection were slightly different (*Section 5.4.2*). Briefly, three different samples were collected from the Δ*slmA* infection; 1) pre-infection sample, which contained an equal mixture of the strains to ensure that there was no skew in the competition assays; 2) sample 1, which was 35 hours post-infection during the dispersal phase where the bacterial cells would have undergone morphological changes and the bladder cells would have erupted and released the bacteria; and 3) sample 2, 100 µL of the dispersal supernatant was added to LB and left to incubate for 10 hours to allow for the reversal of the filaments.

As expected, from the flow cytometry analysis the pre-infection samples contained 48% WT and 52% UTI89Δ*slmA* (Figure 5.4; panel A). Microscopy analysis from the cell count showed that 52% were WT and 48% were UTI89Δ*slmA* demonstrating almost an equal mixture of the strains being added to the infection (Table 5.2). The cell area analysis showed that 41% were WT and 59% were UTI89Δ*slmA* also demonstrating almost an equal mixture of the strains being added to the infection (Table 5.2). After 15 hours of exposure of concentrated urine leading to filamentation, it appeared from the flow cytometry that the average proportion of cells that were UTI89Δ*slmA* in sample 1 was 61% and 39% of cells were WT (Figure 5.4; panel B). Microscopy analysis of the cell

area showed that 65% of the population was WT and 35% was UTI89Δ*slmA* (Table 5.2). Results from this sample were inconclusive however it should be noted that there is variability for the flow cytometry replicates in sample 1 due to the clumping of the cells and the difficulty this creates for the flow cytometer when measuring the fluorescent signal of each cell as it passes through the probe. The clumping may be due to the bacterial cells being released from the IBC and collected in the supernatant where they are known to be sticky. Additionally, the cell fluorescence profiles of the cells stuck together differ and this adds another level of complexity for the flow cytometer. For this reason, the microscopy images were also used to measure total cell fluorescence to provide confidence when analysing this sample.

Upon the completion of the recovery of filaments in LB, it was found from the flow cytometry on average 78% of cells in this sample were WT compared to 22% of cells being UTI89Δ*slmA* (Figure 5.4; panel C; sample 2). This was supported by the microscopy analysis of cell count, where 78% of cells were WT and 22% of cells were UTI89Δ*slmA* also and cell area where 80% of cells were WT and 20% of cells were UTI89Δ*slmA* (Table 5.2). At this stage, all the cells are back to their short form as seen from the microscopy (Figure 5.4; panel C). This suggests that *slmA* important for the recovery of growth during the reversal stage of UEPC infection cycle, confirming the results from the TraDIS screen. Overall, despite sample 1 being complex for analysis the overall trend for pre-infection and sample 2 were the same for all methods of analysis.

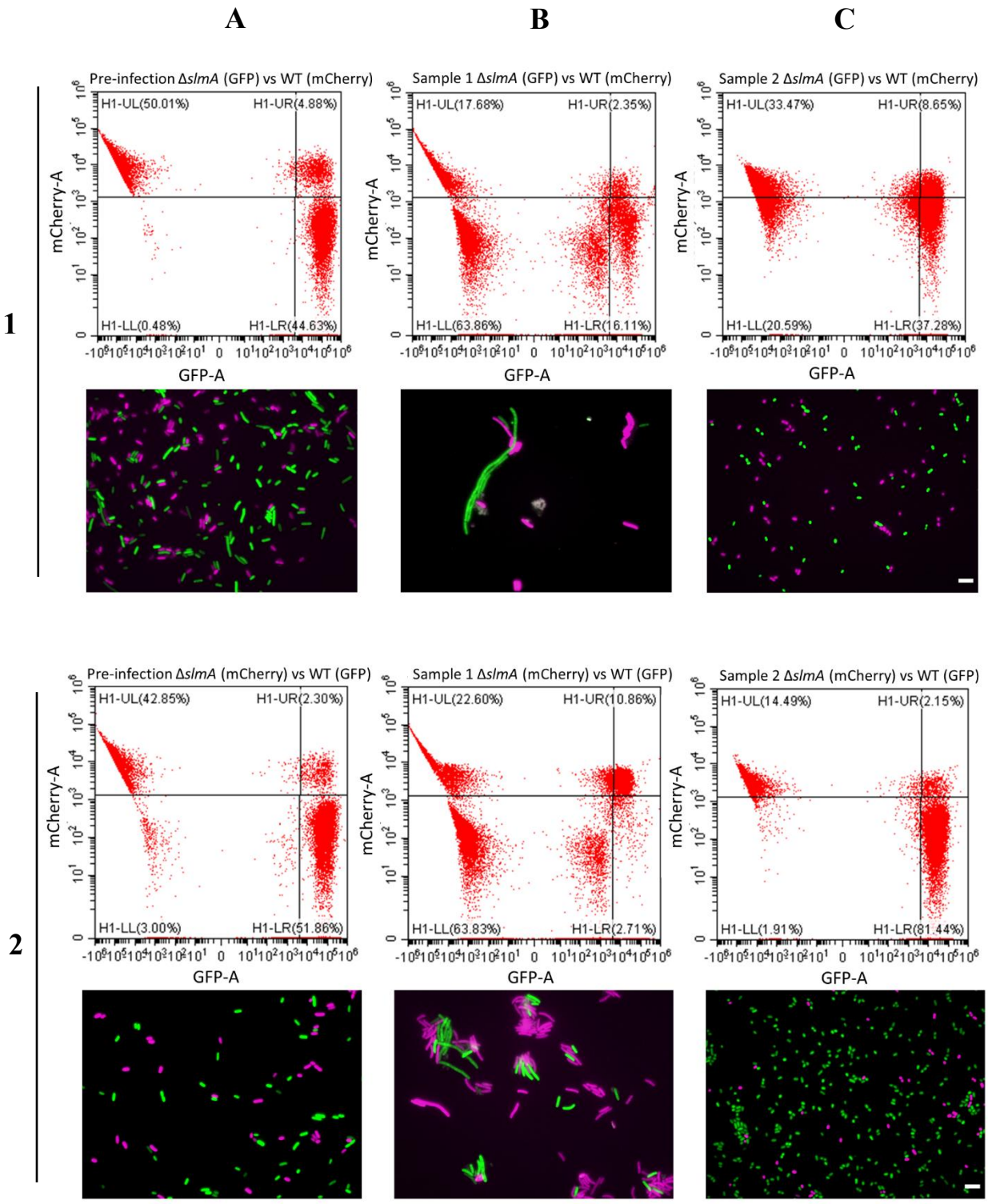

Figure 5.4 slmA is required for the growth recovery of dispersed bacteria.

Competition assays were performed using an up-scaled bladder cell infection model. Two sets of representative data are shown (1&2) (performed 4 times). PD07i bladder cells were infected with an equal mixture of UTI89 and UTI89ΔslmA (both containing a constitutive fluorescent plasmid pGI5 (GFP) or pGI6 (mCherry)) (panel A, pre-infection sample). Concentrated urine was added to induce filamentation and after 15 hours some

of the cells were fixed and analysed (panel B, sample 1). One hundred microliters of the cells were used to inoculate LB containing spectinomycin (100 µg/mL). These cells were left to incubate for 10 hours and then fixed and analysed (panel C, sample 2). All samples were analysed using flow cytometry and compensation was performed to reduce the bleed-through signal. The x-axis shows the GFP labelled cells while the y-axis shows the mCherry labelled cells. The samples were gated using a GFP only control and a mCherry only control. Cells that are only green will appear in the H1-LL quadrant and cells that are red will appear in the H1-LL and H1-UL quadrants. There are some cells that appear to fluoresce both red and green and these make up a small proportion of cells which appear in the H1-UR quadrant. Scale bar = 5 µm (Section 2.9.2).

Table 5.2 Percentages from flow cytometry and microscopy analysis of ΔslmA competition-style infection assays.

	Pre-infection						**Sample 1**						**Sample 2**					
Triplicate	1		2		3		1		2		3		1		2		3	
Strain	WT	Δ*slmA*	WT	Δ*slmA*	WT	Δ*slmA*	WT	Δ*slmA*	WT	Δ*slmA*	WT	Δ*slmA*	WT	Δ*slmA*	WT	Δ*slmA*	WT	Δ*slmA*
Flow cytometry	53	47	53	47	38	62	83	17	3	97	32	68	59	41	83	17	92	8
Microscopy (cell count)	45	55	66	34	45	55	-	-	-	-	-	-	52	48	84	16	98	2
Microscopy (cell area)	35	65	60	40	29	71	60	40	62	38	74	26	62	38	83	17	95	5

To further understand how *slmA* improves growth during the recovery stage of UPECs infection cycle, the reversal was studied in more detail with extra time points. An *in vitro* flow chamber UTI model was utilised (*Section 2.8*) as it produces longer filaments than the 6-well plate infection model which would be essential to monitor the reversal over a longer period. A combination of nucleoid staining and Z-ring positioning (through the use of *zapB-gfp*) was also employed to observe any major differences between WT and UTI89Δ*slmA*. After 20 hours post urine exposure the supernatant from the flow chambers was collected and 100 μL of the sample was added to liquid LB containing chloramphenicol (35 μg/mL, for plasmid maintenance) to allow for the reversal of filaments into rod-shaped bacteria.[11] This culture was sampled at 15, 30, 45, 60, 90, and 120 mins, the samples were fixed in 4% PFA and stained with Hoechst 33342 and analysed by flow cytometry and microscopy.

The data demonstrated that, in these individual infections, UTI89Δ*slmA* was able to undergo filament reversal to the same extent as WT in the same amount of time (Figure 5.5). From the flow cytometry, it is evident that as the right shoulder of the peak (filaments) decreases over time for both strains (Figure 5.5). It was found that on average both WT and UTI89Δ*slmA* began with 7.5% of the population being filaments. After 120 mins in LB during reversal of the filaments, 0.8% of WT cells were filaments and 1.2% of UTI89Δ*slmA* were filaments (Table 5.3). From the microscopy, it is not possible to observe the nucleoid organisation at the earliest time point (Figure 5.6; 0 mins) as they appear to be too faint in fluorescence which was unexpected (Figure 5.6). As time progresses, the nucleoids become clearer and in both strains, the organisation seems to vary from cell to cell, with some cells showing DNA spread along the entire filament, whereas other cells have nucleoids resolved into individual structures evenly separated along the cell length. By the final time point (Figure 5.6; 120 mins), the cells no longer have the extended nucleoid and all nuclei are resolved and spaced regularly. Overall, this indicates that, while it appears from snapshots over time that *ΔslmA* is able to undergo filamentation, it still cannot be ignored that during the competition-style studies Δ*slmA* was outcompeted by WT. Therefore, we next aimed to determine if there were any other defects in cell division that could be seen by visualising the division ring.

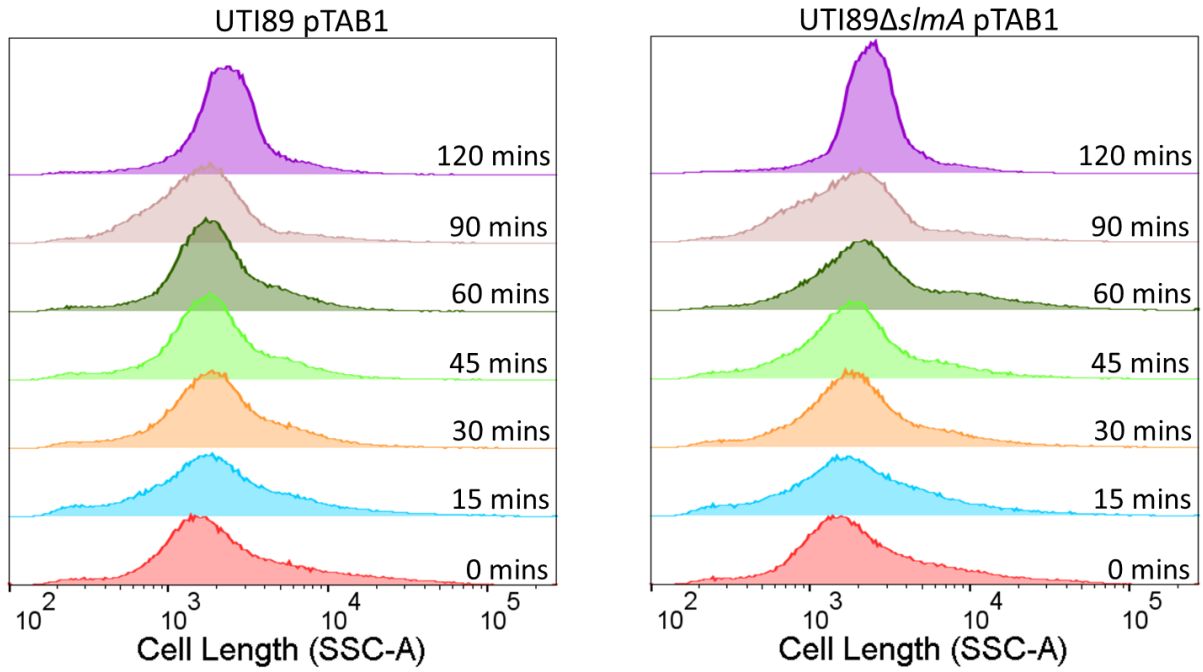

Figure 5.5 UTI89ΔslmA undergoes filament reversal similar to WT.

Twenty-four hours post-infection of PD07i bladder cells with UTI89 and UTI89ΔslmA, concentrated urine was used to induce dispersal and filamentation for 20 hours. After the 20 hour exposure to urine, the supernatant from the flow chambers was collected and 10 µL of the sample was used to inoculate 5 mL of LB. Samples were collected at various time points over 2 hours to track the reversal of the filaments into short rod-shaped cells. The samples were then analysed using flow cytometry. Flow cytometry was performed to determine the size distributions of the strains. As a control, cells from the overnight static culture were used as a reference for short cells when gating the samples. The x-axis depicts the side scatter area (SSC-A) which corresponds to the length of the bacteria.

Table 5.3 The mean percentage and standard deviation (SD) of filaments and short cells for UTI89 and UTI89ΔslmA as determined by flow cytometry.

Time (mins)	Percentage of filaments of WT[a]		Percentage of short cells WT[a]		Percentage of filaments of *ΔslmA*[a]		Percentage of short cells of *ΔslmA*[a]	
	mean	SD	mean	SD	mean	SD	mean	SD
0	7.455	1.591	92.550	1.626	7.595	0.573	92.400	0.566
15	8.000	3.960	92.000	3.960	8.375	5.127	91.650	5.162
30	5.640	4.228	94.350	4.172	5.730	3.507	94.250	3.465
45	2.740	1.061	97.250	1.061	3.870	1.372	96.150	1.344
60	2.550	1.541	97.450	1.485	3.870	0.849	96.00	0.990
90	1.645	0.460	98.350	0.495	2.650	0.156	97.350	0.212
120	0.865	0.092	99.150	0.071	1.250	0.537	98.750	0.495

[a] averaged from replicate experiments

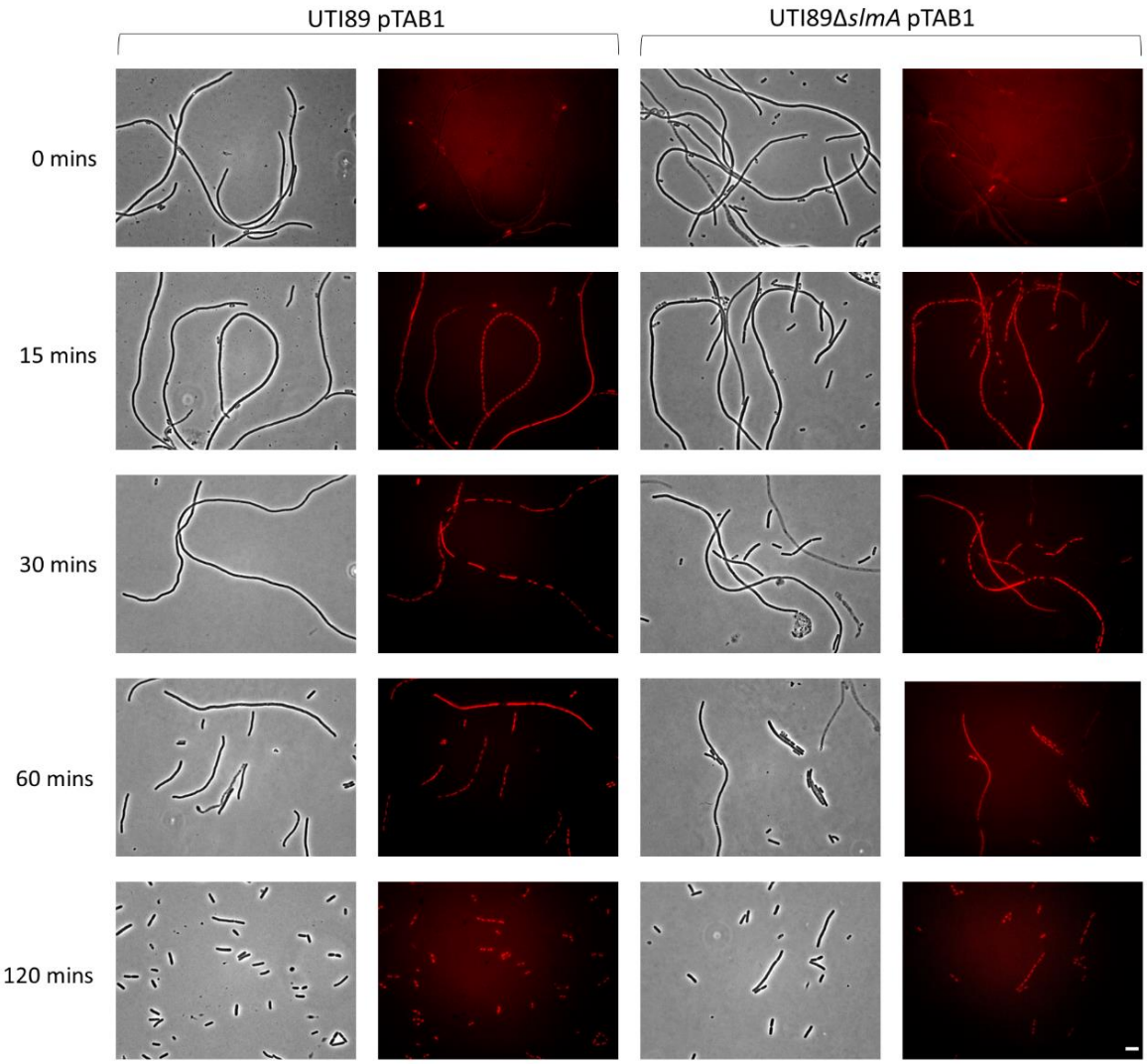

Figure 5.6 Microscopy depicts that UTI89ΔslmA undergoes filament reversal similar to WT.
Twenty-four hours post-infection of PD07i bladder cells with UTI89 and UTI89ΔslmA, concentrated urine was used to induce dispersal and filamentation for 20 hours. After the 20 hour exposure to urine, the supernatant from the flow chambers was collected and 10 µL of the sample was used to inoculate 5 mL of LB. Samples were collected at various time points over 2 hours to track the reversal of the filaments into short rod-shaped cells. The bacterial morphology was observed using microscopy. Phase-contrast and fluorescence microscopy of DAPI staining from the different time points to highlight the morphological changes. Scale bar is 5 µm. The combination of this data demonstrates that the slmA mutant is able to revert to short cells within the same time frame as WT. At 120 mins in LB 99% of both strains populations were short cells. Scale bar = 5µm (Section 2.9.2).

As there were no obvious differences in the nucleoid organisation between WT and UTI89Δ*slmA,* Z-rings were visualized using *zapB-gfp* during reversal (*Section 5.4.3*).

Unexpectedly, the expression of *zapB-gfp* was induced with the urine despite no inducer (IPTG) present at the time (Figure 5.8, 0 mins). This appeared to lead to large inclusion bodies of *zapB-gfp* seen at the poles at 0 mins when the filaments were harvested from the infection. This has also previously been seen when more than 0.05 mM of IPTG is added to LB cultures (Figure 5.1) and is expected to be caused by the build-up and clustering of ZapB-GFP in the cells (these clusters had no obvious impact on cell division). Therefore, to try to limit the number of inclusion bodies to better visualize the division rings at later time points in the reversal, the filaments were diluted into LB containing chloramphenicol and no inducer. At 5 mins before a sample was to be taken 1 mL of the culture was added to a tube containing IPTG (final concentration of 0.05 mM) and left to incubate for 5 mins before being fixed.

As seen in the previous study UTI89Δ*slmA* was able to undergo filament reversal to the same extent as WT in the same amount of time (Figure 5.7). From the quantified flow cytometry, it was shown that WT and UTI89Δ*slmA* began with 9% and 10% of the population being filaments on average, respectively. After 120 mins in LB during reversal of the filaments, less than 1% of the population of cells were filaments for both strains (Table 5.4). Although there are inclusion bodies in the filaments harvested straight from the infection model it is interesting to note that these filaments have *zapB-gfp* along the length of the cells in both strains and in some cases appear to be in a ring formation. From phase microscopy, it can be noted that the majority of these Z-rings have not undergone constriction even though the Z-rings are in place. Also, despite the condensation of the nucleoids in some cases in both WT and Δ*slmA*, the Z-rings were able to form in the spaces between the nucleoids in both strains (Figure 5.8). By the final time point (120 mins) the Z-ring have formed mid-cell in both strains. Overall, this data suggests that Δ*slmA* does not affect the ability of FtsZ to form Z-rings in the correct positions in the bacterial cells. It is possible that the filaments in the Δ*slmA* background may not be able to undergo the process of reversal like WT, and this difference was not detected by the methods we have chosen here. Or we were unable to see a difference in filaments because *slmA* may be required for other functions in other cell types like the short cells that also disperse from the IBCs. These cells would thrive during the filament reversal phase as they are able to continue to grow and divide as per normal, unlike their filamentous

counterparts. These short cells are also more motile which is needed for the infection of new bladder cells and to initiate a new round of the infection cycle.

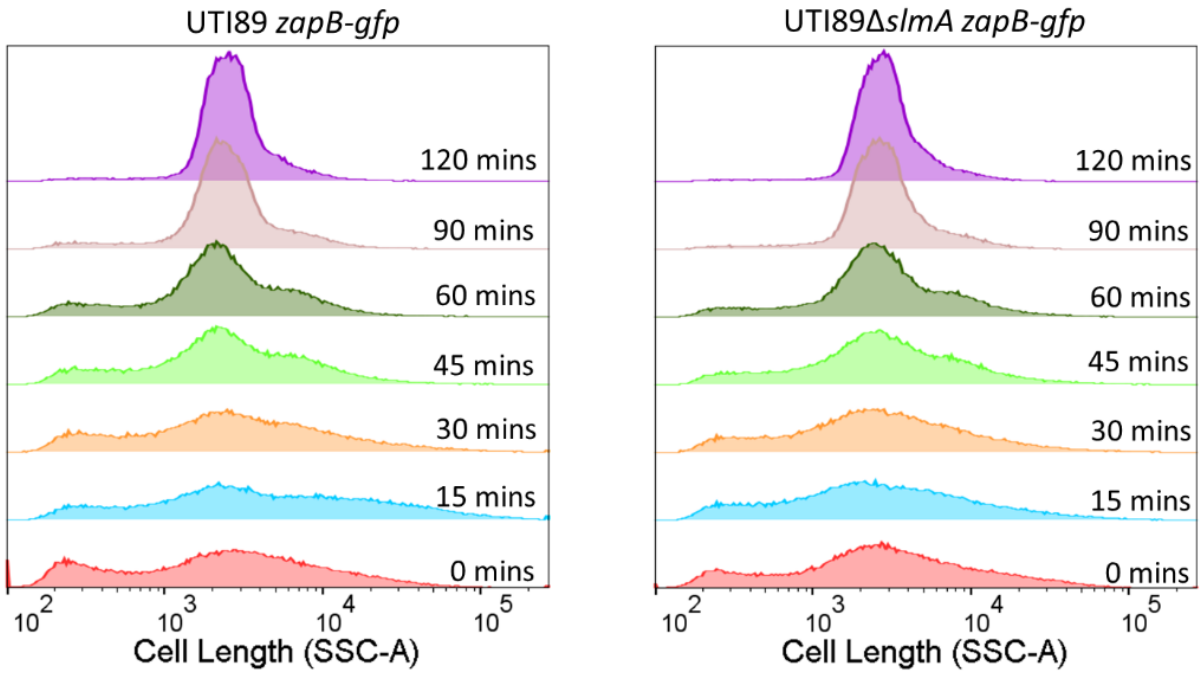

Figure 5.7 UTI89 and UTI89ΔslmA can still undergo reversal with zapB-gfp overexpression.
UTI89 and UTI89ΔslmA were transformed with pTAB1 zapB-GFP. Twenty-four hours post-infection of PD07i bladder cells with UTI89 zapB-gfp and UTI89ΔslmA zapB-gfp, concentrated urine was used to induce dispersal and filamentation for 20 hours. After the 20 hour exposure to urine, the supernatant from the flow chambers was collected and 100 µL of the sample was used to inoculate 10 mL of LB containing 35 µg/mL chloramphenicol. From this main LB culture, 5 mins before a time sample 1 mL of the culture was added to a fresh Eppendorf tube containing IPTG (0.05 mM, final concentration) and after a 5 min exposure to IPTG to induce zapB-gfp the sample was fixed. Samples were collected at various time points over 2 hours to track the reversal of the filaments into short rod-shaped cells. The samples were then analysed using flow cytometry. Flow cytometry was performed to determine the size distributions of the strains. As a control, cells from the overnight static culture were used as a reference for short cells when gating the samples. The x-axis depicts the side scatter area (SSC-A) which corresponds to the length of the bacteria.

Table 5.4 The mean percentage and standard deviation (SD) of filaments and short cells for UTI89 zap-gfp and UTI89ΔslmA zapB-gfp as determined by flow cytometry.

Time (mins)	Percentage of filaments of WT *zapB-gfp*[a]		Percentage of short cells WT *zapB-gfp*[a]		Percentage of filaments of *ΔslmA zapB-gfp*[a]		Percentage of short cells of *ΔslmA zapB-gfp*[a]	
	mean	SD	mean	SD	mean	SD	mean	SD
0	9.055	1.336	90.95	1.344	10.09	1.711	89.9	1.697
15	12.55	3.182	87.45	3.182	9.74	2.913	90.25	2.899
30	8.17	0.651	91.85	0.636	7.495	1.351	92.5	1.414
45	5.58	1.351	94.45	1.344	5.685	0.559	94.3	0.566
60	2.99	0.438	97.00	0.424	4.11	0.877	95.9	0.849
90	1.065	0.163	99.00	0.141	1.82	0.750	98.15	0.778
120	0.455	0.148	99.50	0.141	0.835	0.163	99.2	0.141

[a] averaged from replicate experiments

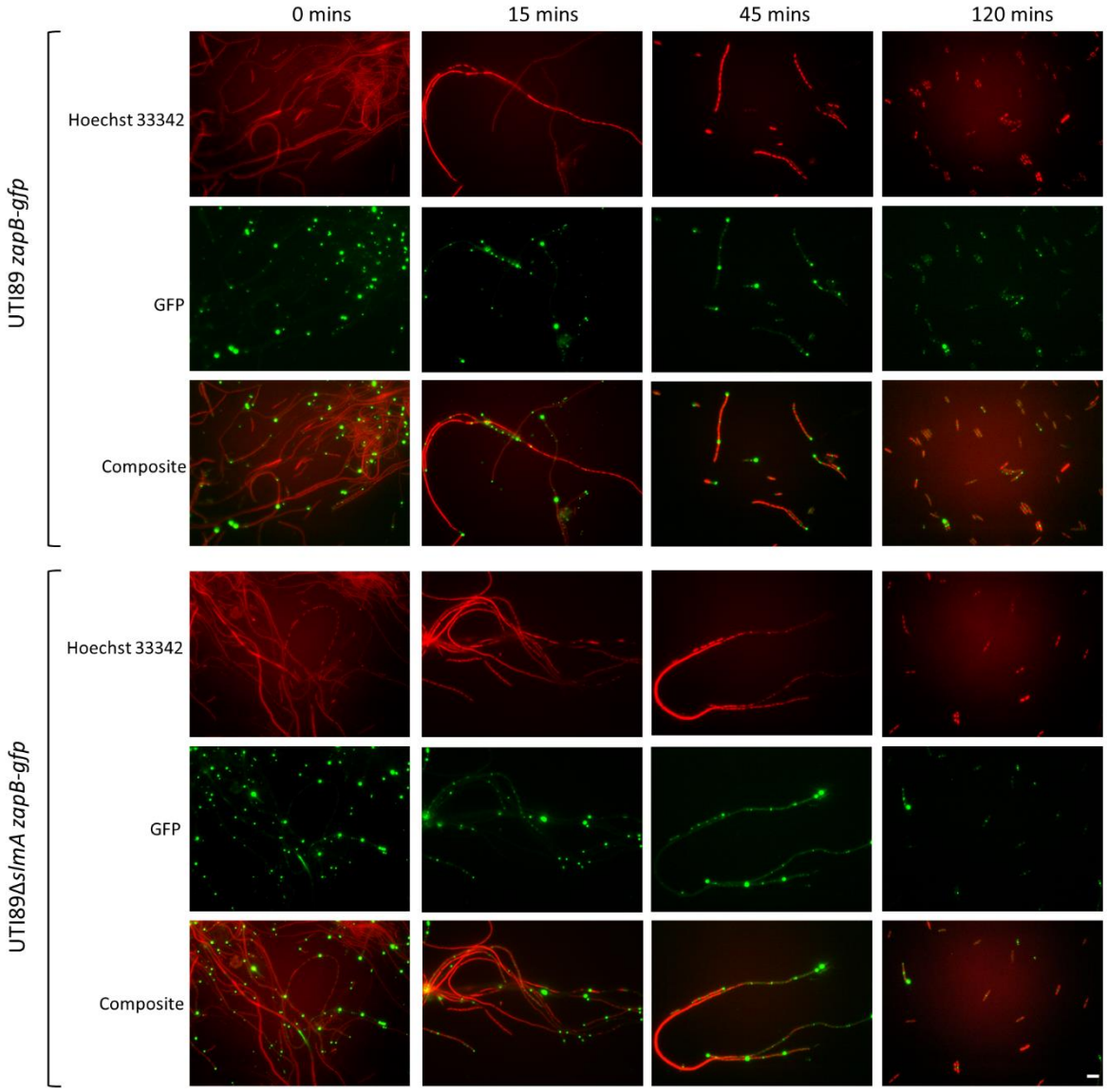

Figure 5.8 There is apparently normal Z-ring formation in the absence of slmA during UPEC reversal.

UTI89 and UTI89ΔslmA were transformed with pTAB1 zapB-GFP. Twenty-four hours post-infection of PD07i bladder cells with UTI89 zapB-gfp and UTI89ΔslmA zapB-gfp, concentrated urine was used to induce dispersal and filamentation for 20 hours. After the 20 hour exposure to urine, the supernatant from the flow chambers was collected and 100 µL of the sample was used to inoculate 10 mL of LB containing 35 µg/mL chloramphenicol. From this main LB culture, 5 mins before a time sample 1 mL of the culture was added to a fresh Eppendorf tube containing IPTG (0.05 mM, final concentration) and after a 5 min exposure to IPTG to induce zapB-gfp the sample was fixed. Samples were collected at various time points over 2 hours to track the reversal of the filaments into short rod-shaped cells. The bacterial morphology was observed using microscopy. Phase-contrast and fluorescence microscopy of DAPI staining and Z-rings from the different time points to highlight the morphological changes. Scale bar is 5 µm. The combination of this data demonstrates that in the absence of slmA Z-rings are able

to form and constrict like WT. Additionally, the data suggests that the Z-rings are not forming over the nucleoid. Scale bar is 5μm (Section 2.9.2).

5.3 Discussion

This chapter set out to confirm the role of *cedA* and *slmA* during UPEC infection. *cedA* and *slmA* were preliminarily identified as being required for the dispersal phase and the reversal of UPEC filaments, respectively.[174] Therefore, this study performed direct competition infection assays in an up-scaled 6-well dish to determine whether these genes were required for UPEC to progress through the relevant stage of infection.

We initially characterised Δ*cedA* in terms of its requirement for normal cell division and initiation of DNA replication. To visualise the Z-rings in the Δ*cedA* background, a plasmid expressing low-levels of *zapB-gfp* was successfully constructed. ZapB tagged with GFP has been used successfully in the literature to observe the Z-rings.[85] The use of this plasmid during normal growth in rich medium demonstrated Z-rings locating to the mid-cell at 0.05 mM IPTG (Figure 5.1). Therefore, this plasmid was used as a tool for observing Z-rings during normal growth conditions and to determine whether Δ*cedA* would lead to any abnormal localisation of the Z-ring. It was found that there was no difference in the cell size, positioning of the Z-ring, the timing of the formation of the Z-ring or the number of chromosomes present in the cell between WT and Δ*cedA* in UTI89 and BW25113 backgrounds (Figure 5.2). Therefore, this data initially suggested that *cedA* is not essential for any processes regarding cell division or the initiation of DNA replication under these standard growth conditions. However, from the transcriptome of WT *E. coli*, it was found that under standard laboratory growth conditions in rich media, there were no reads for *cedA,* suggesting that *cedA* is not transcribed under standard conditions, which may be the reason for not seeing any phenotypes of Δ*cedA* in our studies. In conjunction with the results from Chapter 4, this suggests that *cedA* might only be expressed during certain conditions or a state of stress to continue normal cell division. *katE,* which is situated next to *cedA,* is known to be dependently regulated by sigma factor S or RpoS, which is the master regulator of the general stress response.[177] It should be noted that although *katE* and *cedA* are adjacent to one another and couple at a divergent promoter site, their functions are unrelated.[178]

The RpoS regulon is large with many genes under its control; for example, *otsAB and treA,* which encodes for trehalose-6-phosphate synthase and trehalase, respectively. These genes are involved in trehalose synthesis and metabolism. In *E. coli,* trehalose-6-phosphate synthase converts UDP-glucose and glucose-6-phosphate to trehalose-6-phosphate.[179] *E. coli* uses trehalose as a carbon source during environmental stress and has been shown to serve as an important osmoprotectant and stress protectant.[180] Interestingly, during this thesis it was found that *otsA* and *treA* are significantly downregulated during *cedA* overexpression, suggesting possible negative regulation. Future studies should collect the Δ*cedA* cells from the infection model during the IBC and dispersal phases to determine if there are any changes in expression of *otsAB* and *treA* compared to WT. Nevertheless, due to the results from this thesis, it is still possible that there is a CedA-dependent stress response that specifically works to maintain normal cell division.

CedA has previously been implicated in the UPEC infection cycle, however, its function has not yet been determined.[16,174] It has been suggested from transcriptomics and TraDIS approaches that *cedA* is upregulated and involved in the dispersal phase of UPECs lifecycle.[16,174] During this stage it is reported that there is a mixture of filamentous cells and highly motile short rods.[11] It was hypothesised in this study that in the absence of *cedA* UPEC would have a reduced ability to progress to the dispersal phase as it has been suggested to be required. Competition assays between WT and UTI89Δ*cedA* through IBC development to filamentation and dispersal demonstrated that UTI89Δ*cedA* was able to progress through these stages to approximately the same extent as WT (Figure 5.4). This suggests that *cedA* is not required for the dispersal of UPEC during BEC infection *in vitro*. Upon reanalysing the TraDIS screen it was found that *cedA* appeared to only be required in 1 out of 2 biological replicates. This emphasises the potential limitations of TraDIS and the importance of verification studies like the one performed in this thesis to confirm if a gene is required. One potential limitation was that the TraDIS library experienced a bottleneck effect due to small sample size and this means that the criteria for selected genes from the screen needs to be improved. For example, the gene of interest needs to be shown to be required in both replicates of TraDIS as opposed to averaging the replicates to determine if a gene is essential. In light of the findings in Chapter 4 and

in conjunction with *cedA* being upregulated during the dispersal of UPEC[16] it was found that *cedA* overexpression leads to IBCs being unable to produce filaments and the downregulation of trehalose biosynthesis. This may suggest that there is a link between treholase synthesis and IBC formation and the eventual filamentation of bacteria in the IBCs. It is also possible that in Δ*cedA,* with the requirement of another regulator to compensate for the loss of *cedA*, treholase biosynthesis is able to continue as normal and therefore leads to a stress response that is required for the formation of IBCs or the dispersal of filaments and highly motile cells like WT.

Importantly, in this study, we were able to demonstrate the nucleoid occlusion protein, *slmA*, improves growth for the recovery of UPEC during the reversal phase of infection however it is not required for the reversal of filaments to short rod-shaped bacteria (Figures 5.4 & 5.5). The competition assay between WT and UTI89Δ*slmA* showed that during the reversal of filaments, only 22-27% of the population was UTI89Δ*slmA*. This suggests that *slmA* has a role in growth during the recovery ('reversal') phase of the infection protocol. To observe the difference more closely *in vitro* infections were performed, however, they demonstrated that UTI89Δ*slmA* was able to reverse filaments to rod cells to the same extent as WT (Figures 5.6 and 5.7). Upon observing the Z-rings and nucleoids in these cells, it was apparent that in the absence of *slmA* the Z-rings still did not form over the nucleoids, this may be possible because of the Ter-MatP regulatory system or other nucleoid-related inhibitory systems that regulate division. Future studies should follow filaments from dispersal to reversal using time-lapse microscopy as it is possible that most filaments are undergoing lysis due to their inability to reverse, this may help explain the results from the competition assay. A hypothesis to explain the individual *in vitro* infections may be that as not all IBCs are filamentous before they erupt,[120] the short cells or the short filaments are able to continue normal growth in *slmA*s absence because the nucleoids are not condensed in these cells.

In this chapter, we have demonstrated that *cedA* is not transcribed during normal growth and thus Δ*cedA* had no obvious phenotypes (Figure 5.2). Additionally, we have shown that *cedA* is not required for the IBC development or dispersal of filaments during UPEC lifecycle. Importantly, we successfully revealed that *slmA* is needed for optimal survival

of cells during the recovery phase (post-infection), using a competition style infection assay. Overall, this highlights the importance of understanding the mechanism of SlmAs ability to improve recovery of UPEC during the infection cycle to possibly create therapies that target its action. It also highlights that while we were unable to identify the significance of CedA during UTIs there are many possibilities for its mechanism beginning with regulating metabolism during the infection cycle to ensure that UPEC is able to progress through the different stages.

5.4 Methods

For a detailed description of the general materials and methods used throughout this thesis, refer to Chapter 2. The following section will describe the materials and methods specific to this Chapter.

5.4.1 Bacterial Strains and Growth Conditions

JW1720-1 (referred to as BW25113Δ*cedA*) was obtained from the *E. coli* Genetic Stock Center (Yale University, USA). UTI89Δ*cedA* was kindly provided to this study by D. Mediati. UTI89Δ*slmA* was constructed for this study and is detailed below. Plasmid pGI5 was kindly provided to this study by G. Iosifidis. Plasmids pGI6 and pTAB1 *zapB-gfp* (*Section 2.7.2*) were constructed in this study. Strains were routinely cultured at 37°C on solid or liquid LB. For culturing of strains containing plasmids pGI5 or pGI6, spectinomycin at 100 μg/mL was routinely used. For culturing of strains containing pTAB1 *zapB-gfp*, chloramphenicol at 35 μg/mL was routinely used.

5.4.1.1 Construction of UTI89ΔslmA

Chromosome UTI89 gDNA was extracted and purified using Bioline Isolate II Genomic DNA (Bioline) and *slmA* mutant was constructed using the λ-Red recombinase protocol.[181] The primers used to amplify the kanamycin cassette from pKD4 are forward primer (slmA_del_F) and reverse primer (slmA_del_R) (Table 5.5). The PCR product was DpnI digested overnight following the manufacturers' protocol. The kanamycin cassette was then gel extracted from 0.7% TAE gel. The *slmA* mutants were selected for using kanamycin and confirmed using a combination of gene flanking and internal kanamycin primers. (K1_LamRed, K2_LamRed, slmA_R_UTI89, KT, slmA_F_UTI89) (Table 5.5)

Table 5.5 Oligonucleotides and their respective restriction enzymes used for performing λ red recombination to delete slmA from UTI89.

Name	Sequence (forward 5' → 3')	Source
slmA_del_F	TTT GGT CAC TCT GGT CGT CAG	IDT
slmA_del_R	GGC GTT TAA AGA AAC TCG CCG	IDT
K1 LamRed	CAGTCATAGCCGAATAGCCT	IDT
K2_LamRed	CGG TGC CCT GAA TGA ACT GC	Macrogen
Kt_LamRed	CGG CCA CAG TCG ATG AAT CC	Macrogen
slmA_F_UTI89	CCG GTA GTA CAG GCT GAA TT	IDT
slmA_R_UTI89	CGT ATT GAT TTC GCT CGA TC	IDT

5.4.1.2 Subcloning of pGI6

mCherry was PCR amplified from pIDJL117 using Phusion protocol (NEB) primers listed in Table 5.6. pGI5 and mCherry were digested using restriction enzymes NcoI-HF (NEB) and BamHI (NEB) following the manufacturers' protocol. Overnight ligation was performed using T4 DNA ligase following the manufacturers' protocol. The ligation mixture was then sanitised using restriction enzyme PvulI (NEB) to remove any background pGI5 plasmid containing GFP. The resulting plasmid was named pGI6 and it was confirmed by DNA Sanger sequencing.

Table 5.6 Oligonucleotides and their respective restriction enzymes used for cloning mCherry into pGI5.

Name	Sequence (forward 5' → 3')	Source
mcherry_F_ncoI	GCG CCG CCA TGG GTG AGC AAG GGC GAG GAG GAT	IDT
mcherry_R_bamhI	GGC CCG GGA TCC TTA CTT GTA CAG CTC GTC CAT GCC	IDT

5.4.2 Z-ring positioning and timing of formation in *cedA* deletion strains

Image analysis for Z-ring experiments was performed using microbeJ.[182] Default thresholding was used to outline the cell and determine the cell length. Next, by eye, the shortest side from pole to Z-ring was determined and measured to find the positioning of the Z-ring within the cell. For the timing of the formation of the Z-ring, the cell length

was ranked from shortest to longest with a cumulative frequency of cells containing a Z-ring. This data was then plotted on graphs using GraphPad Prism 8.

5.4.3 UTI Competition Assays in 6-well Dishes for Δ*cedA*

Following the splitting of the PD07i bladder cells into the 6-well dishes (*Section 2.5.1*) the plates were left to incubate overnight at 37°C with 5% CO_2. The bacterial cultures used for the infection were grown in liquid LB containing spectinomycin (100 μg/ml) overnight at 37°C statically. The overnight cultures were then centrifuged for 10 mins at 4000 xg and resuspended to an OD_{600} = 0.1. WT pGI5 and UTI89Δ*cedA* pGI6 were equally mixed with 500 μL of each strain (pre-infection sample) and then 1 mL of bacterial suspension was added to 3 wells and left to sit for 1 min. The dish was centrifuged for 5 mins at 500 g and then left to statically incubate for 2 hours at 37°C with 5% CO_2. The supernatant was discarded and 3 mL of pre-warmed Epilife media containing gentamicin (100 μg/ml) was added to each well. The dish was left to incubate statically for 20 hours at 37°C with 5% CO_2.

After 20 hours, the supernatant was removed and the wells were washed with PBS a total of 4 times. One millilitre of lysis buffer (*Section 2.3*, Table 2.5) was added to 1 well of the competition infections and left to incubate for 10 mins at 37°C with 5% CO_2. The mammalian cells were collected from the well using a cell scraper and pipetted into a new Eppendorf tube. The tube was centrifuged at 5000 xg for 5 mins and resuspended in 20 μL of PBS and fixed with 4% PFA. This sample during the IBC phase was named sample 1.

Following this 3 mL of concentrated urine (*Section 2.8.1*) was added to the remaining wells and left to incubate at 37°C with 5% CO_2 for 10 hours with orbital shaking. After 10 hours the urine was changed every hour until a total of 15 hours. At which point the urine was changed for a final time and collected after 20 mins (dispersal phase, sample 2). This experiment was repeated with the reverse of plasmids in each strain for complementation.

5.4.4 UTI Competition Assays in 6-well Dishes for Δ*slmA*

Following the splitting of the PD07i bladder cells into the 6-well dishes (*Section 2.5.1*) the plates were left to incubate overnight at 37°C with 5% CO_2. The bacterial cultures used for the infection were grown in liquid LB containing spectinomycin (100 μg/ml) overnight at 37°C statically. The overnight cultures were then centrifuged for 10 mins at 4000 xg and resuspended to an OD_{600} = 0.1. WT pGI5 and UTI89Δ*slmA* pGI6 were equally mixed with 500 μL of each strain (pre-infection sample) and then 1 mL of bacterial suspension was added to 3 wells and left to sit for 1 min. The dish was centrifuged for 5 mins at 500 g and then left to statically incubate for 2 hours at 37°C with 5% CO_2. The supernatant was discarded and 3 mL of pre-warmed Epilife media containing gentamicin (100 μg/ml) was added to each well. The dish was left to incubate statically for 20 hours at 37°C with 5% CO_2.

After 20 hours, the supernatant was removed and the wells were washed with PBS a total of 4 times. Following this 3 mL of concentrated urine (*Section 2.8.1*) was added to the remaining wells and left to incubate at 37°C with 5% CO_2 for 10 hours with orbital shaking. After 10 hours the urine was changed every hour until a total of 15 hours. At which point the urine was changed for a final time and collected after 20 mins (dispersal phase, sample 1). Then 10 μL of bacterial cell suspension was used to inoculate 5 mL of liquid LB containing spectinomycin (100 μg/mL). This culture was left to incubate for 12 hours at 37°C with shaking. This experiment was repeated with the reverse of plasmids in each strain for complementation.

5.4.5 Analysis for Competition Assays

Samples from the competition assays were analysed by flow cytometry and microscopy. For flow cytometry, a CytoFLEX instrument was used and 30,000 events were recorded. For mCherry, the yellow laser was used, with the 610/20 filter and for GFP the blue laser was used with the 525/40 laser. The mCherry versus GFP plot was gated on the main population of cells to remove any background debris using the CytExpert software

(version 2.4.0.28). The gating option in the Cytoexpert software determines a percentage and this was used to report the percentages in Tables 5.1 and 5.2.

MicrobeJ was used to count the number of cells that were red (pGI6) versus green (pGI5) during the competition assays (*Sections 5.4.3 and 5.4.4*). The threshold was set using Huang (-40 for red and -80 for green). Using the intensity column, the count for each colour was determined and over 1000 cells for each sample over 3 replicates were recorded. The percentage of cells from each sample that were either red or green was calculated and added to Tables 5.1 and 5.2. Additionally, the total area of fluorescence was measured for each channel and reported as a percentage of the entire fluorescence for each image.

The average percentage from the flow cytometry and microscopy analysis for each sample and colour was calculated from triplicate data and reported in the text.

5.4.6 *zapB-gfp* Expression during *in vitro* Flow Chamber UTI Model

UTI89 and UTI89Δ*slmA* were transformed with pTAB1 *zapB-gfp* (*Section 2.7.2*). These strains were then used for the *in vitro* flow chamber UTI model to infect PDO7i bladder cells (*Section 2*.8). After harvesting the cells from the flow chambers 20 hours post urine exposure, the 100 µL of the supernatant was added to 10 mL of LB containing 35 µg/mL chloramphenicol (main culture), this culture was left to incubate at 37°C with shaking. From this main LB culture, 5 mins before a time sample 1 mL of the culture was added to a fresh Eppendorf tube containing IPTG (0.05 mM, final concentration) and after a 5 mins exposure to IPTG to induce *zapB-gfp* the sample was fixed.

Chapter 6
Discussion and Conclusion

6.1 General Discussion

UTIs are the most common bacterial infections worldwide and 80% of cases are caused by UPEC.[9] With the continuous rise of antibiotic-resistant bacteria, UTIs are increasingly more difficult to treat and therefore, finding new targets for therapeutics is essential. UPEC is naturally occurring in the intestine however, it has adapted to disseminate and colonise the urinary tract. Through extensive research into understanding more about UTIs, it is now widely understood that UPEC undergoes many morphological changes during its multi-stage intracellular infection cycle of the bladder cells within the urinary tract.[10,11] This complex infection cycle involves the attachment of the bacteria to the bladder epithelium, invasion and the formation of intracellular biofilm-like communities (IBCs) where cells differentiate into filaments and highly-motile cells.[10] Once the IBCs overwhelm the bladder cells, the cell ruptures and the bacteria are dispersed.[10,11] UPEC filaments can revert to their short-rod shaped morphology, which is thought to be required for the initiation of a new infection cycle.[10,11] The initial stages of infection (binding and invasion) have been studied extensively, however, little research has focused on the later stages of infection (filamentation and reversal).

Filamentation has been shown to be a mechanism that allows for the survival of bacteria in stressful environments.[14] It has been observed that filaments, such as those seen during the UPEC infection, are able to re-divide and continue with normal division to produce viable normal short rod-shaped bacterial cells.[10,11] Therefore, it is hypothesised that the filamentation mechanism is deliberate and may allow the cells to survive the host immune response or the force of the urine flow in the bladder.[11,25] A well-known mechanism for causing filamentation in *E. coli* is the SOS response, leading to the induction of SulA and YmfM and the inhibition of FtsZ polymerisation.[102,136] However, it was recently shown that there is an independent mechanism of UPEC filamentation involving the cell division gene, *damX*.[16] Nevertheless, the exact mechanism of how *damX* is regulated and the possible involvement of other genes remains unknown.

In addition to *damX*, Khandige, et al.[16] demonstrated that the cell division gene *cedA* was upregulated 8-fold during the dispersal stage of UPEC infection cycle. *cedA* has also been previously linked to the prevention of filamentation in a *dnaA* mutant, *dnaA(cos)*, and is

positively selected for amongst UPEC strains.[12,15] These 3 key pieces of information highlight the potential importance of *cedA* to UPECs infection cycle and is the premise for the work in this thesis.

More recently, a genetic screen performed by our laboratory identified *cedA* as being required for the dispersal of UPEC from the bladder cells.[174] Overall, there is very little known about *cedA* in *E. coli*, and for this reason, the work in this thesis set out to understand the general function of *cedA*. Firstly, as *cedA* was discovered as a multi-copy suppressor of *dnaA(cos)*, *Chapter 3* aimed to determine the mechanism that causes filamentation in the *dnaA(cos)* background in order to shed light on which pathway of filamentation *cedA* is preventing. Secondly, *Chapter 4* used the overexpression of *cedA,* in conjunction with the overexpression of many genes that are known to cause filamentation, to determine if the ability of *cedA* to prevent filamentation was a general response or whether it was specific for particular modes of filamentation. Lastly, *Chapter 5* aimed to verify whether *cedA* was required for UPEC to progress through the dispersal or filamentation stage of the infection cycle. In addition to *cedA, slmA* was also suggested to be required for the later stages of UPECs infection cycle and therefore, its role was also confirmed during this thesis. Additionally, as nucleoid occlusion was tested during the previous aims of this thesis the fact that *slmA* was a hit in the TraDIS screen made it more relevant to the goals of this thesis.

6.1.1 *dnaA(cos)* filamentation is a complex response that requires multiple pathways to cause filamentation

To understand how *cedA* is able to prevent filamentation caused by *dnaA(cos)*, it was considered important to understand how *dnaA(cos)* causes filamentation. It is thought that *dnaA(cos)* filamentation is the result of hyper-initiation at *oriC*, leading to replication forks that collide from behind with stalled or slower forks.[66,68] This creates double-stranded breaks in the DNA, which possibly leads to an arrest of cell division via SOS-induction.[66,68] However, the mechanism that regulates the filamentation response in *dnaA(cos)* is yet to be determined. In *Chapter 3* we used mutants of the SOS response, Min System, and nucleoid occlusion to determine which, if any, of these pathways were required for *dnaA(cos)* filamentation. It has previously been concluded that *dnaA(cos)*

filamentation is independent of *sulA* and *recA* however Kaytama, et al.[15] came to this conclusion with almost no data shown. Thus this study aimed to conclusively demonstrate which pathway was required for *dnaA(cos)* filamentation. Additionally, it has been previously reported that while *cedA* overexpression could prevent the filamentation phenotype it was unable to overcome the hyper-initiation of DNA replication.[15]

This study was unable to conclusively determine which pathway is required for *dnaA(cos)* filamentation through the overexpression of *dnaA(cos)* in the mutant backgrounds. We were able to demonstrate that *dnaA(cos)* filamentation does not require the Min System or Nucleiod occlusion. However, the *slmA* gene was upregulated in the *dnaA(cos)* filaments. We also found from transcriptomics studies that the SOS response was induced during *dnaA(cos)* filamentation (Figure 3.9). Taken together, the results from this study suggested that *dnaA(cos)* filamentation is complex and is the result of more than one pathway leading to filamentation working at the same time. This, in turn, suggested that *cedA* is able to counteract multiple pathways that lead to filamentation. This was tested in Chapter 4.

As the SOS response is induced during *dnaA(cos)* filamentation, this suggested that *cedA* is able to prevent filamentation in *dnaA(cos)* in part by promoting division and preventing the SOS response. In support of this, transcriptomics on samples taken during the prevention of *dnaA(cos)* filamentation by the overexpression of *cedA (Chapter 4)* demonstrated that the SOS response genes were not induced. The mechanism of how *cedA* expression leads to prevention of SOS induction is still unknown, however, DNA damage and/or other lethal damage normally resulting from *dnaA(cos)* expression is also suppressed by *cedA*.[15] Consistent with this, we saw that *cedA* expression causes a wild-type nucleoid morphology in DnaA(cos) cells.

This is the first study to report that *dnaA(cos)* filamentation induces the SOS response even though it does not require *recA*, *ymfM* and *sulA* to produce filaments. Katayama, et al.[15] suggested that *dnaA(cos)* can filament in the absence of *sulA* and *recA* through very limited data and no data, respectively. Moreover, Ogura, et al.[183] observed the induction of the SOS response in *B. subtilis* cells overexpressing *dnaA*. We were unable to demonstrate that *dnaA(cos)* filamentation requires specifically nucleoid occlusion, Min

system or the SOS response. Demonstrating that multiple pathways are involved to induce filamentation in the *dnaA(*cos) pathway. Future studies will use the transcriptomics as a basis for determining what genes are required for *dnaA(cos)* filamentation.

6.1.2 *cedA* can prevent stress-induced filamentation and promote cell division in WT cells

As we determined that *dnaA(cos)* filamentation may be a response to multiple pathways blocking cell division, which can be prevented by cedA expression, we hypothesised that *cedA* could prevent filamentation of multiple pathways, and we tested this in Chapter 4. These included nucleoid occlusion, SOS response, metabolism linked filamentation, direct inhibition of the Z-ring, DamX-reversible filamentation, and UPEC filamentation. From this study, we found that *cedA* could partially prevent filamentation caused by a direct inhibition to the Z-ring formation (*ftsZ-yfp*), SOS response (*recAtif*), metabolism (*zwf*) and DamX-reversible filamentation (*damX)*. Overall, these studies demonstrate that no matter how little the degree of the filamentation is, *cedA* was able to recognise it and was able to continue normal cell division. Interestingly, it was found that while there was no growth rate difference between *cedA* overexpression and WT cells, *cedA* overexpression did significantly cause a smaller cell size (Figure 4.2). This suggests that CedA production can promote cell division even in the WT background. There are not many situations where a gene is known to cause the production of smaller cells, but a well-known case is with the overexpression of *ugpT* in nutrient-poor conditions which allows for the promotion of cell division in *B. subtilis*.[184] UgtP encodes for glucosyltransferase and its localization in the cell is dependent on UDP glucose.[169] During nutrient-poor conditions, the UgpT protein levels are known to reduce 6-fold compared to nutrient-rich conditions.[169] Under these conditions, it is also known to localise away from the Z-ring and forms randomly distributed foci.[169] In the case of UgpT smaller cell size was also observed, independent of growth rate changes.[169] In *E. coli*, OpgH is functionally analogous to UgpT. It has been shown that OpgH interacts with FtsZ to delay the timing of assembly of the division machinery.[185] Also the inactivation of *pgm* in *E. coli* can lead to a ~25% reduction in cell size during nutrient-rich conditions.[186] *pgm* encodes for the phosphoglucomutase enzyme which is required for the glycolysis pathway.[186] From the transcriptomics of *cedA* overexpression, no known cell division

genes were upregulated but we observed regulation of a lot of genes involved in cell metabolism. This suggests that *cedA* may control cell size by having an effect on cell metabolism.

On the other hand, it was hypothesised that the deletion of *cedA* would have an effect on cell division, however, this was found to not be the case. In *Chapter 5, ΔcedA* did not reveal any obvious phenotypic differences from WT, however, transcriptomics showed that in WT cells, *cedA* was not expressed. This suggests that *cedA* is not normally transcribed in the cells unless it is required, and this explains why no phenotypic differences were observed, suggesting that *cedA* as a specific conditional role. It has been shown previously that the deletion of *cedA* in *E. coli* exhibited increased susceptibility to LAL-32, a nanoparticle bactericidal antibiotic which inhibits cell division.[187] Therefore, future studies may aim to determine conditions in which the deletion of *cedA* may affect the cell division processes such as to induce stressful conditions that may lead to filamentation and determine if CedA is being expressed.

There were a couple of instances where *cedA* overexpression led to cells which were unable to continue normal cell division and this was with the overexpression of *slmA* and *slmA*-SBS and the reversal of filamentation caused by *dnaA(cos)* and *ftsZ-yfp*. As it has been shown that *cedA* binds DNA[107,108] it may be possible that this helps to promote cell division and *slmA* may compete for the DNA binding or counteract *cedA's* function. Future studies will use CHiP-seq and protein-protein interaction studies to test this hypothesis.

We are the first study to report that overexpression of *cedA* during UPEC *in vitro* infection of BECs leads to the death of some cells as well as the prevention in others (Figure 4.16). It is hypothesised from these results that during WT UPEC infection, where there is a mixture of filaments and short cells dispersed from IBCs, *cedA* could be responsible for ensuring that there are a population of short cells which would allow for the immediate invasion of nearby bladder cells. Recently, it was published that IBCs during infections have two morphological fates, one being that all of the cells within the IBC become filamentous and then other being that all of the cells stay as short rods.[120] Therefore it is possible that *cedA* is upregulated in a subset of IBCs to ensure that the cells remain short.

Future studies with WT UPEC using a flow cytometer sorter to sort the filaments and short cells after dispersal and then perform transcriptomics or western blots on the subpopulation can help to determine the differences between the two cell shapes and to determine if CedA is expressed more in the short cells to prevent filamentation. Another approach is to use immunofluorescence microscopy (IFM) of the dispersing IBCs to link their morphology to *cedA's* expression level. Further studies need to be performed to determine the viability of the cells after infection and therefore possibly express *cedA* from the chromosome instead to match the levels seen during infection.

A TraDIS screen suggested *cedA* as being required for the dispersal of filaments during UPEC infection cycle. However, competition-style infection assays performed during this thesis were unable to confirm this result and showed that this was likely a false detection in the TraDIS (Figure 5.3). This demonstrates the significance of performing verification experiments on TraDIS results as these are not always correct when data are analysed en masse. Possibly the TraDIS screen experienced a bottleneck effect in which certain mutants were insufficiently represented in the mutant library during the infection studies, such that their absence in the collection after infection occurs by chance rather than by the desired selection against unfit mutants. Also, as the replicates for the TraDIS screen were pooled together and treated as one it was found in the case of *cedA* that when averaged the results appeared significant. However, when the replicates were treated separately it was found that *cedA* was only significant in one out of the two replicates. As we were unable to determine when *cedA* is required during infection, future studies will use IFM at the different stages of infection to determine *cedA's* expression. CedA has been shown to be upregulated during the later stages of UPECs infection cycle however this encapsulates two very significant stages from dispersal to filament reversal.[16] Tracking CedA expression would provide information about a specific time during the infection cycle that CedA is required, as we were unable to demonstrate that CedA was required for the dispersal phase of infection.

Overall, CedA has been shown to be upregulated during the later stages of UPECs infection cycle;[16] positively selected for in UPEC strains[12] and it is found mostly within bacterial strains that are known to inhabit and/or cause infection of the gastrointestinal tract and urinary tract; its overexpression can prevent many pathways that lead to

filamentation especially during UTIs; its overexpression during UPECs infection cycle may cause possible cell death and it appears to only be expressed during certain conditions. There is still a lot to work out about its mechanism however we were able to show that CedA is able to control cell size in many instances and we hypothesise that it may be able to do this through an indirect effect on cell metabolism. Moreover, this highlights the importance of continuing research into the role of *cedA* during UTIs as it may present a future therapeutic target.

6.1.3 *slmA* is required for the reversal of UPEC filaments

The TraDIS screen in our laboratory identified *slmA* as being required for the reversal of filaments to normal short rod-shaped cells.[174] This was of interest to this project as *slmA* and the Nucleoid Occlusion system were used throughout the thesis as an inhibitor of cell division. It also provided us with the opportunity to verify the TraDIS screen using a gene that was shown to be significant in both replicates. Therefore the *slmA* mutant (Δ*slmA*) during the UPEC infection cycle was characterised for its ability to progress through the dispersal and filament reversal stage of infection. Competition-style infection assay between Δ*slmA* and WT confirmed that *slmA* is required for the recovery stage of infection (Figure 5.4). It was observed that during the competition that the number of Δ*slmA* cells was lower than WT, indicating how *slmA* is required for normal UPEC growth during the recovery phase. However, during a follow up *in vitro* flow chamber infection model, *slmA* was able to reverse to the same extent as WT. This indicates that although we know it is required for the recovery phase it may not be specifically required for filaments to reverse into short rod-shaped cells, as was hypothesised initially.

Next, we attempted to visualise the Z-rings in the Δ*slmA* to determine if the filaments were unable to divide and therefore dying and this might have explained why it appeared that filament reversal between Δ*slmA* and WT appeared to be the same. To our knowledge, this is the first study that attempts to track the formation of Z-rings during filament reversal of UPEC. Expression of ZapB-GFP under these conditions lead to the formation of ZapB-GFP inclusion bodies. The inclusion bodies did not affect the bacteria's ability to form short rod-shaped cells. In this set of studies, we did not observe any difference in the formation of Z-rings between WT and Δ*slmA*. In the future, a protein

fusion for the Z-ring that does not lead to the formation of inclusion bodies should be developed so that time-lapse microscopy can be used to visualise what happens to the Δ*slmA* filaments in real-time. Further research on the role of *slmA*s during the reversal of UPEC filaments is essential to understand as it may be a key target in preventing the infection of nearby bladder cells. Therefore, targeting *slmA* could potentially hinder UPECs ability to progress through its infection cycle.

6.1.4 Concluding remarks

There is very little known about the role of *cedA* in *E. coli* despite being implicated in UPECs infection cycle. This thesis initiated research into characterising *cedA* through its overexpression and deletion. With a combination of genetic analyses, transcriptomics, and *in vitro* flow chamber infection models, we were able to demonstrate: 1) *cedA* is only found in the Enterobacteriaceae Family, in bacterial strains that cause gastrointestinal and urinary tract infections; 2) *cedA* can prevent filamentation caused by various blocks but not by slmA; 3) *cedA* promotes cell division in WT backgrounds, and 4) *cedA* is not expressed in normal growth conditions. Further research into *cedA* will shed light onto the function of *cedA* during UTIs. Additionally, this thesis was able to demonstrate the importance of *slmA* during the recovery phase of the in vitro UTI infection model. Further characterisation of both *cedA* and *slmA* may lead to the advancement of novel therapeutics for UTIs in the future.

Appendix

Supplementary Data

Supplementary data is provided within this thesis and as separate excel files for the transcriptomics data (Tables S1, S2, S3 and S4). Supplementary data to support these results are listed below.

Chapter 3:

Supp. data Table S1 *dnaA(cos)* overexpression differential gene expression

Chapter 4:

Supp. data Table S2 *cedA* overexpression differential gene expression

Supp. data Table S3 *dnaA(cos)* + *cedA* versus *dnaA(cos)* differential gene expression

Supp. data Table S4 *dnaA(cos)* + *cedA* versus WT differential gene expression

Supp. data Figure S1 CedA can prevent filamentation that is caused during *in vitro* BEC infection

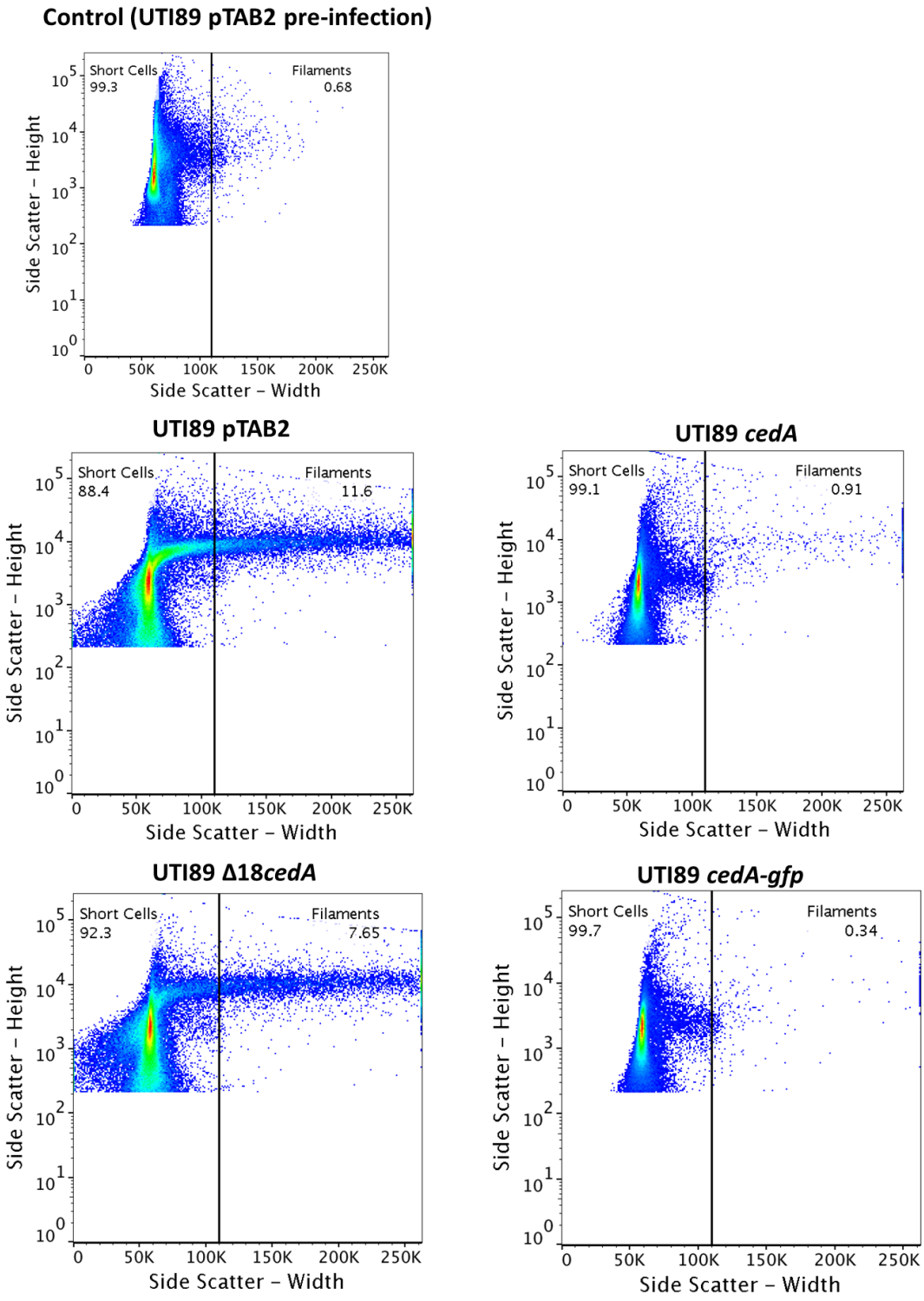

Figure S1 CedA can prevent filamentation that is caused during in vitro BEC infection.

Control (UTI89 pTAB2 grown in LB overnight), UTI89 pTAB2, UTI89 cedA, UTI89 Δ18cedA, and UTI89 cedA-gfp underwent infection of bladder cells (PDO7i) in an in vitro flow chamber infection model. The fraction of filamentous bacteria were obtained from flow cytometry. A scatterplot of the cells was gated based on the control (UTI89 pTAB2 grown overnight in LB) and was named short cells and all other cells were names filaments with side scatter width and height on the x and y axes respectively. This is data

shown from one replicate. The control is the same in both replicates as the samples were run through the flow cytometer on the same day.

References

1. Ulett, G. C. *et al.* Uropathogenic Escherichia coli virulence and innate immune responses during urinary tract infection. *Curr. Opin. Microbiol.* (2013) doi:10.1016/j.mib.2013.01.005.
2. Hooton, T. M. *et al.* Perineal anatomy and urine-voiding characteristics of young women with and without recurrent urinary tract infections. *Clin. Infect. Dis.* **29**, 1600–1601 (1999).
3. Foxman, B. Epidemiology of urinary tract infections: incidence, morbidity, and economic costs. *Am. J. Med.* **113 Suppl**, 5S-13S (2002).
4. Hunstad, D. A. & Justice, S. S. Intracellular lifestyles and immune evasion strategies of uropathogenic Escherichia coli. *Annu Rev Microbiol* **64**, 203–221 (2010).
5. Gupta, K., Hooton, T. M. & Stamm, W. E. Increasing antimicrobial resistance and the management of uncomplicated community-acquired urinary tract infections. *Ann. Intern. Med.* **135**, 41–50 (2001).
6. Flores-Mireles, A. L., Walker, J. N., Caparon, M. & Hultgren, S. J. Urinary tract infections: epidemiology, mechanisms of infection and treatment options. *Nat. Rev. Microbiol.* **13**, 269–284 (2015).
7. Phan, M. D. *et al.* Molecular characterization of a multidrug resistance IncF plasmid from the globally disseminated Escherichia coli ST131 clone. *PLoS One* **10**, e0122369 (2015).
8. Barber, A. E., Norton, J. P., Spivak, A. M. & Mulvey, M. A. Urinary tract infections: current and emerging management strategies. *Clin. Infect. Dis.* **57**, 719–724 (2013).
9. Ronald, A. The etiology of urinary tract infection: traditional and emerging pathogens. *Am. J. Med.* **113 Suppl**, 14S-19S (2002).
10. Justice, S. S. *et al.* Differentiation and developmental pathways of uropathogenic Escherichia coli in urinary tract pathogenesis. *Proc. Natl. Acad. Sci. U. S. A.* **101**, 1333–1338 (2004).
11. Andersen, T. E. *et al.* Escherichia coli uropathogenesis in vitro: invasion, cellular escape, and secondary infection analyzed in a human bladder cell infection model. *Infect. Immun.* **80**, 1858–1867 (2012).
12. Chen, S. L. *et al.* Identification of genes subject to positive selection in uropathogenic strains of Escherichia coli: a comparative genomics approach.

Proc. Natl. Acad. Sci. U. S. A. **103**, 5977–5982 (2006).

13. Foxman, B., Barlow, R., D'Arcy, H., Gillespie, B. & Sobel, J. D. Urinary tract infection: self-reported incidence and associated costs. *Ann. Epidemiol.* **10**, 509–515 (2000).
14. Justice, S. S., Hunstad, D. A., Cegelski, L. & Hultgren, S. J. Morphological plasticity as a bacterial survival strategy. *Nat. Rev. Microbiol.* **6**, 162–168 (2008).
15. Katayama, T., Takata, M. & Sekimizu, K. CedA is a novel Escherichia coli protein that activates the cell division inhibited by chromosomal DNA over-replication. *Mol. Microbiol.* **26**, 687–697 (1997).
16. Khandige, S. *et al.* DamX Controls Reversible Cell Morphology Switching in Uropathogenic Escherichia coli. *MBio* **7**, (2016).
17. Mulvey, M. A., Schilling, J. D. & Hultgren, S. J. Establishment of a persistent Escherichia coli reservoir during the acute phase of a bladder infection. *Infect. Immun.* **69**, 4572–4579 (2001).
18. Hooton, T. M. Uncomplicated urinary tract infection. *N. Engl. J. Med.* **366**, 1028–1037 (2012).
19. Lichtenberger, P. & Hooton, T. M. Complicated urinary tract infections. *Curr. Infect. Dis. Rep.* **10**, 499–504 (2008).
20. Totsika, M. *et al.* Uropathogenic Escherichia coli mediated urinary tract infection. *Curr. Drug Targets* **13**, 1386–1399 (2012).
21. Bien, J., Sokolova, O. & Bozko, P. Role of Uropathogenic Escherichia coli Virulence Factors in Development of Urinary Tract Infection and Kidney Damage. *Int J Nephrol* **2012**, 681473 (2012).
22. Rogers, B. A., Sidjabat, H. E. & Paterson, D. L. Escherichia coli O25b-ST131: a pandemic, multiresistant, community-associated strain. *J. Antimicrob. Chemother.* **66**, 1–14 (2011).
23. Marrs, C. F., Zhang, L. & Foxman, B. Escherichia coli mediated urinary tract infections: are there distinct uropathogenic E. coli (UPEC) pathotypes? *FEMS Microbiol. Lett.* **252**, 183–190 (2005).
24. Wiles, T. J., Kulesus, R. R. & Mulvey, M. A. Origins and virulence mechanisms of uropathogenic Escherichia coli. *Exp Mol Pathol* **85**, 11–19 (2008).
25. Justice, S. S., Hunstad, D. A., Seed, P. C. & Hultgren, S. J. Filamentation by Escherichia coli subverts innate defenses during urinary tract infection. *Proc. Natl. Acad. Sci. U. S. A.* **103**, 19884–19889 (2006).

26. Schaeffer, A. J. Potential role of phase variation of type 1 pili in urinary tract infection and bacterial prostatitis. *Infection* **19**, S144–S149 (1991).
27. Connell, I. *et al.* Type 1 fimbrial expression enhances Escherichia coli virulence for the urinary tract. *Proc Natl Acad Sci U S A* **93**, 9827–9832 (1996).
28. Langermann, S. *et al.* Prevention of mucosal Escherichia coli infection by FimH-adhesin-based systemic vaccination. *Science (80-.).* **276**, 607–611 (1997).
29. Martinez, J. J., Mulvey, M. A., Schilling, J. D., Pinkner, J. S. & Hultgren, S. J. Type 1 pilus-mediated bacterial invasion of bladder epithelial cells. *EMBO J.* **19**, 2803–2812 (2000).
30. Hvidberg, H. *et al.* Development of a long-term ascending urinary tract infection mouse model for antibiotic treatment studies. *Antimicrob. Agents Chemother.* **44**, 156–163 (2000).
31. Anderson, G. G. *et al.* Intracellular bacterial biofilm-like pods in urinary tract infections. *Science (80-.).* **301**, 105–107 (2003).
32. Mulvey, M. A. Induction and Evasion of Host Defenses by Type 1-Piliated Uropathogenic Escherichia coli. *Science (80-.).* **282**, 1494–1497 (1998).
33. Berry, R. E., Klumpp, D. J. & Schaeffer, A. J. Urothelial cultures support intracellular bacterial community formation by uropathogenic Escherichia coli. *Infect. Immun.* **77**, 2762–2772 (2009).
34. Rosen, D. A., Hooton, T. M., Stamm, W. E., Humphrey, P. A. & Hultgren, S. J. Detection of intracellular bacterial communities in human urinary tract infection. *PLoS Med.* **4**, e329 (2007).
35. Wright, K. J., Seed, P. C. & Hultgren, S. J. Development of intracellular bacterial communities of uropathogenic Escherichia coli depends on type 1 pili. *Cell. Microbiol.* **9**, 2230–2241 (2007).
36. Tormo, A., Almiron, M. & Kolter, R. surA, an Escherichia coli gene essential for survival in stationary phase. *J. Bacteriol.* **172**, 4339–4347 (1990).
37. Lazar, S. W. & Kolter, R. SurA assists the folding of Escherichia coli outer membrane proteins. *J. Bacteriol.* **178**, 1770–1773 (1996).
38. Newman, J. V *et al.* Stimulation of Escherichia coli F-18Col− type-1 fimbriae synthesis by leuX. *FEMS Microbiol. Lett.* **122**, 281–287 (1994).
39. Justice, S. S., Lauer, S. R., Hultgren, S. J. & Hunstad, D. A. Maturation of intracellular Escherichia coli communities requires SurA. *Infect. Immun.* **74**, 4793–4800 (2006).

40. Hannan, T. J. *et al.* LeuX tRNA-dependent and-independent mechanisms of Escherichia coli pathogenesis in acute cystitis. *Mol. Microbiol.* **67**, 116–128 (2008).
41. Dobrindt, U. & Hacker, J. Regulation of the tRNA 5 Leu-encoding gene leuX that is associated with a pathogenicity island in the uropathogenic Escherichia coli strain 536. *Mol. Genet. Genomics* **265**, 895–904 (2001).
42. Piechaczek, K. *et al.* Influence of pathogenicity islands and the minor leuX-encoded tRNA5Leu on the proteome pattern of the uropathogenic Escherichia coli strain 536. *Int. J. Med. Microbiol.* **290**, 75–84 (2000).
43. Schafer, K. A. The cell cycle: a review. *Vet. Pathol.* **35**, 461–478 (1998).
44. Wang, J. D. & Levin, P. A. Metabolism, cell growth and the bacterial cell cycle. *Nat. Rev. Microbiol.* **7**, 822–827 (2009).
45. Mott, M. L. & Berger, J. M. DNA replication initiation: mechanisms and regulation in bacteria. *Nat. Rev. Microbiol.* **5**, 343–354 (2007).
46. Reyes-Lamothe, R., Nicolas, E. & Sherratt, D. J. Chromosome replication and segregation in bacteria. *Annu. Rev. Genet.* **46**, 121–143 (2012).
47. Katayama, T. Feedback controls restrain the initiation of Escherichia coli chromosomal replication. *Mol. Microbiol.* **41**, 9–17 (2001).
48. Gilbert, W. & Dressler, D. DNA replication: the rolling circle model. in *Cold Spring Harbor Symposia on Quantitative Biology* vol. 33 473–484 (Cold Spring Harbor Laboratory Press, 1968).
49. Duggin, I. G., Wake, R. G., Bell, S. D. & Hill, T. M. The replication fork trap and termination of chromosome replication. *Mol. Microbiol.* **70**, 1323–1333 (2008).
50. Kornberg, A. & Baker, T. A. DNA replication. WH. *H. Free. New York* (1992).
51. Nordman, J., Skovgaard, O. & Wright, A. A novel class of mutations that affect DNA replication in E. coli. *Mol. Microbiol.* **64**, 125–138 (2007).
52. Fang, L., Davey, M. J. & O'Donnell, M. Replisome assembly at oriC, the replication origin of E. coli, reveals an explanation for initiation sites outside an origin. *Mol. Cell* **4**, 541–553 (1999).
53. Zakrzewska-Czerwińska, J., Jakimowicz, D., Zawilak-Pawlik, A. & Messer, W. Regulation of the initiation of chromosomal replication in bacteria. *FEMS Microbiol. Rev.* **31**, 378–387 (2007).
54. Skarstad, K. & Katayama, T. Regulating DNA replication in bacteria. *Cold*

Spring Harb. Perspect. Biol. **5**, a012922 (2013).

55. Donachie, W. D. & Blakely, G. W. Coupling the initiation of chromosome replication to cell size in Escherichia coli. *Curr. Opin. Microbiol.* **6**, 146–150 (2003).
56. Kato, J. & Katayama, T. Hda, a novel DnaA-related protein, regulates the replication cycle in Escherichia coli. *EMBO J.* **20**, 4253–4262 (2001).
57. Katayama, T., Ozaki, S., Keyamura, K. & Fujimitsu, K. Regulation of the replication cycle: conserved and diverse regulatory systems for DnaA and oriC. *Nat. Rev. Microbiol.* **8**, 163–170 (2010).
58. Fujimitsu, K., Senriuchi, T. & Katayama, T. Specific genomic sequences of E. coli promote replicational initiation by directly reactivating ADP-DnaA. *Genes Dev.* **23**, 1221–1233 (2009).
59. Morigen, M., Flåtten, I. & Skarstad, K. The Escherichia coli datA site promotes proper regulation of cell division. *Microbiology* **160**, 703–710 (2014).
60. Kitagawa, R., Ozaki, T., Moriya, S. & Ogawa, T. Negative control of replication initiation by a novel chromosomal locus exhibiting exceptional affinity for Escherichia coli DnaA protein. *Genes Dev.* **12**, 3032–3043 (1998).
61. Kasho, K. & Katayama, T. DnaA binding locus datA promotes DnaA-ATP hydrolysis to enable cell cycle-coordinated replication initiation. *Proc. Natl. Acad. Sci.* **110**, 936–941 (2013).
62. Skarstad, K., Lueder, G., Lurz, R., Speck, C. & Messer, W. The Escherichia coli SeqA protein binds specifically and co-operatively to two sites in hemimethylated and fully methylated oriC. *Mol. Microbiol.* **36**, 1319–1326 (2000).
63. Katayama, T. & Kornberg, A. Hyperactive initiation of chromosomal replication in vivo and in vitro by a mutant initiator protein, DnaAcos, of Escherichia coli. *J. Biol. Chem.* **269**, 12698–12703 (1994).
64. Katayama, T., Akimitsu, N., Mizushima, T., Miki, T. & Sekimizu, K. Overinitiation of chromosome replication in the Escherichia coli dnaAcos mutant depends on activation of oriC function by the dam gene product. *Mol. Microbiol.* **25**, 661–670 (1997).
65. Felczak, M. M. & Kaguni, J. M. DnaAcos hyperinitiates by circumventing regulatory pathways that control the frequency of initiation in Escherichia coli. *Mol. Microbiol.* **72**, 1348–1363 (2009).

66. Simmons, L. A. & Kaguni, J. M. The dnaAcos allele of Escherichia coli: hyperactive initiation is caused by substitution of A184V and Y271H, resulting in defective ATP binding and aberrant DNA replication control. *Mol. Microbiol.* **47**, 755–765 (2003).
67. Katayama, T. The mutant DnaAcos protein which overinitiates replication of the Escherichia coli chromosome is inert to negative regulation for initiation. *J. Biol. Chem.* **269**, 22075–22079 (1994).
68. Simmons, L. A., Breier, A. M., Cozzarelli, N. R. & Kaguni, J. M. Hyperinitiation of DNA replication in Escherichia coli leads to replication fork collapse and inviability. *Mol. Microbiol.* **51**, 349–358 (2004).
69. Braun, R. E., O'Day, K. & Wright, A. Cloning and characterization of dnaA (Cs), a mutation which leads to overinitiation of DNA replication in Escherichia coli K-12. *J. Bacteriol.* **169**, 3898–3903 (1987).
70. Carr, K. M. & Kaguni, J. M. The 4784V missense mutation of the dnaA5 and dnaA46 alleles confers a defect in ATP binding and thermoiability in initiation of Escherichia coli DNA replication. *Mol. Microbiol.* **20**, 1307–1318 (1996).
71. Wu, L. J. & Errington, J. Nucleoid occlusion and bacterial cell division. *Nat. Rev. Microbiol.* **10**, 8–12 (2012).
72. Weiss, D. S. Bacterial cell division and the septal ring. *Mol. Microbiol.* **54**, 588–597 (2004).
73. Lee, S. Y. Suppression of filamentation in recombinant Escherichia coli by amplified FtsZ activity. *Biotechnol. Lett.* **16**, 1247–1252 (1994).
74. Bi, E. F. & Lutkenhaus, J. FtsZ ring structure associated with division in Escherichia coli. *Nature* **354**, 161–164 (1991).
75. Adams, D. W. & Errington, J. Bacterial cell division: assembly, maintenance and disassembly of the Z ring. *Nat. Rev. Microbiol.* **7**, 642–653 (2009).
76. Strepp, R., Scholz, S., Kruse, S., Speth, V. & Reski, R. Plant nuclear gene knockout reveals a role in plastid division for the homolog of the bacterial cell division protein FtsZ, an ancestral tubulin. *Proc. Natl. Acad. Sci.* **95**, 4368–4373 (1998).
77. Romberg, L. & Mitchison, T. J. Rate-limiting guanosine 5 '-triphosphate hydrolysis during nucleotide turnover by FtsZ, a prokaryotic tubulin homologue involved in bacterial cell division. *Biochemistry* **43**, 282–288 (2004).
78. Hale, C. A. & de Boer, P. A. Direct binding of FtsZ to ZipA, an essential

component of the septal ring structure that mediates cell division in E. coli. *Cell* **88**, 175–185 (1997).

79. Lutkenhaus, J., Pichoff, S. & Du, S. Bacterial cytokinesis: from Z ring to divisome. *Cytoskeleton* **69**, 778–790 (2012).
80. Pichoff, S. & Lutkenhaus, J. Unique and overlapping roles for ZipA and FtsA in septal ring assembly in Escherichia coli. *EMBO J.* **21**, 685–693 (2002).
81. van den Ent, F. & Löwe, J. Crystal structure of the cell division protein FtsA from Thermotoga maritima. *EMBO J.* **19**, 5300–5307 (2000).
82. Geissler, B., Elraheb, D. & Margolin, W. A gain-of-function mutation in ftsA bypasses the requirement for the essential cell division gene zipA in Escherichia coli. *Proc. Natl. Acad. Sci.* **100**, 4197–4202 (2003).
83. Gueiros-Filho, F. J. & Losick, R. A widely conserved bacterial cell division protein that promotes assembly of the tubulin-like protein FtsZ. *Genes Dev.* **16**, 2544–2556 (2002).
84. Harry, E. J., Monahan, L. & Thompson, L. Bacterial cell division: the mechanism and its precison. *Int Rev Cytol* **253**, 27–94 (2006).
85. Ebersbach, G., Galli, E., Moller-Jensen, J., Lowe, J. & Gerdes, K. Novel coiled-coil cell division factor ZapB stimulates Z ring assembly and cell division. *Mol. Microbiol.* **68**, 720–735 (2008).
86. Lutkenhaus, J. Assembly dynamics of the bacterial MinCDE system and spatial regulation of the Z ring. *Annu. Rev. Biochem.* **76**, 539–562 (2007).
87. Shih, Y. & Zheng, M. Spatial control of the cell division site by the Min system in E scherichia coli. *Environ. Microbiol.* **15**, 3229–3239 (2013).
88. Rowlett, V. W. & Margolin, W. The Min system and other nucleoid-independent regulators of Z ring positioning. *Front. Microbiol.* **6**, (2015).
89. Yu, X. C. & Margolin, W. FtsZ ring clusters in min and partition mutants: role of both the Min system and the nucleoid in regulating FtsZ ring localization. *Mol Microbiol* **32**, 315–326 (1999).
90. Mulder, E. & Woldringh, C. L. Actively replicating nucleoids influence positioning of division sites in Escherichia coli filaments forming cells lacking DNA. *J Bacteriol* **171**, 4303–4314 (1989).
91. Bernhardt, T. G. & de Boer, P. A. SlmA, a nucleoid-associated, FtsZ binding protein required for blocking septal ring assembly over Chromosomes in E. coli. *Mol Cell* **18**, 555–564 (2005).

92. Tonthat, N. K. *et al.* Molecular mechanism by which the nucleoid occlusion factor, SlmA, keeps cytokinesis in check. *EMBO J.* **30**, 154–164 (2011).
93. Cho, H., McManus, H. R., Dove, S. L. & Bernhardt, T. G. Nucleoid occlusion factor SlmA is a DNA-activated FtsZ polymerization antagonist. *Proc Natl Acad Sci U S A* **108**, 3773–3778 (2011).
94. Bailey, M. W., Bisicchia, P., Warren, B. T., Sherratt, D. J. & Mannik, J. Evidence for divisome localization mechanisms independent of the Min system and SlmA in Escherichia coli. *PLoS Genet* **10**, e1004504 (2014).
95. Espéli, O. *et al.* A MatP–divisome interaction coordinates chromosome segregation with cell division in E. coli. *EMBO J.* **31**, 3198–3211 (2012).
96. D'Ari, R. & Huisman, O. Novel mechanism of cell division inhibition associated with the SOS response in Escherichia coli. *J Bacteriol* **156**, 243–250 (1983).
97. Bi, E. & Lutkenhaus, J. Cell division inhibitors SulA and MinCD prevent formation of the FtsZ ring. *J Bacteriol* **175**, 1118–1125 (1993).
98. Trusca, D., Scott, S., Thompson, C. & Bramhill, D. Bacterial SOS checkpoint protein SulA inhibits polymerization of purified FtsZ cell division protein. *J. Bacteriol.* **180**, 3946–3953 (1998).
99. Mizusawa, S. & Gottesman, S. Protein degradation in Escherichia coli: the lon gene controls the stability of sulA protein. *Proc. Natl. Acad. Sci.* **80**, 358–362 (1983).
100. Aertsen, A., Van Houdt, R., Vanoirbeek, K. & Michiels, C. W. An SOS response induced by high pressure in Escherichia coli. *J. Bacteriol.* **186**, 6133–6141 (2004).
101. Janion, C. Some aspects of the SOS response system--a critical survey. *Acta Biochim. Pol.* **48**, 599–610 (2001).
102. Radman, M. SOS repair hypothesis: phenomenology of an inducible DNA repair which is accompanied by mutagenesis. *Basic Life Sci* **5A**, 355–367 (1975).
103. Witkin, E. M. RecA protein in the SOS response: milestones and mysteries. *Biochimie* **73**, 133–141 (1991).
104. Iosifidis, G. Investigating the conditions that trigger filamentation in uropathogenic Escherichia coli. (2018).
105. Arends, S. J. *et al.* Discovery and characterization of three new Escherichia coli septal ring proteins that contain a SPOR domain: DamX, DedD, and RlpA. *J Bacteriol* **192**, 242–255 (2010).

106. Lee, D. J., Busby, S. J. W., Westblade, L. F. & Chait, B. T. Affinity isolation and I-DIRT mass spectrometric analysis of the Escherichia coli O157: H7 Sakai RNA polymerase complex. *J. Bacteriol.* **190**, 1284–1289 (2008).
107. Chen, H. A., Simpson, P., Huyton, T., Roper, D. & Matthews, S. Solution structure and interactions of the Escherichia coli cell division activator protein CedA. *Biochemistry* **44**, 6738–6744 (2005).
108. Abe, Y. *et al.* Functional analysis of CedA based on its structure: residues important in binding of DNA and RNA polymerase and in the cell division regulation. *J. Biochem.* **159**, 217–223 (2015).
109. Sharma, P., Tomar, A. K. & Kundu, B. Identification of functional interactome of a key cell division regulatory protein CedA of E. coli. *Int. J. Biol. Macromol.* **106**, 763–767 (2018).
110. Noor, E., Eden, E., Milo, R. & Alon, U. Central carbon metabolism as a minimal biochemical walk between precursors for biomass and energy. *Mol. Cell* **39**, 809–820 (2010).
111. Schaechter, M., Maaløe, O. & Kjeldgaard, N. O. Dependency on medium and temperature of cell size and chemical composition during balanced growth of Salmonella typhimurium. *Microbiology* **19**, 592–606 (1958).
112. Sandoval, J. M., Arenas, F. A. & Vasquez, C. C. Glucose-6-phosphate dehydrogenase protects Escherichia coli from tellurite-mediated oxidative stress. *PLoS One* **6**, (2011).
113. Calloni, G. *et al.* DnaK functions as a central hub in the E. coli chaperone network. *Cell Rep.* **1**, 251–264 (2012).
114. Inouye, M., Shaw, J. & Shen, C. The assembly of a structural lipoprotein in the envelope of Escherichia coli. *J. Biol. Chem.* **247**, 8154–8159 (1972).
115. Cho, H. & Bernhardt, T. G. Identification of the SlmA active site responsible for blocking bacterial cytokinetic ring assembly over the chromosome. *PLoS Genet* **9**, e1003304 (2013).
116. Baba, T. *et al.* Construction of Escherichia coli K-12 in-frame, single-gene knockout mutants: the Keio collection. *Mol Syst Biol* **2**, 2006 0008 (2006).
117. Ansari, S. *et al.* A newly identified prophage-encoded gene, ymfM, causes SOS-inducible filamentation in Escherichia coli. *bioRxiv* (2020).
118. Bernhardt, T. G. & De Boer, P. A. J. The Escherichia coli amidase AmiC is a periplasmic septal ring component exported via the twin-arginine transport

pathway. *Mol. Microbiol.* **48**, 1171–1182 (2003).

119. Guzman, L. M., Belin, D., Carson, M. J. & Beckwith, J. Tight regulation, modulation, and high-level expression by vectors containing the arabinose PBAD promoter. *J. Bacteriol.* **177**, 4121–4130 (1995).
120. Iosifidis, G. & Duggin, I. G. Distinct morphological fates of uropathogenic E. coli intracellular bacterial communities: dependency on urine composition and pH. *Infect. Immun.* (2020).
121. Lau, I. F. *et al.* Spatial and temporal organization of replicating Escherichia coli chromosomes. *Mol Microbiol* **49**, 731–743 (2003).
122. Burke, C. *et al.* Harnessing single cell sorting to identify cell division genes and regulators in bacteria. *PLoS One* **8**, e60964 (2013).
123. Froger, A. & Hall, J. E. Transformation of plasmid DNA into E. coli using the heat shock method. *JoVE (Journal Vis. Exp.* e253 (2007).
124. Aranda, P. S., LaJoie, D. M. & Jorcyk, C. L. Bleach gel: a simple agarose gel for analyzing RNA quality. *Electrophoresis* **33**, 366–369 (2012).
125. Afgan, E. *et al.* The Galaxy platform for accessible, reproducible and collaborative biomedical analyses: 2016 update. *Nucleic Acids Res* **44**, W3–W10 (2016).
126. Langmead, B., Trapnell, C., Pop, M. & Salzberg, S. L. Ultrafast and memory-efficient alignment of short DNA sequences to the human genome. *Genome Biol* **10**, R25 (2009).
127. Anders, S., Pyl, P. T. & Huber, W. HTSeq—a Python framework to work with high-throughput sequencing data. *Bioinformatics* **31**, 166–169 (2015).
128. Love, M. I., Huber, W. & Anders, S. Moderated estimation of fold change and dispersion for RNA-seq data with DESeq2. *Genome Biol.* **15**, 550 (2014).
129. Skarstad, K., Boye, E. & Steen, H. B. Timing of initiation of chromosome replication in individual Escherichia coli cells. *EMBO J.* **5**, 1711–1717 (1986).
130. Gallet, R. *et al.* The evolution of bacterial cell size: the internal diffusion-constraint hypothesis. *ISME J.* **11**, 1559–1568 (2017).
131. Fuller, R. S., Funnell, B. E. & Kornberg, A. The dnaA protein complex with the E. coli chromosomal replication origin (oriC) and other DNA sites. *Cell* **38**, 889–900 (1984).
132. Hansen, F. G. & Rasmussen, K. V. Regulation of the dnaA product in Escherichia coli. *Mol. Gen. Genet. MGG* **155**, 219–225 (1977).

133. Kurokawa, K., Nishida, S., Emoto, A., Sekimizu, K. & Katayama, T. Replication cycle-coordinated change of the adenine nucleotide-bound forms of DnaA protein in Escherichia coli. *EMBO J.* **18**, 6642–6652 (1999).
134. Woelker, B. & Messer, W. The structure of the initiation complex at the replication origin, oriC, of Escherichia coli. *Nucleic Acids Res.* **21**, 5025–5033 (1993).
135. Kellenberger-Gujer, G., Podhajska, A. J. & Caro, L. A cold sensitive dnaA mutant of E. coli which overinitiates chromosome replication at low temperature. *Mol. Gen. Genet. MGG* **162**, 9–16 (1978).
136. Mukherjee, A., Cao, C. & Lutkenhaus, J. Inhibition of FtsZ polymerization by SulA, an inhibitor of septation in Escherichia coli. *Proc. Natl. Acad. Sci.* **95**, 2885–2890 (1998).
137. Tonthat, N. K. *et al.* SlmA forms a higher-order structure on DNA that inhibits cytokinetic Z-ring formation over the nucleoid. *Proc. Natl. Acad. Sci.* **110**, 10586–10591 (2013).
138. Dajkovic, A., Lan, G., Sun, S. X., Wirtz, D. & Lutkenhaus, J. MinC spatially controls bacterial cytokinesis by antagonizing the scaffolding function of FtsZ. *Curr. Biol.* **18**, 235–244 (2008).
139. Chen, Y., Milam, S. L. & Erickson, H. P. SulA inhibits assembly of FtsZ by a simple sequestration mechanism. *Biochemistry* **51**, 3100–3109 (2012).
140. Little, J. W. Mechanism of specific LexA cleavage: autodigestion and the role of RecA coprotease. *Biochimie* **73**, 411–421 (1991).
141. Ansari, S. Bacterial filamentation as a survival strategy: identification and characterisation of a novel cell division inhibitor in Escherichia coli. (2019).
142. Projan, S. J. & Wechsler, J. A. Isolation and analysis of multicopy extragenic suppressors of dnaA mutations. *J. Bacteriol.* **145**, 861–866 (1981).
143. Brüning, J.-G., Myka, K. K. & McGlynn, P. Overexpression of the replicative helicase in Escherichia coli inhibits replication initiation and replication fork reloading. *J. Mol. Biol.* **428**, 1068–1079 (2016).
144. Baev, M. V, Baev, D., Radek, A. J. & Campbell, J. W. Growth of Escherichia coli MG1655 on LB medium: monitoring utilization of sugars, alcohols, and organic acids with transcriptional microarrays. *Appl. Microbiol. Biotechnol.* **71**, 310–316 (2006).
145. Courcelle, J., Khodursky, A., Peter, B., Brown, P. O. & Hanawalt, P. C.

Comparative gene expression profiles following UV exposure in wild-type and SOS-deficient Escherichia coli. *Genetics* **158**, 41–64 (2001).

146. Anderson, D. G. & Kowalczykowski, S. C. The translocating RecBCD enzyme stimulates recombination by directing RecA protein onto ssDNA in a χ-regulated manner. *Cell* **90**, 77–86 (1997).
147. Kuzminov, A. & Stahl, F. W. Stability of linear DNA in recA mutant Escherichia coli cells reflects ongoing chromosomal DNA degradation. *J. Bacteriol.* **179**, 880–888 (1997).
148. Dixon, D. A. & Kowalczykowski, S. C. The recombination hotspot χ is a regulatory sequence that acts by attenuating the nuclease activity of the E. coli RecBCD enzyme. *Cell* **73**, 87–96 (1993).
149. VanBogelen, R. A., Acton, M. A. & Neidhardt, F. C. Induction of the heat shock regulon does not produce thermotolerance in Escherichia coli. *Genes Dev.* **1**, 525–531 (1987).
150. Kitagawa, M., Matsumura, Y. & Tsuchido, T. Small heat shock proteins, IbpA and IbpB, are involved in resistances to heat and superoxide stresses in Escherichia coli. *FEMS Microbiol. Lett.* **184**, 165–171 (2000).
151. Gerding, M. A. *et al.* Self-enhanced accumulation of FtsN at Division Sites and Roles for Other Proteins with a SPOR domain (DamX, DedD, and RlpA) in Escherichia coli cell constriction. *J Bacteriol* **191**, 7383–7401 (2009).
152. Lee, S. K. *et al.* Directed evolution of AraC for improved compatibility of arabinose-and lactose-inducible promoters. *Appl. Environ. Microbiol.* **73**, 5711–5715 (2007).
153. Ehrt, S. *et al.* Controlling gene expression in mycobacteria with anhydrotetracycline and Tet repressor. *Nucleic Acids Res.* **33**, e21–e21 (2005).
154. Stewart, J. B. & Hermodson, M. A. Topology of RbsC, the membrane component of the Escherichia coli ribose transporter. *J. Bacteriol.* **185**, 5234–5239 (2003).
155. Schlegel, A. *et al.* Network regulation of the Escherichia coli maltose system. *J. Mol. Microbiol. Biotechnol.* **4**, 301–307 (2002).
156. Peralta, D. R. *et al.* Enterobactin as part of the oxidative stress response repertoire. *PLoS One* **11**, (2016).
157. Snyder, J. A. *et al.* Transcriptome of uropathogenic Escherichia coli during urinary tract infection. *Infect. Immun.* **72**, 6373–6381 (2004).

158. Muse, W. B., Rosario, C. J. & Bender, R. A. Nitrogen regulation of the codBA (cytosine deaminase) operon from Escherichia coli by the nitrogen assimilation control protein, NAC. *J. Bacteriol.* **185**, 2920–2926 (2003).
159. Vadia, S. *et al.* Fatty acid availability sets cell envelope capacity and dictates microbial cell size. *Curr. Biol.* **27**, 1757–1767 (2017).
160. Hung, M.-N. *et al.* Crystal structure of TDP-fucosamine acetyltransferase (WecD) from Escherichia coli, an enzyme required for enterobacterial common antigen synthesis. *J. Bacteriol.* **188**, 5606–5617 (2006).
161. Goździewicz, T. K., Łukasiewicz, J. & Ługowski, C. The structure and significance of enterobacterial common antigen (ECA). *Postepy Hig. Med. Dosw. (Online)* **69**, 1003–1012 (2015).
162. Viveiros, M. *et al.* Antibiotic stress, genetic response and altered permeability of E. coli. *PLoS One* **2**, (2007).
163. Liu, X. & Ferenci, T. An analysis of multifactorial influences on the transcriptional control of ompF and ompC porin expression under nutrient limitation. *Microbiology* **147**, 2981–2989 (2001).
164. Knight, K. L., Aoki, K. H., Ujita, E. L. & McEntee, K. Identification of the amino acid substitutions in two mutant forms of the recA protein from Escherichia coli: recA441 and recA629. *J. Biol. Chem.* **259**, 11279–11283 (1984).
165. Castellazzi, M., George, J. & Buttin, G. Prophage induction and cell division in E. coli. *Mol. Gen. Genet. MGG* **119**, 153–174 (1972).
166. Mediati, D. G., Burke, C. M., Ansari, S., Harry, E. J. & Duggin, I. G. High-throughput sequencing of sorted expression libraries reveals inhibitors of bacterial cell division. *BMC Genomics* **19**, 781 (2018).
167. Lyngstadaas, A., Lobner-Olesen, A. & Boye, E. Characterization of three genes in the dam-containing operon of Escherichia coli. *Mol. Gen. Genet.* **247**, 546–554 (1995).
168. Chien, A.-C., Hill, N. S. & Levin, P. A. Cell size control in bacteria. *Curr. Biol.* **22**, R340–R349 (2012).
169. Chien, A., Zareh, S. K. G., Wang, Y. M. & Levin, P. A. Changes in the oligomerization potential of the division inhibitor UgtP co-ordinate B acillus subtilis cell size with nutrient availability. *Mol. Microbiol.* **86**, 594–610 (2012).
170. Gerdes, S. Y. *et al.* Experimental determination and system level analysis of

essential genes in Escherichia coli MG1655. *J. Bacteriol.* **185**, 5673–5684 (2003).

171. Potter, S. C. *et al.* HMMER web server: 2018 update. *Nucleic Acids Res.* **46**, W200–W204 (2018).
172. Edgar, R. C. MUSCLE: multiple sequence alignment with high accuracy and high throughput. *Nucleic Acids Res.* **32**, 1792–1797 (2004).
173. Kumar, S., Stecher, G., Li, M., Knyaz, C. & Tamura, K. MEGA X: molecular evolutionary genetics analysis across computing platforms. *Mol. Biol. Evol.* **35**, 1547–1549 (2018).
174. Mediati, D. G. Identification of Escherichia coli genes required for bacterial survival and morphological plasticity in urinary tract infections. (2018).
175. Hashimoto, M. *et al.* Cell size and nucleoid organization of engineered Escherichia coli cells with a reduced genome. *Mol. Microbiol.* **55**, 137–149 (2005).
176. Ferullo, D. J., Cooper, D. L., Moore, H. R. & Lovett, S. T. Cell cycle synchronization of Escherichia coli using the stringent response, with fluorescence labeling assays for DNA content and replication. *Methods* **48**, 8–13 (2009).
177. Weber, H., Polen, T., Heuveling, J., Wendisch, V. F. & Hengge, R. Genome-wide analysis of the general stress response network in Escherichia coli: sigmaS-dependent genes, promoters, and sigma factor selectivity. *J Bacteriol* **187**, 1591–1603 (2005).
178. Yamada, M., Kabir, M. S. & Tsunedomi, R. Divergent promoter organization may be a preferred structure for gene control in Escherichia coli. *J. Mol. Microbiol. Biotechnol.* **6**, 206–210 (2003).
179. Kaasen, I., Falkenberg, P., Styrvold, O. B. & Strøm, A. R. Molecular cloning and physical mapping of the otsBA genes, which encode the osmoregulatory trehalose pathway of Escherichia coli: evidence that transcription is activated by KatF (AppR). *J. Bacteriol.* **174**, 889–898 (1992).
180. Kempf, B. & Bremer, E. Uptake and synthesis of compatible solutes as microbial stress responses to high-osmolality environments. *Arch. Microbiol.* **170**, 319–330 (1998).
181. Datsenko, K. A. & Wanner, B. L. One-step inactivation of chromosomal genes in Escherichia coli K-12 using PCR products. *Proc. Natl. Acad. Sci. U. S. A.* **97**,

6640–6645 (2000).

182. Ducret, A., Quardokus, E. M. & Brun, Y. V. MicrobeJ, a tool for high throughput bacterial cell detection and quantitative analysis. *Nat. Microbiol.* **1**, 16077 (2016).

183. Ogura, Y., Imai, Y., Ogasawara, N. & Moriya, S. Autoregulation of the dnaA-dnaNOperon and Effects of DnaA Protein Levels on Replication Initiation inBacillus subtilis. *J. Bacteriol.* **183**, 3833–3841 (2001).

184. Weart, R. B. *et al.* A metabolic sensor governing cell size in bacteria. *Cell* **130**, 335–347 (2007).

185. Hill, N. S., Buske, P. J., Shi, Y. & Levin, P. A. A moonlighting enzyme links Escherichia coli cell size with central metabolism. *PLoS Genet* **9**, e1003663 (2013).

186. Lu, M. & Kleckner, N. Molecular cloning and characterization of the pgm gene encoding phosphoglucomutase of Escherichia coli. *J. Bacteriol.* **176**, 5847–5851 (1994).

187. Byrne-Nash, R. *et al.* Probing the Mechanism of LAL-32, a Gold Nanoparticle-Based Antibiotic Discovered through Small Molecule Variable Ligand Display. *Bioconjug Chem* **28**, 1807–1810 (2017).